Mixing and reactions in porous media

Pietro de Anna

N° d'ordre: 4519 **ANNÉE 2012**

THÈSE / UNIVERSITÉ DE RENNES 1
sous le sceau de l'Université Européenne de Bretagne

pour le grade de

DOCTEUR DE L'UNIVERSITÉ DE RENNES 1

Mention: Sciences de la Terre

Ecole doctorale Sciences de la Matière Rennes

présentée par

Pietro DE ANNA

préparée à l'unité de recherche UMR6118
Geosciences Rennes
Université de Rennes 1

Mixing and reactions in porous media

Thèse soutenue à Rennes le 2.07.2012

devant le jury composé de :

Philippe ACKERER
D. R. CNRS, Lhyges - Strasbourg, France / rapporteur

Emmanuel VILLERMAUX
Professeur, Université de Aix-Maresille, France / *rapporteur*

Renaud DELANNAY
Professeur, Université de Rennes 1, France / examinateur

Aldo FIORI
Professeur, Université Roma 3, Italie / *examinateur*

Jesus CARRERA
D. R. CSIC, Barcelone, Espagne / examinateur

Yves MEHEUST
Maitre de conference / examinateur

Philippe DAVY
D. R. CNRS, Géosciences Rennes / *directeur de thèse*

Tanguy LE BORGNE
Physicien adjoint CNAP / co-*directeur de thèse*

Acknowledgements

This thesis was funded by the European Commission through FP7 projects ITN project, IMVUL project (Grant Agreement 212298). I had the opportunity to travel and have successful interactions with several scientists in Rennes and internationally. In particular my stay in Barcelona for five months has been supported by a mobility fellowship assigned from the *Collège Doctoral International (CDI) de l'Université européenne de Bretagne (UEB)*.

Abstract

In this thesis we use a stochastic approach to address the upscaling of mixing dominated reactions in flows thorough heterogeneous porous media.

For the case where the transport is represented only by diffusion, fluctuations in spatial concentration distribution lead to segregation of chemicals and thus to anomalous kinetics. We show that the transition from the expected behavior shown by well mixed systems to this anomalous kinetics is intimately linked to the evolution of the concentration PDF from a Gaussian to non-Gaussian shape. This fact establishes a direct relationship between anomalous reaction kinetics, incomplete mixing and the non-Gaussian nature of the concentration PDF.

Introducing advective transport processes in our analysis, we studied the impact of incomplete mixing on effective reaction kinetics at the front between two solutes, one displacing the other, in a $2d$ heterogeneous porous medium. While classical Fickian models predict a scaling for the mass production as $t^{\frac{1}{2}}$, we show that the kinetics follow 2 non-Fickian regimes. An early times the invading reactant is organized in fingers and the mass production scales as t^2. For later times the mass production slows down, but it is still faster then the $t^{\frac{1}{2}}$. It does not depends on diffusion and is totally controlled by advective spreading. In this regime, anomalous kinetics is directly related to superdiffusive advective spreading. In order to relate the pore scale flow heterogeneity to advective spreading and subsequently to anomalous kinetics, we analyze the distribution and correlation of Lagrangian velocities. We show the existence of long range temporal correlation of Lagrangian accelerations, which are at the root of the breakdown of classical Fickian dispersion models. Thus, similarly to turbulent media, flow through porous media displays strong intermittent properties. We demonstrate that they can be quantified by a correlated Continuous Time Random Walk approach, which provides a consistent upscaling framework.

We finally perform a laboratory experiment where a quasi $2D$ system is studied through an Hele-Shaw cell in which two reactive chemicals are injected, one displacing the other. A new experimental set up based on chemiluminescence reactions allows high resolution quantification of the pore scale concentration pdf and reaction rate. The anomalous kinetics of the reactive front is observed and is very consistent with our theoretical predictions.

Contents

1 Introduction **1**

1.1 A framework for reactions 1

1.2 Mixing 3

1.3 Mixing-limited reactions 9

1.4 Organization of the thesis 14

2 Diffusion-limited reactions **17**

2.1 The mean field limit 17

2.2 PDF description of the spatial islands segregation of reactants 18

2.3 An analytical solution for the islands segregation 32

3 Spreading due to advective processes **47**

3.1 Anomalous dispersion from pore scale flow heterogeneity 47

3.2 Intermittency-like behavior of Lagrangian velocities in porous media 56

4 Mixing limited reactions in porous media **65**

4.1 Kinetics scaling of a reaction front 65

4.2 Islands dynamics interpretation for the dispersion regime 76

4.3 The $3d$ case 79

5 Experimental set up for $2d$ reactive transport **81**

5.1 Introduction 81

5.2 A pore scale experiment based on chemiluminescence 86

5.3 Results 99

6 Conclusions and perspectives **101**

A Appendix A **107**

B Appendix B **119**

Chapter 1

Introduction

This thesis focuses on the theoretical and experimental study of rate of reactions between chemicals that mix while transported by flows in porous media.

1.1 A framework for reactions

It is a matter of our daily experience that reactions are not instantaneously transformed into products. Transformations can take place only between molecules that are close enough to exchange electrons forming and breaking chemical bonds *Connors* [1990]. In other words, if reactants are placed at large distance no collisions, and thus no reactions, between them are possible (*Neufeld and Hernandez-Garcia* [2010]). In this thesis we consider a reaction as the ensemble of processes that leads to the transformation of one set of reactants to a set of products through changes that strictly involve a short range interaction between reactants. The short nature of interaction of such a systems requires transport mechanisms in order to produce collisions and thus reactions (*Neufeld and Hernandez-Garcia* [2010]; *Horsthemke et al.* [2010]). Systems made by long range interacting particles (e.g. plasmas or gravitational systems) cannot be described in the presented framework and their behavior will not be discussed here. More generally, many phenomena are based on the short range interactions between particles or agents. Thus, it is possible to model not only the molecular interactions, but also a wide spectrum of processes such as the population dynamics of biological species (e.g. *Tel et al.* [2005]; *de Anna et al.* [2010]), ecological activity (e.g. *Lugo and McKane* [2008]), social behavior (e.g *Schweitzer* [2003]) as a reaction. In this framework, reactive phenomena are omnipresent in our daily lives, in nature and many industrial applications.

In the context of hydrology, chemical reactions of particular interest are those between the

constituents of the soil and solutes dissolved in water flowing through it including, for example, dissolution reactions responsible for karst formations and biochemical reactions that control the dynamics of bacteria population in soil (e.g. denitrification, biodegradation).
The reaction kinetics plays a crucial role in the fate of reactive systems (e.g. *Dentz et al.* [2011]). To describe reactions chemical equations are usually adopted (e.g. *Connors* [1990]). These equations represent the reactions that occur between N chemical species with α_i molecules of the chemical species X_i for $i = 1, \dots N$:

$$\alpha_1 X_1 + \alpha_2 X_2 + \dots \alpha_N X_N \rightarrow \text{products} \tag{1.1}$$

where the numbers α_i are the so called stoichiometric coefficients. A general law that predicts the reaction rate as a function of concentrations c_i of involved reactants X_i is the well known mass action law. This law states that the rate of a reaction is proportional to the product of the concentration of the involved chemicals each one elevated to the power of the representative stoichiometric coefficient

$$\text{reaction rate} = k c_1^{\alpha_1} c_2^{\alpha_2} \dots c_N^{\alpha_N} \tag{1.2}$$

where the proportionality constant k is the so called reaction constant. The fundamental hypothesis behind this law is that the involved chemicals X_i are well mixed. This implies that everywhere in the considered system the concentration of chemical X_i must have the same value. Thus, spatial effects are absent, or can be neglected, and the time evolution of the concentrations of all involved chemicals is provided by a system of ordinary differential equations, called rate equations, derived from the previous mass action law (1.3) (e.g. *Horsthemke et al.* [2010]; *Connors* [1990]):

$$\frac{dc_i}{dt} = -\alpha_i k c_1^{\alpha_1} c_2^{\alpha_2} \dots c_N^{\alpha_N} \tag{1.3}$$

These dynamical systems can be solved through deterministic (e.g. *Strogatz* [2000]), or stochastic (e.g. *Gillespie* [1976]) approaches.
If reactions are very fast compared to the mixing processes, the chemicals are depleted and reactions stop. Only a new mixing of reactants can allow reactions to take place again. Thus, mixing processes play an important role and will dominate the kinetics of such a systems (e.g. *Neufeld and Hernandez-Garcia* [2010]; *Horsthemke et al.* [2010]; *Gálfi and Rácz* [1988]; *Havlin et al.* [1995]; *Kapoor et al.* [1997]; *Gramling et al.* [2002]; *De Simoni et al.* [2007]; *Luo et al.* [2008]; *Edery et al.* [2010]; *Chiogna et al.* [2011]; *de Anna et al.* [2011]).

In this thesis we focus on mixing limited reactive transport systems to understand the impact of incompletely mixed systems (*Ottino* [1989]) on effective reaction rate.

1.2 Mixing

Mixing is the ensemble of mechanisms that change the spatial distribution of an heterogeneous system, to make it more homogeneous. As discussed by, for example, *Ottino* [1989] and *Kitanidis* [1994], two or more given substances, originally segregated into different volumes of space, tend to occupy the same volume due to mixing processes. In other words, as

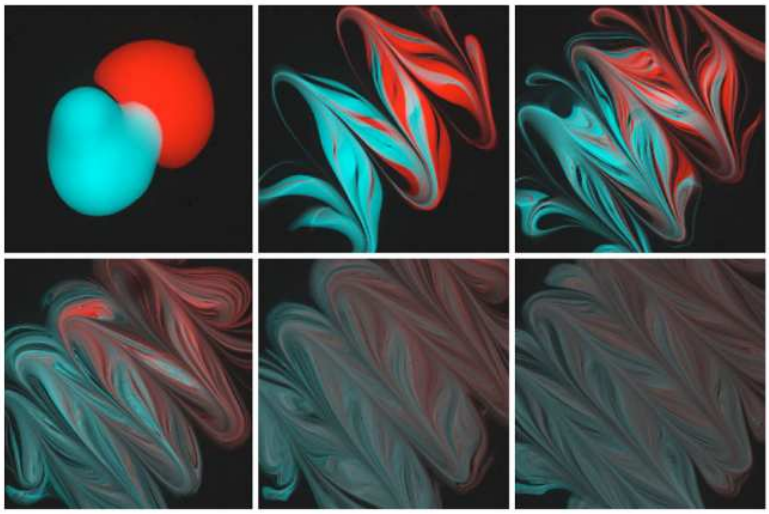

Figure 1.1: *Mixing of two ink spots, initially laid side by side, their mixing process is described in Duplat et al. [2010a], from where the image is taken.*

stated by *Villermaux and Duplat* [2003], a mixture is a transient state between the initial segregation of the constituents and their ultimate homogeneity. This concept is well represented by the image of the experiment performed by *Duplat et al.* [2010a] in Figure 1.1 where the two initially segregated drops of different ink are mixed. As the time goes on, the mixing mechanisms reduce the heterogeneity of the system until the two drops are homogenized and thus indistinguishable. Given the above mixing definition, it is therefore necessary to specify the meaning of homogeneous condition. We define ξ as the smallest length scale over which it is possible to distinguish the given substances. All information at smaller scale than ξ are considered to be already homogenized by mixing. Usually ξ is much smaller then the size L of the considered system (e.g. *Whitaker* [1999]; *Le Borgne et al.* [2011a]), implying that the mixing

shows important features at different, spatial and temporal, scales that are mutually coupled. The governing equations are usually defined at the homogenization scale, also called the microscale (e.g. *Le Borgne et al.* [2011a]), while the observations are typically at a scale much larger then ξ. The dynamics at this larger observations scale L, or macroscale, is the result of the collective action of several local phenomena. To quantify local mixing we can solve at small scale fluid mechanics (e.g. *Bear* [1988]), described by coupled equations that are derived from conservation laws. In general, these equations are not solvable due to our ignorance on the boundary and initial conditions (e.g. *Tel et al.* [2005]; *Dentz et al.* [2011]) or due to mathematical difficulties, as in turbulence for example where the uniqueness of solutions is not guaranteed (e.g. *Pope* [2000]). Alternative solvable descriptions include dynamical system approach (e.g. *Tel et al.* [2005]; *Ottino* [1989]; *Horsthemke et al.* [2010]; *Neufeld and Hernandez-Garcia* [2010]), stochastic approach (e.g. *Dentz et al.* [2011]) or effective models through volume averaging (*Whitaker* [1999]). In any case, a physically consistent description must take into account the first principles formalized by the local equations and provide a link to the macroscale in terms of simple and solvable models.

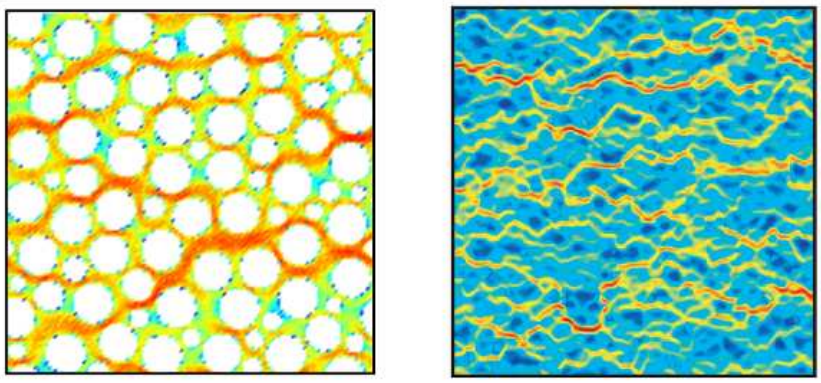

Figure 1.2: *On the left the velocity field resulting from numerical simulations for a given porous medium at the microscale: the flow around the solid grains is a solution of local Navier-Stokes equation. On the right the velocity field of a given porous medium at (Darcy) macroscale: the flow is non-zero everywhere and it is a solution of the Darcy equation.*

With regard to porous media, as explained in more details in the following, at the macroscale the governing equation for flow is the so called Darcy equation (resulting from an upscaling of local Stokes equations), e.g. *Bear* [1988]; *Whitaker* [1999]. We will hence refer to macroscale as the Darcy scale. This Darcy scale is characterized by the fact that the porous structure of

the medium is no longer visible. In Figure 1.3 two velocity fields at the pore scale (on the left) and at Darcy scale (on the right) are compared.

Mixing in porous media

The mechanic processes responsible for mixing in porous media considered in this thesis are advection and diffusion. We define the dimensionless Peclet number $Pe = \frac{\lambda \overline{v}}{D}$ that take into account the effective ratio between advection and diffusion over a given length λ for a given average velocity $\overline{v}$, where D represent the diffusion coefficient. These two processes are coupled in contributing to the degree of mixing. If, on one hand, heterogeneous advection acts to spread the solutes in the local direction of the flow, on the other hand, diffusion tends to homogenize their spatial distribution (e.g. *Ottino* [1989]). This interaction between heterogeneous advection and diffusion is typically lumped in a dispersion coefficient to describe the effective mixing processes of the solute (e.g. *Taylor* [1953]; *Aris* [1956]; *Gramling et al.* [2002]). The pore scale information can be integrated at the Darcy scale into an upscaled picture using, for example, the volume averaging approach (e.g. *Quintard and Whitaker* [1994]; *Whitaker* [1999]) or homogenization approaches (e.g. *Hornung* [1997]). These upscaled models rely on effective transport parameters among the most investigated of which are included macrodispersion coefficients (e.g. *Gelhar and Axness* [1983]; *Janković et al.* [2009]). The range of validity of such macroscopic descriptions has been discussed by *Battiato et al.* [2009].

Anomalous dispersion

The macrodispersion approach (e.g., *Gelhar and Axness* [1983]) models effective transport by the same theoretical framework as local-scale transport: the impact of spatial heterogeneities on larger scales is taken into account by the so called macrodispersion tensor. It measures the influence of pore scale heterogeneities on large scale solute spreading. Although useful in practice, this approach is in general not able to describe qualitatively and quantitatively the so called anomalous or non-Fickian transport behavior, which is frequently observed (*Dentz et al.* [2011]). Such behavior is characterized by non linear growth of the longitudinal (main flow direction) spatial variance of the solute distribution. A schematic view of the longitudinal spreading temporal evolution is given in Figure 1.4. These anomalous behaviors, can be described by various theories usually based on spatially and temporally non-local transport equations. Such transport models are generally non-Markovian: the system state at a

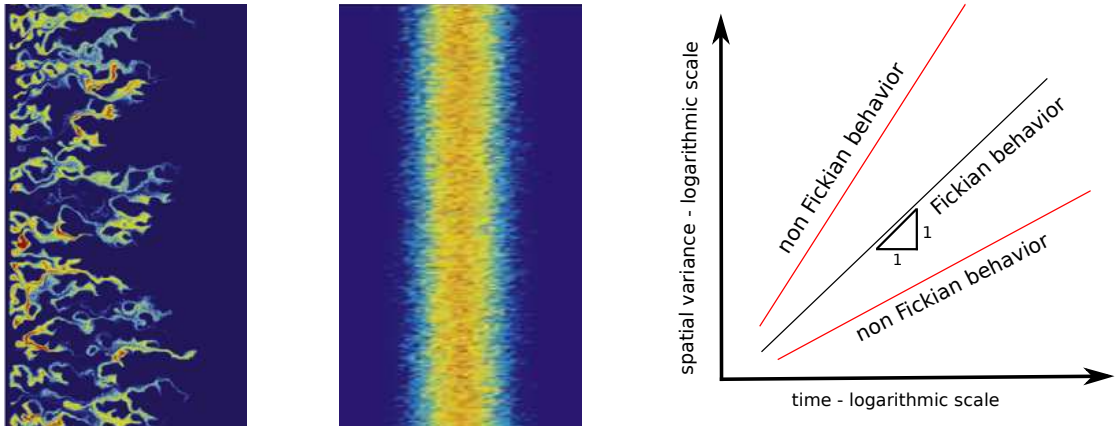

Figure 1.3: *On the left and on the middle the concentration field of an injected plume respectively in an heterogeneous and almost homogeneous porous medium. On the right a schematic view of the scaling of the spatial variance of the distribution of a plume that undergoes Fickian and non Fickian dispersion. The former well represent the behavior of a plume in an homogeneous medium while anomalous scalings are observed for heterogeneous media.*

given time depends on the full system history. Non local models that have been used for the description of effective transport in heterogeneous media include the multirate mass transfer (MRMT) or multicontinuum approach (e.g. *Haggerty and Gorelick* [1995]; *Harvey and Gorelick* [1995]; *Carrera et al.* [1998]; *Haggerty et al.* [2000]), the Continuous Time Random Walk approach (e.g., *Montroll and Weiss* [1965]; *Berkowitz and Scher* [1998]; *Metzler and Klafter* [2000]; *Le Borgne et al.* [2008a]), the moment equation approach (e.g. *Neuman* [1993]; *Neuman and Tartakovsky* [2009]), non equilibrium statistical mechanics using projection formalism approaches (e.g. *Cushman and Ginn* [1993]; *Cushman et al.* [2002]) and the fractional advection dispersion equation approach (e.g., *Meerschaert et al.* [1999]; *Benson et al.* [2000]). The dependence of the upscaling results on the adopted upscaling technique is discussed in *Dagan et al.* [2012].

Difference between spreading and mixing

Spreading and mixing are two concepts that need to be differentiated in porous media, as illustrated in Figure 1.4. Spreading has received a lot of attention, however it does not predict well the degree of mixing of observed solutes. As pointed out by *Kitanidis* [1994], mixing and spreading for transport in homogeneous media can both be characterized in terms of diffusion and dispersion coefficients. In heterogeneous media this is no longer true. Medium

heterogeneities lead to a distortion of the solute plume that, for times smaller than the transport time over a typical heterogeneity scale, increase the solute spreading but not its degree of mixing. Thus, in general these coupled processes of spreading and mixing need to be

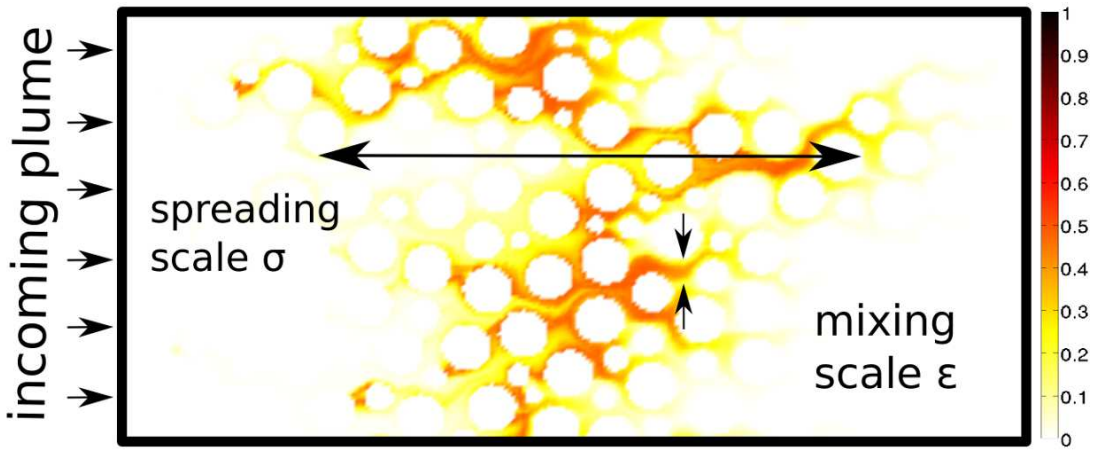

Figure 1.4: *A numerical simulation of a plume of solute A invading a porous medium saturated by another solute B. Here it is represented the difference between the concept of mixing and spreading: intuitively the former measures the length over which the incoming solute A is spread, the latter the size of the length over which A and B coexist (de Anna et al. in preparation).*

separated (e.g. as proposed by *Tartakovsky et al.* [2008a]). To quantify the coupling between those two mechanisms, *Le Borgne et al.* [2011a] introduce and quantify the local mixing scale ϵ, defined as the length for which the scalar distribution is locally uniform. The anomalous evolutions of the dispersion scale σ and the mixing scale ϵ result to be complementary, $\sigma\epsilon \sim t$ relating anomalous global dispersion to the dynamics of local mixing.

Probability density function of solutes concentration

Mixing processes are defined as mechanisms that tends to make heterogeneous physical system more homogeneous. The mixing state can be quantified by the probability density function of solutes concentration $p(C)$, defined as the total (volume averaged) probability of the presence of the concentration value C. Thus, mixing acts to change the shape of $p(C)$ from a wide distribution representing heterogeneity (and thus an heterogeneity of C values) to a sharp distribution about the homogenized C value (e.g. *Villermaux and Duplat* [2003]). From observations in natural formations, it results that the $p(c)$ is typically far from being Gaussian. Thus, the first two concentration moments do not provide sufficient information to well

describe the mixing properties (e.g. *Bellin et al.* [2011]). Currently, the relevant equations to describe $p(C)$ in porous media is still debated (*Dentz et al.* [2011]).

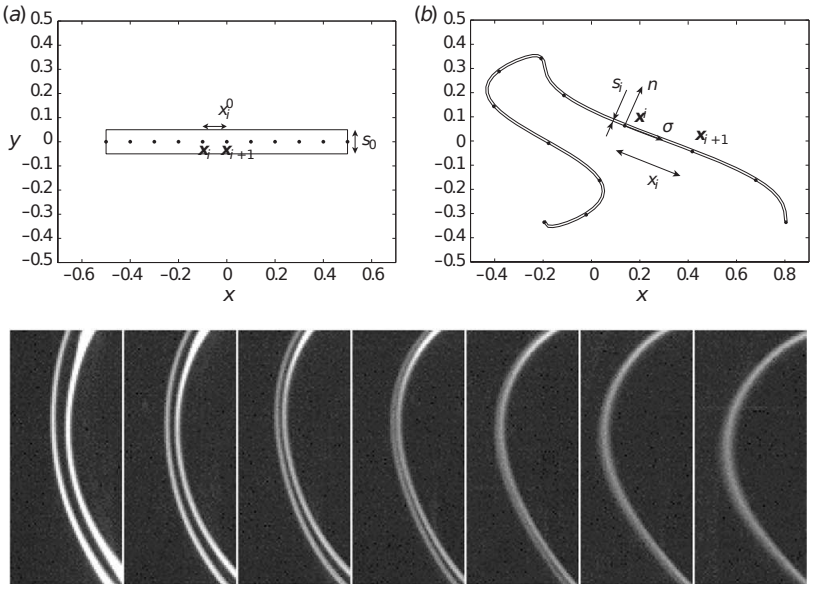

Figure 1.5: *On the top a schematic view of the elongation of a line in a turbulent flow: image taken from Meunier and Villermaux [2010]. On the bottom the lamellas superposition: image taken from Duplat and Villermaux [2008].*

For turbulent flows, full descriptions for $p(C)$ have been derived and observed (e.g. *Villermaux and Duplat* [2003]). When an initial line distribution of solute of size L is injected in a turbulent flow its shape is elongated and its length evolves in time $L(t)$. The $p(C)$ is related to the probability distribution of the elongation $p(L)$ (*Meunier and Villermaux* [2010]), see Figure 1.5. For a blob of solute injected on a turbulent flow, its geometric organization is a convoluted ensemble of interacting strips or lamellas that superpose, see Figure 1.1 or 1.5. In such a case the $p(C)$ is derived by observing the superposition process of lamellas and it is well described by a Γ distribution (*Meunier and Villermaux* [2010]). The validity of such approaches for porous media is subject of current investigations (collaboration between T. Le Borgne and E. Villermaux).

Incomplete mixing

The concentration pdf $p(C)$ provides upscaled global informations about the degree of mixing of solutes. For porous media the evaluation of the full distribution $p(C)$ represents a very important issue because, as already outlined, real systems display local heterogeneities from

which non well mixed conditions for transported solutes arise (*Dentz et al.* [2011]), e.g. see Figure 1.6. This incomplete mixing has been observed through both the use a high resolution numerical method to simulate advective-diffusive transport of a passive tracer at pore scale (e.g. *Tartakovsky and Neuman* [2008]) and laboratory experiments (e.g. *Levy and Berkowitz* [2003]; *Zinn et al.* [2004]). Incomplete mixing is generally not taken into account by Darcy scale models that assume well mixed conditions at scale larger than pores volumes (*Dentz et al.* [2011]).

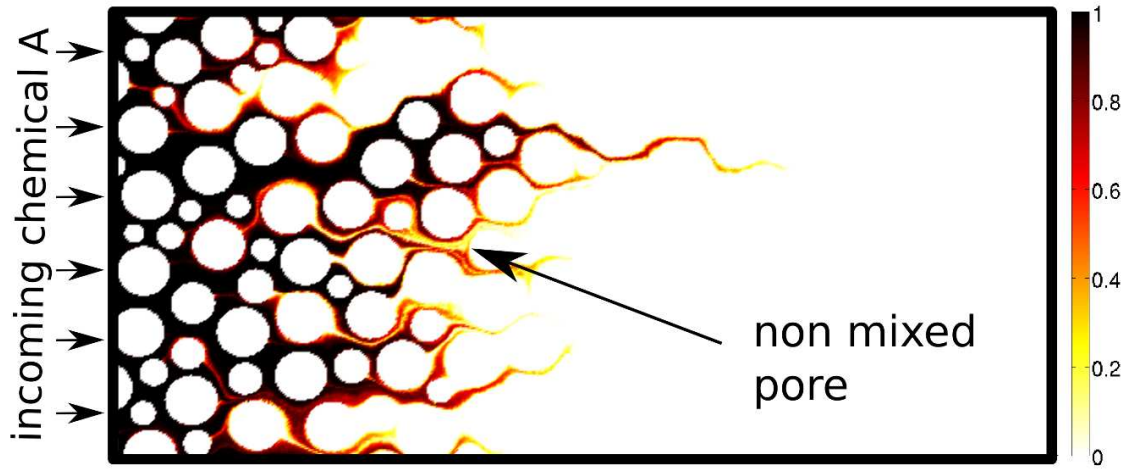

Figure 1.6: *Incomplete mixing at the pore scale between two chemicals A and B. A is injected from the left and is invading the pore space initially saturated by the chemical B (not displayed in figure). The image shows the concentration field (normalized with respect to the injected value) resulting from a numerical pore scale simulation discussed in the following chapters (de Anna et al. in preparation).*

1.3 Mixing-limited reactions

The reactive activity in porous media refers to a large number of aqueous species that react among themselves (e.g. denitrification), with the solid matrix (e.g. solid dissolution) and with gaseous phases (e.g. gas dissolution) through different kinds of reactions (*Pinder and Celia* [2006]), undergoing different kind of kinetics (e.g. *Connors* [1990]). Reactions characterized by slow kinetics compared with mixing kinetics can be well described by rate equations (e.g. *Neufeld and Hernandez-Garcia* [2010]; *Horsthemke et al.* [2010]). Reactive processes involving multiple chemical species represent a very complex and challenging problem that can be analyzed using advanced numerical codes (e.g. *Saaltink* [2004]; *Majdalani and Ackerer* [2011];

Fahs et al. [2010]; *Ackerer* [2010]). For mixing-limited reactions in groundwater, a simplified procedure to solve reactive transport in terms of conservative components was proposed by *De Simoni et al.* [2005]. Here we consider reactions in porous media whose local kinetics are fast enough to be limited by mixing processes.

Anomalous mixing is found to induce reaction kinetics that is different from the ones predicted by Fickian mixing (e.g. *Tel et al.* [2005]; *Gramling et al.* [2002]). As discussed in the previous paragraph, a Fickian description of transport significantly over predicts the degree of mixing between chemicals in porous media (*Dentz et al.* [2011]) and, moreover, the full probability density function of solute concentration is needed, in theory, to model mixing (e.g. *Bellin et al.* [2011]; *Oates* [2007]). Also for reactive systems the probability density function of chemical concentration turns out to be far from a Gaussian shape (e.g. *de Anna et al.* [2011, 2010]; *Di Patti et al.* [2010]): a full distribution of $p(C)$ is thus needed in order to extract information about the underlying dynamics. Effective upscaled models that take into account the local heterogeneity of porous media in reactive transport systems include effective reaction rate coefficients (e.g. *Tartakovsky et al.* [2008b]), Continuous Time Random Walk (e.g. *Edery et al.* [2010]), fractional Advection Diffusion equation (e.g. *Bolster et al.* [2010, 2012]) and effective Langevin models (e.g. *Tartakovsky* [2010]). All these models assume some knowledge about the local properties of the medium, e.g. probability distribution of particle jumps, spatial correlation of velocity field or some other required upscaled physical fitting parameter. Their validity for quantifying mixing is still debated (*Dentz et al.* [2011]). This is one of the key questions addressed in this thesis.

Laboratory experiments

Presently, relatively few experiments aimed to the quantification of mixing and reactions in porous media have been carried out, although they could represent a direct measurement of the impact of incomplete mixing on reaction rates. In order to resolve the whole concentration field, laboratory experiments involving transparent quasi $2d$ chambers are needed (e.g. *Konz et al.* [2009]). To observe and quantitatively measure the reaction product concentration field between two chemicals mixed while transported, a technique used in the past is the colorimetry described in *Zinn et al.* [2004]; *Oates and Harvey* [2006]; *Oates* [2007]. At the interface between two chemicals transported through a thin chamber ($40 \times 20 \times 0.64$) cm packed with glass beads of different sizes, reactions take place. Figure 1.7 shows the concentration

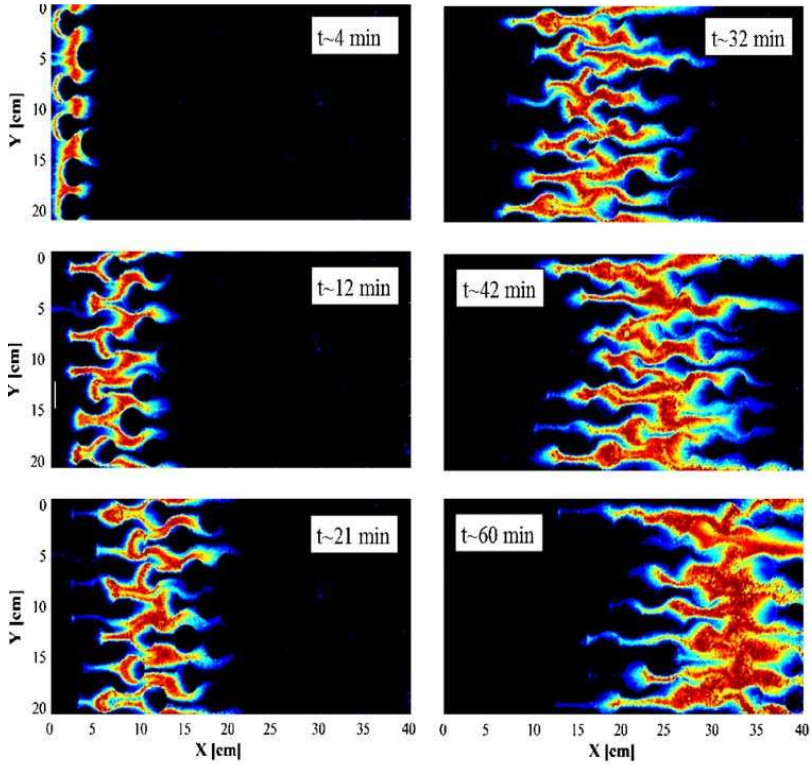

Figure 1.7: *Concentration field of the reaction product from the laboratory experiment performed by Oates and Harvey [2006]*

field of the reaction product obtained with the conversion, through appropriate calibration, of images taken with a CCD camera by *Zinn et al.* [2004] and *Oates and Harvey* [2006]. Due to the ratio between the size of the system and the grain size, the spatial resolution of this experiment does not resolve the pore scale concentration distribution. In figure 1.8 is shown

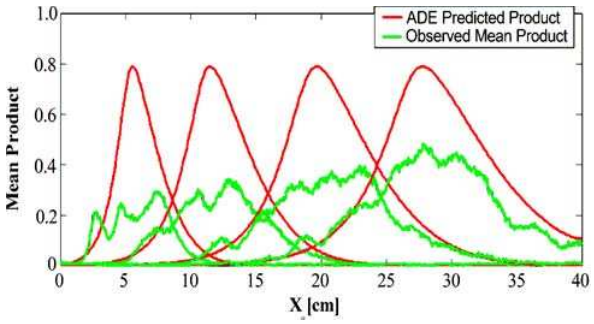

Figure 1.8: *The projection over the main flow direction of the reaction product concentration field of the experiment from Oates and Harvey [2006] (green line) and the solution of the Darcy scale advection-dispersion equation (red line). Different curves represent different times.*

the projection along the main flow direction, for different times, of the measured local concentration field of the reaction product versus the analog quantity derived from a Darcy scale Fickian model. The curves do not superpose due to the incomplete mixing at pore scale. The proposed macroscopic model, which assumes well mixed conditions at the pore scale, fails in predicting the mass production by reactions (see Figure 1.8). A laboratory experiment to quantify pore scale mixing and reactions represents a challenging subject of investigation that we address in this thesis.

Anomalous kinetics scaling

We define mean field behavior as the expected temporal scaling of reaction system in homogeneous media. We will refer to different temporal evolution, with respect to the mean field, as anomalous behaviors. As discussed previously, anomalous kinetics of reaction products arises from anomalous mixing. To understand and consistently describe the impact of incomplete mixing on reaction rates, we focus on the analysis of temporal scaling behavior. The study over several orders of magnitude, with respect to some characteristic time, of the temporal evolution of the mass transformed by reactions, can provide informations about the underlying physical mechanism of reactive transport (*Tel et al.* [2005]; *Neufeld and Hernandez-Garcia* [2010]; *Horsthemke et al.* [2010]).

For the simple case of a mixing limited reaction between two initially well mixed chemicals where transport mechanisms are represented only by diffusion, segregation of reactants take place due to fluctuations in initial spatial distribution of concentrations as discussed by *Ovchinnikov and Zeldovich* [1978]; *Toussaint and Wilczek* [1983]; *Kang and Redner* [1985]; *Monson and Kopelman* [2004]; *Benson and Meerschaert* [2008]. The observed scaling for the reactants decrease for early times and it is well predicted by completely mixed thermodynamics models until reactions deplete most of reactants concentrations. When in the system there are zones where only one reactant is present, locally reactions stop until diffusion mixes reactants again. The observed reactants concentrations decrease slow down from the well mixed prediction t^{-1} to scale as $t^{-\frac{d}{4}}$, where d is the dimensionality of the system (see Figure 1.9). This scaling law can be fully derived from upscaled models only if the basic processes are well understood and consistently formalized. At the same time, the knowledge of such scaling law provides an important way to properly upscale the pore scale physics of the system.

The case of reactive front, i.e. a reactant A that invades a medium initially saturated by another reactant B (e.g. see Figure 1.6) is of primary interest since the heterogeneity determines the

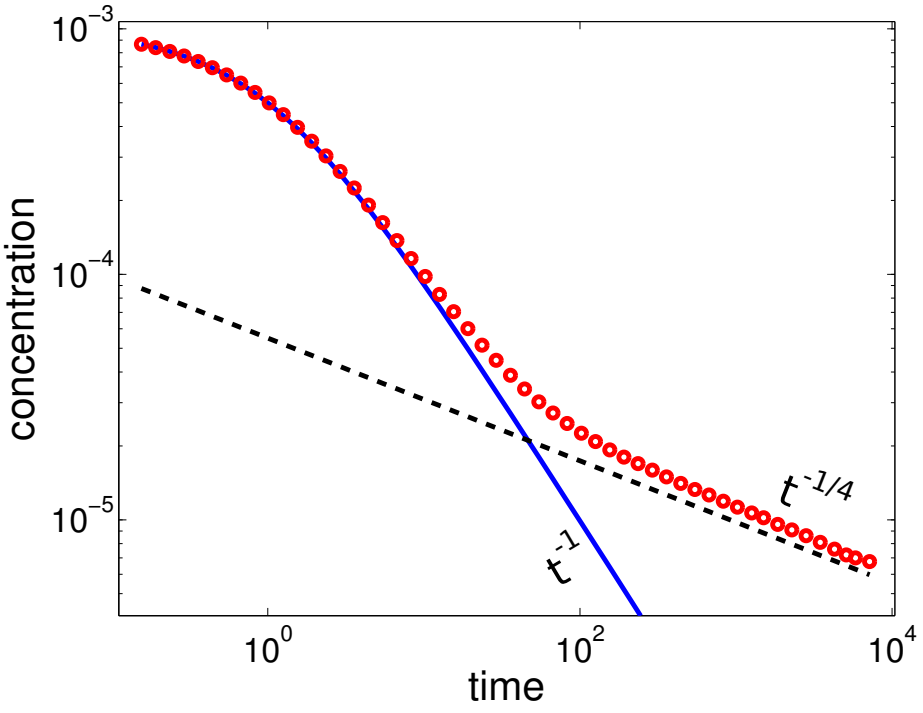

Figure 1.9: *Red dots represent the temporal evolution over several orders of magnitude (scaling law) of a reactant undergoing an irreversible bimolecular reaction in a well mixed one dimensional domain, in presence of initial spatial fluctuations. For the unidimensional case, the anomalous scaling $t^{-\frac{1}{4}}$ deviates from the mean field t^{-1}.*

front geometry. If the transport is due to homogeneous advection, *Gramling et al.* [2002] show that the mass produced by reactions scales in time as $\sqrt{\sigma} \propto \sqrt{t}$, where σ^2 represent the spatial variance of a plume. How the reactants produce mass in the case of heterogeneous advection is an open and challenging question which is addressed in chapters 4 and 5.

Relationship between anomalous dispersion and kinetics

In porous media the degree of mixing of reactants is given by the interplay between the spreading of the solutes due to the transport process associated to the heterogeneous local velocity field and the molecular diffusion. A local description of such a systems is provided by conservation laws, but their associated equations result, in general, impossible to be analytically solved at large scale. The connection between small and larger scales can be provided by scaling laws using upscaling techniques. Classical upscaled models (e.g. macrodisperion) for transport in porous media tend to overestimate the reaction rates since they assume com-

plete mixing at a scale large compared to the pore sizes. As a consequence, scaling laws for temporal behavior of spreading display anomalous behavior compared to the predictions of this upscaled models. The impact of this effect on mixing has primary importance in reactive systems. The derivation of upscaled models for mixing limited reactions in porous media is addressed throughout this thesis.

1.4 Organization of the thesis

To understand and characterize the basic mechanisms behind the complex coupling of mixing and reactions, we focus on the simple case where only two chemicals A and B are involved in a mixing limited reaction. The whole thesis work was carried out with the aim to understand, explain and, thus, predict the scaling laws observed.
To try to give answers to this general problem (i.e. determination of upscaled models for mixing limited reactions in porous media), we proceeded in steps decoupling the individual processes that constitute mixing in order to study their impact on reaction kinetics.

We start studying only diffusion and reactions: we consider the anomalous reaction kinetics related to the segregation of chemicals in the simple $d = 1$ dimensional diffusion limited reaction $A + B \rightarrow C$. We investigate the relationship between the scaling of the produced mass by this reaction and the probability distribution function (pdf) of the species concentrations. In particular, we derive a relationship between the evolution of the concentration pdf from a Gaussian to non-Gaussian shape and the transition from the expected behavior associated to the well mixed case to anomalous reaction kinetics. This analysis leads us to a new view of the problem, thanks to which we have determined a model to predict the evolution of temporal scaling of the system kinetics. This work was made in collaboration with Marco Dentz, research professor at the Department of Geosciences Institute of Environmental Assessment and Water Research of Barcelona (Spain), Diogo Bolster, Assistant Professor at the University of Notre Dame (Indiana, USA), Alexander Tartakovsky, scientist at Pacific Northwest National Laboratory (Washington state, USA) and Dave Benson, Associate Professor of Hydrogeology Department of Geology and Geological Engineering, Colorado School of Mines (Colorado, USA).

As a following step we study the scaling of advective spreading in absence of diffusion and

reactions in heterogeneous porous media. We propose a general framework for upscaling dispersion. A key challenge of the upscaling procedure is to relate the temporal evolution of spreading to the small scale velocity field properties quantified by the Lagrangian velocity distribution and correlation. The resulting effective transport model is a correlated Continuous Time Random Walk allowing us to well represent the dispersion temporal scaling that has a dramatic impact on reaction kinetics, as discussed in the next chapter. This work was made in collaboration with Marco Dentz, research professor at the Department of Geosciences Institute of Environmental Assessment and Water Research of Barcelona (Spain), Diogo Bolster, Assistant Professor at the University of Notre Dame (Indiana, USA) and Alexander Tartakovsky, scientist at Pacific Northwest National Laboratory (Washington state, USA).

Adding diffusion and reactions, we investigate the effective kinetics of the reaction front for the mixing limited bimolecular reaction $A + B \rightarrow C$. We observe that the anomalous behavior of the system kinetics is characterized by two time regimes in which the total product mass evolves faster than the classical prediction obtained with classical Darcy scale description. This anomalous kinetics appears to be consistently related to the incomplete mixing at the pore scale. In particular we derive a direct relationship between the anomalous dispersion and the observed kinetics. This work was made in collaboration with Marco Dentz, research professor at the Department of Geosciences Institute of Environmental Assessment and Water Research of Barcelona (Spain) and Alexander Tartakovsky, scientist at Pacific Northwest National Laboratory (Washington state, USA).

The last step consists in a laboratory experiment where we reproduce the conditions previously numerically simulated. We propose a new technique to measure the local reaction kinetics in a porous medium via a chemiluminescence reaction. This work was made in collaboration with Yves Meheust, assistant Professor at the University of Rennes 1 (France), Herve Tabuteau researcher at the National Council of Research, Rennes (France), Joaquin Jimenez-Martinez, Post-doc position at CNRS - University of Rennes 1 (France), Regis Turuban, Master student at University of Rennes 1 (France), Jean-Jacques kermarrec, engineer at Geosciences Rennes and Pascal Rolland, engineer at Geosciences Rennes.

Chapter 2

Diffusion-limited reactions

To understand and quantify the basic mechanisms behind the coupling of mixing and reactions, we begin with a simple example. We consider the irreversible bimolecular reaction $A + B \rightarrow C$ (*Connors* [1990]). Then mixing processes responsible for the displacement of these chemicals are reduced to the Fickian diffusion. Although simple, this system can lead to anomalous kinetics when considering spatial fluctuations of reactants concentrations. Thus, it provides an interesting framework to understand basic mechanisms underlying anomalous kinetics. Specifically we focus on the deviation of concentration fluctuations pdf from Gaussian distribution.

The work presented in this chapter was made in collaboration with Marco Dentz, research professor at the Department of Geosciences Institute of Environmental Assessment and Water Research of Barcelona (Spain), Diogo Bolster, Assistant Professor at the University of Notre Dame (Indiana, USA), Alexander Tartakovsky, scientist at Pacific Northwest National Laboratory (Washington state, USA) and Dave Benson, Associate Professor of Hydrogeology Department of Geology and Geological Engineering, Colorado School of Mines (Colorado, USA).

2.1 The mean field limit

Classically reactive diffusion systems are described in terms of continuous concentration field (e.g. *Neufeld and Hernandez-Garcia* [2010]) as follows:

$$\frac{\partial \phi_i(x,t))}{\partial t} - D\frac{\partial^2 \phi_i(x,t)}{\partial x^2} = -k\phi_A(x,t)\phi_B(x,t), \tag{2.1}$$

with D the diffusion coefficient and k the reaction constant. The validity of such continuous description relies on the assumption of an infinite number of particles constituting the system.

In this framework the concentration ϕ of a thermodynamic system is called mean field (e.g. *van Kampen* [2007]). If the spatial distribution is perfectly homogeneous the concentration gradients are zero. Thus, for both species in a closed reactor, $\phi_i(x, t = 0) = c_i$, for $i = A, B$ and eq. (2.1) reduces to the rate equation (*Neufeld and Hernandez-Garcia* [2010])

$$\frac{d\phi_i(t)}{dt} = -k\phi_A(t)\phi_B(t). \tag{2.2}$$

The solution for such an equation is $\phi_A(t) = \phi_B(t) = \frac{c_i}{c_i k t+1}$. At long times, the species concentrations decrease as t^{-1}. In the presence of spatial heterogeneities (which can lead to incomplete mixing on a local scale) the real concentration can deviate from the mean field limit (e.g. *Ovchinnikov and Zeldovich* [1978]; *Kang and Redner* [1985]).

2.2 PDF description of the spatial islands segregation of reactants

In natural systems, the number of constituents is finite. Therefore, natural stochastic deviations from the thermodynamic limit arise and the species concentrations are subject to random fluctuations (e.g. *van Kampen* [2007]; *Gardiner* [2004]). In the mean field description reactions never stop, because neither species A nor species B can completely deplete. However, in a finite system size system somewhere A or B can be depleted. Due to the creation such a zones, or islands of non reactive particles, the system is no longer well-mixed, diffusion effects start to play an important role and will dominate the kinetics of the system. This segregation of chemicals is also called Ovchinnikov-Zeldovich (OZ) segregation after its first observation by *Ovchinnikov and Zeldovich* [1978]. In this anomalous regime, the behavior of the species concentrations change to the $t^{-1/4}$ scaling theoretically observed by *Ovchinnikov and Zeldovich* [1978]; *Toussaint and Wilczek* [1983]; *Kang and Redner* [1985] and experimentally measured by *Monson and Kopelman* [2004]. Furthermore, the breakdown of the mean field description has been studied for variety of reaction diffusion systems using Lattice Gas Automata approaches (e.g. *Boon et al.* [1996]).

To study this mixing limited reaction system from a different perspective, we focus on the concentration PDF of the chemical species A and B. The PDF encodes the full statistical information of the species concentrations about the mean field limit. Thus, it quantifies the incomplete mixing non predicted by the mean field description.

We employ a stochastic approach based on population dynamics (e.g. *McKane and Newman* [2005]; *Bernstein* [2005]; *de Anna et al.* [2010]; *Dauxois et al.* [2009]; *Baras and Mansour* [1996]) which can be used for deriving the governing equation for the concentration pdf.

Stochastic Markov processes and the Master Equation

In general, a stochastic process ξ is an object whose future evolution is not predictable without uncertainty, or is predictable in terms of the probability of its future states. In other words ξ is defined by a set, or ensemble, of possible values that it can assume and a probability distribution $p(\xi = x, t)$ on this ensemble (e.g. *Feller* [1966]). The knowledge of the full probability distribution of a stochastic process provides a complete description of its evolution. A class of stochastic processes for which a governing equation for $p(x, t)$ is derivable include Markov processes (e.g. *van Kampen* [2007]; *Gardiner* [2004]).

We define a Markovian process a stochastic process with the property that for any set of successive time steps $t_1 < t_2 < \ldots < t_n < \ldots$, the state of the system (or the $p(x, t)$ that describe it) at step n depends only on the previous step $n - 1$ and not on all its history. This implies that the full process can be described in terms of two functions: the initial distribution p_0 and the transition probability per unit time for the system to jump from the state x' at step $n - 1$ to the state x at the step n. From the definition of Markov process is possible to show that the evolution of the p is subjected to the equation

$$\frac{\partial p(x,t)}{\partial t} = \int \Big[r(x|x')p(x',t) - r(x'|x)p(x,t) \Big] dx' \tag{2.3}$$

where $r(x|x')$ represent the transition probability per unit time that the system jump from the state x' to the state x. This equation is known as the Master Equation of the system and plays a crucial role in the description of many natural systems (e.g. *van Kampen* [2007]; *Gardiner* [2004]). The Master Equation describes the evolution of the probability distribution of a stochastic Markov process. This kind of process have primary importance because for them a governing equation is well defined.

A population dynamics model for reaction-diffusion

We adopt here the population dynamics approach as proposed by *Lugo and McKane* [2008]. The one-dimensional spatial domain is a string discretized into Ω cells of length h, containing reactive particles. Concentrations within each cell is assumed to be well mixed. For the well mixed condition to hold, the characteristic diffusion time over h is required to be less than the characteristic reaction time. This implies, $t_D = \frac{h^2}{2D} \ll t_k = \frac{1}{\phi_0 k}$ with ϕ_0 is a characteristic species concentration. We impose periodic boundary conditions at the domain boundaries. The system is considered to be of finite size, thus in each cell is defined a maximum occupation number N representing the maximum number of particles that can lie in a single cell. N is

assumed to be the same for each cell. The definition of N implies the definition of the empty spaces E, whose number in each cell is given by the difference between N and the total amount of particle that at a given time are present in that cell: $n_E = N - \sum_i n_i$ (i indicate the species of real particles).

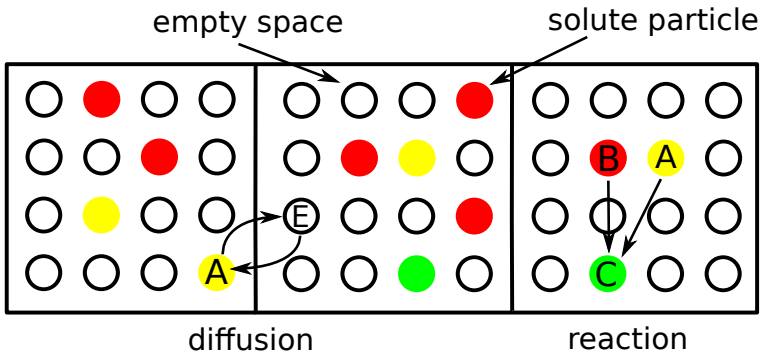

Figure 2.1: *A schematic view of a the numerical model adopted for the one dimensional system. The space is discretized in cells filled with solute particles (colored circles). The cells have a finite volume, thus only a finite number N of particles can lie within each cell. The finite size N define the empty spaces (void circles). Diffusion is represented by the exchange of position between particles and empty spaces, reactions can take place only between particle that lie in the same cell.*

Only particles that are in the same cell can react following the mass action law. Considering this empty spaces, or holes, as virtual particles, diffusion processes are modeled as the exchange of position between a real particle in a cell and a hole in a nearest neighbor cell (see Figure 2.2). This can be thought as a chemical reaction between a particle in one cell and an empty space in a neighboring cell. Thus, diffusion can be modeled with the mass action law: the diffusion rate of the i-th species will be proportional to the product of concentration of ith species and the concentration of holes.

Due to its finite size, the concentrations are to be stochastic variables described in terms of the probability density function for concentrations c (e.g. *de Anna et al.* [2010]). Only a single event can occur per step of the reaction-diffusion process. To each possible event (chemical and physical transitions of any of the particles) a waiting time is associated, which is exponentially distributed (e.g. *Gillespie* [1976, 1977]). The event with the shortest waiting time occurs during a step. The exponential waiting time distribution reflects the fact that the system is locally (within a cell) well mixed and thus a Markov system. Hence, the time series of concentrations in each cell is a Markov process. As discussed at the beginning of the chapter to each Markov process is associated a Master Equation that governs the evolution of the sys-

tem. The transition probabilities per unit time $r(x|x') = r(c|c')$ are defined for each possible transition (a chemical reaction or an exchange of position) by the mass action law. The well known Gillespie algorithm (*Gillespie* [1976]) provides a numerical solution to solve this Master Equation.

To solve the derived Master Equation we use an approximated analytical method: the van-Kampen system size expansion proposed by *van Kampen* [2007]. Such a method represent a Taylor expansion with respect to small fluctuations about the defined mean field. We derive at the first order a set of differential equations for the behavior of the mean field of the system, recovering equations (2.2). Expanding the RDME up to the second order, we derive a Fokker-Plank equation for concentration fluctuations that quantifies the evolution of the joint concentration pdf. We study the evolution of the concentration pdf from a Gaussian to non-Gaussian shape due to the impact of mass transfer limitations on the reaction system. The analytical results are complemented by numerical simulations of the reaction-diffusion system based on the Gillespie algorithm (*Gillespie* [1976]).

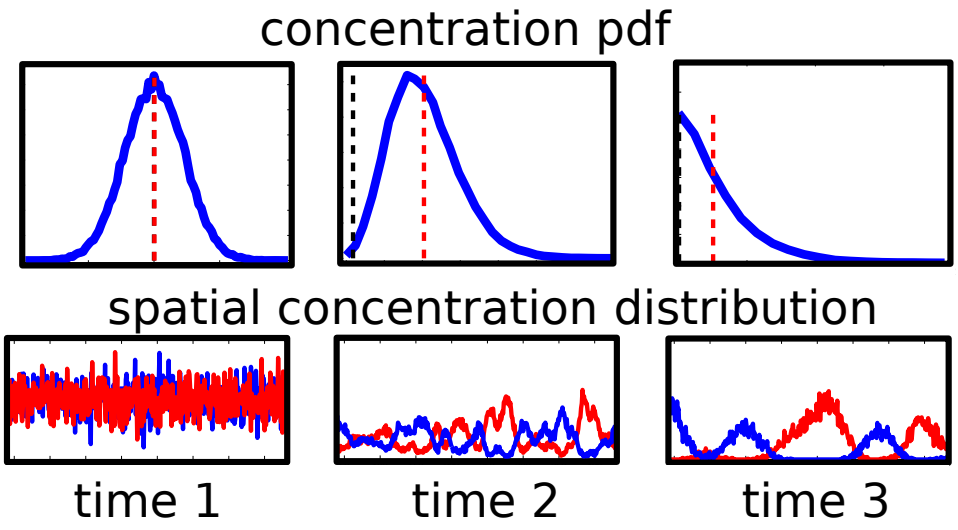

Figure 2.2: *Numerical simulations of the diffusion limited reaction in one dimension for three consecutive times. On the top the concentration pdf $p(C)$: its average (red dashed line) deviate from the mean field limit (black line). On the bottom the spatial distribution of the reactant concentrations (A in red and B in blue). As soon as the islands of segregated reactants arise, the pdf deviate from the Gaussian shape.*

This results have been published in the following manuscript on the *Journal of Chemical Physics* on 2011.

Anomalous kinetics in diffusion limited reactions linked to non-Gaussian concentration probability distribution function

Pietro de Anna,[1,a)] Tanguy Le Borgne,[1] Marco Dentz,[2] Diogo Bolster,[3] and Philippe Davy[1]
[1]*Laboratoire Géosciences Rennes, Unité Mixte de Recherche CNRS Université de Rennes 1, F-35042 Rennes Cedex, France*
[2]*Institute of Environmental Assessment and Water Research, Consejo Superior de Investigaciones Cientìficas, Barcelona, Spain*
[3]*Environmental Fluid Dynamics Laboratory, University of Notre Dame, South Bend, Indiana 46556, USA*

(Received 26 July 2011; accepted 6 October 2011; published online 2 November 2011)

We investigate anomalous reaction kinetics related to segregation in the one-dimensional reaction-diffusion system $A + B \rightarrow C$. It is well known that spatial fluctuations in the species concentrations cause a breakdown of the mean-field behavior at low concentration values. The scaling of the average concentration with time changes from the mean-field t^{-1} to the anomalous $t^{-1/4}$ behavior. Using a stochastic modeling approach, the reaction-diffusion system can be fully characterized by the multipoint probability distribution function (PDF) of the species concentrations. Its evolution is governed by a Fokker-Planck equation with moving boundaries, which are determined by the positivity of the species concentrations. The concentration PDF is in general non-Gaussian. As long as the concentration fluctuations are small compared to the mean, the PDF can be approximated by a Gaussian distribution. This behavior breaks down in the fluctuation dominated regime, for which anomalous reaction kinetics are observed. We show that the transition from mean field to anomalous reaction kinetics is intimately linked to the evolution of the concentration PDF from a Gaussian to non-Gaussian shape. This establishes a direct relationship between anomalous reaction kinetics, incomplete mixing and the non-Gaussian nature of the concentration PDF. © *2011 American Institute of Physics*. [doi:10.1063/1.3655895]

I. INTRODUCTION

Reaction kinetics in heterogeneous reaction-diffusion systems are in general different from the ones observed in well-mixed reactors. Spatial fluctuations in species concentrations in conjunction with diffusion and chemical reactions can have a dramatic impact on the global reaction kinetics.[1–8] Mass transfer limitations can lead to reduced reactivity of the reaction system and slow down the global reaction kinetics.[9] The systematic quantification of the dynamics leading to this behavior is of scientific[1–3,10–12] as well of practical interest for all applications that involve chemical reactions in heterogeneous environments. In natural systems the spatial distribution of reactant concentrations is in general heterogeneous due to fluctuations of the host media that can be represented by porous media,[9,13–15] living cells,[16,17] and turbulent and chaotic flows,[18,19] for example. We focus here on the bimolecular irreversible reaction,

$$A + B \rightarrow C, \tag{1}$$

between species A and B which diffuse in one-dimensional space. The host medium is assumed to be homogeneous and transport is limited to molecular diffusion. The classical approach to describe such a reaction-diffusion system is by the combination of mass transfer for each species concentration $\phi_i(x, t)$ $(i = A, B)$ and a reaction term such that

$$\frac{\partial \phi_i(x,t))}{\partial t} - D\frac{\partial^2 \phi_i(x,t)}{\partial x^2} = -k\phi_A(x,t)\phi_B(x,t), \tag{2}$$

with D is the diffusion coefficient and k is the reaction rate constant. This description is valid in the mean-field limit of an infinite system size, that is, for an infinite number of particles of A and B. For a uniform initial distribution of both species in a closed reactor, $\phi_i(x, t = 0) = c_i$, (2) reduces to the rate equation,

$$\frac{d\phi_i(t)}{dt} = -k\phi_A(t)\phi_B(t). \tag{3}$$

At long times, the species concentrations decrease as t^{-1}. This behavior can be observed if (i) both species are well-mixed and (ii) the number of particles is infinite. In the presence of spatial heterogeneities (which can lead to incomplete mixing on a local scale) and for finite numbers of particles of A and B, this behavior can change. In natural systems, the number of constituents is finite. Therefore, stochastic deviations from the thermodynamic limit arise and the species concentrations are subject to random fluctuations.[20] The thermodynamic limit effectively prevents the formation of zones where only one reactant is present, and where reactions stop, because neither species A nor species B can completely deplete. Due to the creation of such a zones, or islands of non-reactive particles, the system is no longer well-mixed and diffusion effects start to play an important role and will dominate the kinetics of the system. While diffusion attenuates initial concentration contrasts, chemical reaction can

a)Electronic mail: pietro.deanna@univ-rennes1.fr.

amplify them by depleting the species concentrations wherever they are in contact. This leads to segregation, the formation of islands of the respective species. In this regime, the behavior of the species concentrations shows the characteristic $t^{-1/4}$ scaling.[1–3] Kang and Redner[3] used a scaling approach to characterize the anomalous evolution of the species concentrations caused by mass transfer limitations in conjunction with reaction. An analogous scaling has been shown to occur in super-diffusive Levy-flight reaction system.[12,21,22] In this case, the mean concentration scales asymptotically as $t^{-1/2\gamma}$, where $1 < \gamma < 2$ characterizes the Levy-enhanced diffusion operator. Furthermore, the breakdown of the mean-field description has been studied for variety of reaction diffusion systems using lattice gas automata approaches.[11]

In this paper, we study this fluctuation phenomenon from a different perspective. We focus on the description of the reaction diffusion system in terms of the joint concentration PDF of the chemical species and study its evolution as the reaction behavior changes from the mean field to the anomalous scaling. The concentration PDF encodes the full statistical information of the fluctuations of the species concentrations about the mean-field limit. Thus, it quantifies the uncertainty of the concentration values predicted by the mean field. At the same time, it allows for the systematic quantification of the impact of concentration fluctuations on the average behavior.

We employ a stochastic approach based on population dynamics,[23,24,27–29] which can be used for deriving the master equation for the concentration pdf. This framework has been used for the analysis of complex systems that show spontaneous deviations from the average behavior such as proteins and molecules in living cells[27,28,30] and predator-prey systems.[23,31,32] The system state is fully characterized by the joint PDF of the species concentrations at any point in space and time. Its evolution is governed by a reaction-diffusion master equation (RDME).[29,30,33–35] Using the van Kampen system size expansion, we derive at the first order a set of differential equations for the behavior of the system in the mean-field limit. Expanding the RDME up to the second order, we derive a Fokker-Plank equation for concentration fluctuations that quantifies the evolution of the joint concentration PDF through advective and diffusive probability fluxes in the multi-dimensional space of the concentration fluctuations. When the concentration fluctuations are small compared to the average, the PDF can be approximated by a multi-variate Gaussian distribution. This approximation, however, breaks down in the regime in which fluctuations dominate, that is, when the reaction kinetics show anomalous scaling. We study the evolution of the concentration PDF from a Gaussian to non-Gaussian shape due to the impact of mass transfer limitations on the reaction system. The analytical results are complemented by numerical simulations of the reaction-diffusion system based on the Gillespie algorithm.[34–37]

II. REACTION-DIFFUSION MASTER EQUATION AND CONCENTRATION PDF

We adopt here the population dynamics approach as proposed by Lugo and McKane.[32] The one-dimensional spatial domain is discretized into Ω cells of length h, each of which is assumed to be well-mixed.[24] For the well mixed condition to hold, the characteristic diffusion time over h is required to be less than the characteristic reaction time,[24] this means, $\tau_D = h^2/(2D) \leq \tau_k = 1/(\phi_0 k)$ with ϕ_0 is a characteristic species concentration. Notice that more precise criteria can be defined depending on the chemical reaction under consideration.[25,26]

We impose periodic boundary conditions at the domain boundaries. In the adopted model, only particles that are in the same cell can react, and diffusion is modeled as a reaction between a particle in one cell and an empty space in a neighboring cell. Considering empty spaces, or holes, as virtual particles, diffusion processes are modeled as the exchange between a real particle in a cell and a hole in a nearest neighbor cell.[32]

The maximum occupation number of a cell N is equal to the sum of particles and holes. The number of particles of species s in cell j is denoted by $n_s(j)$, the number of holes, or empty spaces by $n_E(j)$. The local concentration of species s is defined as $\rho_s(j) = n_s(j)/N$. It denotes the probability to find a particle of species s in cell j. The system size is given by ΩN, that is, the maximum number of chemical species that can be in the system. Only a single event can occur per step of the reaction-diffusion process. To each possible event (chemical and physical transitions of any of the particles) a waiting time is associated, which is exponentially distributed.[36,37] The event with the shortest waiting time occurs during a step. The exponential waiting time distribution reflects the fact that the system is locally (within a cell) well mixed and thus a Markov system.

The evolution of the reaction-diffusion system is stochastic. The system state at a given time t is characterized by the random vector,

$$\boldsymbol{\rho}(t) = [\rho_A(1,t), \rho_B(1,t), \rho_C(1,t), \ldots, \rho_A(\Omega,t), \rho_B(\Omega,t), \times \rho_C(\Omega,t)]^T, \quad (4)$$

of species concentrations in each cell. The superscript T denotes the transpose. The process $\boldsymbol{\rho}(t)$ is by definition a Markov process. Its realizations are characterized by series of reaction and diffusion waiting times and initial distributions of species concentrations. The joint concentration PDF is obtained by sampling concentration values in each cell from this process,

$$P(\boldsymbol{\rho}, t) = \lim_{R\to\infty} \frac{1}{R} \sum_{r=1}^{R} N\delta_{N\boldsymbol{\rho}, N\boldsymbol{\rho}^{(r)}(t)} \equiv \overline{\delta_N[\boldsymbol{\rho} - \boldsymbol{\rho}(t)]}, \quad (5)$$

in which R is the number of realizations, $\boldsymbol{\rho}^{(r)}(t)$ denotes the concentration vector in realization r. The Kronecker delta $\delta_{N\boldsymbol{\rho}, N\boldsymbol{\rho}(t)}$ is 1 if $\boldsymbol{\rho} = \boldsymbol{\rho}(t)$ and 0 otherwise. The distribution $\delta_N[\boldsymbol{\rho} - \boldsymbol{\rho}(t)] = N\delta_{N\boldsymbol{\rho}, N\boldsymbol{\rho}(t)}$ converges to the Dirac delta in the thermodynamic limit of $N \to \infty$. The overbar denotes the ensemble average. Note that we use the same letter for the stochastic process $\boldsymbol{\rho}(t)$ and the associated sampling vector $\boldsymbol{\rho} = [\rho_A(1), \ldots, \rho(\Omega)]^T$. The probability distribution function $P(\boldsymbol{\rho}, t)$ denotes the joint probability of the particle numbers of all species in all cells and thus encodes the full statistical information about the reaction-diffusion system. The

probability that the concentrations of all reacting species in all cells is in $[\boldsymbol{\rho}, \boldsymbol{\rho} + d\boldsymbol{\rho}]$ is given by $P(\boldsymbol{\rho}, t)d\boldsymbol{\rho}$.

The evolution of the joint concentration PDF $P(\boldsymbol{\rho}, t)$ can be described by the reaction-diffusion master equation,[34,35]

$$\frac{\partial P(\boldsymbol{\rho}, t)}{\partial t} = \sum_j [\epsilon_A^+(j)\epsilon_B^+(j)\epsilon_C^-(j) - 1]T_{AB}(j)P(\boldsymbol{\rho}, t) + \sum_{s[jj']} [\epsilon_s^+(j)\epsilon_s^-(j') - 1]T_s(j|j')P(\boldsymbol{\rho}, t). \quad (6)$$

The step operators are defined through their action on $P(\boldsymbol{\rho}, t)$ as

$$\epsilon_s^{\pm}(j)P[\rho_A(1), \ldots, \rho_s(j), \ldots, \rho_C(\Omega), t] = P[\rho_A(1), \ldots, \rho_s(j) \pm N^{-1}, \ldots, \rho_C(\omega), t]. \quad (7)$$

The notation $\sum_j$ indicates summation over all cells j and $\sum_{s[jj']}$ denotes summation over all species s and over all nearest neighbor pairs j and j'.

Following Refs. 27 and 32, we determine the transition probabilities per unit time from the mass action law, according to which the probability per time of a transition is proportional to the product of the concentrations of the two species that are involved in the chemical reaction or in the position exchange. The probability per time for a transition due to a reaction event in cell j, $T_{AB}(j)$, is given by

$$T_{AB}(j) = Nk\rho_A(j)\rho_B(j). \quad (8)$$

The rate constant k is assumed to be the same in all cells. The transition probability $T_s(j|j')$ for diffusion of a reactant particle of species s from cell j to the nearest neighbor cell j' is given by

$$T_s(j|j') = \frac{ND_s}{2h^2}\rho_s(j)\left[1 - \sum_m \rho_m(j')\right]. \quad (9)$$

The proportionality constant D_s ($s = A, B, C$) is assumed to be the same in all cells, but can vary between species. The system dynamics are fully defined by these transition probability rates. Note that the definition of the transition probability rates used here differs from the one employed in Lugo and McKane[32] by a factor of $N\Omega$. Using the definition of the transition rates given there,[27,32] requires rescaling of the rates *a posteriori*. For clarity, we did it *a priori*.

In the following, we will focus on the mean species concentrations defined by

$$\overline{\boldsymbol{\rho}}(t) = \lim_{R\to\infty} \frac{1}{R}\sum_{r=1}^{R} \boldsymbol{\rho}^{(r)}(t) = \int d\boldsymbol{\rho}\, \boldsymbol{\rho} P(\boldsymbol{\rho}, t). \quad (10)$$

Furthermore, we will illustrate the evolution of the concentration PDF by studying the PDF of concentration values of species s averaged over the whole domain, that is,

$$P_s(\rho, t) = \frac{1}{\Omega}\sum_{j=1}^{\Omega} \overline{\delta_N[\rho - \rho_s(j, t)]}. \quad (11)$$

The RDME (6) is solved numerically using the Gillespie algorithm,[36,37] which is modified to account for transitions between cells[27,32] as outlined above. The numerical simulations are performed in $R = 10^4$ realizations of the stochastic process. The maximum occupation number per cell is set to $N = 10^6$. The cell length is $h = 1$. The number of cells and thus the length of the spatial domain is $\Omega = 10^3$. In each realization, the initial concentrations $\rho_A(j, t_0)$ and $\rho_B(j, t_0)$ are chosen from independent Gaussian distributions with mean values $\overline{\rho}_A(j, t_0) = \overline{\rho}_B(j, t_0) = \rho_0 = 10^{-3}$ and variances $\sigma^2_{\rho_s} = \overline{\rho}_s(j, t_0)/N = 10^{-9}$ for $s = A, B$. The concentration of species C is initially set to zero. The total number of particles at time t_0 is 10^5. Note that the Gaussian initial distribution of concentration values could, in principle, have unphysical negative values. For the setup used here, we did not record any negative concentrations. The diffusion rate constant is $D_s = 0.5$ for all species $s = A, B, C$ and the reaction rate constant is $k = D/\rho_0 = 5 \times 10^2$. As outlined above, the assumption that the cell is well-mixed requires that the characteristic diffusion time $\tau_D = h^2/(2D)$ is of the order of or smaller than the characteristic reaction time $\tau_k = 1/(k\rho_0)$. Figure 1 illustrates the behavior of the spatial average of the mean concentration of species A, $\|\overline{\rho(t)}_A\|$ defined as

$$\|\overline{\rho(t)}_A\| = \frac{1}{\Omega}\sum_{j=1}^{\Omega}\left[\frac{1}{R}\sum_{r=1}^{R}\rho_A^{(r)}(j, t)\right]. \quad (12)$$

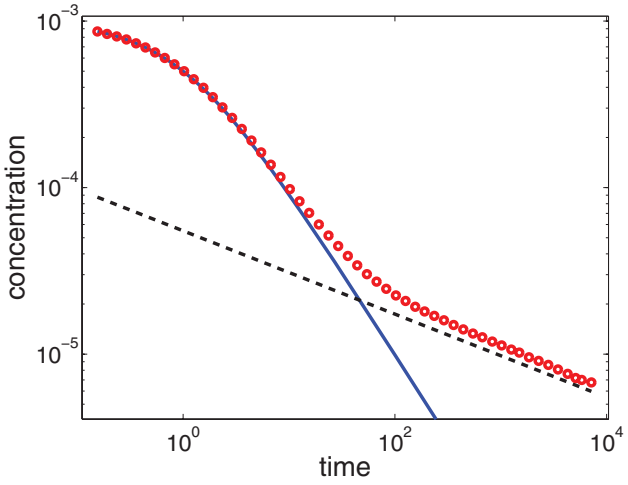

FIG. 1. Temporal behavior of the mean concentration of the A species. For early times the system follows the thermodynamic law, but for large times it deviates from t^{-1} to scale as $t^{-1/4}$. The blue solid line represents the slope t^{-1} and the black line $t^{-1/4}$. The red circles corresponds to results measured in simulations with the adopted model.

At early times, the mean-field behavior t^{-1} is observed, as expected for the solution of a diffusive-reactive system under well-mixed conditions.[3] For larger times, when $\|\overline{\rho(t)}_A\|$ is of the order of the fluctuations, the spatial average of the mean concentration scales as $t^{-1/4}$, as observed by.[1–3] The crossover time can be obtained by equating the mean field behavior $1/(k\rho_0 t)$ and the anomalous $\sqrt{\rho_0}(Dt)^{-1/4}$ behavior derived by Ref. 3. Using $k = D/\rho_0$ as indicated above, one obtains for the crossover time t_c the scaling $t_c \propto \rho_0^{-2/3}$. When one of the two reactants is locally consumed, the reaction stops until diffusion mixes the reactants again and allow for further reactions to take place. Figure 2 shows the evolution of the concentration PDF with time. For small times, the concentration PDF

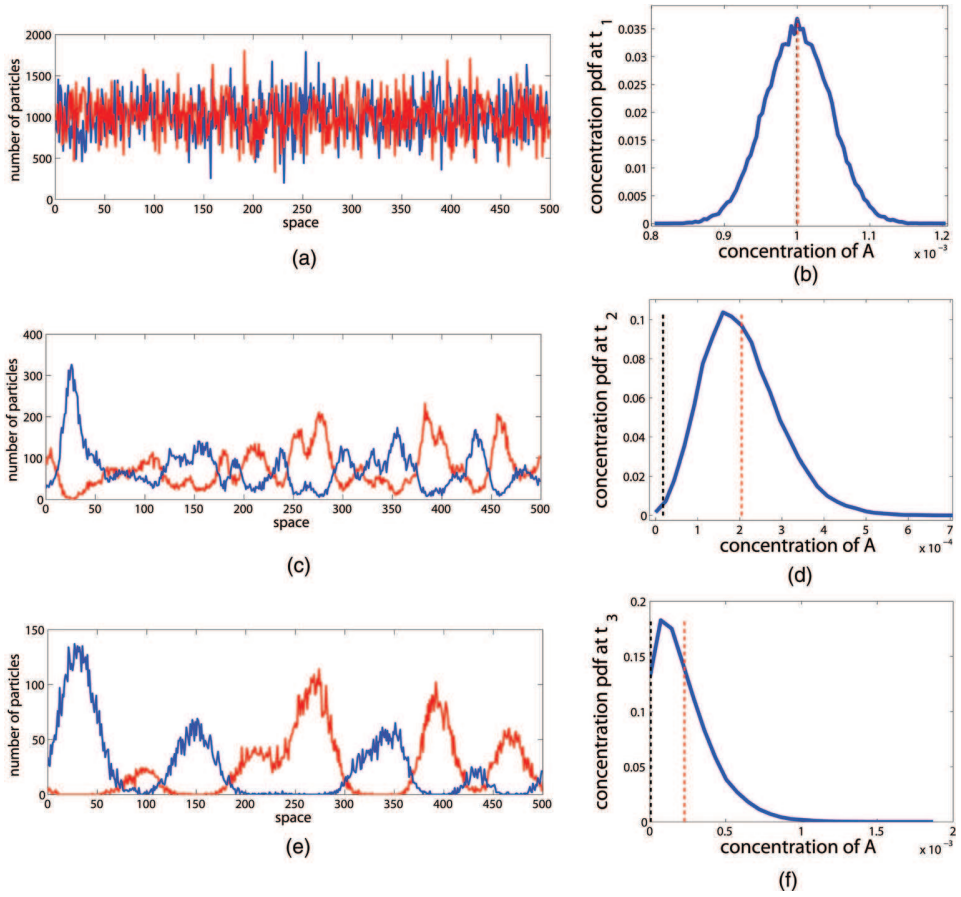

FIG. 2. Spatial distribution of particles in a single realization, (a), (c), and (e), and the ensemble probability density function $P_A(\rho, t)$ of concentration of species A averaged over the domain, see Eq. (11), (b), (d) and (f) at three times: $t_1 = 0$, $t_2 = 55.7$, and $t_3 = 178.7$ in arbitrary time units. On the right, the dashed vertical black line represents the mean field $\phi_A(t)$, and the red dashed vertical line represents the mean $\|\overline{\rho(t)}_A\|$ of the distribution $P_A(\rho, t)$. For $P_A(\rho, t)$ symmetric, the two values coincide. When $P_A(\rho, t)$ starts to become skewed the ensemble average of the concentration becomes larger than the mean-field value. The blue and red solid lines in (a), (c), and (e) correspond to the number of A and B particles, respectively. The top, middle, and bottom rows correspond to the times t_1, t_2, and t_3, respectively. The late times t_2 and t_3 correspond to the situation where islands are formed.

maintains the Gaussian shape of the initial distribution. As the mean concentration decreases and changes its scaling to the anomalous $t^{-1/4}$ behavior, the PDF becomes asymmetric. This change towards an asymmetric shape is due to the emerging segregation regime described in the literature.[1–3] On physical grounds concentration must be positive. Thus, as the mean concentration decreases, negative deviations are more limited than positive fluctuations.

To quantify the evolution of this PDF, and subsequently the first moment of the fluctuation distribution as well as the mean concentration, we apply the van Kampen system size expansion[20,38] to the RDME (6).

III. VAN KAMPEN EXPANSION AND FOKKER-PLANK EQUATION WITH MOVING BOUNDARIES

The RDME (6) encodes both deterministic dynamics and fluctuations due to the intrinsic stochasticity of the system. In order to systematically analyze these two phenomena we proceed as proposed by van Kampen.[20,38] We decompose the system state $\rho_s(j, t)$ into its mean field $\phi_s(j, t)$ and stochastic fluctuations $\xi_s(j, t)$,

$$\rho_s(j, t) = \phi_s(j, t) + \frac{\xi_s(j, t)}{\sqrt{N}}. \tag{13}$$

The deterministic mean-field concentration $\phi_s(j, t)$ is obtained in the thermodynamic limit of infinite system size, $\phi_s(j, t) = \lim_{N\to\infty} \rho_s(j, t)$. The ensemble average over the fluctuations $\xi_s(j, t)/\sqrt{N}$ goes to zero in the limit of infinite system size N. In the following we focus on the PDF of the fluctuations $\boldsymbol{\xi}(t)$, which is defined by $\Pi(\boldsymbol{\xi}, t) = \overline{\delta_{\boldsymbol{\xi},\boldsymbol{\xi}(t)}}$. In terms of the concentration PDF $P(\boldsymbol{\rho}, t)$, it is obtained by variable transform as

$$\Pi(\boldsymbol{\xi}, t) = N^{-1/2} P[\phi_s(j, t) + N^{-1/2}\xi_s(j, t)]. \tag{14}$$

The evolution equation for $\Pi(\boldsymbol{\xi}, t)$ is obtained from a van Kampen expansion of the RDME (6). In Appendix A we obtain, at first order, the classical reaction-diffusion equations (A8) for the mean field and the following Fokker-

Planck equation for the fluctuations, at second order

$$\frac{\partial \Pi(\boldsymbol{\xi},t)}{\partial t} = -\nabla_{\boldsymbol{\xi}} \cdot [\boldsymbol{\mathcal{A}}(t) \cdot \boldsymbol{\xi}\, \Pi(\boldsymbol{\xi},\tau)] + \nabla_{\boldsymbol{\xi}} \cdot [\boldsymbol{\mathcal{B}}(t) \cdot \nabla_{\boldsymbol{\xi}}\, \Pi(\boldsymbol{\xi},\tau)]. \quad (15)$$

Matrices $\boldsymbol{\mathcal{A}}(t)$ and $\boldsymbol{\mathcal{B}}(t)$ are defined in Appendix A.

For changing system size N, numerical simulations show that the deviation from the t^{-1} law is an effect of order of $N^{-1/2}$. This implies that higher order terms in the van Kampen expansion are not needed to describe this phenomenon. Notice that this is different for well-mixed chemical systems in which higher order terms of the van Kampen expansion are generally needed.[8,39] Thus, for incompletely mixed systems for which diffusion is the limiting factor, anomalous kinetics effects may arise already as a second-order effect.

The solution of Eq. (15) with natural boundary conditions is a multi-variate Gaussian distribution. However, the concentration $\rho_s(j) = \phi_s(j) + \xi_s(j)/\sqrt{N}$ is positive; thus the support of $\boldsymbol{\xi}$ is bounded. This implies that the fluctuations $\xi_s(j)$ are within the subdomains

$$\Xi_{sj} = \{\xi_s(j) | -\sqrt{N}\phi_s(j) \le \xi_s(j) \le \sqrt{N}[1-\phi_s(j)]\}, \quad (16)$$

in which $\Xi = \prod_{sj} \Xi_{sj}$ is the full domain of the fluctuations, see Appendix C. Here, we focus on dilute systems characterized by small particle numbers, for which the anomalous scaling of reaction kinetics arises. Therefore, the upper bound of Eq. (15) is never reached and the lower bound is shown here to be responsible for anomalous kinetics. The domain of fluctuations $\boldsymbol{\xi}$ is a hypercube and each component $\xi_s(j)$ is confined within a segment whose size varies over time. Thus, the fluctuation PDF $\Pi(\boldsymbol{\xi},t)$ evolves according to the Fokker-Plank equation (15) with moving boundaries.[39] Fluctuations about the mean field can be characterized by the moments,

$$\overline{\boldsymbol{\Pi}_{i=1}^{n} \xi_{s_i}(j_i)} = \int_{\Xi} d\boldsymbol{\xi}\, \boldsymbol{\Pi}_{i=1}^{n} \xi_{s_i}(j_i) \Pi(\boldsymbol{\xi},t). \quad (17)$$

An evolution equation for the first moment is obtained using Eqs. (15) and (17). In Appendix B, we derive

$$\frac{d\overline{\xi}_s(j)}{dt} = \overline{(\mathcal{A}\cdot\boldsymbol{\xi})}_s + S_s(j,t). \quad (18)$$

We identify the volume term $\overline{(\mathcal{A}\cdot\boldsymbol{\xi})}_s$ and the surface term $S_s(j,t)$, which is defined by

$$S_s(j,t) = \int_{\partial\Xi} d\mathbf{n}_s(j) \cdot [\boldsymbol{\mathcal{A}}(t)\cdot\boldsymbol{\xi}\, \Pi(\boldsymbol{\xi},\tau)] + \nabla_{\boldsymbol{\xi}} \cdot [\boldsymbol{\mathcal{B}}(t)\cdot\nabla_{\boldsymbol{\xi}}\, \Pi(\boldsymbol{\xi},\tau)]\xi_s(j), \quad (19)$$

where $\partial\Xi$ denotes the surface of the domain Ξ and $d\mathbf{n}_s(j)$ is the vector normal to the boundary surface. Physically, $\partial\Xi$ represents all possible states of the system given that at least one island is created, i.e., somewhere in the system at least one of the two species is absent and the chemical reaction stops locally. Note that for natural boundary conditions the surface terms are zero. As shown in Sec. II, at early times, when boundary effects play no role (i.e., no islands have formed), $\Pi(\boldsymbol{\xi},t)$ can be approximated by a Gaussian with zero mean. With increasing time, the fluctuation PDF is growing more and more skewed because the left boundary is approaching zero, see Eq. (16). Also note that the mean fluctuation is nonzero, see Figure 2, and the system behavior deviates from the mean field.

We now consider the mean concentration $\|\overline{\rho}_s\| = \frac{1}{\Omega}\sum_j \overline{\rho}_s(j,t)$, averaged over the spatial domain,

$$\|\overline{\rho}_s(t)\| = \|\phi_s(t)\| + \frac{\overline{\|\xi_s(t)\|}}{\sqrt{N}}. \quad (20)$$

At late times, $\|\phi_s(t)\|$ decreases as t^{-1}. Therefore, the scaling behavior $\|\overline{\rho}_s(t)\| \propto t^{-1/4}$ is governed by the mean fluctuation $\|\overline{\xi}_s(t)\|$. The scaling behavior of the latter can be obtained from the spatial average of Eq. (18). As outlined in Appendix A, to leading order, the space average of the volume term is zero. Thus, we obtain

$$\frac{d\|\overline{\xi}_s\|}{dt} = \|S_s(t)\|. \quad (21)$$

The surface term $\|S_s(t)\|$ controls the behavior of the mean fluctuation. Note that the surface of the fluctuation domain, $\partial\Xi$, corresponds to all possible fluctuation values when at least one island is formed, that is, when at least one species disappears locally. Mathematically this means that at least one of the lower subdomain boundaries, see Eq. (16), is reached, that is, $\xi_s(j) = -\sqrt{N}\phi_s(j)$.

In order to identify the scaling behavior of $\|\xi_s(t)\|$, we need to determine the surface term $\|S_s(t)\|$. The leading order contribution to $\|S_s(t)\|$ is given by

$$\|S_s(t)\| = \frac{1}{\Omega}\sum_j \sum_{s'j'} \int_{\partial\Xi_{sj'}} \xi_s(j) D_{s'} h^2 \xi_{s'}(j') \Pi(\boldsymbol{\xi},t) d(\partial\Xi_{sj'}), \quad (22)$$

see Appendix A. Note that Eq. (22) represents a closure problem because the right side depends on the local values of $\xi_s(j)$. Here, we close the equation by evaluating the surface term numerically. We find that $\|S_s(t)\|$ scales as $t^{-5/4}$, see Figure 3. Direct integration of Eq. (21) shows that the mean fluctuation $\|\xi_s(t)\|$ scales as $t^{-1/4}$, which explains the scaling of the average concentration as $t^{-1/4}$, see Eq. (20).

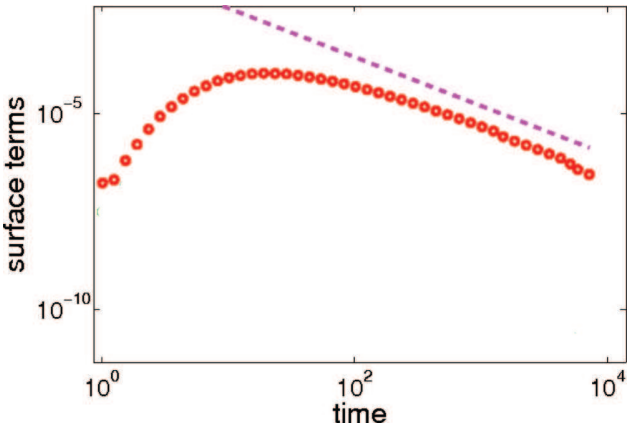

FIG. 3. The temporal behavior of the leading surface integral in Eq. (22) that describes the fluctuations. As expected it scales as $t^{-5/4}$. The red dots correspond to the numerical evaluation of this term with the adopted model. The magenta dashed line depicts a power law of $t^{-5/4}$.

IV. SUMMARY AND CONCLUSIONS

We study anomalous reaction kinetics that arise from the segregation of reactants in diffusion reaction systems. In the diffusion limited regime, islands containing a single reactant are created by self organization of the system. We adopt a stochastic approach based on the population dynamics and a numerical method based on a suitably modified Gillespie algorithm to study these dynamics. It is found that the breakdown of the mean field behavior and the transition to anomalous reaction scaling is related to the transition of the concentration PDF from a Gaussian to non-Gaussian shape.

At large time, the behavior of the reaction-diffusion system is dominated by the concentration fluctuations, whose impact on the reaction behavior can be quantified by its first moment, which, for finite system size, is different from zero. We apply the van Kampen system size expansion to the RDME. The first order of the expansion provides equations for the mean field. The second order provides a Fokker-Plank equation with moving boundaries for the PDF of the concentration fluctuations. The fluctuation domain is bounded because the concentration has non-negative values by definition. The lower limit is given in terms of the mean-field concentration, which decreases to zero as t^{-1}. At large mean concentrations, the lower boundary is negligible and the fluctuation PDF is close to a Gaussian with zero mean. As the mean-field concentration goes to zero, the fluctuation PDF deviates significantly from the Gaussian shape. In this regime, the mean concentration is dominated by the mean fluctuation, which is completely determined by the surface terms, Eq. (22), at the lower concentration boundary. These terms reflect the formation of islands. This result establishes a link between anomalous reaction kinetics and non-Gaussian concentration PDF.

ACKNOWLEDGMENTS

Pietro de Anna wishes to acknowledge Etienne Bresciani, Christoff Andermann and Romain Le Goc for useful discussions. It is gratefully acknowledged the financial support of the European Commission through FP7 projects: ITN, IMVUL (Grant Agreement No. 212298) and Marie Curie ERG grant ReactiveFlows (Grant Agreement No. 230947). Diogo Bolster would like to express thanks for financial support via NSF Grant No. EAR-1113704. Any opinions, findings, conclusions, or recommendations do not necessarily reflect the views of the funding agencies.

APPENDIX A: THE VAN KAMPEN EXPANSION

Using relation (14) in Eq. (6), we obtain the following governing equation for $\Pi(\boldsymbol{\xi}, t)$:

$$\frac{\partial \Pi(\boldsymbol{\xi}, t)}{\partial t} - \sqrt{N}\frac{d\boldsymbol{\phi}}{dt} \cdot \nabla_{\boldsymbol{\xi}} \Pi(\boldsymbol{\xi}, t) = \sum_{j} [\epsilon_A^+(j)\epsilon_B^+(j)\epsilon_C^-(j) - 1) T_{AB}(j) \Pi(\boldsymbol{\xi}, t) + \sum_{s[jj']} (\epsilon_s^+(j)\epsilon_s^-(j') - 1) T_s(j|j') \Pi(\boldsymbol{\xi}, t). \quad \text{(A1)}$$

For large N, the step operator (7) can be expanded in powers of $N^{-1/2}$ and expressed in differential form as[20,38]

$$\epsilon_s^{\pm}(j)\Pi[\xi_A(1), \ldots, \xi_s(j), \ldots \xi_C(\Omega), t] = \left[1 + \sum_{k=1}^{\infty} \frac{(\pm 1)^k}{k!} N^{-k/2} \frac{\partial^k}{\partial \xi_s(j)^k}\right] \Pi(\boldsymbol{\xi}, t). \quad \text{(A2)}$$

Inserting Eqs. (13) and (A2) into the right side of Eq. (A1) yields an expansion of the RDME in powers of $N^{-1/2}$. It has to be noticed that the transition probabilities are proportional to N.

The governing equations for the mean field $\phi_s(j, t)$ can be obtained from the leading order term of the van Kampen expansion. Expanding the right side of Eq. (A1) up to order $\sqrt{N}$, we obtain in leading order

$$\frac{d\boldsymbol{\phi}}{dt} \cdot \nabla_{\boldsymbol{\xi}} \Pi(\boldsymbol{\xi}, t) = (\boldsymbol{r} + \boldsymbol{D}) \cdot \nabla_{\boldsymbol{\xi}} \Pi(\boldsymbol{\xi}, t), \quad \text{(A3)}$$

where the vector $\boldsymbol{r}$ is defined by

$$r_s(j, t) = -k\phi_A(j, t)\phi_B(j, t), \quad r_C(j, t) = k\phi_A(j, t)\phi_B(j, t) \quad \text{(A4)}$$

for $s = A, B$. The vector $\boldsymbol{D}$ is given by

$$D_s(j, t) = D_s \left\{ \Delta\phi_s(j, t) \left[1 - \sum_m \phi_m(j, t)\right] + \phi_s(j, t) \sum_m \Delta\phi_m(j, t) \right\}, \quad \text{(A5)}$$

in which we defined the discrete Laplacian $\Delta\phi_s(j, t) = h^{-2} \sum_{[j'|j]} [\phi_s(j', t) - \phi_s(j, t)]$; $\sum_{[j'|j]}$ denotes the sum over the nearest neighbors of j. Thus, we obtain for the mean field $\phi_s(j, t)$,

$$\frac{d\phi_s(j)}{dt} = D_s \left\{ \Delta\phi_s(j, t) \left[1 - \sum_m \phi_m(j, t)\right] + \phi_s(j, t) \sum_m \Delta\phi_m(j, t) \right\} - k\phi_A(j, t)\phi_B(j, t), \quad \text{(A6)}$$

$$\frac{d\phi_C(j)}{dt} = D_C \left\{ \Delta\phi_C(j, t) \left[1 - \sum_m \phi_m(j, t)\right] + \phi_C(j, t) \sum_m \Delta\phi_m(j, t) \right\} + k\phi_A(j, t)\phi_B(j, t), \quad \text{(A7)}$$

for $s = A, B$. In the spatial continuum limit for an observation scale $L \gg h$ and for dilute solutions, $\phi_s(j) \ll 1$, Eqs. (A6) and (A7) reduce to

$$\frac{\partial \phi_s(x, t)}{\partial t} = D_s \Delta\phi_A(x, t) - k\phi_A(x, t)\phi_B(x, t),$$
$$\frac{\partial \phi_C(x, t)}{\partial t} = D_C \Delta\phi_C(x, t) - k\phi_A(x, t)\phi_B(x, t). \quad \text{(A8)}$$

We identified here $\phi_s(j,t) = \phi_s(x,t)$. If the system is not dilute, Eqs. (A6) and (A7) do not reduce to the classical reaction-diffusion equations as discussed in Ref. 40.

The governing equation for the fluctuation PDF, $\Pi(\boldsymbol{\xi}, t)$ is obtained from the contributions to Eq. (A1) of the order one. Thus, we obtain

$$\frac{\partial \Pi(\boldsymbol{\xi}, t)}{\partial t} = (G_1 + R_1 + G_2 + R_2)\Pi(\boldsymbol{\xi}, t). \tag{A9}$$

The R_i $(i = 1, 2)$ refers to terms that originate in the reactive transitions and are given by

$$R_1 = \sum_j \left\{ -\left[\frac{\partial}{\partial \xi_C(j)} - \frac{\partial}{\partial \xi_A(j)} - \frac{\partial}{\partial \xi_B(j)} \right] \times k[\xi_A(j)\phi_B(j) + \xi_B(j)\phi_A(j)] \right\}, \tag{A10}$$

$$R_2 = \sum_j \left[\frac{\partial}{\partial \xi_C(j)} - \frac{\partial}{\partial \xi_A(j)} - \frac{\partial}{\partial \xi_B(j)} \right]^2 k\phi_A(j)\phi_B(j). \tag{A11}$$

The terms G_i $(i = 1, 2)$ are due to the diffusion transitions. They read as

$$G_1 = -D_s \sum_{js} \frac{\partial}{\partial \xi_s(j)} \left[\Delta\xi_s(j) + \xi_s(j) \sum_m \Delta\phi_m(j) - \Delta\phi_s(j) \times \sum_m \xi_m(j) + \phi_s(j) \sum_m \Delta\xi_m(j) - \Delta\xi_s(j) \sum_m \phi_m(j) \right], \tag{A12}$$

$$G_2 = \frac{D_s}{4} \sum_s \sum_{s[jj']} \left\{ \phi_s(j) \left[1 - \sum_m \phi_m(j') \right] + \phi_s(j') \left[1 - \sum_m \phi_m(j) \right] \right\} \times \left[\frac{\partial^2}{\partial \xi_s(j)^2} + \frac{\partial^2}{\partial \xi_s(j')^2} - 2\frac{\partial^2}{\partial \xi_s(j)\partial \xi_s(j')} \right]. \tag{A13}$$

From the analytical expressions obtained for R_1, R_2, G_1, and G_2, it is possible to express the sums as scalar product between the matrix $\boldsymbol{\mathcal{A}}(t)$ and $\boldsymbol{\mathcal{B}}(t)$ and the vector $\boldsymbol{\xi}$ of all the fluctuations. Doing this we can express Eq. (A9) as

$$\frac{\partial \Pi(\boldsymbol{\xi}, t)}{\partial t} = -\nabla_{\boldsymbol{\xi}} \cdot [\boldsymbol{\mathcal{A}}(t) \cdot \boldsymbol{\xi}\, \Pi(\boldsymbol{\xi}, t)] + \nabla_{\boldsymbol{\xi}} \cdot [\boldsymbol{\mathcal{B}}(t) \cdot \nabla_{\boldsymbol{\xi}}\, \Pi(\boldsymbol{\xi}, t)]. \tag{A14}$$

The latter is a linear multi-variate Fokker-Planck equation, where $\boldsymbol{\mathcal{A}}(t)$ and $\boldsymbol{\mathcal{B}}(t)$ are $3\Omega \times 3\Omega$ matrices that we can write as a $\Omega \times \Omega$ block matrices

$$\mathcal{A} = \begin{bmatrix} \mathcal{A}_0(1) & \mathcal{C}_1(2) & 0 & \dots & \mathcal{C}_1(\Omega) \\ \mathcal{C}_1(1) & \mathcal{A}_0(2) & \mathcal{C}_1(3) & \dots & 0 \\ \dots & \dots & \dots & \dots & \dots \\ \mathcal{C}_1(1) & 0 & 0 & \dots & \mathcal{A}_0(\Omega) \end{bmatrix} \quad \text{with blocks} \quad \mathcal{A}_0(j) = \begin{bmatrix} a_{AA}(j) & a_{AB}(j) & a_{AC}(j) \\ a_{BA}(j) & a_{BB}(j) & a_{BC}(j) \\ a_{CA}(j) & a_{CB}(j) & a_{CC}(j) \end{bmatrix}, \quad \mathcal{C}_1(j') = \begin{bmatrix} c_{AA}(j') & c_{AB}(j') & c_{AC}(j') \\ c_{BA}(j') & c_{BB}(j') & c_{BC}(j') \\ c_{CA}(j') & c_{CB}(j') & c_{CC}(j') \end{bmatrix}, \tag{A15}$$

in which

$$a_{AA}(j) = -k\phi_B(j) + D_A h^2 (2 - \sum_m \Delta\phi_m(j) - \Delta\phi_A(j) + 2\phi_A(j) - 2\sum_m \phi_m(j)), \tag{A16}$$

$$a_{AB}(j) = -k\phi_A(j) + D_A h^2 (\Delta\phi_A(j) + 2\phi_A(j)), \tag{A17}$$

$$a_{AC}(j) = D_A h^2 (\Delta\phi_A(j) + 2\phi_A(j)), \tag{A18}$$

$$a_{BA}(j) = -k\phi_B(j) + D_B h^2 (\Delta\phi_B(j) + 2\phi_B(j)), \tag{A19}$$

$$a_{BB}(j) = -k\phi_A(j) + D_B h^2 (2 - \sum_m \Delta\phi_m(j) - \Delta\phi_B(j) + 2\phi_B(j) - 2\sum_m \phi_m(j)), \tag{A20}$$

$$a_{BC}(j) = D_B h^2 (\Delta\phi_B(j) + 2\phi_B(j)), \tag{A21}$$

$$a_{CA}(j) = k\phi_B(j) + D_C h^2 (\Delta\phi_C(j) + 2\phi_C(j)), \tag{A22}$$

$$a_{CB}(j) = -k\phi_A(j) + D_C h^2 (\Delta\phi_C(j) + 2\phi_C(j)), \tag{A23}$$

$$a_{CC}(j) = D_C h^2 \left(2 - \sum_m \Delta\phi_m(j) - \Delta\phi_C(j) + 2\phi_C(j) - 2\sum_m \phi_m(j)\right), \quad \text{(A24)}$$

$$c_{ss}(j') = -D_s h^2 (1 + \phi_s(j') - \sum_m \phi_m(j')), \quad \text{(A25)}$$

$$c_{sr}(j') = -D_s h^2 \phi_s(j'), \quad \text{(A26)}$$

and

$$\mathcal{B} = \begin{bmatrix} \mathcal{B}_0(1) & \mathcal{D}_1(2) & 0 & \dots & \mathcal{D}_1(\Omega) \\ \mathcal{D}_1(1) & \mathcal{B}_0(2) & \mathcal{D}_1(3) & \dots & 0 \\ \dots & \dots & \dots & \dots & \dots \\ \mathcal{D}_1(1) & 0 & 0 & \dots & \mathcal{B}_0(\Omega) \end{bmatrix} \quad \text{with blocks} \quad \mathcal{B}_0(j) = \begin{bmatrix} b_{AA}(j) & b_{AB}(j) & b_{AC}(j) \\ b_{BA}(j) & b_{BB}(j) & b_{BC}(j) \\ b_{CA}(j) & b_{CB}(j) & b_{CC}(j) \end{bmatrix}, \quad \text{(A27)}$$

$$\mathcal{D}_1(j) = \begin{bmatrix} d_{AA}(j) & 0 & 0 \\ 0 & d_{BB}(j) & 0 \\ 0 & 0 & d_{CC}(j) \end{bmatrix}$$

where

$$b_{AA}(j) = k\phi_A(j)\phi_B(j) - \frac{D_s}{2}\left(\phi_A(j)\left(1 - \sum_m \phi_m(j')\right) + \phi_A(j')\left(1 - \sum_m \phi_m(j)\right)\right), \quad \text{(A28)}$$

$$b_{AB}(j) = k\phi_A(j)\phi_B(j), \quad \text{(A29)}$$

$$b_{AC}(j) = -k\phi_A(j)\phi_B(j), \quad \text{(A30)}$$

$$b_{BA}(j) = k\phi_A(j)\phi_B(j), \quad \text{(A31)}$$

$$b_{BB}(j) = k\phi_A(j)\phi_B(j) - \frac{D_s}{2}\left(\phi_B(j)\left(1 - \sum_m \phi_m(j')\right) + \phi_B(j')\left(1 - \sum_m \phi_m(j)\right)\right), \quad \text{(A32)}$$

$$b_{BC}(j) = -k\phi_A(j)\phi_B(j), \quad \text{(A33)}$$

$$b_{CA}(j) = -k\phi_A(j)\phi_B(j), \quad \text{(A34)}$$

$$b_{CB}(j) = -k\phi_A(j)\phi_B(j), \quad \text{(A35)}$$

$$b_{CC}(j) = k\phi_A(j)\phi_B(j) - \frac{D_s}{2}\left(\phi_C(j)\left(1 - \sum_m \phi_m(j')\right) + \phi_s(j')\left(1 - \sum_m \phi_m(j)\right)\right), \quad \text{(A36)}$$

$$d_{ss}(j) = -D_s\phi_s(j)\left(1 - \sum_m \phi_m(j')\right). \quad \text{(A37)}$$

At large times we disregard contributions to matrices $\boldsymbol{\mathcal{A}}$ and $\boldsymbol{\mathcal{B}}$ that are of the order of t^{-1}, that is, the terms that are proportional to the mean field $\phi_{sj}(t)$ and powers thereof. In this approximation, the matrix $\boldsymbol{\mathcal{B}}$ is zero and the only non-zero components of matrix $\boldsymbol{\mathcal{A}}$ are

$$a_{AA}(j) = 2D_A h^2, \quad \text{(A38)}$$

$$a_{BB}(j) = 2D_B h^2, \quad \text{(A39)}$$

$$a_{CC}(j) = 2D_C h^2, \quad \text{(A40)}$$

$$c_{ss}(j) = -D_s h^2. \quad \text{(A41)}$$

Thus, matrix $\boldsymbol{\mathcal{A}}$ reduces to the discrete Laplacian operator. Inserting this approximation into Eq. (18) and summing over j, the volume term on the right side is zero. Furthermore, inserting the approximations for $\boldsymbol{\mathcal{A}}$ and $\boldsymbol{\mathcal{B}}$ into Eq. (19) and summation over j directly gives Eq. (22).

APPENDIX B: FIRST MOMENT OF THE FLUCTUATIONS

To calculate the first moment of the sj-th component of the fluctuations, we multiply the Fokker-Planck equation by $\xi_s(j)$. Integrating over the fluctuations domain Ξ, we obtain

$$\int_\Xi \xi_s(j)\frac{\partial \Pi(\boldsymbol{\xi}, t)}{\partial t} d\boldsymbol{\xi} = -\int_\Xi \xi_s(j)(\nabla_{\boldsymbol{\xi}} \cdot [\mathcal{A} \cdot \boldsymbol{\xi}\Pi(\boldsymbol{\xi}, t)] + \nabla_{\boldsymbol{\xi}}[\mathcal{B} \cdot \nabla_{\boldsymbol{\xi}}\Pi(\boldsymbol{\xi}, t)])d\boldsymbol{\xi}. \quad \text{(B1)}$$

We integrate this expression by parts, obtaining volume and surface terms. Using the Divergence theorem, we can evaluate the integrals of divergence over a domain as integrals of the argument of the divergence over the surface of the domain. Considering that the system is dilute, we assume that $\Pi(\boldsymbol{\xi}, t) = 0$ at the upper boundary (for $\boldsymbol{\xi} \to \sqrt{N}(1 - \boldsymbol{\phi})$) and we obtain,

$$\begin{aligned}\frac{d\overline{\xi_s}}{dt} &= (\overline{\mathcal{A} \cdot \boldsymbol{\xi}})_s + \sum_{s'j'} \int_{\partial \Xi} [\xi_s(j) \mathcal{A}_{s'j's'j'} \xi_{s'}(j') \Pi(\boldsymbol{\xi}, t)] \cdot d\mathbf{n} \\ &+ \frac{1}{2} \sum_{s'j'} \int_{\partial \Xi} [\xi_s(j) \mathcal{B} \cdot \nabla_{s'j'} \Pi(\boldsymbol{\xi}, t)] \cdot d\mathbf{n} \\ &- \frac{1}{2} \sum_{s'j'} \sum_{s''j''} \int_{\Xi} \boldsymbol{e}_{sj} \cdot (\mathcal{B}^T \cdot \nabla_{s''j''}) \Pi(\boldsymbol{\xi}, t) d\boldsymbol{\xi} \\ &- \sum_{s'j'} \int_{\partial \Xi} \xi_s(j) \partial_t \xi_{s'}(j') \partial_t \Pi(\boldsymbol{\xi}, t) \boldsymbol{e}_{s'j'} \cdot d\mathbf{n}, \end{aligned} \tag{B2}$$

where $\partial \Xi$ is the surface of the domain Ξ, $d\mathbf{n}$ is the vector orthogonal to the surface $\partial \Xi$, and $\boldsymbol{e}_s$ is a vector with all components equal to zero except the sj-th component which is equal to one. This quantity derives from the integration of the term ∇_s. For compactness of notation in the previous expression, we denoted $f_s(j) = f_s$, $f_{s'}(j') = f_{s'}$, and $f_{s''}(j'') = f_{s''}$.

APPENDIX C: THE FOKKER-PLANK EQUATION IN THE NON-REACTIVE ISLANDS REGIME

The number of reactants is a positively defined quantity. Therefore the support of $\boldsymbol{\xi}$ is bounded, because $\rho_s(j) = \phi_s(j) + \xi_s(j)/\sqrt{N}$ is bounded between 0 and N. This implies that the fluctuations $\xi_s(j)$ are bounded in the subdomains

$$\Xi_s(j) = \{\xi_s(j) | -\sqrt{N}\phi_s(j) \le \xi_s(j) \le \sqrt{N}[1 - \phi_s(j)]\}, \tag{C1}$$

with $\Xi = \prod_{sj} \Xi_{sj}$. As such the domain of fluctuations $\boldsymbol{\xi}$ is a hypercube and each component of $\xi_s(j)$ is confined within a segment whose size varies over time. In Appendix A, we derived the Fokker-Planck equation for the evolution of $\Pi(\boldsymbol{\xi}, t)$. We specify zero flux of $\Pi(\boldsymbol{\xi}, t)$ at the boundaries of the 3Ω-dimensional domain Ξ. For an infinite fluctuation domain Ξ and natural boundary conditions for $\Pi(\boldsymbol{\xi}, t)$, the solution of Eq. (15) is a multi-variate Gaussian distribution.[20,41] In this approximation, the solution is fully characterized by its first and second moments. The boundary terms in Eq. (B2) are zero. The average fluctuations $\overline{\xi}_s(j)$ decrease exponentially with time. As long as the natural boundary conditions are a valid approximation, the average behavior of the whole system will not be affected by fluctuations. For situations in which the mean field is not very large compared with the size of fluctuations, the approximation of infinite fluctuation domain is no longer reasonable and boundary effects arise.

[1] A. I. A. Ovchinnikov and Y. B. Zeldovich, Chem. Phys. **28**, 215 (1978).
[2] D. Toussaint and F. Wilczek, J. Chem. Phys. **78**, 2642 (1983).
[3] K. Kang and S. Redner, Phys. Rev. A **32**, 435 (1985).
[4] A. Lin, R. Kopelman, and P. Argyrakis, Phys. Rev. E **53**, 1502 (1996).
[5] D. A. Benson and M. M. Meerschaert, Water Resour. Res. **44**, 1, doi:10.1029/2008WR007111 (2008).
[6] D. Bolster, D. Benson, T. Le Borgne, and M. Dentz, Phys. Rev. E **82**, 021119 (2010).
[7] C. A. Gómez-Uribe and G. C. Verghese, J. Chem. Phys **126**, 024109 (2007).
[8] R. Grima, J. Chem. Phys. **133**, 035101 (2010).
[9] C. I. Steefel, D. J. DePaolo, and P. C. Lichtner, Earth Planet. Sci. Lett. **240**, 539 (2005).
[10] D. ben-Avraham, M. A. Burschka, and C. Doering, J. Stat. Phys. **60**, 695 (1990).
[11] J. P. Boon, D. Dab, R. Kapral, and A. Lawniczak, Phys. Rep. **273**, 55 (1996).
[12] G. Zumofen, J. Klafter, and M. Shlesinger, Phys. Rev. Lett. **77**, 2830 (1996).
[13] M. De Simoni, J. Carrera, X. Sánchez-Vila, and A. Guadagnini, Water Resour. Res. **41**, 1, doi:10.1029/2005WR004056 (2005).
[14] V. Kapoor and P. K. Kitanidis, Water Resour. Res. **34**, 1181, doi:10.1029/97WR03608 (1998).
[15] T. Le Borgne, M. Dentz, P. Davy, D. Bolster, J. Carrera, J. R. de Dreuzy and O. Bour, Phys. Rev. E **85**, 015301(R) (2011).
[16] Z. Neufeld and E. Hernandez-Garcia, *Chemical and Biological Processes in Fluid Flows: A dynamical System Approach* (Imperial College Press, London, 2010).
[17] P. Thomas, A. V. Straube, and R. Grima, J. Chem. Phys. **133**, 195101 (2010).
[18] T. Tel, A. Demoura, C. Grebogi, and G. Karolyi, Phys. Rep. **413**, 91 (2005).
[19] J. Ottino, *The Kinematics of Mixing: Stretching, Chaos, and Transport* (Cambridge University Press, Cambridge, England, 1989).
[20] N. van Kampen, *Stochastic Processes in Physics and Chemistry*, 3rd ed. (Elsevier, Amsterdam, 2007).
[21] G. Zumofen and J. Klafter, Phys. Rev. E **50**, 5119 (1994).
[22] F. Leyvraz and S. Redner, Phys. Rev. A **46**, 3132 (1992).
[23] A. J. McKane and T. J. Newman, Phys. Rev. Lett. **94** (2005).
[24] D. Bernstein, Phys. Rev. E **71**, 041103 (2005).
[25] D. Fange, O. G. Berg, P. Sjoberg and J. Elf, Proc. Natl. Acad. Sci. U.S.A. **107**, 19820 (2010).
[26] R. Erban and S. J. Chapman, Phys. Biol. **6**, 046001 (2009).
[27] P. de Anna, F. Dipatti, D. Fanelli, A. McKane, and T. Dauxois, Phys. Rev. E **81**, 056110 (2010).
[28] T. Dauxois, F. Di Patti, D. Fanelli, and A. McKane, Phys. Rev. E **79**, 036112 (2009).
[29] F. Baras and M. Mansour, Phys. Rev. E **54**, 6139 (1996).
[30] S. A. Isaacson and C. S. Peskin, SIAM J. Sci. Comput. (USA) **28**, 47 (2006).
[31] A. McKane and T. Newman, Phys. Rev. E **70**, 041902 (2004).
[32] C. Lugo and A. McKane, Phys. Rev. E **78**, 010102 (2008).
[33] C. W. Gardiner, K. J. McNeil, D. F. Walls, and I. S. Matheson, J. Stat. Phys. **14**, 307 (1976).
[34] S. A. Isaacson, J. Phys. A **41**, 065003 (2008).
[35] S. A. Isaacson, Phys. Rev. E **80**, 066106 (2009).
[36] D. T. Gillespie, J. Comput. Phys. **22**, 403 (1976).
[37] D. T. Gillespie, J. Phys. Chem. **81**, 2340 (1977).
[38] C. W. Gardiner, *Handbook of Stochastic Methods*, 3rd ed. (Springer-Verlag, Berlin, 2004).
[39] F. Dipatti, S. Azaele, J. R. Banavar, and A. Maritan, Phys. Rev. E **83**, 010102 (2010).
[40] D. Fanelli and A. McKane, Phys. Rev. E **82**, 021113 (2010).
[41] H. Risken, *The Fokker-Planck Equation*, 2nd ed. (Springer-Verlag, Berlin, 1996).

2.3 An analytical solution for the islands segregation

In the same physical framework we now investigate the described OZ segregation from another viewpoint. We use the method of moment equations (e.g. *Neuman* [1993]; *Neuman and Tartakovsky* [2009]) to solve analytically the anomalous kinetics that deviates from the mean field t^{-1} to $t^{-\frac{d}{4}}$ behavior. We consider the well known reaction diffusion equations (e.g. *Neufeld and Hernandez-Garcia* [2010]):

$$\frac{\partial \phi_i(x,t))}{\partial t} - D\frac{\partial^2 \phi_i(x,t)}{\partial x^2} = -k\phi_A(x,t)\phi_B(x,t), \tag{2.4}$$

and we treat the concentrations as random variables:

$$\phi_A(x,t) = \overline{\phi_A(x,t)} + \phi_A(x,t)' \quad \text{and} \quad \phi_B(x,t) = \overline{\phi_B(x,t)} + \phi_B(x,t)' \tag{2.5}$$

where the overbar designates an ensemble average and the prime denotes zero-mean fluctuations about the average. The full solution of this equation is the pdf for distribution of A and B. Here, we are mainly interested in the average behavior of the concentrations and we focus on the leading moments of the distributions. We derive equations for both, the mean concentration that satisfy an ordinary differential equation:

$$\frac{\partial \overline{\phi_A(x,t)}}{\partial t} = -k\overline{\phi_A(x,t)}\;\overline{\phi_B(x,t)} - k\overline{\phi_A(x,t)'\phi_B(x,t)'} \tag{2.6}$$

and the variance $\overline{\phi_A(x,t)'\phi_B(x,t)'}$. We close the system neglecting third order moments. The previous equation is a Riccati differential equation whose solution is given in terms of the Bessel functions of the first and second kind. We define the characteristic transition time t^* when this anomalous kinetics arises. In this analytical framework we derive analytical expressions for t^*. All physical and mathematical derivation of the analytical solution are summarized in the following manuscript that has been published on *Water Resources Research* on 2011.

An analogous scaling has been shown to occur when the transport mechanisms are described by super-diffusive Levy-Flight (e.g. *Zumofen et al.* [1996]; *Leyvraz and Redner* [1992]). In this case, the mean concentration scales asymptotically as $t^{-\frac{1}{2\gamma}}$ where $1 < \gamma < 2$ characterizes the Levy-enhanced diffusion operator. Also for this case we derive an analytical full time expression for the mean concentration and for the characteristic transition time when the anomalous kinetics arises (see paper in Appendix).

Effect of spatial concentration fluctuations on effective kinetics in diffusion-reaction systems

A. M. Tartakovsky,[1] P. de Anna,[2] T. Le Borgne,[2] A. Balter,[1] and D. Bolster[3]

Received 29 March 2011; revised 7 December 2011; accepted 29 December 2011; published 21 February 2012.

[1] The effect of spatial concentration fluctuations on the reaction of two solutes, A + B → C, is considered. In the absence of fluctuations, the concentration of solutes decays as $A_{det} = B_{det} \sim t^{-1}$. Contrary to this, experimental and numerical studies suggest that concentrations decay significantly slower. Existing theory suggests a $t^{-d/4}$ scaling in the asymptotic regime (d is the dimensionality of the problem). Here we study the effect of fluctuations using the classical diffusion-reaction equation with random initial conditions. Initial concentrations of the reactants are treated as correlated random fields. We use the method of moment equations to solve the resulting stochastic diffusion-reaction equation and obtain a solution for the average concentrations that deviates from $\sim t^{-1}$ to $\sim t^{-d/4}$ behavior at characteristic transition time t^*. We also derive analytical expressions for t^* as a function of Damköhler number and the coefficient of variation of the initial concentration.

Citation: Tartakovsky, A. M., P. de Anna, T. Le Borgne, A. Balter, and D. Bolster (2012), Effect of spatial concentration fluctuations on effective kinetics in diffusion-reaction systems, *Water Resour. Res.*, *48*, W02526, doi:10.1029/2011WR010720.

1. Introduction

[2] Incomplete mixing of solutes and spatial fluctuations in concentration fields have been identified as a major cause of failure of deterministic effective models, such as deterministic diffusion-reaction equations, to accurately simulating mixing-controlled reactions. Spatial fluctuations in the concentration of the reactive species can be caused by the thermal fluctuations of molecules [*Ovchinnikov and Zeldovich*, 1978; *Toussaint and Wilczek*, 1983], turbulent flows [*Hill*, 1976] or highly nonuniform laminar flows (e.g., flow in porous media) [*Tartakovsky et al.*, 2008, 2009; *Raje and Kapoor*, 2000; *Luo et al.*, 2008; *Bolster et al.*, 2011; *Le Borgne et al.*, 2011].

[3] In the case of porous media, the fluctuations cause the classical advection-dispersion-reaction (ADR) equations with constant transport coefficients to overestimate the extent of the mixing controlled reactions [*Battiato and Tartakovsky*, 2011; *Battiato et al.*, 2009; *Tartakovsky et al.*, 2009; *Le Borgne et al.*, 2010]. Similar problems occur in a purely diffusive systems where thermal fluctuations of molecules lead to incomplete mixing [*Ovchinnikov and Zeldovich*, 1978; *Toussaint and Wilczek*, 1983]. In order to tackle the discrepancies with traditional homogenous (ADE) equations, a variety of novel models have emerged. These include stochastic Langevin approaches [*Tartakovsky et al.*, 2008; *Tartakovsky*, 2010], perturbation models [*Luo et al.*, 2008], and adaptations of a variety of popular nonlocal models such as continuous time random walks [*Edery et al.*, 2009, 2010], fractional ADEs [*Bolster et al.*, 2010], multirate mass transfer [*Donado et al.*, 2009; *Willmann et al.*, 2010], memory effect models [*Dentz et al.*, 2011] and models with time-dependent rate coefficients [*Sanchez-Vila et al.*, 2010]. However, many of these approaches involve effective parameters, which cannot be computed a priori from the physical properties of the system and have to be found through model calibration with experimental data.

[4] In this work, we use the moment equation approach [e.g., *D. M. Tartakovsky et al.*, 2002, 2003; *A. M. Tartakovsky et al.*, 2003, 2004a, 2004b] to quantify the effect of incomplete mixing in diffusion-reaction systems. We focus on a nonlinear reaction involving diffusion of two species, A and B, that react with each other kinetically as A + B → C. We assume that A and B have the same initial concentration and are macroscopically well mixed before the onset of the reaction. In the absence of spatial fluctuations (i.e., a fully mixed system at all times), a well known analytical solution exists and the average concentrations decay as $A_{det} = B_{det} \sim t^{-1}$.

[5] Recent numerical studies by *Benson and Meerschaert* [2008] and *de Anna et al.* [2011] suggest that while this analytical solution may be valid at early times, at late times a different slower scaling emerges. These observations are in line with previous observations from the physics community [*Hill*, 1976; *Toussaint and Wilczek*, 1983; *Kang and Redner*, 1985] and a variety of theoretical models [*Ovchinnikov and Zeldovich*, 1978; *Toussaint and Wilczek*, 1983; *Kang and Redner*, 1985]. The latter are based on late time asymptotic arguments, and suggest a late asymptotic decay of the concentrations that is proportional to $t^{-d/4}$, where d is the spatial dimensionality of the problem. These models established that, for sufficiently fast

[1]Pacific Northwest National Laboratory, Richland, Washington, USA.
[2]Géosciences Rennes, UMR 6118, CNRS, Université de Rennes 1, Rennes, France.
[3]Environmental Fluid Dynamics Laboratories, Department of Civil Engineering and Geological Sciences, University of Notre Dame, Notre Dame, Indiana, USA.

0043-1397/12/2011WR010720

reactions, initial fluctuations in the concentrations cause segregation of the reactants into separate islands of A and B, (i.e., parts of the domain occupied dominantly by species A or B). In this situation, reactions are limited by how quickly diffusion of particles can cause mixing of A and B across the boundaries of the islands. Thus, the mixing of species is limited and the temporal decay of the concentrations slows down. This anomalous scaling of diffusion-limited reactions, related to segregation of reactants into islands, was experimentally observed by *Monson and Kopelman* [2004].

[6] These past theoretical works have focused primarily on the establishment of the late asymptotic behavior of the concentrations. Also, in the previous studies the initial fluctuations of each species were assumed to be uncorrelated (fluctuations with zero correlation length). The standard deviation of the fluctuations was implicitly assumed to be equal to the square root of the initial number of the reactive particles. In a number of important applications (e.g., turbulent mixing and transport in porous media), the initial fluctuations in concentrations may have nonzero correlation lengths. For example, if the reactive solutions are rapidly brought in contact by nonuniform advection (and allowed to diffuse and react), then the initial correlation length of the concentration fluctuations will depend on the statistics of the velocity field, and can in principle be as large as the size of the domain. The standard deviation of the concentrations in these applications represents the degree of mixing, and can also be arbitrarily large.

[7] To study the effect of fluctuations, we employ a diffusion-reaction equation with random initial conditions. In the past, diffusion-reaction type equations have been used to study the effect of random concentration fluctuations on scales ranging from the molecular scale [*Ovchinnikov and Zeldovich*, 1978] to the field scale [*Sanchez-Vila et al.*, 2008], though advection is usually also considered in the latter case. Here the initial concentrations of the reactants are treated as correlated random fields with spatially constant and equal statistical means and variances. The random initial conditions render the diffusion-reaction equation stochastic. We use the moment equation approach to derive deterministic equations for the mean and variance of the concentrations. The solution for the mean concentrations shows that the average concentration deviates from $\sim t^{-1}$ to $\sim t^{-d/4}$ behavior at a characteristic transition time t^*, which depends on the Damköhler number, *Da*. We obtain analytical expressions for t^* as a function of *Da*. The solutions are used to study the effect of initial average concentration, variance, correlation length, cross correlation, and the size of the domain on the A + B $\rightharpoonup$ C reaction.

2. Problem Formulation

[8] Our goal is to study the effect of random fluctuations in concentration fields on chemical reactions. Specifically, we study an irreversible reaction between two species, A and B, that is described by a diffusion-reaction equation:

$$\frac{\partial I(\mathbf{x},t)}{\partial t} = D\Delta I(\mathbf{x},t) - kA(\mathbf{x},t)B(\mathbf{x},t), \qquad \mathbf{x}\in\Omega \qquad I = A,B, \tag{1}$$

where A and B are the concentrations of species A and B, D is the diffusion coefficient, k is the rate coefficient of the irreversible reaction, and $\Delta = \nabla^2$ is the Laplace operator. We consider two special cases: (1) diffusion in an infinite d-dimensional domain Ω ($d = 1, 2, 3$) and (2) diffusion in a finite one-dimensional domain $\Omega = (0, L)$ subject to periodic boundary conditions.

[9] We treat the concentrations as random variables:

$$A(\mathbf{x},t) = \overline{A}(\mathbf{x},t) + A'(\mathbf{x},t) \qquad B(\mathbf{x},t) = \overline{B}(x,t) + B'(\mathbf{x},t), \tag{2}$$

where the overbar designates an ensemble average and the prime denotes zero-mean fluctuations about the average. We assume equal initial ensemble averaged concentrations of A and B:

$$\overline{A}(\mathbf{x},0) = \overline{B}(\mathbf{x},0) = C_0. \tag{3}$$

Unlike previous work [*Ovchinnikov and Zeldovich*, 1978; *Toussaint and Wilczek*, 1983], we assume the initial fluctuations, $A'(\mathbf{x},0)$ and $B'(\mathbf{x},0)$, to be spatially correlated fields. This allows us to study the effect of spatial correlation of the concentrations on the chemical reaction. In the following we study this system for several initial autocovariance functions. Specifically, we consider initial exponential and delta autocovariance functions. The exponential autocovariance function has a form:

$$\overline{A'(\mathbf{x},0)A'(\mathbf{y},0)} = \overline{B'(\mathbf{x},0)B'(\mathbf{y},0)} = \sigma^2 e^{-\frac{|\mathbf{x}-\mathbf{y}|}{l}}, \tag{4}$$

where σ^2 is the initial variance of the concentrations (σ is the initial standard deviation of fluctuations) and l is the initial correlation length. Assuming that the initial fluctuations of A and B are caused by the same physical processes, we prescribe the same variances and correlation for both reactants.

[10] When the correlation length is small relative to the size of the domain, one can replace the exponential autocovariance function with the delta autocovariance function:

$$\overline{A'(\mathbf{x},0)A'(\mathbf{y},0)} = \overline{B'(\mathbf{x},0)B'(\mathbf{y},0)} = \sigma^2 l^d \delta(\mathbf{x}-\mathbf{y}). \tag{5}$$

[11] In a well-mixed purely diffusive system (in the absence of reactions), the fluctuations in the concentrations are caused by thermal fluctuations of particles. In this case, the fluctuations have a correlation length, l, of the order of the particle diameter, and under most circumstances the delta autocovariance function will provide an accurate representation of the spatial correlation of the fluctuations. In other nonreactive, but hydrologically related stochastic model studies the delta correlation has been shown to give asymptotically similar results as short-range correlation functions such as exponential and Gaussian [e.g., *Neuweiler et al.*, 2003]. We show in section 4.2.2 that the delta function approximation can be used only to predict the mean and variance of the concentrations for times larger than $t_D/8\pi$, where t_D is the diffusion time:

$$t_D = \frac{l^2}{D}. \tag{6}$$

In the absence of reaction, t_D is the time it takes for a region of size l to become well mixed by diffusion. For

smaller times, the delta function approximation leads to unphysical behavior of the ensemble average and/or variance of the concentrations.

[12] Initial large-scale concentration fluctuations can be caused by poor mechanical mixing of two solutes due to fluctuations in advective velocities that brought two solutes in contact. In this case, the correlation length depends on the degree of mixing and can be of the same order (or smaller) as the domain size. Under such conditions, we chose the exponential autocovariance function (4) to describe initial correlation of the fluctuations of A and B, but one could also consider other correlation functions.

[13] To complete the problem formulation, we specify a cross-covariance function $\overline{A'(\mathbf{x},0)B'(\mathbf{y},0)}$ at time $t = 0$. We consider two types of cross correlations: anticorrelation and no cross correlation. The initial anticorrelation assumes that in a volume with a large concentration of one reactant (relative to the average value of the concentration) the concentration of another reactant is small. The anticorrelation is described by a cross-covariance function:

$$\overline{A'(\mathbf{x},0)B'(\mathbf{y},0)} = -\sigma^2 e^{-\frac{|\mathbf{x}-\mathbf{y}|}{l}} \tag{7}$$

if both concentrations, A and B, have the initial exponential correlation and

$$\overline{A'(\mathbf{x},0)B'(\mathbf{y},0)} = -\sigma^2 l^d \delta(\mathbf{x}-\mathbf{y}) \tag{8}$$

if A and B are initially δ correlated.

[14] For completeness, we also consider a case where the initial cross covariance is zero,

$$\overline{A'(\mathbf{x},0)B'(\mathbf{y},0)} = 0. \tag{9}$$

[15] *Kang and Redner* [1985] previously justified the emerging scaling law $t^{-\frac{d}{4}}$ with the formation of islands of segregated solutes. The initial anticorrelation is a necessary but not a sufficient condition for the existence of the islands and the initial condition (7) or (8) does not imply presence of islands at $t = 0$. Furthermore, the following analysis shows that after the onset of the reaction, the scaling changes from t^{-1} to $t^{-\frac{d}{4}}$ regardless of the initial cross correlation, but the transition time from one scaling law to another depends on variance, correlation length and the form of cross-covariance function.

[16] The random initial concentrations render the diffusion-reaction equation (1) stochastic. The full solution of this equation is the probability density functions for distribution of A and B. In this work, we are mainly interested in the average behavior of the concentrations and we focus on the leading moments of the distributions namely the mean (ensemble averaged) concentrations and the concentration variances (a measure of uncertainty). The differential equations for the leading moments are obtained using the method of moment equations [*D. M. Tartakovsky et al.*, 2003]. The details of the derivation of the moment equations are given in Appendix A.

[17] The average concentrations $\overline{A}$ and $\overline{B}$ satisfy an ordinary differential equation:

$$\frac{\partial \overline{I}}{\partial t} = -k\overline{A}\,\overline{B} - k\overline{A'B'}, \qquad I = A, B, \tag{10}$$

where $\overline{A'(\mathbf{x},t)B'(\mathbf{x},t)} = \overline{B'(\mathbf{x},t)A'(\mathbf{x},t)}$. In equation (10), $\overline{A}$ and $\overline{B}$ satisfy the same initial condition (equation (3)), and hence,

$$\overline{A}(t) = \overline{B}(t). \tag{11}$$

[18] Now let us define $f(\mathbf{x},\mathbf{y},t) = \overline{A'(\mathbf{x},t)B'(\mathbf{y},t)} - \overline{A'(\mathbf{x},t)A'(\mathbf{y},t)}$ and $g(\mathbf{x},\mathbf{y},t) = \overline{A'(\mathbf{x},t)B'(\mathbf{y},t)} + \overline{A'(\mathbf{x},t)A'(\mathbf{y},t)}$. The governing equations for these functions are (Appendix A)

$$\frac{\partial f(\mathbf{x},\mathbf{y},t)}{\partial t} = 2D\Delta f(\mathbf{x},\mathbf{y},t) \tag{12}$$

$$\frac{\partial g(\mathbf{x},\mathbf{y},t)}{\partial t} = 2D\Delta g(\mathbf{x},\mathbf{y},t) - 4k\overline{A}(\mathbf{x},t)g(\mathbf{x},\mathbf{y},t), \tag{13}$$

where $\mathbf{y} \in \Omega$.

[19] It is important to note that in the derivations of (13) we disregard the third moment. Once we have solved for f and g, the autocovariance and cross covariance can be calculated as $2\overline{A'(\mathbf{x},t)A'(\mathbf{y},t)} = g(\mathbf{x},\mathbf{y},t) - f(\mathbf{x},\mathbf{y},t)$ and $2\overline{A'(\mathbf{x},t)B'(\mathbf{y},t)} = g(\mathbf{x},\mathbf{y},t) + f(\mathbf{x},\mathbf{y},t)$.

[20] The autocovariances $\overline{A'(\mathbf{x},t)A'(\mathbf{y},t)}$ and $\overline{B'(\mathbf{x},t)B'(\mathbf{y},t)}$ ($\overline{A'(\mathbf{x},t)A'(\mathbf{y},t)} = \overline{B'(\mathbf{x},t)B'(\mathbf{y},t)}$) satisfy either initial conditions (4) or (5) and the cross covariance $\overline{A'(\mathbf{x},t)B'(\mathbf{y},t)}$ satisfies initial conditions (7), (8) or (9) depending on the type of initial autocorrelation and cross correlation of the fluctuations. These initial conditions define initial conditions for f and g.

[21] The boundary conditions for the autocovariance and cross covariance defined on the infinite d-dimensional domain Ω are

$$g(\mathbf{x},\mathbf{y},t) = 0, \qquad x_i = \pm\infty, \qquad i = 1, \ldots, d, \tag{14}$$

$$f(\mathbf{x},\mathbf{y},t) = 0, \qquad x_i = \pm\infty, \qquad i = 1, \ldots, d, \tag{15}$$

respectively, where $\mathbf{x} = (x_1, x_2, x_3)^T$ and $\mathbf{y} = (y_1, y_2, y_3)^T$. These boundary conditions specify that the autocovariance and cross covariance are zero far away from the point $\mathbf{y}$. Furthermore, without loss of generality, we set $y_i = 0$ ($i = 1, \ldots, d$).

[22] In the case of the one-dimensional periodic finite size domain $(0, L)$, the domain can always be centered around the point y (i.e., y in the one-dimensional version of (12) and (13) can be set to $y = y^* = L/2$). For the considered initial conditions, only homogeneous Neumann boundary conditions for equations (12) and (13) can satisfy the periodic conditions. Then the appropriate boundary conditions for equations (12) and (13) are

$$\frac{\partial f(x,y,t)}{\partial x} = 0, \qquad x = 0, L, \tag{16}$$

$$\frac{\partial g(x,y,t)}{\partial x} = 0, \qquad x = 0, L, \tag{17}$$

respectively.

3. Solution of the Deterministic Diffusion-Reaction Equation

[23] If the initial fluctuations are absent or very small and can be disregarded, then the diffusion-reaction equation reduces to a deterministic equation:

$$\frac{\partial I_{det}}{\partial t} = -kI_{det}^2, \qquad I_{det} = A_{det}, B_{det}, \tag{18}$$

where the subscript *det* stands for the deterministic concentrations (with zero initial fluctuations). The solution of this equation, subject to the initial conditions $A_{det}(0) = B_{det}(0) = A_0$, is

$$A_{det}(t) = B_{det}(t) = \frac{A_0}{A_0 kt + 1}. \tag{19}$$

4. Moment Equations for Initially Anti-Cross-Correlated A and B

[24] For initially anticorrelated A and B, the auto-covariance and cross-covariance functions satisfy the initial condition

$$\overline{A'(\mathbf{x},0)A'(\mathbf{y},0)} = -\overline{A'(\mathbf{x},0)B'(\mathbf{y},0)} = \sigma^2\rho(\mathbf{x}-\mathbf{y}), \tag{20}$$

where $\rho(\mathbf{x}-\mathbf{y})$ is the exponential or delta correlation function. For this initial condition, we can solve the moment equations (12) and (13) by recognizing that $\overline{A'(\mathbf{x},t)A'(\mathbf{y},t)} = -\overline{A'(\mathbf{x},t)B'(\mathbf{y},t)}, f = 2\overline{A'(\mathbf{x},t)B'(\mathbf{y},t)}$ and $g \equiv 0$. Then equation (12) can be reduced to

$$\frac{\partial \overline{A'(\mathbf{x},t)B'(\mathbf{y},t)}}{\partial t} = 2D\Delta\overline{A'(\mathbf{x},t)B'(\mathbf{y},t)}, \tag{21}$$

subject to initial condition (20). The boundary conditions for the infinite d-dimensional domain are given by equation (15). For the one-dimensional domain, equation (21) is subject to the homogeneous boundary conditions that can be obtained from equations (16) and (17). Note that equation (12) for f is exact, and therefore, the system of the moment equations (10) and (21) is also exact.

4.1. Solution of the Moment Equations for Finite One-Dimensional Domain

[25] In a one-dimensional domain, the one-dimensional version of the diffusion equation for the cross covariances satisfies the homogeneous Neumann boundary conditions (17) and the initial condition (7). The solution can be found using the method of separation of variables and is given by

$$\overline{A'(x,t)B'(y^*,t)} = c_0 + \sum_{n=1}^{\infty} c_n(y^*)e^{-2D\frac{n^2\pi^2}{L^2}t}\cos\left(\frac{n\pi x}{L}\right), \tag{22}$$

where $y^* = L/2$,

$$c_0 = -\frac{2l\sigma^2}{L}\left[1 - e^{-\frac{L}{2l}}\right], \tag{23}$$

$$c_n = -\frac{2l\sigma^2}{L}\left[2\cos\left(\frac{n\pi}{2}\right) - e^{-\frac{L}{2l}} - e^{-\frac{L}{2l}}\cos(n\pi) + \frac{n\pi l}{L}e^{-\frac{L}{2l}}\sin(n\pi)\right] \times \left(1 + \frac{n^2\pi^2 l^2}{L^2}\right)^{-1}. \tag{24}$$

[26] The variance of the concentrations A and B is

$$\overline{A'A'}(t) = \overline{B'B'}(t) = -\overline{A'(y^*,t)B'(y^*,t)}, \tag{25}$$

and the mean concentrations $\overline{A}(t)$ and $\overline{B}(t)$ ($\overline{A}(t) = \overline{B}(t)$) satisfy the nonlinear ordinary differential equation:

$$\frac{\partial \overline{I}}{\partial t} = -k\overline{I}^2 - k\overline{A'(y^*,t)B'(y^*,t)}, \qquad I = A, B. \tag{26}$$

[27] In general, this equation should be solved numerically. For very large domains and/or early times ($Dt/L^2 \ll 1$), the series in equation (22) converges slowly, but the solution for this case can be simplified by solving the diffusion-reaction equation in the infinite domain ($L \to \infty$ limit).

4.2. Solution in the $L \to \infty$ Limit

[28] In a system with observation time much smaller than $\frac{L^2}{D}$, we can assume that the domain Ω is infinite. Then equation (21), subject to boundary condition (15) and initial cross covariance $\overline{A'(\mathbf{x},0)B'(\mathbf{y}^*,0)}$, has a solution [*Carslaw and Jaeger*, 1972]:

$$\overline{A'(\mathbf{x},t)B'(\mathbf{y}^*,t)} = \frac{1}{\sqrt{8\pi Dt}}\int_{\Omega}\exp\left[-\frac{(\mathbf{x}-\mathbf{z})^2}{8Dt}\right]\overline{A'(\mathbf{x},0)B'(\mathbf{y}^*,0)}\,d\mathbf{z}. \tag{27}$$

4.2.1. Initial Exponential Correlation of Fluctuations

[29] In a one-dimensional domain, the cross covariance (27), subject to the initial condition (7), is given by

$$\overline{A'(x,t)B'(y^*,t)} = -\frac{\sigma^2}{\sqrt{8\pi Dt}}\int_{-\infty}^{\infty}\exp\left[-\frac{(x-z)^2}{8Dt}\right]\cdot\exp\left[-\frac{|z-y^*|}{l}\right]dz. \tag{28}$$

[30] The variance and covariance of the concentrations can be found by setting $x = y^*$ in equation (28) such that

$$\overline{A'(y^*,t)A'(y^*,t)} = \overline{B'(y^*,t)B'(y^*,t)} = -\overline{A'(y^*,t)B'(y^*,t)} = \sigma^2\exp\left[\frac{2Dt}{l^2}\right]\left[\mathrm{erf}\left(\frac{\sqrt{2Dt}}{l}\right) - 1\right]. \tag{29}$$

This is a function of time only, and not of space. Expanding this solution in a Taylor series and gathering low-order terms yields a simplified form for the cross variance (and the variances of the concentrations):

$$\overline{A'(y^*,t)B'(y^*,t)} = \overline{A'B'}(t) = \begin{cases} -\sigma^2\left(1 - \left(\frac{8D}{\pi l^2}\right)^{\frac{1}{2}}t^{\frac{1}{2}}\right), & t \ll \frac{t_D}{2} \\ -\sigma^2\left(\frac{l^2}{2\pi D}\right)^{\frac{1}{2}}t^{-\frac{1}{2}}, & t \gg \frac{t_D}{2}. \end{cases} \tag{30}$$

4.2.2. Initially Delta-Correlated Fluctuations

[31] For initially delta function correlated A and B, the cross covariance in the d-dimensional domain takes the form

$$\overline{A'(\mathbf{x},t)B'(\mathbf{y}^*,t)} = -\frac{\sigma^2 l^d}{(8\pi Dt)^{d/2}}\int_\Omega \exp\left[-\frac{(\mathbf{x}-\mathbf{z})\cdot(\mathbf{x}-\mathbf{z})}{8Dt}\right]\delta(\mathbf{z}-\mathbf{y}^*)dz = -\frac{\sigma^2 l^d}{(8\pi Dt)^{d/2}}\exp\left[-\frac{(\mathbf{x}-\mathbf{y}^*)\cdot(\mathbf{x}-\mathbf{y}^*)}{8Dt}\right]. \tag{31}$$

Setting $\mathbf{x}=\mathbf{y}^*$, we obtain an expression for the variance and covariance of the concentrations:

$$\overline{A'(t)A'(t)} = -\overline{A'(t)B'(t)} = \frac{\sigma^2 l^d}{(8\pi Dt)^{d/2}}. \tag{32}$$

[32] The solution for the variance of A, equation (32), is obtained by approximating the exponential autocorrelation function with a delta autocorrelation function. This approximation is not valid for small times. For example, at time $t = 0$ the variance of the concentration should be equal to σ^2, but equation (32) results in an infinite variance. Also, the averaged concentration, obtained from equations (10) and (32), increases for times smaller than

$$t < \frac{t_D}{8\pi}, \tag{33}$$

which is unphysical for the reaction system considered here. To rectify the situation with equation (32), we neglect time smaller than $t=t_D/8\pi$, essentially assuming that no, or negligible, reaction occurs until then. At time $t=t_D/8\pi$ the variance of A, given by equation (32), is equal to the initial variance, $\overline{A'A'}(t_D)=\sigma^2$, and for time $t>t_D$ the average concentration decreases with time, as should be the case for the irreversible reaction studied here. We shift time by introducing a new variable, $\tau=t-t_D/8\pi$, and rewrite equation (10) as

$$\frac{\partial\bar{\tilde{A}}}{\partial\tau} = -k\bar{\tilde{A}}^2 + k\frac{\sigma^2 l^d}{(8\pi D)^{d/2}}\left(\tau+\frac{t_D}{8\pi}\right)^{-d/2}, \quad \tau>0, \tag{34}$$

subject to the initial condition

$$\bar{\tilde{A}}(\tau=0) = A_0, \tag{35}$$

where $\tilde{A}(\tau)=A(t+t_D/8\pi)$. The solution of equation (34) can be found analytically as

$$\bar{\tilde{A}}(\tau) = -\frac{\sqrt{-ak}\left(\tau+\frac{t_D}{8\pi}\right)^{1-\frac{d}{4}}\left(c_1 J_{b_1}(w) - c_1 J_{b_2}(w) - 2J_{-b_1}(w)\right) - c_1 J_{b_3}(w)}{2k\left(\tau+\frac{t_D}{8\pi}\right)\left(c_1 J_{b_3}(w) + J_{-b_3}(w)\right)}, \tag{36}$$

where c_1 is given by the initial condition (35), $J_a(z)$ is a Bessel function of the first kind, and

$$a = \frac{\sigma^2 l^d}{(8\pi D)^{\frac{d}{2}}}, \qquad w = \frac{4\sqrt{-ak}}{4-d}\left(\tau+\frac{t_D}{8\pi}\right)^{1-\frac{d}{4}}, \qquad b_1 = \frac{2-d}{4-d}, \qquad b_2 = \frac{6-d}{4-d}, \tag{37}$$

$$b_3 = -\frac{2}{4-d}. \tag{38}$$

Setting $d = 1$ in equation (32) recovers the scaling behavior of the one-dimensional covariance with initial exponential correlation, equation (30), for $t > t_D/2$. This means that for times greater than $t > t_D/2$, the average concentration forgets the initial correlation of the fluctuations and the initial δ correlated can be taken as a good approximation. For time smaller than t_0, the solution can be obtained using the covariance function (30).

[33] Defining a new variable, $r = |\mathrm{x}-\mathrm{y}|$, we rewrite equation (31) as $\overline{A'A'}(r,t) = -\frac{\sigma^2 l^d}{(8\pi Dt)^{d/2}}\exp\left[-\frac{r^2}{8Dt}\right]$. The correlation length of the fluctuations can be defined as

$$\lambda(\tau) = \int_0^\infty \frac{\overline{A'A'}(r,\tau)}{\overline{A'A'}(0,\tau)}dr = \int_0^\infty \exp\left(-\frac{r^2}{8D\left(\tau+\frac{t_D}{8\pi}\right)}\right)dr = \sqrt{2\pi D\left(\tau+\frac{t_D}{8\pi}\right)}. \tag{39}$$

[34] The correlation length is a measure of the average size of a subdomain where one of the two reactants is absent. For time $\tau \gg \frac{t_D}{8\pi}$, λ grows as $(D\tau)^{\frac{1}{2}}$. In this regime, the concentration field is composed of segregated "islands" of A and B [*Kang and Redner*, 1985]. Then $\lambda(t)$ becomes a statistical measure of the size of these islands, and according to equation (39) the size grows with time as $t^{\frac{1}{2}}$. A similar scaling law for the size of the islands was phenomenologically postulated, but not explicitly derived, by *Kang and Redner* [1985].

5. Moment Equations for A and B With Initially Zero Cross Correlation

[35] Here we consider a case when A and B are initially uncorrelated, $\overline{A'(x,0)B'(y,0)} = 0$. We obtain a solution for the mean and variance of the concentrations in a one-dimensional infinite domain. For conciseness, here we consider a solution for the delta function correlation. The solution for the exponential correlation function can be obtained in a similar way. Using the delta function approximation of the exponential autocovariance function for A and B, equations for the mean and variance of the concentration have the form (Appendix B)

$$\overline{A'B'}(t) = \frac{\sigma^2 l}{2\sqrt{8\pi Dt}}\left[e^{-4k\int_0^t \overline{A}(t')dt'} - 1\right], \qquad t>0, \tag{40}$$

$$\frac{\partial\overline{A}}{\partial t} = -k\overline{A}^2 - k\frac{\sigma^2 l}{2\sqrt{8\pi Dt}}\left[e^{-4k\int_0^t \overline{A}(t')dt'} - 1\right], \qquad t>0, \tag{41}$$

$$\overline{A'A'}(t) = \frac{\sigma^2 l}{2\sqrt{8\pi D t}}\left[e^{-4k\int_0^t \overline{A}(t')dt'} + 1\right], \qquad t > 0, \tag{42}$$

subject to the initial condition $\overline{A}(t=0) = A_0$.

[36] As in the case of initially anticorrelated A and B, using the δ correlation approximation of the exponential correlation function leads to an unphysical behavior such as infinite variance of the concentrations, $\overline{A'A'}(t)$, at time zero. To make use of the δ correlation approximation, we assume that the reaction does not occur until $t = t_D/8\pi$ and equations (40)–(42) can be rewritten using a new variable, $\tau = t - t_D$, as

$$\overline{A'B'}(\tau) = \frac{\sigma^2 l}{2\sqrt{8\pi D(\tau + t_D/8\pi)}}\left[e^{-4k\int_0^\tau \overline{A}(\tau')d\tau'} - 1\right], \quad \tau > 0, \tag{43}$$

$$\frac{\partial \overline{A}}{\partial \tau} = -k\overline{A}^2 - k\frac{\sigma^2 l}{2\sqrt{8\pi D(\tau + t_D/8\pi)}}\left[e^{-4k\int_0^\tau \overline{A}(\tau')d\tau'} - 1\right], \quad \tau > 0, \tag{44}$$

$$\overline{A'A'}(\tau) = \frac{\sigma^2 l}{2\sqrt{8\pi D(\tau + t_D/8\pi)}}\left[e^{-4k\int_0^t \overline{A}(\tau')d\tau'} + 1\right], \quad \tau > 0, \tag{45}$$

subject to the initial condition $\overline{A}(\tau = 0) = A_0$.

[37] The covariance of A is given by equation (B16). The correlation length is given by

$$\lambda(\tau) = \int_0^\infty \frac{\overline{A'A'}(r,\tau)}{\overline{A'A'}(0,\tau)}\,dr = \int_0^\infty \exp\left(-\frac{r^2}{8D(\tau + t_D/8\pi)}\right)dr = \sqrt{2\pi D(\tau + t_D/8\pi)}, \tag{46}$$

which at late times scales as $\tau^{\frac{1}{2}}$. This is the same scaling behavior as we saw earlier for the correlation length for fluctuations with initial anticorrelation (equation (39)). The comparison of equations (39) and (46) shows that the correlation length of A (and B) for initially anticorrelated A and B grows with the same rate as the correlation length for initially uncorrelated A and B.

6. Results: Impact of Concentration Fluctuations on Effective Kinetics

6.1. Infinite Domain

[38] For the anticorrelated case, Figures 1 and 2 show the averaged concentration and the standard deviation of the concentration for two different Damköhler numbers, $Da = \frac{t_D}{t_k} = \frac{A_0 k l^2}{2D}$, defined as the ratio between the characteristic diffusion and reaction times, $t_D = \frac{l^2}{2D}$ and $t_k = \frac{1}{A_0 k}$. In Figure 3 we compare the anticorrelated case with the zero cross-correlated case. In Figures 1–3, at early times when variance and covariance of the concentrations are relatively small, $\overline{A}$ and $\overline{B}$ follow the deterministic solution (19). At later times, when $\overline{A}$ and $\overline{B}$ become comparable to $\sqrt{-\overline{A'B'}}$,

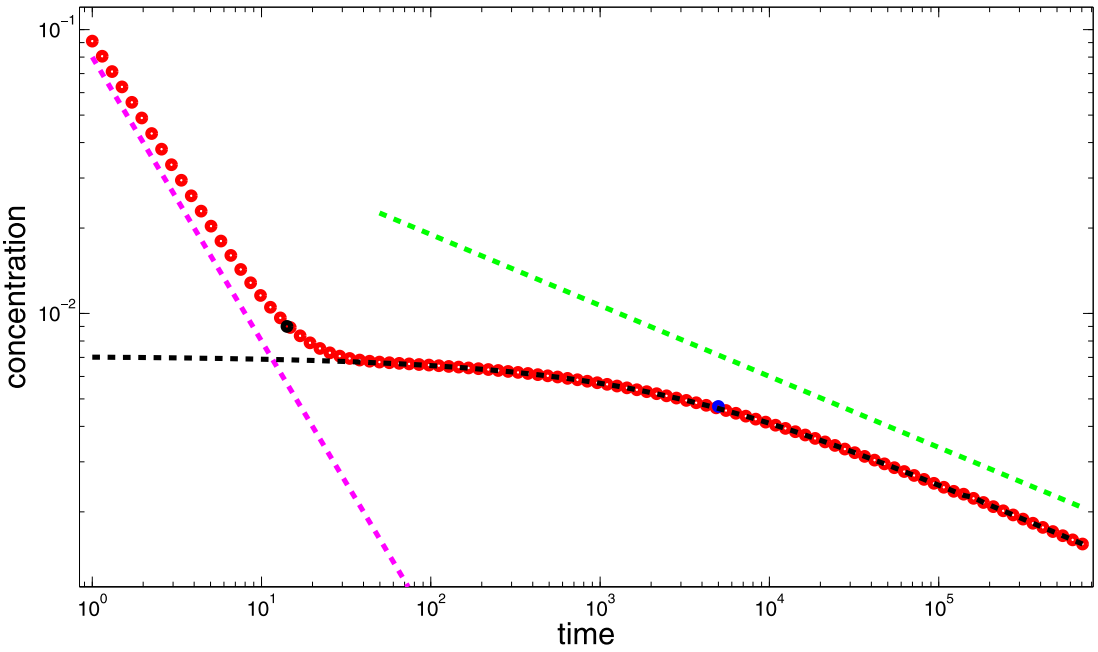

Figure 1. Average concentration (red dotted line) versus time in a one-dimensional infinite domain. The blue dot is the concentration at the diffusion time $t_D = \frac{l^2}{2D}$, and the black dot is the concentration at the transition time given by equation (50). The black dashed line is $\sqrt{-\overline{A'B'}}$, the magenta dashed line shows t^{-1} scaling, and the green line shows $t^{-1/4}$ scaling. The parameters are $l = 0.1$, $D = 10^{-6}$, $\sigma^2 = 10^{-5}$, and $k = 10$, which correspond to $Da > C_{\nu 0}$.

the average concentration deviates from the deterministic solution. Note that the term $\overline{A'B'}$ is negative for all the initial conditions considered (equations (29), (32) and (43)). Therefore, $-\overline{A'B'}$ is a source term while $-A^2$ is a sink term for equation (10), and the system dynamically balances at $\overline{I} \approx \sqrt{-\overline{A'B'}}$ $(I = A, B)$. Since $\overline{A'B'} \approx t^{-d/2}$ (equations (30), (32) and (43)), the average concentration switches its behavior from t^{-1} to $t^{-d/4}$. The coefficient of variation,

$$C_v(t) = \frac{\sqrt{\overline{A'A'}(t)}}{\overline{A}(t)}, \tag{47}$$

increases with time and asymptotically approaches unity. For the early times, $\overline{A}^2 \gg \overline{A'A'} = -\overline{A'B'}$ and the term $k\overline{A'B'}$ in equation (26) can be ignored. Thus, $\overline{A}$ behaves like the deterministic concentration, $A_{det} = \frac{\overline{A}_0}{\overline{A}_0 kt+1}$. As time increases, so does the covariance term $-k\overline{A'B'}$ relative to the reaction term $k\overline{A}^2$, and this slows the decay of $\overline{A}$.

[39] Figure 3 compares the mean and the standard deviation of the concentrations for different initial cross correlations of fluctuations of A and B. The solutions are obtained for one-dimensional infinite domains for initially anticorrelated (equation (8)) and uncorrelated (equation (9)) fluctuations. In both cases, the initial autocovariance function (5) is assumed. Figure 3 shows that the variance of the concentration A (and B) is larger for initially anti-cross-correlated fluctuations than for initially uncorrelated fluctuations for all times greater than zero. The same is true for the average concentrations. Also, average concentrations for initially anti-cross-correlated fluctuations transition earlier to the $t^{-1/4}$ behavior than the average concentrations with initially uncorrelated fluctuations.

6.2. Finite Domain

[40] Figures 4–6 show the average one-dimensional concentration $\overline{A}(t)$ versus time for various parameters obtained from the numerical integration of equation (26). Figure 4 depicts $\overline{A}$ versus t for various domain sizes L. The azure line shows the deterministic solution (19) without the fluctuations. This solution decreases to zero as t^{-1} after $t > (A_0 k)^{-1}$. As for the infinite domain, the average concentration first follows the deterministic solution (scales as t^{-1}), but later the scaling of the average concentration changes to $t^{-1/4}$ and finally asymptotically approaches c_0. Thus, the fluctuations slow the rate of decrease in the concentration. As the domain size L increases, the solution rapidly approaches the solution for the infinite domain.

[41] As a result of the reaction, the average concentration decreases from its initial value to an asymptotic value c_0 (equation (23)) that depends on the initial variance of the concentration, the correlation length, and the size of the domain. This means that, on average, not all of A and B react. This is because owing to initial random fluctuations in concentrations A and B, in a domain of finite size in each particular realization, the initial total mass of A is not exactly equal to the initial total mass of B. This shows that the random concentration field in a finite domain has not attained

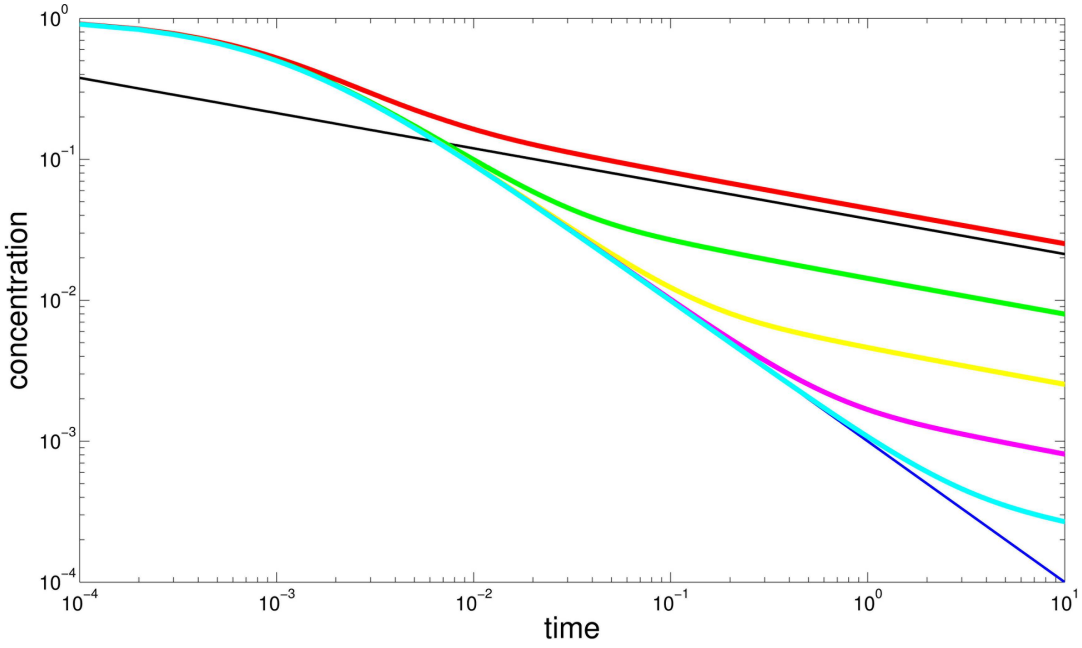

Figure 2. Average concentration (red dotted line) versus time in a one-dimensional infinite domain. The blue dot is the concentration at the diffusion time $t_D = \frac{l^2}{2D}$, and the black dot is the concentration at the transition time given by equation (50). The black dashed line is $\sqrt{-\overline{A'B'}}$, the magenta dashed line shows t^{-1} scaling, and the green line shows $t^{-1/4}$ scaling. The parameters are $l = 0.1$, $D = 10^{-2}$, $\sigma^2 = 10^{-5}$, and $k = 10$, which correspond to $1 < Da < C_{v0}$.

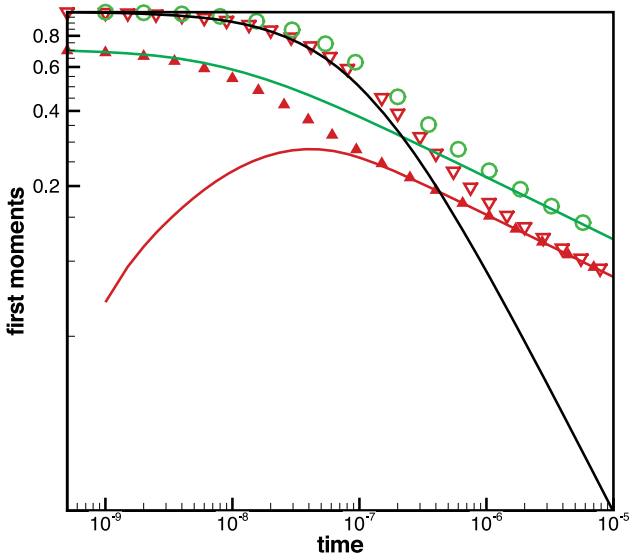

Figure 3. Average concentration and the standard deviation of the concentration for initial fluctuations with zero cross correlation and anti–cross correlation in an infinite one-dimensional domain. Red open triangles depict the average concentration for initially uncorrelated fluctuations. Open green circles denote the average concentration for initially anticorrelated fluctuations. The red line is $\sqrt{-\overline{A'B'}(t)}$ for initially uncorrelated fluctuations. Red solid triangles depict $\sqrt{\overline{A'A'}(t)}$ for initially uncorrelated fluctuations. The green line is $\sqrt{-\overline{A'B'}(t)} = \sqrt{\overline{A'A'}(t)}$ for initially anticorrelated fluctuations. The black line is A_{det}. The values of the parameters are $l = 0.00015$, $D = 0.1$, $\sigma^2 = 0.5$, $k = 10^7$, and $Da = 2.25$.

ergodic conditions and the spatial average of the concentration in each particular realization is not equal to its ensemble average. Problems associated with ergodicity are common in the application of stochastic models to water resources. The system becomes ergodic as the domain size approaches infinity. The standard deviation of the concentrations decreases from its initial value to the constant c_0. The asymptotic value c_0 goes to zero with decreasing l/L and decreasing initial variance of the fluctuations.

[42] Figure 5 displays $\overline{A}$ versus t for various correlation lengths l. The solution for the average concentration with initial correlation length $l = 0$ is equivalent to the solution for deterministic concentration (blue line). For $l > 0$, the average concentration follows the deterministic solution (decreases as t^{-1}) at early times, but later the average concentration decays as $t^{-1/4}$ and eventually approaches the asymptotic value c_0.

[43] Figure 6 shows $\overline{A}$ versus t for different σ^2. In the limit $\sigma^2 = 0$, the system is a deterministic homogeneous mixture and the solution for $\overline{A}$ is given by A_{det} (blue line). For $\sigma^2 > 0$, $\overline{A}$ follows A_{det} (decreases as t^{-1}) at the early time, and later $\overline{A}$ decays as $t^{-1/4}$ and eventually approaches the asymptotic value c_0.

[44] It is evident from Figures 4–6 that disregarding fluctuations leads to an overestimation of the extent of the reaction and an underestimation of the averaged concentration. The error increases with increasing σ^2 and l and decreasing L. Such quantitative results play an important role in determining reaction rates in real systems such as porous media or turbulent streams where mixing is often incomplete and segregation of reactants into islands is commonplace. The analysis in this work is presented to provide an analytical foundation for extensions to such cases.

7. Characteristic Transition Time t^*

[45] In a purely diffusive system, the variance of the fluctuations, σ^2, is usually small, regardless of the origin of the fluctuations. Therefore, the initial coefficient of variation, C_{v0}, should be a small number:

$$0 < C_{v0} = \frac{\sigma}{A_0} < 1. \tag{48}$$

[46] We demonstrated above that in the diffusion-reaction system, equation (1), for any nonzero $C_{v0} = C_v(0)$ at late times $C_v(t)$ approaches unity. The asymptotic increase of the coefficient of variation from an arbitrarily small value to unity is the primary cause of different early and late time scalings of the average concentrations.

[47] Here we derive estimates for the characteristic transition time t^* after which the scaling behavior of the average concentrations change to $t^{-d/4}$. We obtain the estimates of t^* for diffusion and reaction in infinite d-dimensional domains for fluctuations with different initial autocorrelation and cross correlation.

7.1. Infinite One-Dimensional Domain: Initially Anticorrelated Fluctuations With Exponential Autocovariance Function

[48] For early times, $C_v \ll 1$; therefore, the average concentrations are well described by the solution for the deterministic concentration A_{det}. The solution will deviate from A_{det} at time t^*, when the term $\overline{A'B'}$ is comparable to $-A^2$.

[49] The characteristic time t^* can be found as the solution of an algebraic equation:

$$A_{det}(t^*) = \sqrt{-\overline{A'B'}(t^*)}. \tag{49}$$

The solution of this equation depends on the Damköhler number, $Da = \frac{A_0 k l^2}{D}$. For times greater than the characteristic chemical time $t_k = \frac{1}{A_0 k}$, the deterministic solution decreases as $A_{det} \sim (kt)^{-1}$.

[50] We consider t^* for different Damköhler numbers: (1) $Da > C_{v0}^{-1}$, fast reaction and $t_k < t_D$ (Figure 1); (2) $1 < Da < C_{v0}^{-1}$, medium reaction and $t_k < t_D$ (Figure 2); and (3) $Da < 1$, slow reaction and $t_k > t_D$.

7.1.1. Case 1: $Da > C_{v0}^{-1}$

[51] The curves for $A_{det}(t)$ and $\sqrt{-\overline{A'B'}(t)}$ intersect at time t^* such that: $t_k \ll t^* \ll t_D$. Within this interval, $A_{det}(t) \approx \frac{1}{kt}$ and $\sqrt{-\overline{A'B'}} \approx \sigma$, and the solution of equation (49) is

$$t^* = \frac{1}{k\sigma} = t_k C_{v0}^{-1}. \tag{50}$$

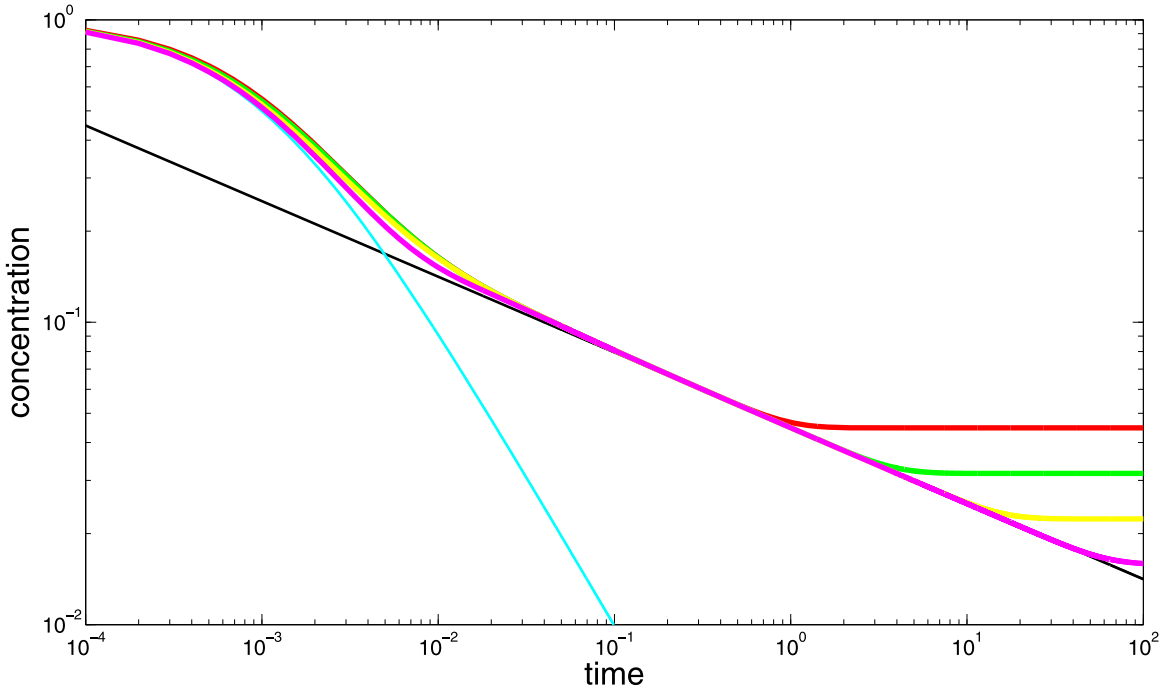

Figure 4. Average concentration in the finite one-dimensional domain versus time as a function of the domain of size L: red line, $L = 0.5$; green line, $L = 1$; yellow line, $L = 2$; magenta line, $L = 4$. For all curves, $l = 0.001$, $D = 0.01$, $\sigma^2 = 0.5$, and $k = 1000$. The azure line is the A_{det} solution. The black line represents the law $t^{-\frac{1}{4}}$.

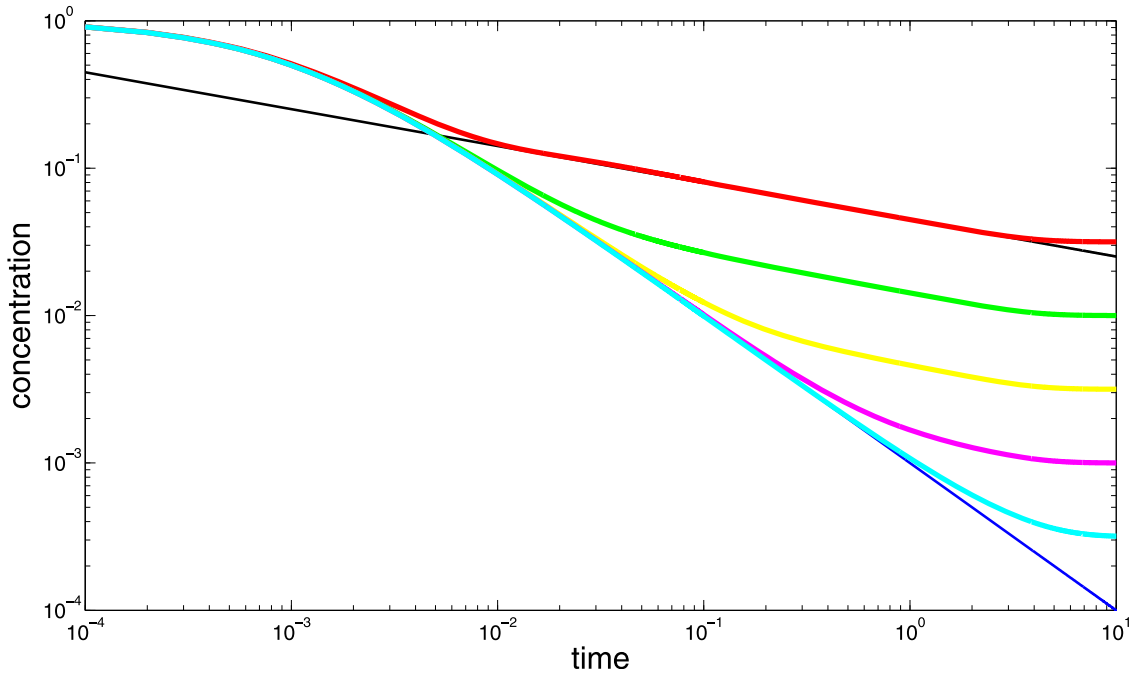

Figure 5. Average concentration in the finite one-dimensional domain versus time as a function of the correlation length l: red line, $l = 10^{-3}$; green line, $l = 10^{-4}$; yellow line, $l = 10^{-5}$; magenta line, $l = 10^{-6}$; azure line, $l = 10^{-7}$; blue line, $l = 0$. For all curves, $L = 1$, $D = 0.01$, $\sigma^2 = 0.5$, and $k = 1000$. The black line represents the law $t^{-\frac{1}{4}}$.

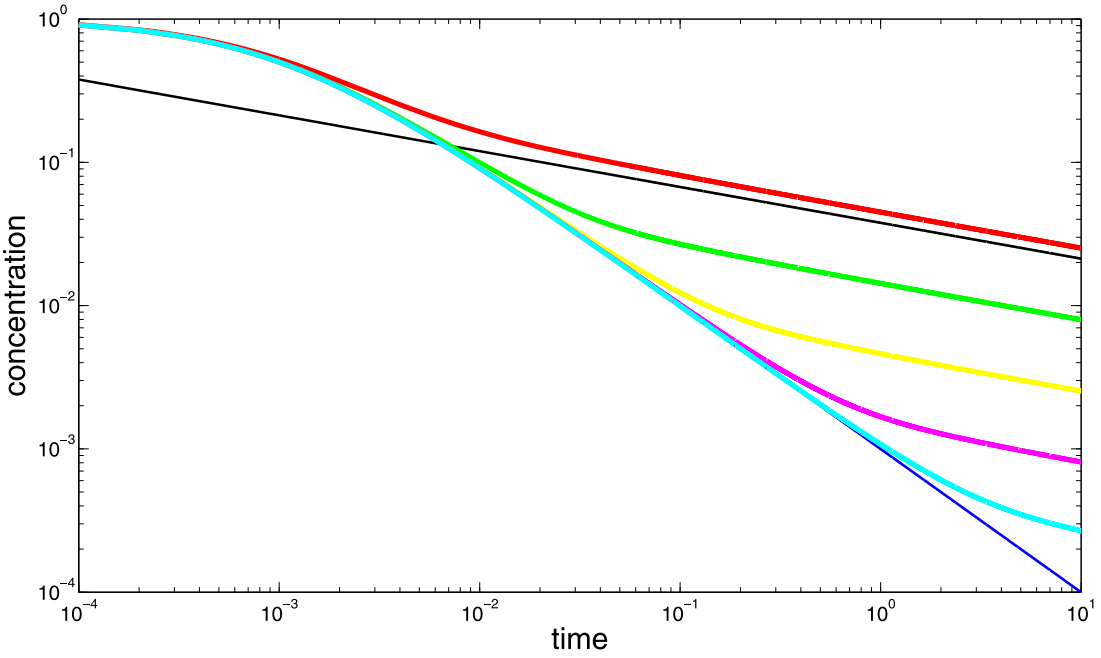

Figure 6. Average concentration versus time in the finite domain of size L: red line, $\sigma^2 = 5 \times 10^{-2}$; green line, $\sigma^2 = 5 \times 10^{-3}$; yellow line, $\sigma^2 = 5 \times 10^{-4}$; magenta line, $\sigma^2 = 5 \times 10^{-5}$; azure line, $\sigma^2 = 5 \times 10^{-6}$. For all curves, $L = 1$, $D = 5 \times 10^{-6}$, $l = 0.001$, and $k = 1000$. The blue curve is the A_{det} solution, and the black line represents the scaling $t^{-\frac{1}{4}}$.

7.1.2. Case 2: $C_{v0}^{-1} > Da > 1$

[52] The two curves, A_{det} and $\sqrt{-\overline{A'B'}}$, cross at time $t^* > t_D$. For $t > t_D$, $A_{det}(t) \approx \frac{1}{kt}$ and $\sqrt{-\overline{A'B'}} \approx \sigma(\frac{l^2}{2\pi D})^{\frac{1}{4}} t^{-\frac{1}{4}}$, and the solution of equation (49) is

$$t^* = t_k \left(\frac{\pi}{Da C_{v_0}^4} \right)^{\frac{1}{3}}. \tag{51}$$

[53] Figures 1 and 2 show the exact solutions for $Da > C_{v0}^{-1}$ and $C_{v0}^{-1} > Da > 1$, respectively. Figures 1 and 2 demonstrate that t^*, calculated from equations (50) or (51) (depending on the magnitude of Da), accurately predicts deviation of the average concentration from $A_{det}(t) \sim t^{-1}$ to $\sim t^{-1/4}$ behavior.

7.1.3. Case 3: $\mathcal{D} < 1$

[54] In this case, $t_k > t_D$. To estimate t^*, we can use the same approximations for A_{det} and $\sqrt{-\overline{A'B'}}$ as in case 2. Then t^* is given by equation (51). The characteristic transition time increases with decreasing Damköhler number (and the reaction rate k). Consequently, for very small Da the average concentrations will not be affected by the spatial fluctuations and will be well described by the solution $A_{det}(t)$.

7.2. Infinite d-Dimensional Domain: Initially Anticorrelated Fluctuations With δ Autocovariance Function

[55] Next we consider an approximate solution for an infinite n-dimensional domain with initial delta-autocorrelated and anti-cross-correlated fluctuations. The two curves, A_{det} and $\sqrt{-\overline{A'B'}}$, cross at time $t^* > t_k$. For $t > t_k$, $A_{det}(t) \approx \frac{1}{kt}$ and $\sqrt{-\overline{A'B'}} = \sigma \left[\frac{l^2}{8\pi D} \right]^{\frac{d}{4}} t^{-\frac{d}{4}}$, and the solution of equation (49) is

$$t^* = t_k^{\frac{4}{4-d}} t_D^{\frac{d}{d-4}} C_{v0}^{\frac{4}{d-4}} (4\pi)^{\frac{d}{4-d}}. \tag{52}$$

[56] For time $t > t^*$, the average concentrations are given by

$$\overline{A(t)} = \overline{B(t)} = \sqrt{-\overline{A'(t)B'(t)}} = \frac{A_0 C_{v0}}{(8\pi)^{d/4}} t_D^{\frac{d}{4}} t^{-\frac{d}{4}}. \tag{53}$$

[57] This asymptotic scaling of the average concentrations with time, $t^{-d/4}$ agrees with the asymptotic scaling results of *Toussaint and Wilczek* [1983], *Kang and Redner* [1985], and *Benson and Meerschaert* [2008].

7.3. Infinite One-Dimensional Domain With Zero Cross Correlation

[58] Finally, to study the effect of the initial cross correlation between fluctuations of A and B we consider an approximate solution for an infinite one-dimensional domain with delta-autocorrelated and zero-cross-correlation fluctuations. The two curves, A_{det} and $\sqrt{-\overline{A'B'}}$, cross at time $t^* > t_k$. For $t > t_k$, $A_{det}(t) \approx \frac{1}{kt}$ and $\sqrt{-\overline{A'B'}} \approx \sqrt{0.5}\sigma \left[\frac{l^2}{8\pi D} \right]^{\frac{1}{4}} t^{-\frac{1}{4}}$, and the solution of equation (49) is

$$t^* = t_k^{\frac{4}{3}} t_D^{-\frac{1}{3}} C_{v0}^{-\frac{4}{3}} (8\pi)^{\frac{1}{3}}. \tag{54}$$

[59] Comparing equation (54) and the one-dimensional version of equation (52) shows that the characteristic

transition time t^* for initially uncorrelated fluctuations is $2^{1/3}$ times greater than the transition time for the initially anti-cross-correlated concentrations.

8. Conclusions

[60] In the absence of fluctuations, the concentration of solutes during chemical reaction $A + B -> C$ decays as $A_{det} = B_{det} \sim t^{-1}$. Contrary to this, experimental and numerical studies suggest that concentrations decay significantly slower. Existing theory suggests a $t^{-d/4}$ scaling in the asymptotic regime (d is the dimensionality of the problem). We have studied the effect of spatial concentration fluctuations in this nonlinear irreversible reaction using the classical diffusion-reaction equation with random initial conditions, where the initial concentrations of the reactants were treated as correlated random fields. We used the moment equation approach to derive equations for the mean and variance of the concentrations and for the characteristic transition time t^*, a time when scaling of the concentration with time changes to $t^{-d/4}$. The moment equations were used to study the effect of the initial autocorrelation and cross correlation of the concentrations on the leading moments of the concentrations. When fluctuations are driven by thermal noise, the initial statistics of the concentration fluctuations can be found from statistical mechanics [*Ovchinnikov and Zeldovich*, 1978]. If fluctuations are caused by the fluctuations in the advective velocities that mixed two solutes (our analysis is for the case when the flow ceased after fluids were mixed), then the initial statistics of the fluctuations can be found from the moment equation method or polynomial chaos solution of the stochastic advection-dispersion equations [*Morales-Casique et al.*, 2006; *Jarman and Tartakovsky*, 2011; *Lin and Tartakovsky*, 2009, 2010; *Lin et al.*, 2010].

[61] We first considered a case of initially anticorrelated A and B. For d-dimensional ($d = 1, 2, 3$) infinite domain and delta-autocorrelated initial concentrations, we obtained analytical solutions for the mean and variance of the concentrations. At late times, the average concentrations scale as $t^{-d/4}$, which agrees with the classical results of *Toussaint and Wilczek* [1983] and numerical observations [*Benson and Meerschaert*, 2008; *de Anna et al.*, 2011]. For infinite domains, we obtained analytical expressions for t^* as function of Da. The characteristic transition time t^* increases with increasing reaction time, $t_k = \frac{1}{kA_0}$ and decreasing diffusion time and the initial coefficient of variation, C_{v0}.

[62] For equations defined on a one-dimensional finite domain, we obtain an analytical solution for the variance of concentrations. The variance decreases asymptotically from the prescribed value to c_0^2, where the constant c_0 is proportional to initial variance of the concentrations σ^2 and the ratio of the initial correlation length of the concentration l to the size of the domain L. We also obtain a one-dimensional solution for the average concentrations via numerical integration of the corresponding ordinary differential equation. This solution shows that the scaling behavior of the average concentrations changes from $\sim t^{-1}$ to $\sim t^{-1/4}$ at t^* that increases with increasing L and decreasing l and σ^2.

[63] Our analytical results support earlier explanations of the change in the scaling behavior of the average concentrations from $A_{det} = B_{det} \sim t^{-1}$, that attributed it to the presence of islands of segregated A and B. Our solutions for various parameters indicate that the transition in the scaling behavior occurs at t^* when (1) A and B are anticorrelated and (2) the cross covariance $\overline{A'B'}$ is equal to the square mean concentration $\overline{A}^2$ (or $\overline{B}^2$). Hence, we conclude that these are the conditions describing the formation of the islands of A and B (i.e., parts of the domain occupied dominantly by species A or B).

[64] The comparison of different initial cross correlations of A and B shows that, for initially uncorrelated fluctuations, t^* is $2^{1/3}$ times greater than the transition time for the initially anti-cross-correlated concentrations. On the other hand, the correlation length of the concentrations growth as $(Dt)^{\frac{1}{2}}$ regardless of the initial cross correlation. The increasing autocorrelation of the concentrations A and B and negative (anti) cross correlation between A and B indicate that A and B segregate into separate islands. The size of the islands is statistically related to the correlation length of the concentrations and our solution suggests that the islands grow as $(Dt)^{\frac{1}{2}}$. A similar scaling law for the size of the islands was phenomenologically postulated in [*Kang and Redner*, 1985].

[65] For very small Da, our results show that the chemical reaction is slow and that diffusion has enough time to mix the system, destroying all the islands of segregated A and B.

[66] We illustrate that fluctuations in concentration have an important role on reactive transport and disregarding the fluctuations can lead to erroneous results. Even though our solutions are derived for the diffusion-reaction equation, they can also be applied to the advection-dispersion-reaction (ADR) equations ($\partial I/\partial t + \mathbf{u} \cdot \nabla I = \mathbf{D}\nabla^2 I - kAB$, $I = AB$) with a uniform advection velocity field ($\mathbf{u}$ = const) and a constant dispersion coefficient $\mathbf{D}$. This is because the ADR equation can be reduced to a diffusion-reaction equation with an anisotropic diffusion coefficient via the Galilean transformation [e.g., *Farlow*, 1982]. We should note that while there are convincing experimental and numerical findings that our analysis accurately describes the behavior of purely diffusive-reactive systems, we are not aware of any experimental results or direct pore-scale simulations that confirm transition to $t^{-d/4}$ scaling for advection-dispersion-reaction systems. Furthermore, the ADR equation accounts only for the first and second moments of a pore-scale velocity distribution (the first moment gives the Darcy scale advective velocity, and the second moment contributes to the dispersion coefficient). Hence, the ADR equation may not be a good model for a multicomponent reactive transport in porous media, because pore-scale velocity affects mixing-controlled reactions in many different ways. For example, variations in pore-scale velocity may prevent or delay segregation of reactants. On the other hand, there is much evidence showing that the deterministic advection-diffusion-reaction equation, which disregards the effect of the concentration fluctuations, overestimates the effective rate of mixing controlled reactions. Further investigations are needed to understand the effect of concentration and pore-scale velocity fluctuations on multicomponent reactive transport in porous media.

Appendix A: Moment Equations

[67] Substituting equation (2) into the diffusion equation yields

$$\frac{\partial(\overline{I}+I')}{\partial t} = D\Delta(\overline{I}+I') - k(\overline{A}+A')(\overline{B}+B'), \qquad I = A, B. \tag{A1}$$

[68] Taking ensemble average yields

$$\frac{\partial \overline{I}}{\partial t} = D\Delta\overline{I} - k\overline{A}\,\overline{B} - k\overline{A'B'}, \qquad I = A, B, \tag{A2}$$

where all the variables are functions of $\mathbf{x}$ and t

[69] Subtracting equation (A2) from equation (A1) gives a diffusion-reaction equation for fluctuations:

$$\frac{\partial I'}{\partial t} = D\Delta I' - k\overline{A}B' - k\overline{B}A' - kA'B' + k\overline{A'B'}, \qquad I = A, B. \tag{A3}$$

[70] To obtain the equations for the variance $\overline{A'(\mathbf{x},t)A'(\mathbf{x},t)}$ and covariance $\overline{A'(\mathbf{x},t)B'(\mathbf{x},t)}$, we write equations for $A'-B'$ and $A'+B'$:

$$\frac{\partial(A'-B')}{\partial t} = D\Delta(A'-B'), \tag{A4}$$

and

$$\frac{\partial(A'+B')}{\partial t} = D\Delta(A'+B') - 2k\overline{A}B' - 2k\overline{B}A' - 2kA'B' + 2k\overline{A'B'}. \tag{A5}$$

[71] We first obtain an equation for $f(\mathbf{x},\mathbf{y},t) = \overline{A'(\mathbf{x},t)B'(\mathbf{y},t)} - \overline{A'(\mathbf{x},t)A'(\mathbf{y},t)}$. To do so, we multiply equation (A4) with $A'(\mathbf{y},t)$:

$$A'(\mathbf{y},t)\frac{\partial(A'(\mathbf{x},t)-B'(\mathbf{x},t))}{\partial t} = D\Delta(A'(\mathbf{x},t)A'(\mathbf{y},t) - B'(\mathbf{x},t)A'(\mathbf{y},t)). \tag{A6}$$

[72] Next, we multiply equation (A4) with $B'(\mathbf{y},t)$:

$$B'(\mathbf{y},t)\frac{\partial(A'(\mathbf{x},t)-B'(\mathbf{x},t))}{\partial t} = D\Delta(A'(\mathbf{x},t)B'(\mathbf{y},t) - B'(\mathbf{x},t)B'(\mathbf{y},t)). \tag{A7}$$

[73] Summing the last two equations, taking ensemble average, and recognizing that for considered boundary conditions,

$$\overline{A}(t) = \overline{B}(t) \tag{A8}$$

$$\overline{A'(\mathbf{x},t)A'(\mathbf{y},t)} = \overline{B'(\mathbf{x},t)B'(\mathbf{y},t)}, \tag{A9}$$

we obtain the equation for f:

$$\frac{\partial f(\mathbf{x},\mathbf{y},t)}{\partial t} = 2D\Delta f(\mathbf{x},\mathbf{y},t). \tag{A10}$$

[74] In a similar manner, we obtain an equation for $g(\mathbf{x},\mathbf{y},t) = \overline{A'(\mathbf{x},t)B'(\mathbf{y},t)} + \overline{A'(\mathbf{x},t)A'(\mathbf{y},t)}$:

$$\frac{\partial g(\mathbf{x},\mathbf{y},t)}{\partial t} = 2D\Delta g(\mathbf{x},\mathbf{y},t) - 4k\overline{A}(\mathbf{x},t)g(\mathbf{x},\mathbf{y},t). \tag{A11}$$

[75] It is important to notice that in the derivations of equation (A11) we disregarded the third moment $\overline{A'B'B'}$. This approximation is only valid for $\sigma/\overline{A}_0 < 1$.

Appendix B: Moment Equations for Uncorrelated A and B

[76] Here we solve the moment equations in one-dimensional infinite domain for A and B with zero cross correlation. Fluctuations of A and B satisfy the initial conditions (5) and (9). We first solve for

$$f(x,y,t) = \overline{A'(x,t)B'(y,t)} - \overline{A'(x,t)A'(y,t)}, \tag{B1}$$

which satisfies

$$\frac{\partial f(x,y,t)}{\partial t} = 2D\Delta_x f(x,y,t), \qquad x,y \in (0,L). \tag{B2}$$

[77] This equation is subject to the initial condition

$$f(x,y,0) = -\sigma^2 l\delta(x-y) \tag{B3}$$

and the homogeneous Dirichlet boundary condition at $x = \pm\infty$. The solution of this equation is [*Carslaw and Jaeger*, 1972]

$$f(x,y^*,t) = -\frac{\sigma^2 l}{(8\pi Dt)^{1/2}}\exp\left[-\frac{(x-y^*)^2}{8Dt}\right] \tag{B4}$$

$$f(t) = \frac{\sigma^2 l}{(8\pi Dt)^{1/2}}. \tag{B5}$$

[78] Next, we solve for $g = \overline{A'(x,t)A'(y,t)} + \overline{A'(x,t)B'(y,t)}$ that satisfies

$$\frac{\partial g(x,y^*,t)}{\partial t} = 2D\Delta_x(x,y^*,t) - 4k\overline{A}(t)g(x,y^*,t). \tag{B6}$$

[79] The Fourier transform of g is

$$\hat{g}(\psi) = \int_{-\infty}^{+\infty} g(x)e^{-2\pi ix\psi}dx. \tag{B7}$$

[80] Multiplying both parts of the equation with $e^{-2\pi ix\psi}$ and integrating over x yields

$$\frac{\partial \hat{g}(\psi,y^*,t)}{\partial t} = -2D\psi^2\hat{g}(\psi,y^*,t) - 4k\overline{A}(t)\hat{g}(\psi,y^*,t), \tag{B8}$$

subject to the initial condition

$$\hat{g}(\psi,y^*,0) = \sigma^2 l e^{-2\pi iy^*\psi}. \tag{B9}$$

[81] The solution of this equation is

$$\hat{g}(\psi, y^*, t) = \sigma^2 l e^{-2\pi i y^* \psi} e^{-2D\psi^2 t - 4k\int_0^t \overline{A}(t')dt'} \tag{B10}$$

[82] The inverse Fourier transform is

$$g(x, y^*, t) = \sigma^2 l \int_{-\infty}^{+\infty} e^{-2\pi i y^* \psi} e^{-2D\psi^2 t - 4k\int_0^t \overline{A}(t')dt'} e^{2\pi i x \psi} d\psi, \tag{B11}$$

or

$$g(x, y^*, t) = \frac{\sigma^2 l}{\sqrt{8\pi D t}} \exp\left[-\frac{(x-y^*)^2}{8Dt} - 4k\int_0^t A(t')dt'\right], \tag{B12}$$

$$g(y^*, y^*, t) = \frac{\sigma^2 l}{\sqrt{8\pi D t}} e^{-4k\int_0^t \overline{A}(t')dt'}. \tag{B13}$$

[83] The covariance is found as

$$\overline{A'B'}(t) = \frac{1}{2}(f(y^*, y^*, t) + g(y^*, y^*, t)) = \frac{\sigma^2 l}{2\sqrt{8\pi D t}}\left[e^{-4k\int_0^t \overline{A}(t')dt'} - 1\right]. \tag{B14}$$

[84] Substituting this into the equation for the average concentration yields

$$\frac{\partial \overline{A}}{\partial t} = -k\overline{A}^2 - k\frac{\sigma^2 l}{2\sqrt{8\pi D t}}\left[e^{-4k\int_0^t \overline{A}(t')dt'} - 1\right]. \tag{B15}$$

[85] The autocovariance of A is

$$\overline{A'(x,t)A'(y^*,t)} = \frac{1}{2}\frac{\sigma^2 l}{\sqrt{8\pi D t}}\left[\exp\left(-4k\int_0^t A(t')dt'\right) + 1\right] \times \exp\left(-\frac{(x-y^*)^2}{8Dt}\right), \tag{B16}$$

and the variance of the concentration is equal to

$$\overline{A'A'}(t) = \overline{A'(y^*,t)A'(y^*,t)} = \frac{\sigma^2 l}{2\sqrt{8\pi D t}}\left[e^{-4k\int_0^t \overline{A}(t')dt'} + 1\right]. \tag{B17}$$

[86] **Acknowledgments.** This research was supported in part by the Advanced Scientific Computing Research Program of the Office of Science, U.S. Department of Energy, at the Pacific Northwest National Laboratory. The Pacific Northwest National Laboratory is operated for the U.S. Department of Energy by Battelle under contract DE-AC06-76RL01830. P. de Anna and T. Le Borgne would like to express thanks for the financial support of the European Commission through FP7 projects: ITN, IMVUL (grant agreement 212298), and Marie Curie ERG grant Reactive Flows (grant agreement 230947). D. Bolster would like to express thanks for financial support via NSF grant EAR-1113704. Any opinions, findings, conclusions, or recommendations do not necessarily reflect the views of the funding agencies.

References

Battiato, I., and D. Tartakovsky (2011), Applicability regimes for macroscopic models of reactive transport in porous media, *J. Contam. Hydrol.*, *120-121*, 18–26.

Battiato, I., D. Tartakovsky, A. Tartakovsky, and T. Scheibe (2009), On breakdown of macroscopic models of mixing-controlled heterogeneous reactions in porous media, *Adv. Water Resour.*, *32*, 1664–1673.

Benson, D., and M. Meerschaert (2008), Simulation of chemical reaction via particle tracking: Diffusion-limited versus thermodynamic rate-limited regimes, *Water Resour. Res.*, *44*, W12201, doi:10.1029/2008WR007111.

Bolster, D., D. Benson, T. Le Borgne, and M. Dentz (2010), Anomalous mixing and reaction induced by superdiffusive nonlocal transport, *Phys. Rev. E*, *82*, 021119.

Bolster, D., F. Valdes-Parada, T. Le Borgne, M. Dentz, and J. Carrera (2011), Mixing in confined stratified aquifers, *J. Contam. Hydrol.*, *120-121*, 198–212.

Carslaw, H. S., and J. C. Jaeger (1972), *Conduction of Heat in Solids*, 2nd ed., Oxford Univ. Press, Oxford, U. K.

de Anna, P., T. Le Borgne, M. Dentz, D. Bolster, and P. Davy (2011), Anomalous kinetics in diffusion limited reactions linked to non-Gaussian concentration, *J. Chem. Phys.*, *135*, 174104, doi:10.1063/1.3655895.

Dentz, M., P. Gouze, and J. Carrera (2011), Effective non-local reaction kinetics for transport in physically and chemically heterogeneous media, *J. Contam. Hydrol.*, *120-121*, 222–236.

Donado, L., X. Sanchez-Vila, M. Dentz, J. Carrera, and D. Bolster (2009), Multicomponent reactive transport in multicontinuum media, *Water Resour. Res.*, *45*, W11402, doi:10.1029/2008WR006823.

Edery, Y., H. Scher, and B. Berkowitz (2009), Modeling bimolecular reactions and transport in porous media, *Geophys. Res. Lett.*, *36*, L02407, doi:10.1029/2008GL036381.

Edery, Y., H. Scher, and B. Berkowitz (2010), Particle tracking model of bimolecular reactive transport in porous media, *Water Resour. Res.*, *46*, W07524, doi:10.1029/2009WR009017.

Farlow, F. J. (1982), *Partial Differential Equations for Scientists and Engineers*, John Wiley, New York.

Hill, J. (1976), Homogeneous turbulent mixing with chemical reactions, *Annu. Rev. Fluid Mech.*, *8*, 135–161.

Jarman, K., and A. Tartakovsky (2011), Divergence of solutions to perturbation-based advection-dispersion moment equations, *Adv. Water Resour.*, *34*, 659670, doi:10.1016/j.advwatres.2011.03.002.

Kang, K., and S. Redner (1985), Fluctuation-dominated kinetics in diffusion controlled reactions, *Phys. Rev. A*, *32*, 435–447.

Le Borgne, T., M. Dentz, D. Bolster, J. Carrera, J. de Dreuzy, and P. Davy (2010), Non-Fickian mixing: Temporal evolution of the scalar dissipation rate in heterogeneous porous media, *Adv. Water Resour.*, *33*, 1468–1475.

Le Borgne, T., M. Dentz, D. Bolster, J. Carrera, J. de Dreuzy, and O. Bour (2011), Persistence of incomplete mixing: A key to anomalous transport, *Phys. Rev. E*, *84*, 4.

Lin, G., and A. M. Tartakovsky (2009), An efficient, high-order probabilistic collocation method on sparse grids for three-dimensional flow and solute transport in randomly heterogeneous porous media, *Adv. Water Resour.*, *32*, 712–722, doi:10.1016/j.advwatres.2008.09.003.

Lin, G., and A. M. Tartakovsky (2010), Numerical studies of three-dimensional stochastic Darcy's equation and stochastic advection-diffusion-dispersion equation, *J. Sci. Comput.*, *43*, 92–117, doi:10.1007/s10915-010-9346-5.

Lin, G., A. M. Tartakovsky, and D. M. Tartakovsky (2010), Random domain decomposition for probabilistic collocation on sparse grids, *J. Comput. Phys.*, *229*, 6995–7012, doi:10.1016/j.jcp.2010.05.036.

Luo, J., M. Dentz, J. Carrera, and P. Kitanidis (2008), Effective reaction parameters for mixing controlled reactions in heterogeneous media, *Water Resour. Res.*, *44*, W02416, doi:10.1029/2006WR005658.

Monson, E., and R. Kopelman (2004), Nonclassical kinetics of an elementary $A + B \rightarrow C$ reaction-diffusion system showing effects of a speckled initial reactant distribution and eventual self-segregation: Experiments, *Phys. Rev. E*, *69*, 021103, doi:10.1103/PhysRevE.69.021103.

Morales-Casique, E., S. Neuman, and A. Guadagnini (2006), Non-local and localized analyses of non-reactive solute transport in bounded randomly heterogeneous porous media: Theoretical framework, *Adv. Water Res.*, *29*, 123855, doi:10.1016/j.advwatres.2005.10.002.

Neuweiler, I., S. Attinger, W. Kinzelbach, and P. King (2003), Large scale mixing for immiscible displacement in heterogeneous porous media, *Transp. Porous Media*, *51*, 287–314.

Ovchinnikov, A., and Y. Zeldovich (1978), Role of density fluctuations in bi-molecular reaction kinetics, *Chem. Phys.*, *28*, 215–218.

Raje, D., and V. Kapoor (2000), Experimental study of biomolecular reaction kinetics in porous media, *Environ. Sci. Technol.*, *34*, 1234–1239.

Sanchez-Vila, X., A. Guadagnini, and D. Fernandez-Garcia (2008), Conditional probability density functions of concentrations for mixing-controlled reactive transport in heterogeneous aquifers, *Math. Geosci.*, *41*, 323–351, doi:10.1007/s11004-008-9204-2.

Sanchez-Vila, X., D. Fernandez-Garcia, and A. Guadagnini (2010), Interpretation of column experiments of transport of solutes undergoing an irreversible bimolecular reaction using a continuum approximation, *Water Resour. Res.*, *46*, W12510, doi:10.1029/2010WR009539.

Tartakovsky, A. (2010), Langevin model for reactive transport in porous media, *Phys. Rev. E*, *82*, 026302.

Tartakovsky, A. M., S. P. Neuman, and R. Lenhard (2003), Immiscible front evolution in randomly heterogeneous porous media, *Phys. Fluids*, *15*(11), 3331–3341.

Tartakovsky, A. M., L. Garcia-Naranjo, and D. M. Tartakovsky (2004a), Transient flow in a heterogeneous vadose zone with uncertain parameters, *Vadose Zone J.*, *3*(1), 154–163.

Tartakovsky, A. M., P. Meakin, and H. Huang (2004b), Stochastic analysis of immiscible displacement of the fluids with arbitrarily viscosities and its dependence on support scale of hydrological data, *Adv. Water Resour.*, *27*, 1151–1166.

Tartakovsky, A. M., D. M. Tartakovsky, and P. Meakin (2008), Stochastic Langevin model for flow and transport in porous media, *Phys. Rev. Lett.*, *101*, 044502, doi:10.1103/PhysRevLett.101.044502.

Tartakovsky, A. M., G. D. Tartakovsky, and T. D. Scheibe (2009), Effects of incomplete mixing on multicomponent reactive transport, *Adv. Water Resour.*, *32*, 1674–1679.

Tartakovsky, D. M., A. Guadagnini, F. Ballio, and A. M. Tartakovsky (2002), Localization of mean flow and apparent transmissivity tensor for bounded randomly heterogeneous aquifers, *Transp. Porous Media*, *49*(1), 41–58.

Tartakovsky, D. M., Z. Lu, A. Guadagnini, and A. M. Tartakovsky (2003), Unsaturated flow in heterogeneous soils with spatially distributed uncertain hydraulic parameters, *J. Hydrol.*, *275*, 182–193.

Toussaint, D., and F. Wilczek (1983), Particle-antiparticle annihilation in diffusive motion, *J. Chem. Phys.*, *78*, 2642–2647.

Willmann, M., J. Carrera, X. Sanchez-Vila, O. Silva, and M. Dentz (2010), Coupling of mass transfer and reactive transport for nonlinear reactions in heterogeneous media, *Water Resour. Res.*, *46*, W07512, doi:10.1029/2009WR007739.

A. Balter and A. M. Tartakovsky, Pacific Northwest National Laboratory, PO Box 999, Richland, WA 99352, USA. (alexandre.tartakovsky@pnl.gov)

D. Bolster, Environmental Fluid Dynamics Laboratories, Department of Civil Engineering and Geological Sciences, University of Notre Dame, Notre Dame, IN 46556, USA.

P. de Anna and T. Le Borgne, Géosciences Rennes, UMR 6118, CNRS, Université de Rennes 1, F-35042 Rennes, France.

Chapter 3

Spreading due to advective processes

In this chapter we focus on the advective component of mixing. Due to the complex spatio-temporal organization of flow fields in heterogeneous media, advective processes are often described in a stochastic framework (e.g. *Dentz et al.* [2011]; *Tel et al.* [2005]). In a Lagrangian framework, the velocity of the particles that constitute the fluid system fluctuate in space and time. Here we analyze pore scale numerical simulations for the flow in a heterogeneous porous medium, observing anomalous dispersion of an advected plume of fluid Lagrangian particles (that do not diffuse). We relate this observation to the spatial correlation of Lagrangian velocities at the pore scale and we derive an effective upscale model based on Continuous Time random Walk of particles that move due to random velocities that are stochastically distributed and spatially correlated.

The work presented in this chapter was made in collaboration with Marco Dentz, research professor at the Department of Geosciences Institute of Environmental Assessment of Barcelona (Spain), Diogo Bolster, Assistant Professor at the University of Notre Dame (Indiana, USA) and Alexander Tartakovsky, scientist at Pacific Northwest National Laboratory (Washington state, USA).

3.1 Anomalous dispersion from pore scale flow heterogeneity

We consider the two dimensional heterogeneous porous medium studied by *Tartakovsky et al.* [2008b], see Figure 3.1. The porous medium is considered fully saturated. To simulate the fluid flow at the pore scale we adopt the smoothed particle hydrodynamics (SPH) approach described in *Tartakovsky et al.* [2008b]. In this SPH model, the fluid is discretized in N_p particles

that flow through the pores with velocities given by the solution of the Navier-Stokes equation

$$\frac{d\boldsymbol{v}}{dt} = -\frac{\nabla p}{\rho} + \frac{\mu}{\rho}\nabla \cdot (\nabla \boldsymbol{v} + \nabla \boldsymbol{v}^T) + \boldsymbol{b} \tag{3.1}$$

for a given set of physical parameters (density ρ, viscosity μ, the body forces $\boldsymbol{b}$ and local pressure p). We will refer to this Lagrangian particle as SPH particles. The porous medium is composed of circular grains of average size $d = 10$ with mean porosity $\phi = 0.42$. The boundary conditions for flux are periodic on all sides. In this numerical method SPH particles, representing elementary fluid volumes, are advected with the flow that is solution of equation (3.1). Advective Lagrangian trajectories are thus given by the trajectories of the SPH particles. The resulting stationary velocity field shows the existence of a braided network of preferential flow paths in channels as well as low velocity, or stagnation, zones (see Figure 3.1a).

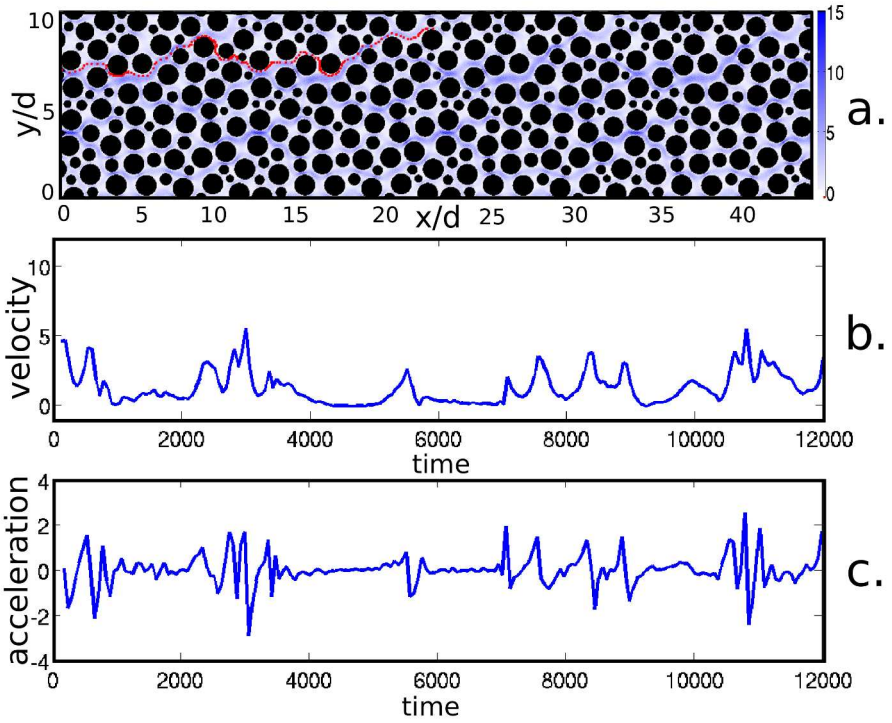

Figure 3.1: *a) the modulus $|v|$ of the flow velocity rescaled by the modulus of the spatially averaged flow velocity $\overline{v}$. The Reynolds number value is $Re = 4$. Coordinates are normalized with d, the average grain diameter. The trajectory of a Lagrangian particle (red dots) is superposed on the amplitude of the velocity field. For the same particle we display: b) the time series of its velocity and c) the time series of its accelerations (both projected along the longitudinal direction).*

The pore scale velocity field, shown in Figure 3.1a, is characterized by high velocity channels and stagnation zones. An example of particle trajectory superposed on the amplitude of the

velocity field is displayed in Figure 3.1a. The particle slows down as it travels close to stagnation zones and accelerates when entering the high velocity channels. Examples of Lagrangian longitudinal velocity v_x and acceleration a_x series along the trajectory are plotted as a function of travel time in Figure 3.1b and 3.1c respectively. A first qualitative observation is that Lagrangian accelerations cannot be represented as a white noise. At each time increment Δt the force driving the motion of a Lagrangian particle is not independent from the force that acted during the previous Δt. Lagrangian accelerations are characterized by periods of high variability, corresponding to the high velocity channels, and periods of low variability and, thus, of high correlation with low velocity, corresponding to the stagnation zones. The non Gaussian nature of Lagrangian velocity distribution is shown in Figure 3.2.

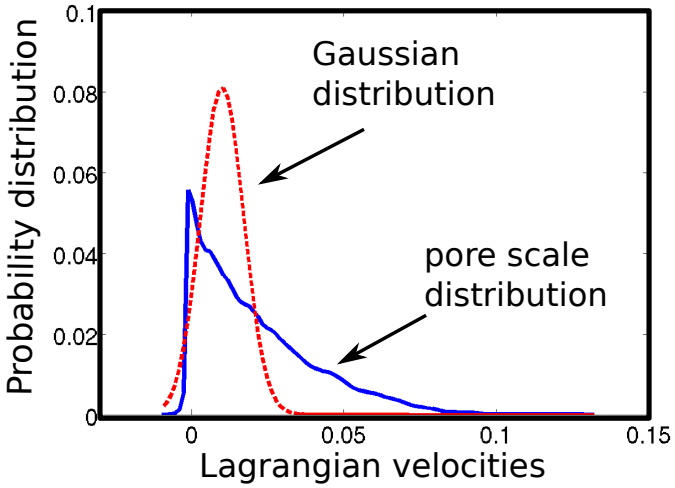

Figure 3.2: *The probability distribution of the pore scale Lagrangian velocities (blue line) compared with a Gaussian (red dashed line) distribution centered at the mean Lagrangian velocity value.*

Longitudinal dispersion and its anomalous scaling

In the SPH pore scale Lagrangian framework, the fluid in motion is represented by in an ensemble of N_p particles that follow the stream lines of the local velocity field. The dispersion of this advected fluid particles can be characterized in terms of the longitudinal width σ of their spatial distribution, defined as:

$$\sigma(t)^2 = \sum_{i}^{N_p} \Big(x_i(t) - x_i(0) - \overline{x}(t) \Big)^2 \tag{3.2}$$

where $x_i(t)$ is the position (projected along the main flow direction) of the i-th particle at time t and $\overline{x}(t)$ is the average of $x_i(t) - x_i(0)$ over all the N_p particles constituting the fluid. Please

note that the considered particles move along streamlines of the velocity field and diffusion is not taken into account here.

Figure 3.3 show the temporal scaling of the width σ of the simulated flow's longitudinal spreading. It displays anomalous scaling with respect to Fickian dispersion characterized by linear temporal scaling, $\sigma^2 \propto t^{\frac{1}{2}}$. In the simulated case the Lagrangian fluid particles display superdiffusive behavior characterized by an evolution of σ that is faster than the Fickian case. This can be expected by the qualitative observation of the existence of stagnation zones where particles get trapped and become long time correlated.

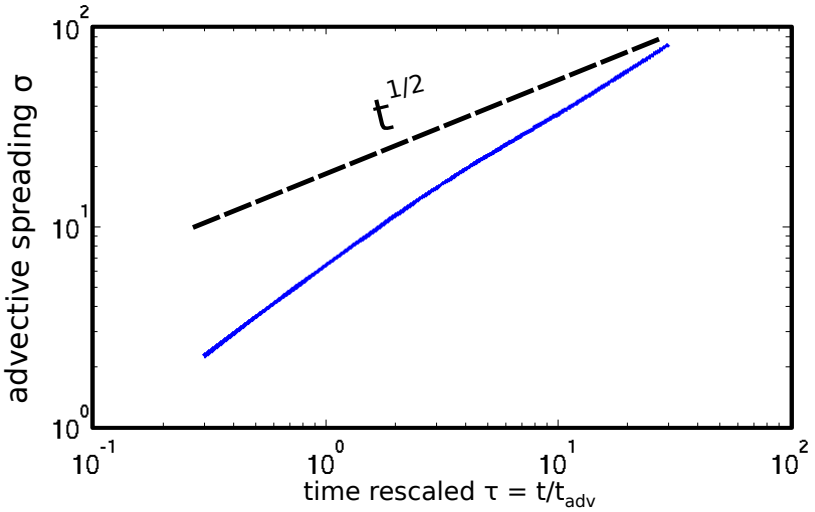

Figure 3.3: *The temporal scaling of the square root of the longitudinal variance of fluid particles simulated via SPH technique. For early time σ is almost ballistic, for late time slows down, but is still faster than the classical Fickian behavior $t^{\frac{1}{2}}$*

Upscaled models

As discussed in the introduction of this thesis, due to the large degree of freedom and our ignorance about boundary and initial conditions, for complex flows a statistical description is necessary (e.g. *Dentz et al.* [2011]). In a Lagrangian framework the particles velocities time series can be assumed to be stochastic processes characterized by certain distributions. As discussed below, depending on the nature of the stochastic process and its correlations, different upscaled picture can be represented.

Random walk and Fickian dispersion

The dynamical picture of classical Fickian models considers the Lagrangian velocities time series to be non autocorrelated. The stochasticity of the advective process is described by a Gaussian white noise about an average behavior (e.g. *Bouchaud* [1990]; *Delay et al.* [2005]). This picture corresponds to the well known Brownian motion for each Lagrangian particle that constitute the fluid. A typical Brownian walk of a single particle, is schematically displayed on a two-dimensional lattice in Figure 3.4. At each discrete time step $t_n = t_{n-1} + \Delta t$,

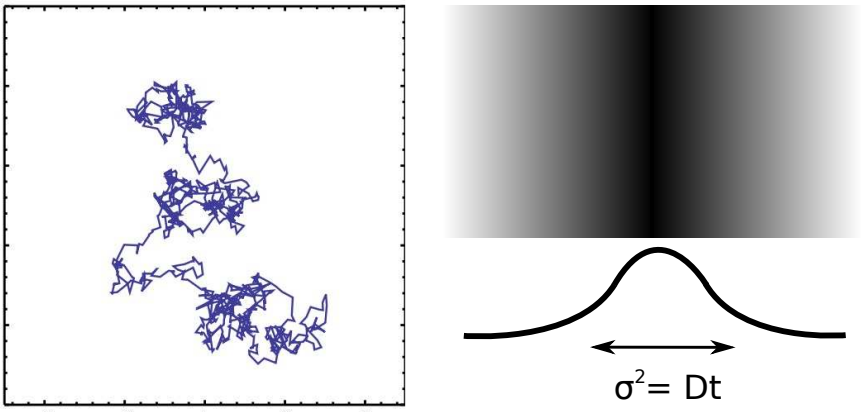

Figure 3.4: *On the left, a schematic view of a* 2*d Brownian motion On the right, a cloud of particles that are moved advected by stochastic velocities. The velocities time series are Brownian walkers about the mean velocity. The spreading of this ensemble of particles is characterized by* $\sigma^2 \propto Dt$

that increases with constant time increment Δt, a Lagrangian particle is assumed to jump and change position to $x_n = x_{n-1} + \xi$. Here $\xi = \frac{v}{\Delta t}$ is the spatial increment given by the stochastic velocity v. This latter quantity is assumed to be a white noise and, hence, a Markov process. The state of the system can be described by the probability density function $p(x,t)$ of positions of the particles. As discussed in the previous chapter, the evolution of the state of a Markov process depends only on the state that the process had at the previous time step. The transitions between states are quantified by the rate of transitions $r(x|x')$. This quantity represents the conditional probability that from the position x' at time t' a walker move to the position x at successive time $t = t' + \Delta t$. The stochastic process is governed by the corresponding Master Equation

$$\frac{\partial p(x,t)}{\partial t} = \int \Big[r(x|x')p(x',t) - r(x'|x)p(x,t) \Big] dx' \tag{3.3}$$

representing a gain-loss equation for the probabilities of the states (e.g. *van Kampen* [2007]). The first term is the gain due to the transitions between states x' to state x, while the second is the loss due to transitions from the state x to any other state x'. Solving this equation, it is demonstrated that the longitudinal dispersion of such an ensemble of random walkers evolves as $\sigma^2 \propto t$ (e.g. *Bouchaud* [1990]), providing a good description for Fickian dispersion.

The Continuous Time Random Walk (CTRW) for anomalous dispersion

Anomalous dispersion, characterized by non linear growth of σ^2 (as for the flow in the considered heterogeneous porous medium), cannot be modeled in terms of Brownian motion. A possible dynamical description of such an anomalous behavior is CTRW (e.g. *Montroll and Weiss* [1965]; *Berkowitz et al.* [2006]). In order to introduce the CTRW, let's consider a one dimensional system. If the classical random walk is based on the idea that for constant time steps Δt the particle position evolves with continuous jumps of size ξ stochastically distributed, the CTRW model is based on the idea that also the time increments τ, elapsing between two successive jumps, are variable, continuous and stochastic. Thus after n steps (or jumps) the position and the time of a particle test will be

$$\begin{aligned} x_n &= x_{n-1} + \xi \\ t_n &= t_{n-1} + \tau. \end{aligned} \tag{3.4}$$

We here consider the simple case where the spatial increment $\xi = \Delta x$ is constant. The successive temporal increments, or waiting times, are related to the spatial series of stochastic velocities as $\tau = \frac{\Delta x}{v}$. In other words, at each spatial increment Δx the particles change velocity and generate a new effective waiting time τ. If the stochastic system defined by (3.4) is Markovian in space, it can be described by

$$R(x,t) = \sum_{x'} \int_0^t dt' \psi(x - x', t - t') R(x', t') \tag{3.5}$$

where where $R(x,t)$ is the probability per time for a walker to arrive at position x at time t and $\psi(x,\tau)$ is the probability per unit time for a displacement x with a waiting time τ. The function ψ determines the nature of the transport, as it has been discussed by *Berkowitz et al.* [2006]. Equation (3.5) describes a semi-Markovian process, or a process that is Markovian in space but not in time. In other words the position difference of particles at fixed time increments depends on the history of the travel of the particle, while the waiting times distribution over fixed spatial increments depends only on the previous position. It has been demonstrated

that for a spatial Markov process a Master Equation for the stochastic process x, described by $R(x,t)$, exists.

Please note the importance of the Markovian property in space of the random walkers defined by (3.4). If over a fixed spatial increment Δx the transition rate $\psi(x,t)$ at the position x depends only on the previous position $x - \Delta x$ the governing equation of CTRW is shown to be equivalent to a Generalized Master Equation (e.g. *Berkowitz et al.* [2006]). If this condition does not hold no Master Equation is defined for the considered ensemble of walkers.

The spreading of CTRW particles, characterized by a σ^2, depends on the particular conditional probability density $\psi(x - x', t - t')$ (e.g. *Berkowitz et al.* [2006]) and can well describe and represent observed anomalous dispersion. However, the relationship between its parameters, in particular the space time jump probability ψ, and the flow velocity field properties is a key open question (e.g. *Le Borgne et al.* [2008b]), which we address in the following for pore sale dispersion.

Spatial Markov property

The key property for the CTRW dynamical description to hold is the Markovian property of spatial velocity series, across a given spatial increment Δx. To test this property we consider the conditional probability density $r(v_n|v_{n-1})_{\Delta x}$ along the Lagrangian trajectories. This quantity represents the probability that the next velocity will be $v_n = \frac{\Delta x}{\tau_n}$ after n spatial increments Δx , given that it was $v_{n-1} = \frac{\Delta x}{\tau_{n-1}}$ after $n-1$ spatial increments. τ_n is the waiting time associated to the nth jump. We numerically compute this conditional probability density from SPH pore scale simulations over consecutive spatial increments Δx along the Lagrangian particle trajectories. To do so we define an equispaced grid over the porous medium and we evaluate the particle velocities transitions over the grid (see Figure 3.5).
From the definition of Markovian process,

$$r(v_n|v_{n-q})_{\Delta x} = r(v_n|v_{n-1})^q_{\Delta x} \quad \forall q \quad \text{integer} \tag{3.6}$$

Thus, for a Markov process the conditional probability density evaluated after q steps Δx has to be equal to the q-th power of r evaluated after a single jump (e.g. *Le Borgne et al.* [2008c,a]; *Kang et al.* [2011]). This reflects the fact that the state of a Markovian process is defined by the initial distribution and the transition probability between successive states and does not

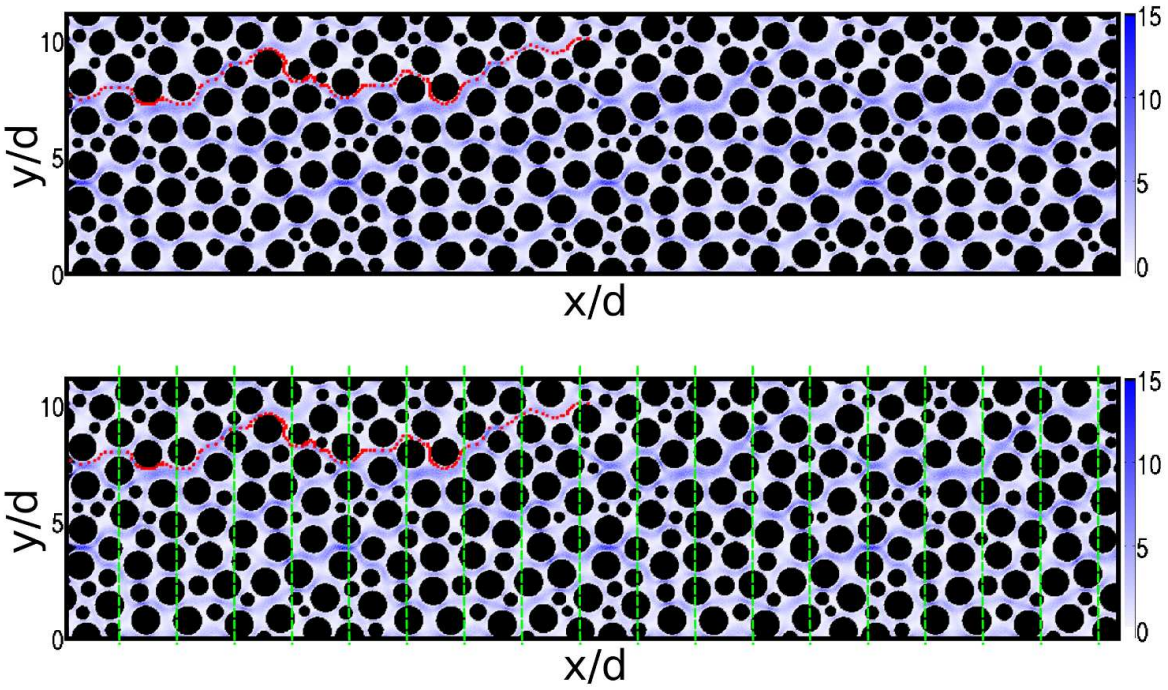

Figure 3.5: *On the top the considered pore scale velocity field where the trajectory of a Lagrangian particle has been superposed (red dots). On the bottom, to the same image has been superposed an equispaced grid. In the spatial framework here proposed we evaluate the particles velocities on the defined grid.*

depends on the history of the spatial series of positions.

We demonstrate that this relationship is not verified for small Δx. Increasing the value of the spatial increment we show that the spatial series of velocities become a Markov process. If the size Δx is very large, in the conditional probability density will be mixed all the information about stagnation zones and channels. The resulting distribution of velocities for large Δx turns out to be a white noise and the upscaled picture will be equivalent to the one associated to the classical Random Walk.

Thus, there exist a minimum spatial increment Δx for which the Markov property holds. This minimum Δx_m allows deriving a consistent CTRW model, which maintains information about the pore scale organization of the flow. We show that the minimum Δx for which equation (3.1) is satisfied, results to be $\Delta x_m = 0.25d$, where d is the average size of a grain that corresponds also to the average stagnation zones size (see Figure 3.1). Figure 3.6 shows the conditional

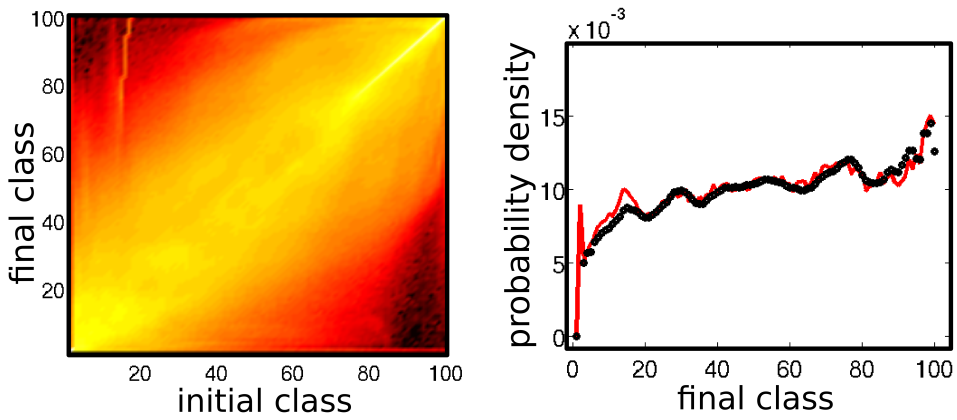

Figure 3.6: *On the left, the matrix representing $r(v_n|v_{n-1})_{\Delta x}$ for a spatial increment $\Delta x = 0.25d$. These probabilities are defined over 100 classes. On the right, the superposition of the transition probabilities evaluated for a jump $5\Delta x$ (in red) and the 5-th power of the transition probabilities evaluated after a single Δx (in black) for the 64-th initial velocity class.*

probability $r(v_n|v_{n-1})_{\Delta x_m}$ associated to Δx_m and the good agreement between $r(v_n|v_{n-1})_{\Delta x_m}$ and $r(v_n|v_{n-1})^5_{\Delta x_m}$.

We now consider an ensemble of random walkers that move following (3.4) where $r(\tau_n|\tau_{n-1})_{\Delta x_m}$ is derived from pore scale analysis over a fixed spatial lattice with lattice spacing $\Delta x_m = 0.25d$. We compute the longitudinal particles distribution σ defined as in equation (3.1). Figure 3.7

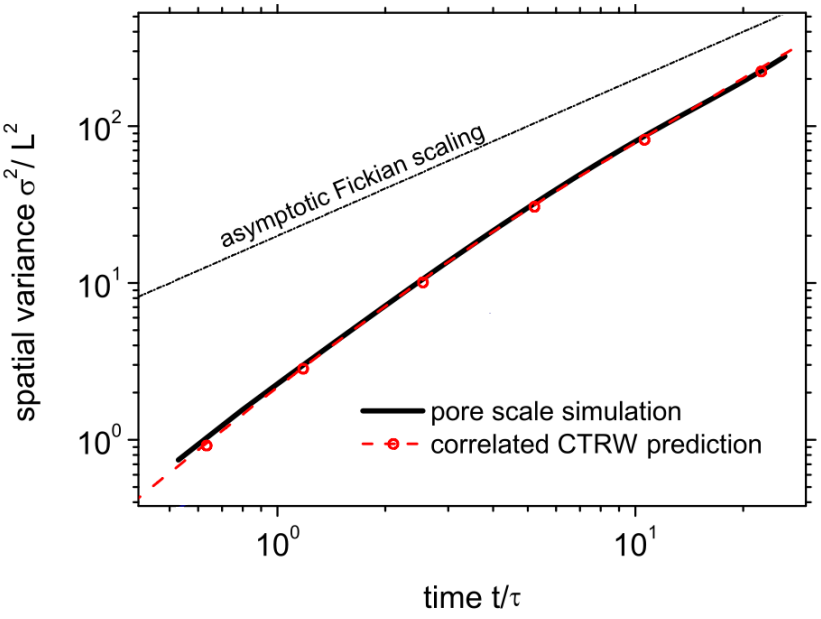

Figure 3.7: *Comparison of the prediction of the correlated CTRW model (red dashed line with dots) with the numerical pore scale simulations (black line).*

shows the good agreement between the scaling of dispersion σ predicted by the correlated CTRW model and the pore scale observation. This means that the size of the spatial increment Δx_m is big enough to ensure the Markov properties of the waiting times, but is small enough to capture, within $r(v_n|v_{n-1})_{\Delta x_m}$, the complex flow organization from which arises the anomalous behavior of dispersion. Please note that no fitting parameters are used to determine the waiting time distribution (or the Lagrangian velocities), since we relate the conditional probability $r(v_n|v_{n-1})_{\Delta x_m}$ to the local pore scale Lagrangian velocities evaluated from SPH simulations.

This work has been published (*Le Borgne et al.* [2011b]) to validate, on a realistic case of an heterogeneous medium, the framework of correlated CTRW proposed for a more simple periodic porous medium.

3.2 Intermittency-like behavior of Lagrangian velocities in porous media

As shown at the beginning of this chapter, the Lagrangian velocities in porous medium exhibit an intermittent behavior between high and variable versus low and correlated velocities (see Figure 3.1). This behavior reflects the complex organization of the pore scale flow in channels and stagnation zones. We shown that this correlated velocities are responsible for non Fickian dispersion. Thus, the classical upscaled descriptions of flows in porous media based on pore scale well mixed conditions (e.g. *Dentz et al.* [2011]) breaks down when the observation scales (temporal and spatial) are fine enough to appreciate the non homogenized conditions of the pore scale. Fickian dispersion models are based on the assumption that Lagrangian accelerations are represented as a white noise. At each time increment the force driving the motion of a Lagrangian particle is independent from the force that acted during the previous temporal increment. This leads to an effective description in terms of a Langevin type equation with white noise. A similar breakdown of classical models emerges in turbulent flows, that exhibit intermittency.

Turbulent flows are characterized by high Reynold number and are locally governed by Navier-Stokes equation. Due to the uncertainty of the uniqueness of the solution of such an equation and of boundary conditions, turbulence cannot be described as a deterministic chaos phenomenon. Given the huge number of degree of freedom of turbulent systems, a statistical approach is necessary. An upscaled description of turbulence is provided by the

statistical picture of Kolmogorov (e.g. *Pope* [2000]). From a dynamical point of view, this description is equivalent to the motion of particles subjected to a Langevin type equation where the added white noise represent a stochastic force the move the particles. The choice for the stochastic term of white noise, implies uncorrelation of successive particle accelerations. The Kolmogorov upscaled description can fail when the underlying hypothesis are not satisfied, as in the case of intermittency (e.g. *Pope* [2000]; *Mordant et al.* [2002]).

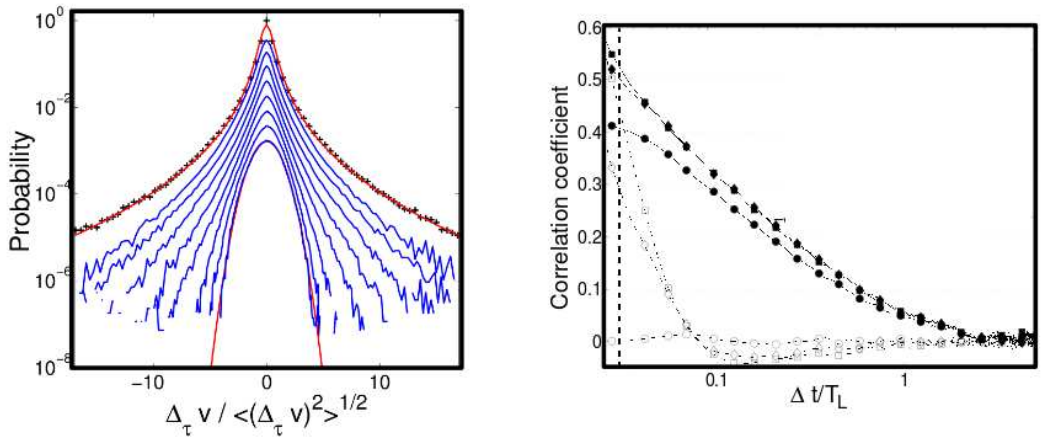

Figure 3.8: *On the left the velocity increments distribution observed by Mordant et al. [2002] for severtal time lags, normalized to the standard deviation and displayed with vertical shift for clarity. Increasing the time lag the distributions tend from a heavy tailed to a Gaussian shape.*

In a Lagrangian framework, *Mordant et al.* [2002] propose to model the anomalous behavior of turbulent flows (and thus the breakdown of the upscaled Kolmogorov theory) related to intermittency in terms of correlation of successive particle accelerations. In particular *Mordant et al.* [2002] studied experimentally the Lagrangian velocities of particles advected in a von Karaman flow. They observe non Gaussian distribution of velocity increments $\Delta v_\tau = v(t+\tau) - v(t)$ for time lag τ (see Figure 3.8). Such a distributions tends to a Gaussian shape if the time lag increase (recovering the upscaled Kolmogorov picture). They quantified this observations by the autocorrelation coefficient χ of accelerations that appear to be long range correlated when considering its absolute value (see Figure 3.8). The correlation coefficient χ is defined as

$$\chi = \frac{< [a(t+\tau) - \overline{a}][a(t) - \overline{a}] >}{\sigma_a^2} \tag{3.7}$$

where $\overline{a}$ and σ_a^2 are the average and the variance of the Lagrangian accelerations a; angular brakets represents ensemble averages. To define an upscaled model, *Mordant et al.* [2002]

adopt a Multifractal Random Walk model that take into account Lagrangian correlations.

For the considered porous medium we follow a similar approach quantifying the correlation coefficient χ of accelerations and the velocities increments distribution $p(\Delta v_\tau)$. The resulting picture is similar to the one of intermittency of turbulent flows. However, the origin of intermittency is different. In porous media this phenomenon arises from the existence channels of high and variable velocities and stagnation zones, where particle and move very slowly with very correlated velocities. To give a dynamical interpretation of such behavior, we propose the correlated CTRW model described in previous paragraphs to reproduce the intermittent-like behavior observed in porous medium flow. The model predicts correctly the intermittent property of Lagrangian velocities. It hence provides a link between CTRW and intermittency, suggesting a new dynamical picture of intermittency.

This results has been formalized in the manuscript, reported below, that is in preparation.

Intermittent properties of transport in porous media

Pietro de Anna,* Tanguy Le Borgne, and Philippe Davy
Géosciences Rennes, UMR 6118, CNRS, Université de Rennes 1, Rennes, France

Alexander Tartakovsky
Pacific Northwest National Laboratory, Washington, USA

Diogo Bolster
Environmental Fluid Dynamics Laboratories, University of Notre Dame, Department of Civil Engineering & Geological Sciences, Notre Dame, IN 46556, USA

Marco Dentz
Spanish National Research Council (IDAEA-CSIC), Barcelona, Spain

From numerical simulations of pore scale flow in porous media, we demonstrate the existence of an intermittent-like behavior of Lagrangian velocities similar to observations in turbulent flows. This phenomenon, characterized by non Gaussian pdfs of Lagrangian velocity increments and long range correlation of Lagrangian accelerations, is at the origin at the breakdown of the classical upscaled models. For transport in porous media this is manifested by anomalous scaling of the temporal evolution of the characteristic dispersion length, called anomalous dispersion. Long range correlation is related to the existence of stagnation zones and localized high velocity channels. While for turbulence, intermittency of Lagrangian velocities can be represented by Multifractal Random Walk, for porous media we show that the dynamical picture is different and that this process is well captured by a correlated Continuous Time Random Walk.

The breakdown of Fickian models of dispersion in porous media has been recognized as a key issue upscaling dispersion, mixing and reaction processes ([3, 7, 15]). Different formalisms have been proposed to represent this process including Continuous Time Random Walk (e.g., [2, 12, 13]), non equilibrium statistical mechanics (e.g. [4, 5]) and fractional advection dispersion (e.g., [11]). Although successful at representing important characteristics of anomalous transport, these models have often failed in relating their parameters to the local velocity field properties (e.g. [15]).

The Fickian transport representation can be described by a Langevin type equation with white noise representing a random force driving the motion ([16]). Thus, the main underlying assumption is the decorrelation of successive Lagrangian accelerations. One of the central elements for upscaling anomalous dispersion is the representation of the dynamics of long range temporal correlation of Lagrangian velocities. The existence of correlation is related to incomplete mixing at pore scale (e.g. [10]). Here we investigate the correlation properties of Lagrangian velocities and accelerations starting from pore scale high resolution numerical simulations. We relate explicitly the long range correlation of local velocities as quantified by intermittent-like properties to the upscaled CTRW dispersion formalism. This phenomenon is similar to the breakdown of the upscaled picture of Kolmogorov for turbulent flows, although the dynamics of the velocity correlation are fundamentally different (e.g. [14]).

We consider a two dimensional porous medium composed by circular grains with mean porosity $\phi = 0.42$. The average velocity of $\overline{v} \sim 10^{-2}$ results from application of a hydraulic head gradient from left to right. The boundary conditions for flux are periodic on all sides. We use Smoothed Particles Hydrodynamics (SPH) to solve numerically the flow [17]. SPH is a Lagrangian particle

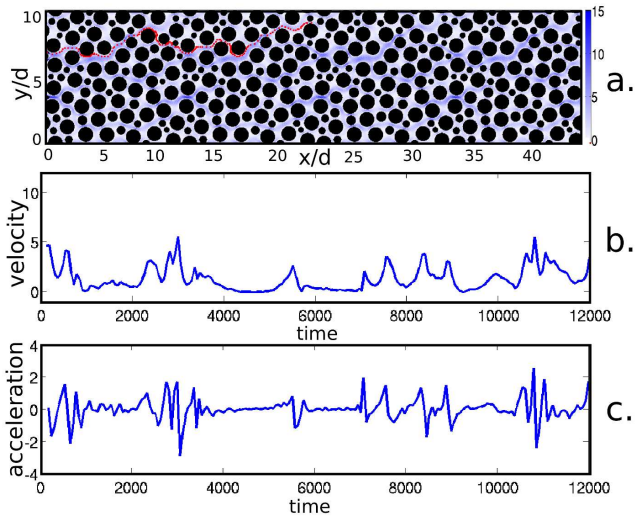

Figure 1. a) The amplitude of the pore scale velocity field normalized by the average Lagrangian velocity. The trajectory of a Lagrangian particle is shown with red dots at equidistant time increments Δt. b) The time series of the Lagrangian velocity for the particle displayed on the top. c) The time series of the Lagrangian accelerations.

*E-mail: pietro.deanna@univ-rennes1.fr

method where particles representing elementary fluid volumes are advected with the flow: advective Lagrangian trajectories are thus given by the trajectories of the SPH particles. Figure 1a shows the simulated pore scale velocity field. It is characterized by high velocity channels and low velocity regions. The spreading size that characterize the advective spreading in the pore volume, can be measured by of the longitudinal width σ_x of the particles distribution $\sigma_x(t)^2 = \sum_i^{N_p}(x_i(t) - x_i(0) - \overline{x}(t))^2$ where $x_i(t)$ is the position (projected along the main flow direction) of the i-th particle at time t and $\overline{x}(t)$ is the average of $x_i(t) - x_i(0)$ over the N_p particles constituting the fluid. In this heterogeneous medium the temporal evolution of spreading size σ_x shows anomalous dispersion when compared to the predictions of the Fickian dispersion, $\sigma_x \neq t^{\frac{1}{2}}$ [6] (see Figure 2).
An example of Lagrangian trajectory is displayed in Figure 1a. The particle slows down as it travels close to stagnation zones and accelerates when entering the high velocity channels. Examples of Lagrangian longitudinal velocity v_x and acceleration a_x series along the trajectory are plotted as a function of travel time in Figure 1b and 1c respectively. A first qualitative observation is that Lagrangian accelerations cannot be represented as a white noise. At each time increment Δt the force driving the motion of a Lagrangian particle is not independent from the force that acted during the previous Δt.

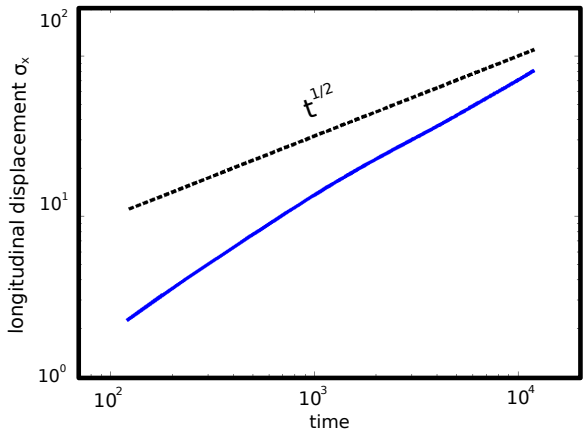

Figure 2. The temporal behavior of the longitudinal displacement variance of Lagrangian particles. In this log-log plot is clear the non Fickian nature (characterized by $t^{\frac{1}{2}}$ scaling) of advective spreading.

We distinguish two regimes in the motion of Lagrangian particles: one characterized by low variability and the other by strong fluctuations in the velocity and acceleration signals. The first regime corresponds to low velocities in stagnation zones. In these stagnation zones, the Lagrangian longitudinal velocities and accelerations are small and strongly autocorrelated. The second regime corresponds to high velocities in flow channels. Thus, the Lagrangian velocities and acceleration time series display qualitatively an intermittent-like behavior.

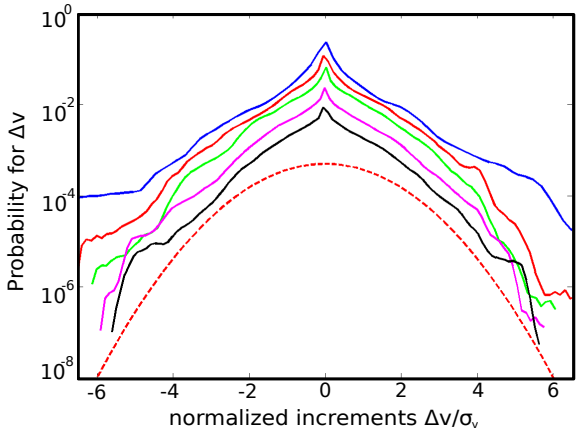

Figure 3. Probability distributions of normalized Lagrangian longitudinal velocity increments $v_x/\sigma(\tau)$. The curves are shifted for clarity, $\sigma(\tau)$ is the variance of velocity increments for each lag time $\tau = 1, 2, 5, 7, 9$.

To quantify the correlation and intermittent-like behavior of Lagrangian particles, we define the Lagrangian velocity increment of the ith particle, associated to the time lag τ, as

$$\Delta_\tau v_i = v_i(t+\tau) - v_i(t) \tag{1}$$

The probability density function of Lagrangian velocity increments normalized with respect to the square root of increments variance $P(\Delta_\tau v/\sigma(\Delta_\tau v))$ is plotted in Figure 3 for different different time lags τ. For small lag time τ, the distribution of Lagrangian velocity increments is characterized by exponential tails and a sharp peak close to zero acceleration due to the stagnation zones where particles are almost at rest. As the lag time increases, the slopes of the exponential tails increase and the sharpness of the peak decreases, approaching a Gaussian distribution. A Gaussian distribution of velocity increments would be equivalent to dynamics described by a Langevin type equation with a white noise representing a stochastic force, whose characteristic dispersion is Fickian [18]. Here the Gaussian shape of the distribution of Lagrangian velocity increments is not reached, even for very large time lags. This is consistent with the fact that during the observation time, or the duration of the simulation, the dispersion size σ_x never follows a Fickian scaling (see Figure 2).
These results are similar to turbulent flow observations of [14]. In the context of turbulent flow the Lagrangian velocity increment distributions show heavy tails and evolve towards a Gaussian distribution at large lag times. The normalized correlation function of a stochastic signal r as

$$\chi = \frac{< [r(t+\tau) - \overline{r}][r(t) - \overline{r}] >}{\sigma_r^2} \tag{2}$$

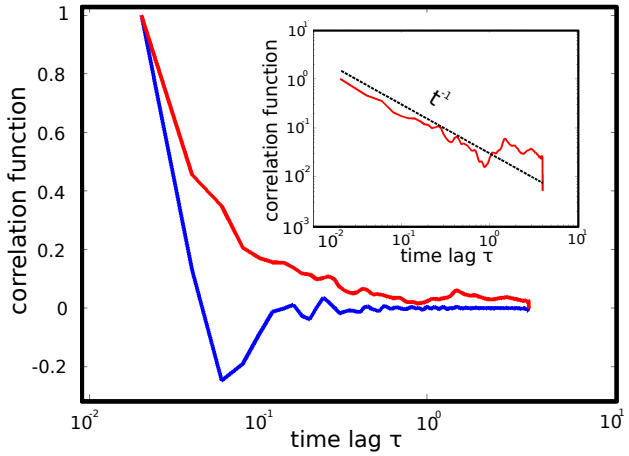

Figure 4. The normalized autocorrelation function χ of Lagrangian particles accelerations a_x (blue curve) and absolute values of acclerations $|a_x|$ (red curve) as function of normalized time lags τ'. We defined $\tau' = \frac{\tau}{t_{adv}}$, where t_{adv} is the average time needed for a Lagrangian particle to cross the whole medium.

where $\overline{r}$ and σ_r^2 are the average and the variance of the process r; angular brakets represents ensemble averages. Figure 4 displays χ for the longitudinal Lagrangian accelerations a_x and for its amplitude $|a_x|$, for the studied flow. The correlation of the longitudinal Lagrangian acceleration decreases rapidly with lag time. We observe a slight anticorrelation at early times, which is possibly due to the rapid fluctuations of acceleration in high velocity channels, as illustrated in Figure 1c. The correlation of the absolute value of the longitudinal Lagrangian acceleration $|a_x|$ is slowly decaying, as obtained by [14] for turbulent flow. While [14] observed an exponential decay, here we obtain a power law decay $C_{|a|} \propto t^{-1}$ (see inset of Figure 4). Thus, the amplitude of accelerations in porous media appear to be more correlated than in turbulent flows. From this analysis, we conclude that transport in porous media share several intermittent-like anomalous scaling properties with transport in turbulent flow. Although the origin of velocity fluctuations in both types of flow are fundamentally different. The existence of such anomalous scaling properties in porous media is related mainly to the low velocity regions.

To upscale the longitudinal flow properties discussed, including correlation of Lagrangian velocities, we use a stochastic method where Lagrangian particles are moved randomly in a one dimensional system representing the longitudinal direction. The considered Lagrangian velocities times series do not represent a Markov process, due to the strong correlation in the stagnation zones. A possible generalization of the Random Walk to a semi-Markovian process, Markovian in space but not in time, accounting for memory in particle transitions, is Continuous Time Random Walk. The basic motion of CTRW for N particles is defined as:

$$\begin{aligned} x_i^{n+1} &= x_i^n + \Delta x \\ t_i^{n+1} &= t_i^n + \frac{\Delta x}{v_i^n} \end{aligned} \tag{3}$$

where $i = 1, \ldots, N$ denotes the particle, n the step, x the position, t the time and v the velocity. In this Lagrangian framework, the Continuous Time Random Walk is completely defined by the initial velocities distribution and transition probability $r(v_x|v_x')$ representing the conditional probability that at a given spatial step the velocity is v_x given that at the previous step the velocity was v_x' [1].

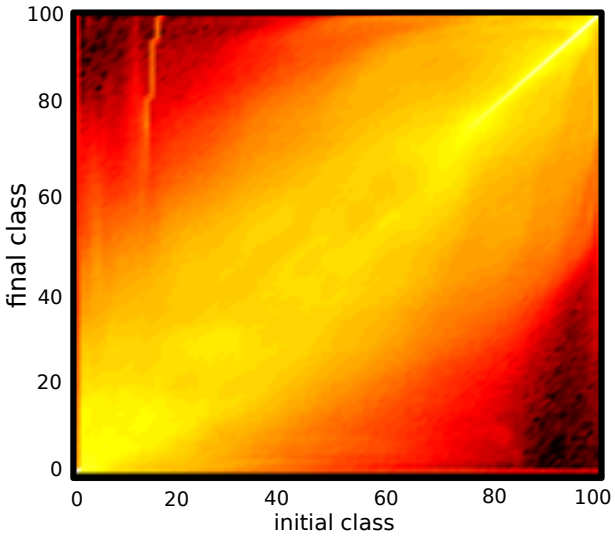

Figure 5. The matrix representing $r(v_n|v_{n-1})_{\Delta x}$ for a spatial increment $\Delta x = 0.25d$. These probabilities are defined over 100 classes.

Most CTRW formulations assume uncorrelated successive jump times [12], hence $r(v_x|v_x') = p(v_x)$ regardless of the previous v_x'. This assumption is true when the jump size is larger than the velocity correlation length. However in order to relate the temporal increments to the local velocity $\tau = \Delta x/v_x$, the spatial increment should be small enough so that the pore scale flow dynamics is not lost by averaging. To relate the CTRW parameters to the local velocity distribution one minimize the spatial increment while maintaining the Markov property that allows writing a CTRW model. The minimum Δx was shown to be equal to $\Delta x_m = d/4$ for the studied porous medium [6], where d is the average grain size. We evaluate from the pore scale simulations this transitions $r(v_x|v_x')_{\Delta x_m}$ associated to the spatial increment Δx_m. Figure 5 shows the matrix representing the evaluated $r(v_x|v_x')_{\Delta x_m}$: each column of the matrix represent the pdf for the next velocity

v_x given that the previous one was v'_x. To different initial velocities v'_x different distribution of v_x are associated. Following [8, 9], we take a series of velocities $\{v_i^n\}_{n=0}^M$ for the random walkers in agreement with this transitions $r(v_x|v'_x)_{\Delta x_m}$: $\{v_i^n\}_{n=0}^M$ form a Markov chain, where M is the considered number of steps for the CTRW simulation. The resulting Continuous Time Random Walk model is characterized by correlated waiting times. Correlated CTRW simulations are done

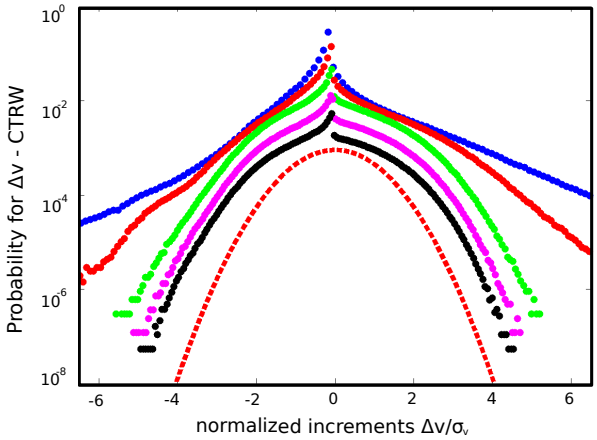

Figure 6. Probability distributions of normalized Lagrangian longitudinal velocity increments $v_x/\sigma(\tau)$ for the CTRW model adopted. The curves are shifted for clarity, $\sigma(\tau)$ is the variance of velocity increments for each lag time $\tau = 1, 2, 5, 7, 9$.

for 10^5 particles. The resulting trajectories are given at equidistant positions for a given spatial increment Δx. To compare the velocities increments distribution and autocorrelation of acceleration to the analogous results of the pore scale simulation analysis, we convert the results of simulations from a discretized space to a discretized constant time Δt framework. Figure 6 shows the probability distribution of the velocity increments for CTRW simulations for different time lags τ. For small time lags the distribution is characterized by heavy tails. Increasing τ the distribution approaches a Gaussian. This is in good agreement with the observation of the pore scale longitudinal Lagrangian velocities. We then calculated the correlation function as defined in equation (2) of the Lagrangian accelerations and their absolute value, for the CTRW simulations. Figure 7 shows the good agreement between the model and the pore scale simulations observations. Furthermore the correlated CTRW provides good predictions for the anomalous scaling of the spreading size [6](see Figure 2)

Following a similar analysis, we show that a key property of complex pore scale flows in porous media are the long time correlations of Lagrangian velocities, associated to the low velocity stagnation zones. As for turbulence, this correlations represent the breakdown of upscaled classical models that assumes pore scale well mixed conditions and

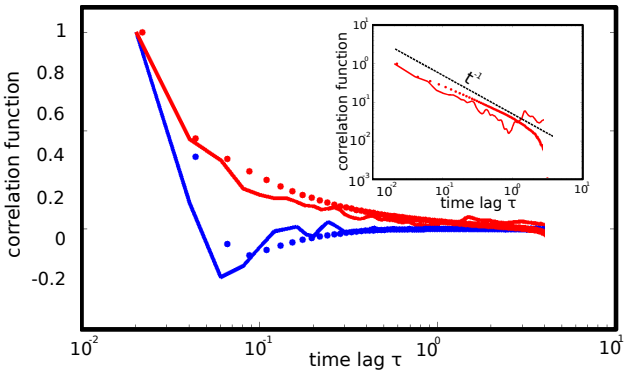

Figure 7. Comparison between pore scale observations (solid lines) and the upscaled CTRW model (dots). In blue is represented the normalized autocorrelation function χ of Lagrangian particles accelerations a_x and in red the absolute values of these acclerations $|a_x|$ as function of normalized time lags τ'.

no correlations. As an alternative description, we use a CTRW model, accounting for the correlation between velocities, that captures the essential features of such a complex pore scale flow. The resulting picture is similar to the one of intermittency of turbulent flows, although the origin of intermittency is different. It hence provides a link between CTRW and intermittency, suggesting a new dynamical picture of intermittency.

Acknowledgements

Pietro de Anna and Tanguy Le Borgne acknowledge the financial support of the European Commission through FP7 projects ITN project, IMVUL project (Grant Agreement 212298) and Marie Curie ERG grant ReactiveFlows (Grant Agreement Number 230947).

[1] Brian Berkowitz, Andrea Cortis, Marco Dentz, and Harvey Scher. Modeling non-Fickian transport in geological formations as a continuous time random walk. *Reviews of Geophysics*, 44(2):1–49, 2006.

[2] Brian Berkowitz and Harvey Scher. Theory of anomalous chemical transport in random fracture networks. 57(5):5858–5869, 1998.

[3] Branko Bijeljic, Peyman Mostaghimi, and Martin Blunt. Signature of Non-Fickian Solute Transport in Complex Heterogeneous Porous Media. *Physical Review Letters*, 107(20):20–23, November 2011.

[4] J. H. Cushman and T. R. Ginn. Non local dispersion in media with continuously evolving scales of heterogeneity. *Transp. in Porous Media*, 13(1):123–138, 1993.

[5] John H. Cushman, Lynn S. Bennethum, and Bill X. Hu. A primer on upscaling tools for porous media. *Advances*

in Water Resources, 25(8-12):1043–1067, August 2002.

[6] T. Le Borgne, D Bolster, M Dentz, P. de Anna, and A Tartakovsky. Effective pore-scale dispersion upscaling with a correlated continuous time random walk approach. *Water Resources Research*, 47(12):1–10, December 2011.

[7] Tanguy Le Borgne, Marco Dentz, and Jesus Carrera. Lagrangian Statistical Model for Transport in Highly Heterogeneous Velocity Fields. *Physical Review Letters*, 101(9):1–4, August 2008.

[8] Tanguy Le Borgne, Marco Dentz, and Jesus Carrera. Lagrangian Statistical Model for Transport in Highly Heterogeneous Velocity Fields. *Physical Review Letters*, 101(9):1–4, August 2008.

[9] Tanguy Le Borgne, Marco Dentz, and Jesus Carrera. Spatial Markov processes for modeling Lagrangian particle dynamics in heterogeneous porous media. *Physical Review E*, 78(2):1–9, August 2008.

[10] Tanguy Le Borgne, Marco Dentz, Philippe Davy, Diogo Bolster, Jesus Carrera, Jean-Raynald de Dreuzy, and Olivier Bour. Persistence of incomplete mixing: A key to anomalous transport. *Physical Review E*, 84(1):1–4, July 2011.

[11] Mark Meerschaert, David Benson, and Boris Bäumer. Multidimensional advection and fractional dispersion. *Physical Review E*, 59(5):5026–5028, May 1999.

[12] Ralf Metzler and Joseph Klafter. The random walk's guide to anomalous diffusion: a fractional dynamics approach. *Physics Reports*, 339, 2000.

[13] E. W. Montroll and G. H. Weiss. Random walks on lattices. *J. Math. Phys.*, 6(2):167, 1965.

[14] N. Mordant, J. Delour, E. Léveque, a. Arnéodo, and J.-F. Pinton. Long Time Correlations in Lagrangian Dynamics: A Key to Intermittency in Turbulence. *Physical Review Letters*, 89(25):2–5, December 2002.

[15] Shlomo P Neuman and Daniel M Tartakovsky. Perspective on theories of non-Fickian transport in heterogeneous media. *Advances in Water Resources*, 32(5):670–680, May 2009.

[16] Alexandre Tartakovsky. Langevin model for reactive transport in porous media. *Physical Review E*, 82(2):1–11, August 2010.

[17] Alexandre M Tartakovsky and Shlomo P Neuman. Effects of Peclet number on pore-scale mixing and channeling of a tracer and on directional advective porosity. *Geophysical Research Letters*, 35(21), November 2008.

[18] N.G. van Kampen. *Stochastic Processes in Physics and Chemistry*. Elsevier, Amsterdam, third edition, 2007.

Chapter 4

Mixing limited reactions in porous media

We now consider the porous medium and the flow analyzed in the previous chapter, adding diffusion and reactions. We investigate the case for which mass transfer is a limiting processes for the chemical reactions. So, we investigate the effective kinetics of the mixing limited reactions that take place at front between two reactive solute A and B that undergo to the irreversible bimolecular reaction $A + B \rightarrow C$.
The work presented in this chapter was made in collaboration with Marco Dentz, research professor at the Department of Geosciences Institute of Environmental Assessment of Barcelona (Spain) and Alexander Tartakovsky, scientist at Pacific Northwest National Laboratory (Washington state, USA)

4.1 Kinetics scaling of a reaction front

We consider the two dimensional porous medium of Figure 4.3 initially saturated of a solute B. A continuous injection of another solute A is produced in the system. The two solute react when in contact in the portion of the pores volume where A and B are mixed by the combination of advection and diffusion (as shown in Figure 4.1). The heterogeneous advection stretches the concentration field of both A and B, while diffusion locally mixes the two solute. While the two reactant are mixed a bimolecular reaction $A + B \rightarrow C$ take place. The reaction is assumed to be fast enough to be limited by mixing processes. In other words the characteristic reaction time defined for a bimolecular reaction $t_k = \frac{1}{k}$, where k is the reaction rate (*Connors* [1990]), is assumed to be much smaller then the characteristic transport time t_T.

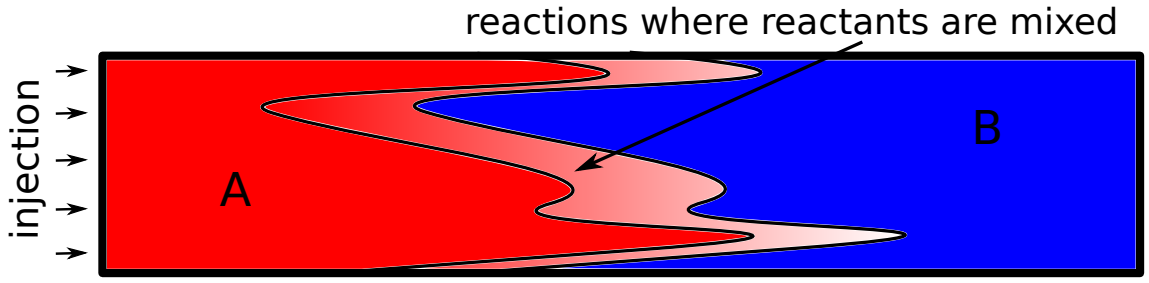

Figure 4.1: *A schematic view of the configuration of the mixing limited reaction considered. A solute A is continuously injected in a medium saturated by another chemical B. Where the two are mixed reactions take place.*

This is quantified by the Damkohler number $Da = \frac{t_T}{t_k}$ (*Dentz et al.* [2011]), that in our case is assumed to be much larger then 1. To simulate the fluid flow at the pore scale we adopt the

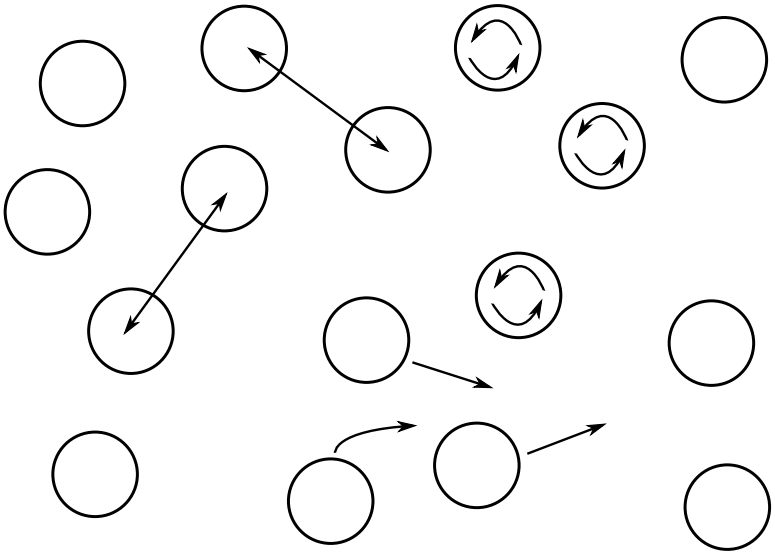

Figure 4.2: *A schematic view of the numerical simulation method. Void circles represent SPH particles that are advected in the porous medium following the flow stream lines. Molecular diffusion is modeled as the exchange of mass between particles, carrying mass. Reactions can take place only between chemicals that are inside the same particle and their kinetics is modeled with mass action law.*

Smoothed Particle Hydrodynamics (SPH) approach as described in *Tartakovsky et al.* [2008a]. As introduced in the previous chapter, in this SPH model the fluid is discretized in N_p particles that flow through the pores with velocities given by the solution of the Navier-Stokes equation for a given set of physical parameters (density ρ, viscosity μ, the body forces $\boldsymbol{b}$ and local pressure p). The porous medium is composed of circular grains of average size $d = 10$

with mean porosity $\phi = 0.42$. The boundary conditions for flux are periodic on all sides. In the adopted numerical method particles carry the mass of the solutes A and B. Molecular diffusion is modeled as the exchange of mass between these particles. We consider that the volume represented by each particle is well mixed. In other words, each particle has a size that represents the homogenization scale ξ defined by *Le Borgne et al.* [2011a]. Since solutes in each particle are well mixed, reactions kinetics within particles follow the mass action law. No reactions can take place between solutes that are not in the same particle. A schematic view of such a numerical method is shown in Figure 4.3 Advective Lagrangian trajectories are thus given by the trajectories of the SPH particles. The validation of this numerical method is discussed by *Tartakovsky and Meakin* [2005]; *Tartakovsky* [2010]. To provide a further validation of the method we run simulations for different particles size (or different spatial resolution) but same physical parameters, obtaining the same results. For the same pore scale flow (with

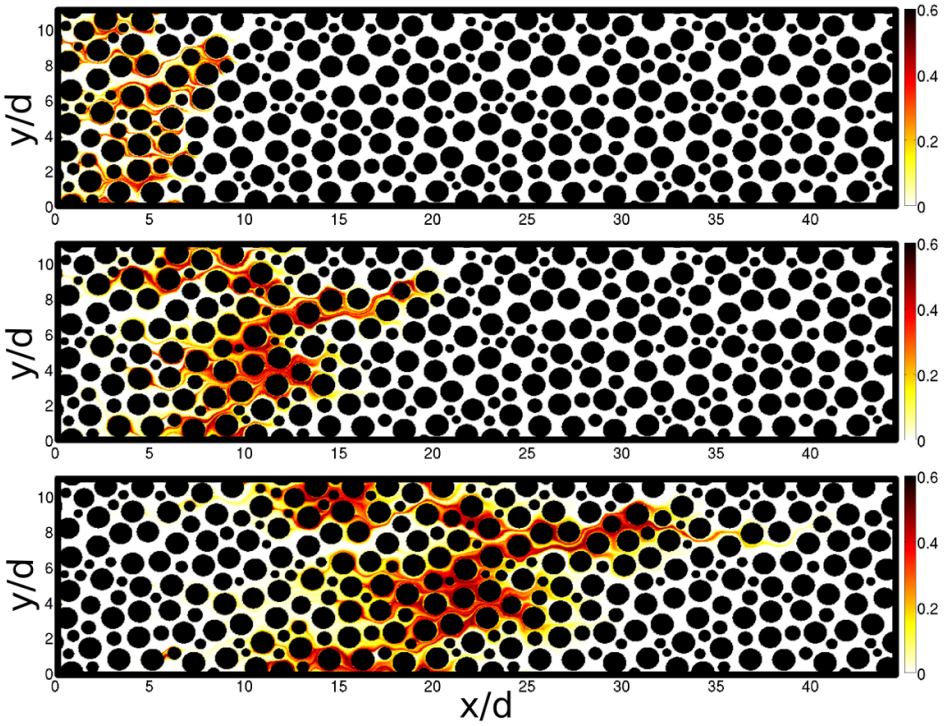

Figure 4.3: *Three consecutive snapshot of the concentration field of the reaction product C at the front between the injected solute A and the solute already present in the system B. Coordinates are normalized with d, the average grain diameter. Concentration is normalized with respect to the constant injected concentration of A. The Peclet number is* 10^5

average value $\overline{v}$), we performed several simulations for different values of the diffusion coefficient D in order to study the impact of different mixing configurations on reaction kinetics.

We thus define the Peclet number of the system $Pe = \frac{t_D}{\tau_a} = \frac{\lambda \overline{v}}{D}$ as the ratio between characteristic diffusion time scale over characteristic advection time scale over the length $\lambda = 10$ representing the average pore space. Here we focus on the temporal scaling of the mass M_C produced by reactions at the front between A and B, defined as

$$M_C(t) = \int_V c_C(x, y, t) dx dy \tag{4.1}$$

where V represent the volume of the $2d$ porous medium. Fickian dispersion models that assume complete mixing at the pore scale predict a scaling $M_C(t) \propto (D_{disp} t)^{\frac{1}{2}}$, where D_{disp} represent the effective dispersion coefficient (e.g. *Gramling et al.* [2002]). From pore scale simulations the resulting upscaled picture is quite far from the one derived in the framework of Fickian dispersion. The time evolution of $M_C(t)$ follows two regimes as shown in Figure 4.4. At early times the total mass of C grows faster then the classical Fickian case $t^{1/2}$. At late times the reaction rate slows down, but is still faster than the classical $t^{1/2}$ behavior. A key observation in this late time regime is that the total mass does not depend the Peclet number. We propose a simple physical model that explains both regime and the transition time between them, providing a global upscaled framework for this mixing limited reaction. The results have been summarized in the following manuscript in preparation.

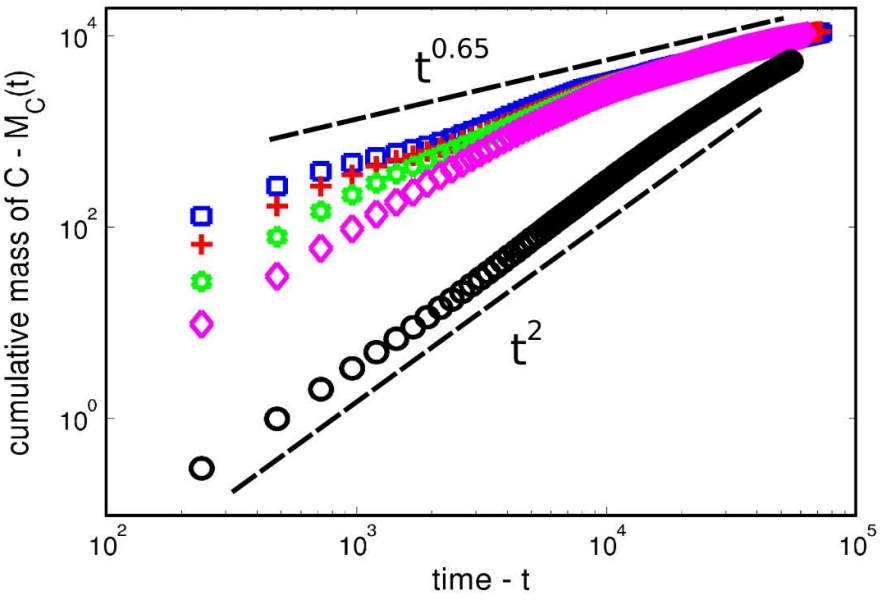

Figure 4.4: *The temporal scaling of the cumulative mass M_C produced by reactions. Different colors represents different Pe numbers: blue $Pe = 10^{-2}$, red $Pe = 3 \cdot 10^{-3}$ green $Pe = 10^{-3}$ magenta $Pe = 3 \cdot 10^{-4}$ and black $Pe = 10^{-5}$.*

Anomalous Reaction Kinetics of reactive front in Porous Media

Pietro de Anna* and Tanguy Le Borgne
Géosciences Rennes, UMR 6118, CNRS, Université de Rennes 1, Rennes, France

Marco Dentz
Spanish National Research Council (IDAEA-CSIC), Barcelona, Spain

Alexander Tartakovsky
Pacific Northwest National Laboratory, Washington, USA

We investigate the effective kinetics of a reaction front for mixing limited bimolecular reaction $A + B \to C$ in a porous medium. While Fickian diffusion predicts a scaling of the cumulative mass produced as $M_C \propto t^{1/2}$, we observe two time regimes in which the total product mass evolves faster then $t^{1/2}$. At early times the invading solute is organized in fingers of high velocity. Reactions take place only at the fingers boundaries whose surface grows linearly in time. We show that this configuration leads to a mass scaling $M_C \propto t^2$. When diffusion mixes reactants and destroy these finger structures, the effective reaction rate slows down and we relate it to the longitudinal advective spreading providing $M_C \propto \sigma_x$. The transition time between these two regimes is characterized by the diffusion time over the transverse fingers cross section.

Reactive transport phenomena are ubiquitous in natural systems, medical and industrial applications. Their dynamics derive from the interaction of microscopic mass transfer and reaction processes [9, 21]. The understanding of observed reaction behavior requires the quantification of these microscale processes and their impact on the large scale reaction and transport behavior. This task is challenging because the probability of reactive species to meet and react depends on the complex flow organization [14, 23, 26]. In general, reactions take place when reagents are close enough to chemically interact. Due to mixing processes two or more given substances, originally segregated into different volumes of space, tend to occupy the same volume allowing the reactions to take place [19]. Reactive transport systems can be divided into two main categories. In the chemically dominated systems the transport phenomena are efficient enough to mix the reagents before the chemical reactions can significantly reduce their concentration. In the mixing dominated systems reactions are fast enough to be limited by transport of reactants [4–6, 10–14, 16, 18, 26].

In this Letter we focus on the mixing limited reactive transport system $A + B \to C$ on the pore-scale, and its effective behavior on the mesoscale. To this end we consider the invasion of the dissolved chemical A into a domain in which only the dissolved chemical B is present, illustrated in Figure 2. When viscous effects are absent, mixing processes in porous media are controlled by the combination of heterogeneous advection and diffusion [4, 7, 10, 12, 20]. The former acts to spread the reactants in the local direction of the flow. Diffusion, on the other hand tends to homogenize the spatial distribution of chemicals. In the framework of classical dispersion theory, at the mesoscale, these two phenomena are lumped into a single dispersion coefficient [10, 12, 22]. This approach is valid if the microscale can be assumed to be well mixed. This means, for situations, in which the diffusion time over the characteristic microscopic length scales is much smaller than the mesoscopic mass transfer scales. Furthermore, the validity of the classical mesoscale advection-diffusion reaction equation requires the typical reaction time scale to be much larger than the microscopic diffusion scale. The conditions under which such mesoscopic models provide an adequate average description of pore scale transport and reaction processes are discussed in detail in Battiato et al. [1]. In many situations these conditions for the microscale mass transfer and reaction processes are not met, one observes anomalous transport and reaction behaviors. Thus, mass transfer cannot be described by Fickian diffusion and transport is in general non-Markovian. Such behaviors have been observed for a range of disordered and fractal systems [2], and in the presence of stochastic fluctuations [5, 15].

We consider the $d = 2$ dimensional heterogeneous porous medium, presented in Figure 2. The medium is composed of circular grains of different sizes and average diameter $d = 10$ with mean porosity $\phi = 0.42$. The pore volume is initially fully saturated with a solution containing the chemical species, B with concentration $c_B(x = 0, y, t = 0) = c_0$. At time $t = 0$ a solution with dissolved chemical A with concentration $c_A(x = 0, y, t = 0) = c_0$ is injected through the left boundary of the porous domain. The pore-scale steady-state fluid flow is driven by a body force acting in the positive x-direction, as illustrated in Figure 1. The fluid motion is subjected to periodic boundary conditions for velocity and pressure at the external boundaries in the x- and y-directions. At the initial time $t = 0$, the interface between the two chemicals is a line (interrupted

*E-mail: pietro.deanna@univ-rennes1.fr

by the grains of the porous medium) located at $x = 0$ transverse to the main flow direction (x axis). As time increases the two chemicals are mixed by heterogeneous advection and diffusion, and reactions take place where both A and B coexist. Due to advective-diffusive mass transfer, the mixing zone is stretched and increases in width. The chemical C is produced in this mixing zone and then transported by advection and diffusion in the pore space.

To simulate reactive transport at the pore scale we adopt the smoothed particle hydrodynamics (SPH) approach described in [3, 20]. In this SPH model, fluid is discretized with N_p particles that flow through the pores with velocities given by the solution of the Navier-Stokes equation

$$\frac{d\boldsymbol{v}}{dt} = -\frac{\nabla p}{\rho} + \frac{\mu}{\rho}\nabla\cdot(\nabla\boldsymbol{v} + \nabla\boldsymbol{v}^T) + \boldsymbol{b} \qquad (1)$$

for a given set of physical parameters (density ρ, viscosity μ, the body forces $\boldsymbol{b}$...), see Figure 1 *a.* Each particle

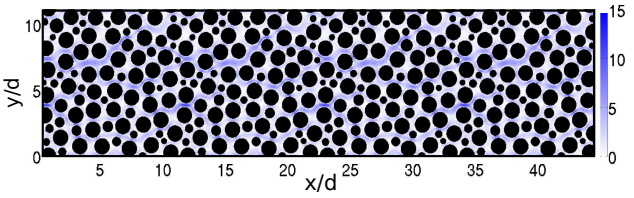

Figure 1. The modulus $|v|$ of the flow velocity scaled by the modulus of the spatially averaged flow velocity denoted by $\overline{v}$. The Reynolds number value is $Re = 4$. Coordinates are normalized with d, the average grain diameter.

carries a certain amount of mass and thus of concentration. The concentration of solute within each particle is given by the total mass of solute in the particle divided by the total mass carried by the particle. Molecular diffusion is modeled as the exchange of mass, or concentration, of solute between particles. Each particle represents a volume that is assumed to be well mixed. Therefore we do not describe any process that takes place at length scales smaller than the particles size, which is taken here equal to $d/40$. The resulting stationary velocity field shows the existence of a braided network of preferential flow paths in channels as well as low velocity or stagnation zones, see Figure 2. The evolution of the species concentrations is described by the advection-diffusion reaction equations

$$\frac{\partial c_i}{\partial t} = -\boldsymbol{v}\cdot\nabla c_i + \nabla\cdot(D\nabla c_i) + r_i, \qquad (2)$$

where $i = A, B, C$, D is the diffusion coefficient, which is assumed to be the same for all chemicals, and r_i is the local reaction rate. We assume that reactions take place only inside the fluid particles. Due to the well mixed assumption in each particle, reactions can be described via the mass action law and a reaction constant k. For the reaction $A+B \rightarrow C$, in a fluid particle placed at point (x, y)

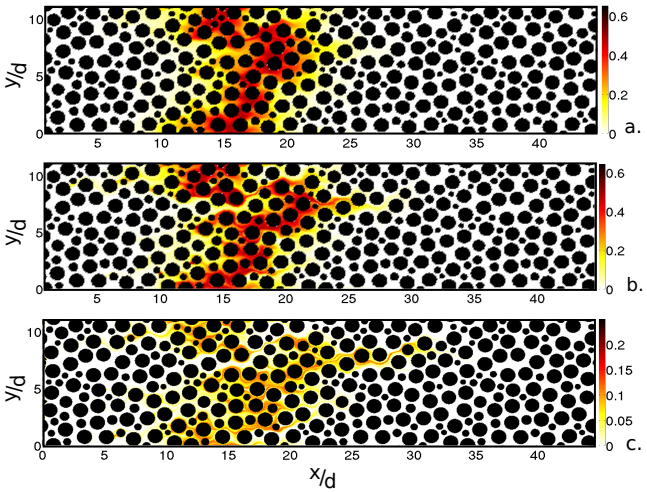

Figure 2. Dimensionless concentration of the reaction product C. The panels *a.*, *b.* and *c.* show results of pore scale simulations respectively related to the case $Pe = 5$, $Pe = 50$ and $Pe = 5000$, at time $t = 9\tau_a$.

at time t the reaction rate is $r_i = -kc_Ac_B$ for $i = A, B$ and $r_C = kc_Ac_B$. The numerical details of the SPH model and its validation are given in Refs. [3, 20]. At the mesoscale, reactive transport of averaged concentrations $\overline{c}_i$ is classically described by the advection-dispersion reaction equation [25]

$$\phi\frac{\overline{c}_i}{\partial t} + q\frac{\partial\overline{c}_i}{\partial x} - (D + D^*)\nabla^2\overline{c}_i = r_i^*, \qquad (3)$$

with $i = A, B, C$, D^* the hydrodynamic dispersion coefficient, and the reaction rates $r_i^* = -k\overline{c}_A\overline{c}_B$ for $i = A, B$ and $r_C^* = k\overline{c}_A\overline{c}_B$. The constant Darcy velocity satisfies the Darcy equation $q = -K\partial h/\partial x$ with K hydraulic conductivity and h hydraulic head [8, 12, 20]. In this framework the total mass of C, defined as the integral of $c_C(\boldsymbol{x}, t)$ over the fluid volume V is [12]

$$M_C(t) = \int_V c_C dV = c_0\sqrt{\frac{4(D + D^*)t}{\pi}} = c_0\sqrt{\frac{2\sigma^2}{\pi}} \qquad (4)$$

where $\sigma^2 = 2(D + D^*)t$ is the characteristic variance of the displacement of a Fickian transported conservative solute. σ is the characteristic spreading length [17].
The pore scale simulations display significant deviations with respect to the expected classical result (4). We performed 5 simulations for 5 different values of the diffusion coefficient D: 10^{-2}, $3\cdot10^{-3}$, 10^{-3}, $3\cdot10^{-4}$ and 10^{-5}. The Peclet number is defined as $Pe = \frac{\overline{v}\lambda}{2D}$ where $\overline{v} = 10^{-2}$ is the average velocity and $\lambda = 10$ the average pore size. We vary the Peclet number between 5 and 5000, by varying the diffusion coefficient. The characteristic advection time over the average pore size is $\tau_a = \lambda/\overline{v}$. A snapshot of concentration field in the porous medium for different value of the Peclet number is shown in Figure 2. The time evolution of $M_C(t)$

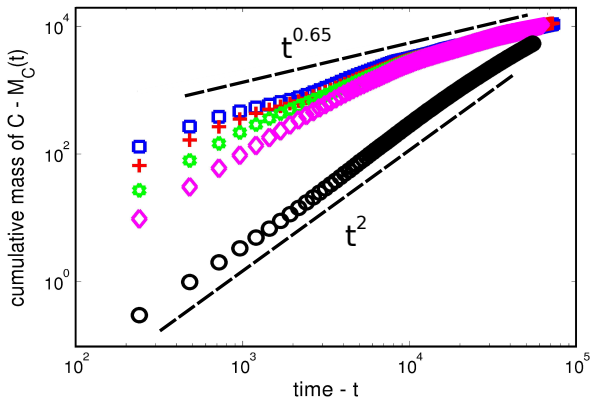

Figure 3. Time evolution of the total mass $M_C(t)$. At early time $M_C \propto Dt^2$, at late times $M_C(t) \propto t^{0.65}$ ad does not depend on diffusion coefficient D. Different colors correspond to different values of D: blue squares corresponds to $D = 10^{-2}$, red cross to $D = 3 \cdot 10^{-3}$, green starts to $D = 10^{-3}$, magenta diamond to $D = 3 \cdot 10^{-4}$ and black circles to $D = 10^{-5}$.

follows two regimes as shown in Figure 3. At early times the total mass of C grows much faster then the classical Fickian case $t^{1/2}$. At late times the reaction rate slows down, but is still faster than the classical $t^{1/2}$ behavior. A key observation in this late time regime is that the total mass does not depend on local diffusion D, in this framework.

Invasion regime - For early times the incoming chemical A is organized in fingers that invade the pores occupied by B, (Figure 4). Since the velocity field is stationary, the size of the fingers, and thus the interface between chemicals, grows linearly with time. We consider the characteristic diffusion time over the average finger cross-section size $h = 2$ defined as $t_D = \frac{h^2}{2D}$. For $t \ll t_D$, diffusion is not efficient enough to mix the chemical over the fingers cross-sections h and thus reactions take place at finger surfaces, which are stretched in the direction of the local velocity field (Figure 4). After volume averag-

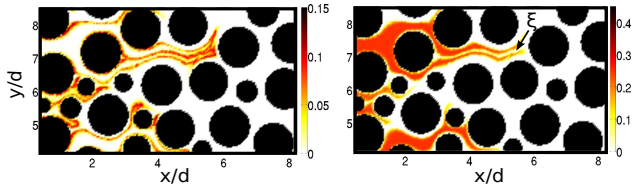

Figure 4. Magnification around the fingers structures: image of the invasion regime at time $t = 1.26\tau_a$ related to the case $Pe = 5000$. On the right the incoming reactant A organized in fingers. On the left C produced at the finger surfaces.

ing of (2) for $i = C$ and considering that the chemical C is not injected in the system, the transport terms (both advection and diffusion) vanish and the variation of total mass of C produced is

$$\frac{dM_C(t)}{dt} = \int kc_A c_B dV. \tag{5}$$

For $i = A$ we obtain

$$\int \frac{dc_A}{dt} dV = \int (D\nabla^2 c_A - kc_A c_B) dV \tag{6}$$

where we used the total derivative for c_A, $\frac{dc_A}{dt} = \frac{\partial c_A}{\partial t} + \boldsymbol{v} \cdot \nabla c_A$. In this early time regime the portion of the system where reactants are mixed by diffusion is small. Thus, the variation of the mass of A due to reaction is negligible compared to the variation of the mass of A due to the continuous injection. Therefore, $\int \frac{\partial c_A}{\partial t} dV \sim -\int \boldsymbol{v} \cdot \nabla c_A dV$. Hence, the total amount of mass that react and disappear can be approximated as

$$\frac{dM_C(t)}{dt} = \int kc_A c_B dV \sim \int D\nabla^2 c_A dV = D \int_\Sigma \nabla c_A d\Sigma \tag{7}$$

where we used the Gauss theorem to derive the last equality, Σ is the finger boundaries. Equation (7) quantifies the fact that the rate of reaction equals the diffusive flux across the fingers surface. When A or B crosses the interface Σ by diffusion, it is converted into C.
Defining ξ as the characteristic width of the finger boundaries Σ, the gradient of c_A across Σ can be approximated as $\nabla c_A \sim \frac{c_A^0 - 0}{\xi}$. This approximation relies on the fact that the concentration inside the fingers is almost constant and equal to the injected concentration c_A^0, while it is almost zero outside (see Figure 4). Assuming that ξ is constant due to the competition between shear, diffusion and reactions the mass of C is

$$\frac{dM_C(t)}{dt} \sim D\frac{c_A^0}{\xi} \int_\Sigma d\Sigma \propto D\Sigma(t) \tag{8}$$

Given that the finger boundaries grows linearly in time, equation 8 implies that the mass of produced C scales as $M_C(t) \propto Dt^2$. This correspond to the fast evolution observed in simulations, Figure 3. Note that this is equivalent to state that locally at the fingers boundaries, where reactions take place, the production of C is constant.

This observation validates the assumption of a constant characteristic size of the fingers boundaries ξ, independent on diffusion. This is in contrast with results obtained in turbulent flow, for which the Batchelor scale, representing the local equilibrium between shear and diffusion, scales as $D^{\frac{1}{2}}$ (e.g. [24]). A possible explanation for this constant width ξ is that it is physically determined by geometry of the solid matrix of the porous medium. The no-slip boundary conditions at the grains walls create stagnation zones. Furthermore, the flow organization around the grains creates a stream

line division down stream of the grains. As illustrated in Figure 4 the reaction production in the first regime is localized in these stagnation zones and streamline divisions which form the contours of the fingers.

Dispersion regime - For times $t \geq t_D$ the fingers structures are destroyed by diffusion. The scaling of the total mass of C produced slows down from the previous regime (Figure 3), but is still faster than the prediction of equation (4), $t^{1/2}$, and the total mass does not depend on local diffusion D. In classical upscaled models [10, 12, 22] reactants are considered to be well mixed in each cross-section transverse to the main flow. At pore scale this condition is not full-filled as shown in Figure 2 and 4.
To describe the anomalous kinetics in this second regime we seek to relate the reactive production to the mixing properties as quantified by the probability density function of conservative components (as defined below). We consider the local probability density $p(\widetilde{c}_C, x, y, t)$ that at location (x, y), at time t the concentration of C is $\widetilde{c}_C$. We can thus express M_C as

$$M_C(t) = \int_V dV c_C = \int_0^{c_0} d\widetilde{c}_C \widetilde{c}_C \phi(\widetilde{c}_C, t) \tag{9}$$

where we introduced the total probability density $\phi(\widetilde{c}_C, t) = \int_V dV p(\widetilde{c}_C, x, y, t)$ and the tilde over the local concentration c_C indicate the associated ensemble variable. We define the conservative species $R = A + C$ and $S = B + C$ whose concentrations c_R and c_S are subjected only to diffusion and advection, due to the linearity of the transport processes considered in equation (2). For the mixing limited reactions considered here, the coexistence of the chemicals A and B is very short: when mixed A and B react before transport processes can act. As pointed out by [12], locally the concentration of C can be written as $c_C = min[c_R, c_S]$ and the total mass $M_C(t)$ can be expressed as:

$$M_C(t) = \int_0^{\frac{c_0}{2}} d\widetilde{c}_R \widetilde{c}_R \phi(\widetilde{c}_R, t) + \int_{\frac{c_0}{2}}^{c_0} d\widetilde{c}_R (c_0 - \widetilde{c}_R) \phi(\widetilde{c}_R, t) \tag{10}$$

Note that $min[c_R, c_S]$ is c_R when $c_R < \frac{c_0}{2}$ and is $c_S = c_0 - c_R$ if $c_R > \frac{c_0}{2}$. We hence relate the cumulative mass of produced C to the concentration of the conservative species R and S. The total probability density $\phi(\widetilde{c}_R, t)$ can be written as the sum of tree terms

$$\phi(\widetilde{c}_R, t) = \int_{V_{mix}} dV p(\widetilde{c}_R, x, y, t) + \int_{V_0} dV \delta(\widetilde{c}_R) + \int_{V_1} dV \delta(\widetilde{c}_R - c_0) \tag{11}$$

The domain of integration V_{mix} is the portion of the system where the conservative component are mixed and thus their concentration are different from 0 or c_0. V_0 and V_{c_0} are defined as the portion of the system where c_R have concentration 0 and c_0 respectively. Since in equation (11) the values 0 and c_0 for $\widetilde{c}_R$ give no contribution, we focus on the integral over V_{mix}. The production of C is fully determined by the conservative species in the mixing volume V_{mix}.

In order to simplify the first term of equation (11), we define a new reference system (x', y') with the components oriented, respectively, parallel and transverse to the local direction of flow. We thus discretize the volume V_{mix} in N_Ω slices Ω_i locally parallel to the direction x'. In each slice the concentration of the conservative species c_R along the local x' direction goes from c_0 to 0. We assume that this dependence scales as a function of $\frac{x'}{w(y',t)}$, where $w(y', t)$ is the size of the i-th slice in the x' direction. Thus $\int_{V_{mix}} dV p(\widetilde{c}_R, x, y, t)$ can be rewritten as

$$\phi(\widetilde{c}_R, t) = \int_{L(t)} dy' w(y', t) \int d\widetilde{x} p(\widetilde{c}_R, \widetilde{x}) = L(t) \overline{w(t)} f(\widetilde{c}_R) \tag{12}$$

where $\widetilde{x} = \frac{x'}{w(y',t)}$ is an ensemble variable varying between 0 and 1 and f is a function that is independent on time and space. Inserting equation 12 in equation 10, provides the relationship between the mass of produced C and the geometrical characteristics of the mixing volume, as quantified by the average width $\overline{w}$ and L, which represents the length of the line that joins all the centers of the slices Ω_i.
The geometrical characteristic of the mixing zone, L and $\overline{w}$ are related to the spreading properties of the porous medium. Advective spreading can be quantified by the variance of the fluid particles displacement

$$\sigma_x^2(t) = \sum_i \int_V dV \Big(x_i(t) - x_i(0) - \overline{x}(t) \Big)^2 \tag{13}$$

where $x_i(t) - x_i(0)$ represent the longitudinal displacement of the i-th particle that constitute a fluid plume, $\overline{x}(t)$ its average position and the sum is done over all the N_p SPH particles. As illustrated in Figure 2, the length of the line that joins the local center of masses, L, decreases when increasing the diffusion coefficient. For large diffusion coefficient the local center of mass position depends on the averaging of a large number of fluid particles. therefore the variability of the local center of mass positions decreases when increasing diffusion. On the other hand the local width w increases when increasing diffusion.
We thus make the conjecture that $L(t) \propto \frac{\sigma_x(t)}{\overline{w}(t)}$. For an heterogeneous porous medium this conjecture can be supported by the following intuitive arguments. The center of each slice depends on the position of all the fluid particles in a disk of radius proportional to its size, w. The size of each disk is large enough to contain stagnation zones and channels. Thus, it is much larger than the characteristic velocity field correlation length and hence within it the statistics of all the fluid particles is well

represented. Assuming that each disk includes N independent fluid particles, with N growing with the disk volume $\overline{w}^2$, the variance of the center of mass position can be approximated as $\sigma_\chi^2 \sim \sigma_x^2/N = \sigma_x^2/\overline{w}^2$. Hence the length L can be estimated as $L = \sqrt{\sigma_\chi^2} \sim \sigma_x/\overline{w}$. This simple conjecture implies that the mixing volume scales as $L\overline{w} \sim \sigma_x$.

Thus, using this relationship in equations (10) and (12), the time evolution of M_C is found to be independent of diffusion and controlled only by the longitudinal advective dispersion $M_C(t) \propto \sigma_x$. A direct measure of σ_x from the analysis of the N_p Lagrangian SPH particles confirm this result (see Figure3).

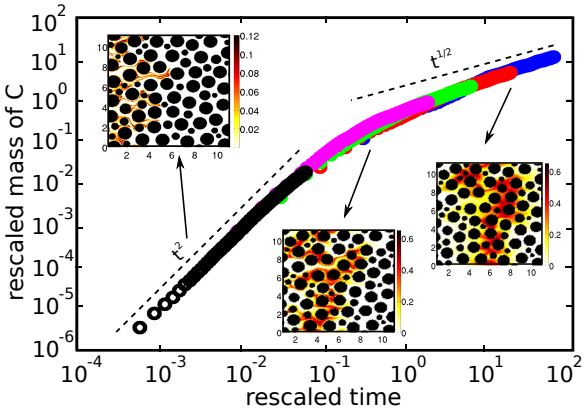

Figure 5. The rescaled mass of produced C in a $\log - \log$ scale versus the rescaled time τ. Colors are defined as in previous figures.

To provide a global picture of the evolution of the considered mixing limited system, we rescale the time with respect to the characteristic transition time t_D and the cumulative mass $M_C(t)$ with respect to $\sigma_x(t_D)$. Figure 5 shows the rescaled mass versus the rescaled time $\tau = \frac{t}{t_D}$ for all the simulated cases. The 5 curves collapse on each other, confirming the observations for the two regimes and the transition between them.

The analyzed high resolution pore scale simulations display anomalous transport and reaction behavior compared with classical Fickian models that assume complete mixing at the pore scale. Thus, incomplete mixing is found to have a dramatic impact on reaction kinetics. The results provide a link between anomalous kinetics and anomalous transport. Specifically we relate purely advective processes to the kinetics scaling.

Acknowledgements

Pietro de Anna and Tanguy Le Borgne acknowledge the financial support of the European Commission through FP7 projects ITN project, IMVUL project (Grant Agreement 212298) and Marie Curie ERG grant ReactiveFlows (Grant Agreement Number 230947).

[1] I. Battiato, D.M. Tartakovsky, a.M. Tartakovsky, and T. Scheibe. On breakdown of macroscopic models of mixing-controlled heterogeneous reactions in porous media. *Advances in Water Resources*, 32(11):1664–1673, November 2009.

[2] D. ben Avraham and S. Havlin. *Diffusion and Reactions in Fractals and Disordered Systems*. Cambridge University Press, 2000.

[3] Tanguy Le Borgne, Diogo Bolster, Marco Dentz, and Alexandre Tartakovsky. Upscaling dispersion with the correlated CTRW model. *Water Resources*, pages 1–27.

[4] Gabriele Chiogna, Olaf A. Cirpka, Peter Grathwohl, and Massimo Rolle. Transverse mixing of conservative and reactive tracers in porous media: Quantification through the concepts of flux-related and critical dilution indices. *Water Resources Research*, 47(2), February 2011.

[5] Pietro de Anna, Tanguy Le Borgne, Marco Dentz, Diogo Bolster, and Philippe Davy. Anomalous kinetics in diffusion limited reactions linked to non-Gaussian concentration probability distribution function. *The Journal of chemical physics*, 135(17):174104, November 2011.

[6] M. De Simoni, X. Sanchez-Vila, J. Carrera, and M. W. Saaltink. A mixing ratios-based formulation for multicomponent reactive transport. *Water Resources Research*, 43(7):1–10, July 2007.

[7] a. De Wit. Fingering of Chemical Fronts in Porous Media. *Physical Review Letters*, 87(5):1–4, July 2001.

[8] Marco Dentz, Tanguy Le Borgne, Andreas Englert, and Branko Bijeljic. Mixing, spreading and reaction in heterogeneous media: A brief review. *Journal of contaminant hydrology*, May 2010.

[9] Marco Dentz, Tanguy Le Borgne, Andreas Englert, and Branko Bijeljic. Mixing, spreading and reaction in heterogeneous media: a brief review. *Journal of contaminant hydrology*, 120-121:1–17, March 2011.

[10] Yaniv Edery, Harvey Scher, and Brian Berkowitz. Particle tracking model of bimolecular reactive transport in porous media. *Water Resources Research*, 46(7):1–12, July 2010.

[11] L. Gálfi and Z. Rácz. Properties of the reaction front in an A+BC type reaction-diffusion process. *Physical Review A*, 38(6):3151–3154, September 1988.

[12] Carolyn M. Gramling, Charles F. Harvey, and Lucy C. Meigs. Reactive Transport in Porous Media: A Comparison of Model Prediction with Laboratory Visualization. *Environmental Science & Technology*, 36(11):2508–2514,

June 2002.

[13] S. Havlin, M. Araujo, H. Larralde, A. Shehter, and H.E. Stanley. Anomalous kinetics in A + B C with initially-separated reactants. *Chaos, Solitons & Fractals*, 6:157–169, January 1995.

[14] Werner Horsthemke, Sergei Fedotov, and Vicenc Mendez. *Reaction-Transport Systems*. Springer Series in Synergetics. Springer Berlin Heidelberg, Berlin, Heidelberg, 1st edition, 2010.

[15] K. Kang and S. Redner. Fluctuation-dominated kinetics in diffusion-controlled reactions. *Physical Review A*, 32(1):435, 1985.

[16] Vivek Kapoor, Lynn W. Gelhar, and Fernando Miralles-Wilhelm. Bimolecular second-order reactions in spatially varying flows: Segregation induced scale-dependent transformation rates. *Water Resources Research*, 33(4):527, 1997.

[17] Tanguy Le Borgne, Marco Dentz, and Jesus Carrera. Lagrangian Statistical Model for Transport in Highly Heterogeneous Velocity Fields. *Physical Review Letters*, 101(9):1–4, August 2008.

[18] Jian Luo, Marco Dentz, Jesus Carrera, and Peter Kitanidis. Effective reaction parameters for mixing controlled reactions in heterogeneous media. *Water Resources Research*, 44(2):1–12, February 2008.

[19] J.M. Ottino. *The kinematics of mixing: stretching, chaos, and transport*. Cambridge University Press, 1989.

[20] Alexandre Tartakovsky. Langevin model for reactive transport in porous media. *Physical Review E*, 82(2):1–11, August 2010.

[21] Alexandre Tartakovsky, Daniel Tartakovsky, and Paul Meakin. Stochastic Langevin Model for Flow and Transport in Porous Media. *Physical Review Letters*, 101(4):1–4, July 2008.

[22] A.M. Tartakovsky, G.D. Tartakovsky, and T.D. Scheibe. Effects of incomplete mixing on multicomponent reactive transport. *Advances in Water Resources*, 32(11):1674–1679, November 2009.

[23] T Tel, A Demoura, C Grebogi, and G Karolyi. Chemical and biological activity in open flows: A dynamical system approach. *Physics Reports*, 413(2-3):91–196, July 2005.

[24] E Villermaux and J Duplat. Coarse Grained Scale of Turbulent Mixtures. 144506(October):4–7, 2006.

[25] S. Whitaker. *The Method of Volume Averaging*. Kluwer Academic Publishers, 1999.

[26] Z. Neufeld and E. Hernandez-Garcia. *Chemical and Biological Processes in Fluid Flows: A dynamical System Approach*. Imperial College Press, 2010.

4.2 Islands dynamics interpretation for the dispersion regime

For the considered mixing limited reaction, due to the pore scale incomplete mixing, we observe two time regimes in which the total product mass evolves faster then the classical prediction $t^{\frac{1}{2}}$ obtained with a Fickian dispersion description (e.g. *Gramling et al.* [2002]). For early times the invading solute is organized in fingers and the cumulative mass of the produced C scales as Dt^2, see Figure 4.4. For late times the longitudinal spreading of the solute controls the anomalous scaling $M_C \propto \sigma$. Here we propose another interpretation for this second regime that is consistent with the one already discussed and that involves dispersion transverse to the main flow direction. It also provides a link with the (OZ) segregation problem discussed in the second chapter of this thesis.

When for $t > t_D$ the fingers structures of the invading chemical are destroyed by diffusive mixing, the scaling of the total mass of produced C slows down from the previous regime, but is still faster than the prediction of Fickian models $t^{1/2}$ (e.g. *Gramling et al.* [2002]; *Edery et al.* [2010]; *Tartakovsky et al.* [2009]) and the total mass does not depend on local diffusion D (or on the Peclet number for the given flow). In classical Fickian models, reactants are considered to be well mixed in each cross-section transverse to the main flow. The mass produced by reactions is proportional to the longitudinal width of the plume of C (measured by Fickian dispersion) and the concentration of the reaction product c_C at the center of the plume is constant (e.g. *Gramling et al.* [2002]). Figure 4.5 shows the projection along the x axis of c_C for different values of D at time $t = 9\tau_a$, where $\tau_a = \frac{\lambda}{\overline{v}}$ is the characteristic advection time over the average pore size $\lambda = 10$. Contrary to the well mixed models, large diffusion coefficients lead to smaller longitudinal plume size as quantified by the spatial concentration variance,

$$\sigma_C = \int (x - \overline{x})^2 c_C(x, y, t) dxdy \tag{4.2}$$

where $\overline{x}$ is the position of the center of mass (Figure 4.5 and 4.6). This phenomenon is consistent with the fact that diffusion tends to reduce the correlation of Lagrangian velocities by allowing particles to jump from one strem line to another with the consequent reducing of spreading. This complex dependency has been studied and discussed by, for example, *Bijeljic et al.* [2011]. Another effect of increasing diffusion is to increase the peak of reactive plume (see Figrue 4.5). These two effect balance each other and the area under the curves in Figure 4.5, representing the total mass of C, does not depend on D. This key observation implies that the behavior of this reactive system is different of that assumed by classical models where well mixed conditions at each position x is postulated.

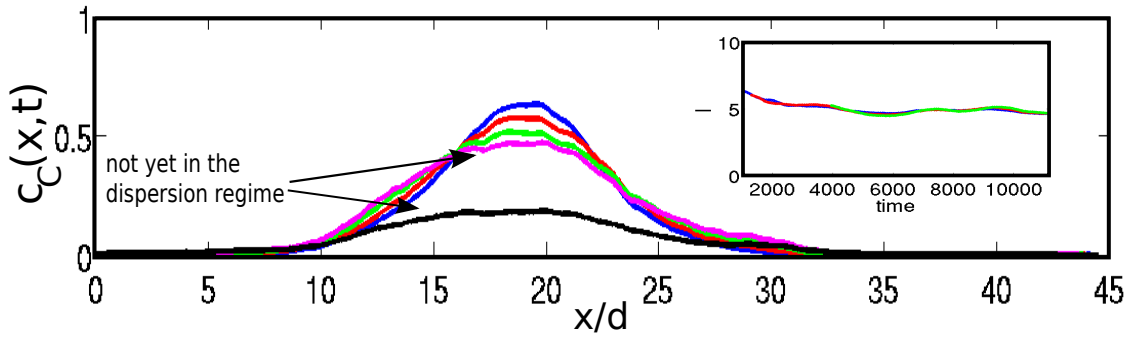

Figure 4.5: *a, the projection of the dimensionless concentration of C along the main flow direction (x) at time $t = 9\tau_a$; b. the total mass of C; c. the scaling of the size of the plume σ_C. Blue, red, green, magenta and black curve represent data for Peclet values of: blue $Pe = 10^{-2}$, red $Pe = 3 \cdot 10^{-3}$ green $Pe = 10^{-3}$ magenta $Pe = 3 \cdot 10^{-4}$ and black $Pe = 10^{-5}$., respectively.*

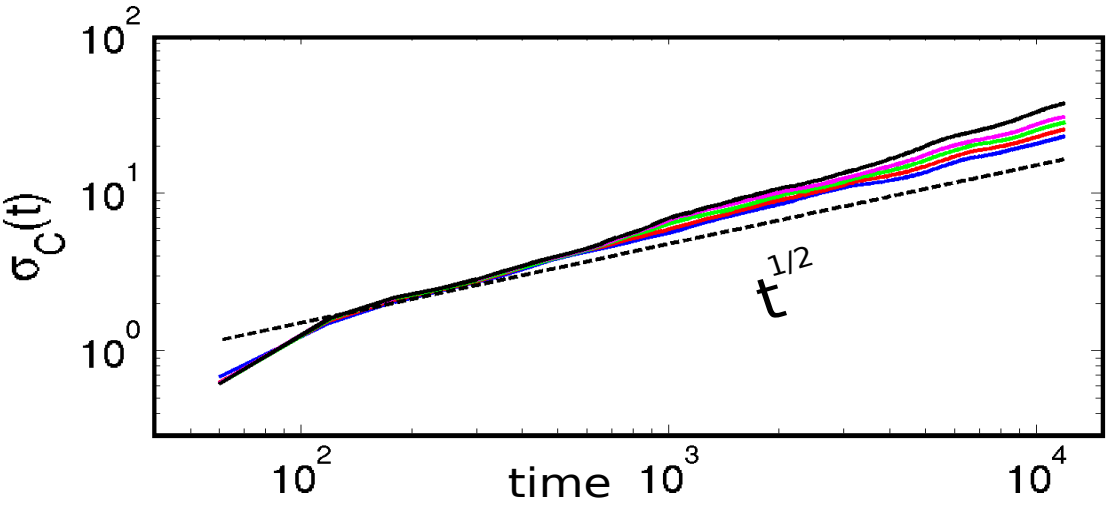

Figure 4.6: *Different lines represent the temporal scaling of the longitudinal variance of reaction product concentration for different Peclet values: blue $Pe = 10^{-2}$, red $Pe = 3 \cdot 10^{-3}$ green $Pe = 10^{-3}$ magenta $Pe = 3 \cdot 10^{-4}$ and black $Pe = 10^{-5}$.*

the mass of C can be rescaled with respect to $\sigma_C(t)$ and the peak value $C_p(t) = \int c_C(x = peak, y, t)dy$:

$$M_C(t) = \sigma_C(t)C_p(t)I(t) \tag{4.3}$$

where $I(t) = \int_x \frac{c_C(x,y,t)}{\sigma_C(t)C_p(t)}dxdy$. In the dispersion regime, I results to be constant and does not depends on the Peclet number (as shown in inset of Figure 4.5), showing that $\sigma_C(t)$ and

$C_p(t)$ are the only control parameters for $M_C(t)$. Thus the projection of the longitudinal c_C distribution is shape invariant. The degree of mixing at a longitudinal position x can be quan-

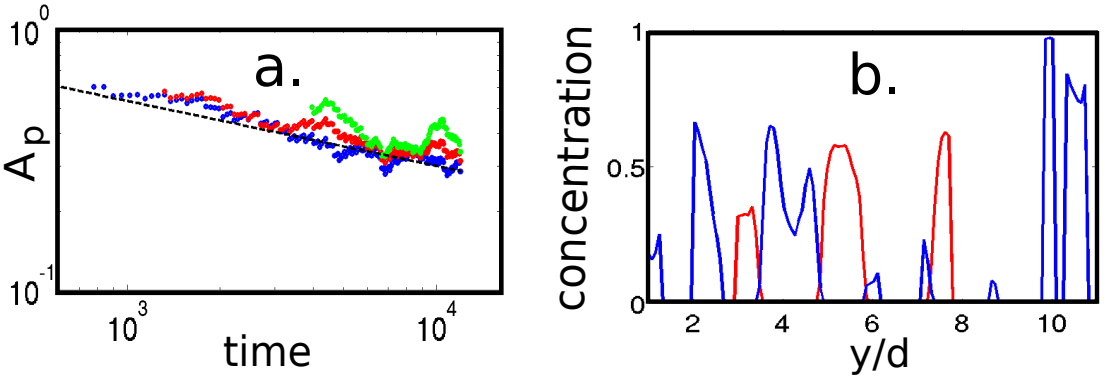

Figure 4.7: *a, the time scaling of A_p decreasing as $t^{-\frac{1}{4}}$. b, the cross section of the concentration field at peak position in the direction transverse to the main flow: in blue is represented A in red B.*

tified by analyzing the spatial distribution of A and B in a cross section transverse to the main flow (Figure4.7b). A and B are found to be organized in segregated islands. We compare their dynamics to the $1D$ diffusion limited reactive system studied by in the second chapter of this thesis. The spatial segregation of reactants (see Figure 4.7b) is progressively reduced by transverse diffusion. The resulting reactions tend to increase the mass of C produced at the center of the reactive plume. Under this analogy we can expect the production of mass at the peak to follow the anomalous scaling discussed in the second chapter of the thesis. In this framework the mass of A at the center, $A_p(t) = \int c_A(x = peak, y, t)dy$ should scale as $t^{-\frac{1}{4}}$. Figure 4.7a shows that the pore scale simulation results are compatible with this description. By mass conservation the increase of $C_p(t)$ can be predicted by adding the total mass of C produced until time t_D at the center, when the islands dynamics start, to the variation of A at the peak: $C_p(t) = C_p(t_D) + A_p(t_D) - A_p(t)$.

This second interpretation for the dispersion regime observed in this mixing limited reaction provides a connection between reactive diffusive systems and more complex advection diffusion reactive systems. In particular, the dynamics $t^{-\frac{d}{4}}$ of the the diffusion-limited segregation problem results to control the anomalous scaling of this incomplete mixed reactive system. Moreover this result shows the importance of transverse dispersion of solutes while transported in heterogeneous porous media.

4.3 The $3d$ case

A reactive front simulation similar to the one described previously in this chapter has been performed in a $3d$ flow, for three values of the Peclet number. As for the $2d$ case we observe anomalous scaling of kinetics if compared with classical Fickian models. The invading chemical A is organized in fingers and the mass of C produced at the front scales in time as t^2. This results to be true for times smaller than the characteristic diffusion time t_D over the fingers boundaries. For $t > t_D$, the produced mass of C change tis scaling and slow down. In Figure 4.8 are displayed the simulations results for the cumulative mass of C versus the rescaled time $\tau = \frac{t}{t_D}$. M_C scales as $\tau < 1$. This $3d$ results are consistent with the physical model proposed for the $2d$ case.

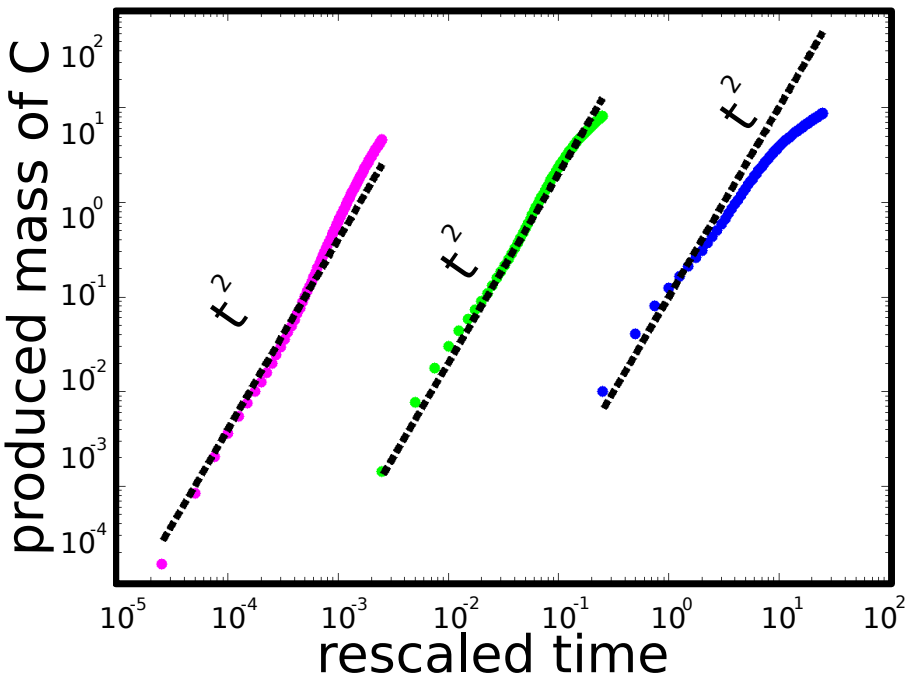

Figure 4.8: *Scaling of the cumulative mass of C in 3d pore scale simulation versus time rescaled with respect to the characteristic diffusion time over the average transverse finger cross section. Different colors represent different Peclet number: magenta $Pe = 500$, green $Pe = 50$ and blue $Pe = 5$.*

Chapter 5

Experimental set up for $2d$ reactive transport

5.1 Introduction

Numerical simulations provide the opportunity to study and investigate physical systems under certain assumptions (e.g. well mixed condition over the scale of the spatial resolution). Experiments are a direct measure of natural phenomena that are not subject to any assumption. On one hand they allow a direct observation of new phenomena, on the other they provide a general reference to test the validity of a theory. Measuring the impact of incomplete mixing on global reaction kinetics represent a challenging goal. Thus, there exist relatively few experiments in the framework of reactive transport in porous media laboratory experiments for which both pore scale mixing and reaction rates are quantified (e.g. *Gramling et al.* [2002]). Here we present a new laboratory experiment that allow for high spatial resolution quantification of pore scale incomplete mixing, concentration pdf and reaction rate in a porous medium.

We study the case of the reactive front studied numerically in the previous chapter of the thesis (i.e. a reactant A that invades a medium initially saturated by another reactant B) represented in Figure 5.1. This case is of primary interest since the heterogeneity of the porous medium determines the front geometry. The physical system discussed in the previous chapter is a $2d$ porous medium within which a flow, solution of Navier-Stokes equations, transport the two reactants A and B. To experimentally reproduce the same system as in the simulations, the main issues to solve are: i) the design of a $2d$ porous medium, across which a flow is imposed,

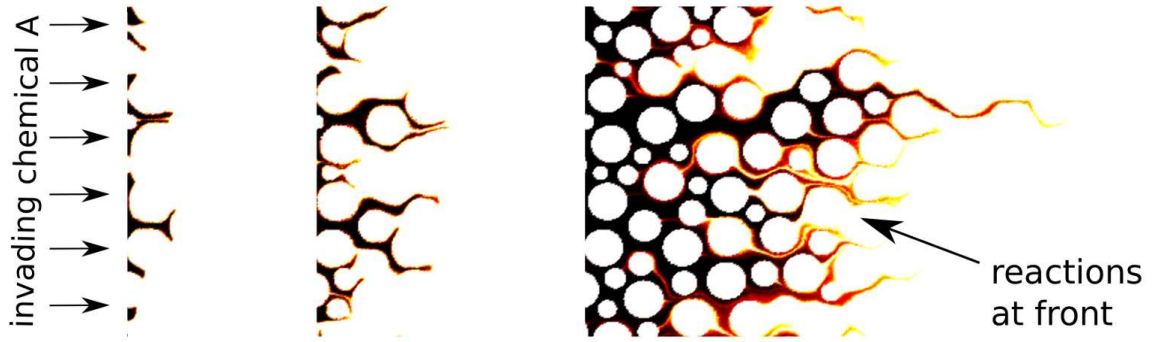

Figure 5.1: *The invading chemical analyzed in the previous chapter: three snapshot for three consecutive times from pore scale numerical simulations.*

such that we can observe pore scale mixing; ii) the observation and quantification of chemical reactions simultaneous to the transport of reactants at the pore scale.
The work presented in this chapter was made in collaboration with Yves Meheust, assistant Professor at the University of Rennes 1 (France), Herve Tabuteau researcher at the National Council of Research, Rennes (France), Joaquin Jimenez-Martinez, Post-doc position at CNRS - University of Rennes 1 (France) and Regis Turuban, Master student at University of Rennes 1 (France).

Homogenization scale for chemical reactions

Real chemical reactions are the ensemble of processes that transform chemical species in other chemical species due to their local interactions. The mass action law states that the elementary reaction rate is proportional to the product of the reactant concentrations each one elevated to the power of the corresponding stoichiometric coefficient. As discussed in previous chapters, behind the mass action law there is a strong hypothesis: the involved chemicals are in dynamical equilibrium and are assumed to be well mixed (e.g. *Connors* [1990]). Thus, studying the impact of incomplete mixing on chemical kinetics at pore scale implies the definition of an homogenization scale ξ where chemicals can be assumed to be well mixed. For the case of the numerical method Smoothed Particles Hydrodynamics (SPH) adopted in the previous chapter, the homogenization scale is represented by the size of each SPH particle. This implies that the numerical method cannot resolve the system at scales smaller than the particle size. In other words, it is assumed that over the smaller observation time scale all the processes that occur at scale smaller than the particle size are assumed to be homogenized and well

represented by the concentration of chemicals in each particle. The choice of the size for that homogenization scale has thus a crucial impact on the results of the simulations. For a given time discretization τ, the homogenization scale is usually taken to be the characteristic diffusion length over duration τ, $\xi = 2D\tau$ (e.g. *Tartakovsky* [2010]). In such a way it is assumed that diffusion processes mix all quantities over the length ξ during τ.
An experimental verification of this hypothesis is alway needed in order to provide correct models and predictions. This is a first motivation to do a laboratory experiment in the framework of this thesis that focuses on modeling reactive transport phenomena.

The dimensionality of the considered system

Transport and reactive processes in natural media occur in $d = 3$ dimension. Thus, in principle, to reproduce them three dimensional experiments are necessary. Optical visualization techniques are often used in experimental fluid mechanics (e.g. *Duplat et al.* [2010b]). In flow studies addressing natural objects (fractured or porous rocks), direct optical visualization is difficult to attain as the media are usually opaque to visible light. Even if the solid objects in the experimental setup happens to be transparent to light, the existence of complex boundaries between the fluid and the surrounding solid phase leads to distortion of the images through light refraction at interfaces, unless the solid and fluid are nearly perfectly matched in optical index. This is in particularly true for porous media, due to the many optical interfaces present in the system. The matched fluid allows tracking of individual particles inside the porous medium. Moreover, if we are interested in concentration fields the experimental set up become more complicated. A laser sheet can be used to visualize just a layer of the whole medium (see Figure 5.2). The following images processing allows the reconstruction of the $3d$ concentration field. Here we are interested in reproducing a $2d$ porous medium obtain a $2d$ concentration pdf. The simple two dimensional case can provides informations about the basic mechanisms that govern also more complex three dimensional systems. Thus we will reproduce experimentally the same geometric configuration of the simulated porous medium and we will impose within it a flow in the same physical conditions. After having initially saturated the system with a reactant B, we will inject in the medium another chemical A so that we will be able to observe chemical reaction at the front (see Figure 5.1). Such a system can be studied with relatively high resolution digital camera that takes images of the $2d$ concentration field.

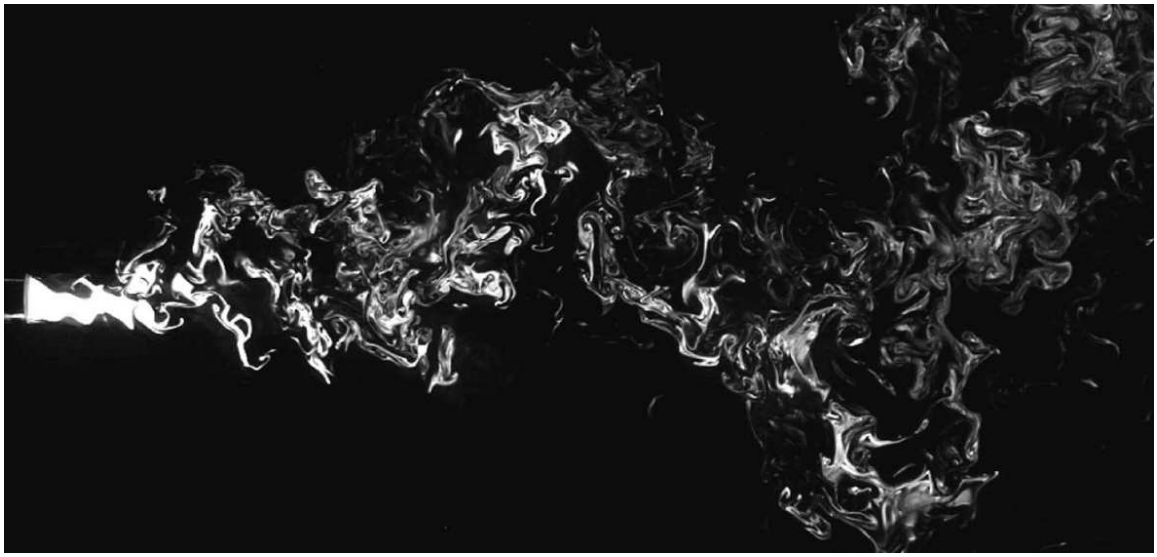

Figure 5.2: *2d image of a 3d turbulent flow: measurements of a fluorescent field done by shining a plane with an argon laser sheet through the water tank in a plane containing the axis of the mean flow. Image taken from Duplat et al. [2010b].*

As an additional motivation, nowadays technologies allow us to measure such a local concentrations at spatial resolutions of the same order or even higher than that of numerical simulations. This implies the possibility to upscale local (mesoscopic) quantities to macroscopic scale.

Temporal scaling for anomalous kinetics

In the presence of certain symmetries a spatial system can be described in terms of its projection along one direction, and then be modeled as one dimensional (e.g. *Gramling et al.* [2002]). The mixing limited reactions at the front between two solutes, one displacing the other, has a preferred direction, parallel to the main flow. At the Darcy scale the projection of the averaged concentrations is classically written as a unidimensional mass transport and reaction equation

$$\phi \frac{\overline{c}_i}{\partial t} + q \frac{\partial \overline{c}_i}{\partial x} - (D + D^*) \nabla^2 \overline{c}_i = r_i^*, \tag{5.1}$$

where $i = A, B, C$, D^* is the hydrodynamic dispersion coefficient, and the reaction rates are $r_i^* = -k\overline{c}_A\overline{c}_B$ for $i = A, B$ and $r_C^* = k\overline{c}_A\overline{c}_B$. The constant Darcy velocity satisfies the Darcy equation $q = -K\partial h/\partial x$, K being hydraulic conductivity and h the hydraulic head *Gramling et al.* [2002]; *Tartakovsky* [2010]; *Dentz et al.* [2010] and ϕ the porosity of the medium (e.g. *Bear* [1988]). In this framework the mass produced by reactions scales in time as $t^{\frac{1}{2}}$ (e.g. *Gramling*

et al. [2002]). As already discussed in the previous chapters, incomplete mixing at the pore scale implies an anomalous behavior of the reaction rates with respect to this classical results.

The scaling of the produced mass by reactions in the case of pore scale advection is an open question which has not been investigated so far for porous media and represents one of the main goal of the present work.

The need for improved visualization and quantification of reactions

Previous experimental methods for obtaining $2d$ concentration fields and reaction rates have relied on colorimetry methods. To visualize and quantify chemical reactions in a transparent porous medium *Oates and Harvey* [2006] propose a chemical reaction between two (almost) transparent chemicals whose reaction product is colored. The chemical reaction is

$$CuSo_4(aq) + Na_2EDTA^{2-} \rightarrow CuEDTA^{2-} + 2Na^+ + SO_4^{2+} \tag{5.2}$$

The reactants $CuSo_4(aq)$ and Na_2EDTA^{2-} are respectively light blue and transparent, while the product of the reaction $CuEDTA^{2-}$ is dark blue. Considering a $2d$ transparent porous medium it is possible to take images and visualize the concentration field of the produced colored chemical. In practice what can be measured is the change in the amount of transmitted light by the the colored solution in the porous medium. This quantity can be related to the concentration the solution in the fluid by the relationship described by the Beer-Lambert law (e.g. *Oates and Harvey* [2006]; *Oates* [2007]). This law fixes the functional relationship between the transmitted light intensity I which has passed through the concentration C in a chamber of thickness a as

$$\log_{10} \frac{I}{I_0} \propto -aC \tag{5.3}$$

where I_0 is the intensity of the incident light. Thus to convert the light intensity value, obtained from the images of the chamber, to concentrations, we can use an empirically determined calibration curve between known concentrations and their observed light intensity needs to be used (e.g. *Gramling et al.* [2002]).

The non linear relationship between transmitted light intensity and concentration field is one of disadvantage of this method. The smaller is the variation in concentration we want to measure, the smaller is the variation in transmitted light and the less it will be observable. Thus, to measure small concentration gradients, that is of primary interest in incomplete

mixed systems, a linear relationship between the light intensity (or other measured quantities) and concentrations would be preferable. Another goal of this thesis is to propose a new efficient method to visualize and quantify local reaction rate at high spatial resolution.

5.2 A pore scale experiment based on chemiluminescence

Here, we propose a new experimental set up to visualize and quantify chemical reaction rate with pore scale resolution in a $2d$ transparent porous medium. The main ingredients for such an experiment are:

- a (quasi) $2d$ porous medium P
- a (quasi) $2d$ flow q in P that will transport the reactants
- a chemiluminescence (optically detectable) chemical reaction
- a camera to take pictures of pore scale concentration fields

With an injection system a pressure gradient ∇p is imposed at the extremities of the porous medium P. The produced flow carries two reactants whose reaction at the front is optically visible. The digital camera takes picture with an imposed time interval Δt. A chemiluminescence reaction between the reactants produces light and is optically detectable. As discussed in more details in the following, we choose a chemical reaction that produces photons proportionally to the amount of reactions that has taken place.

A quasi-Hele-Shaw cell

To produce a (quasi) $2d$ flow q in a porous medium P we consider a transparent chamber, or cell, made by two glass plates whose separation distance is a. We fill the chamber with cylinders representing the grains of a real porous medium. The size and the spatial distribution of these cylinders is the same as in the numerical simulations described in the previous chapter. The cell is closed on two sides and a pressure gradient between the open sides is imposed, causing a flow between the two apertures of the cell. Such a flow is used in several domains where low Reynolds number are needed, e.g. microfluidic flows *Tabeling* [2005]. When the thickness a is much smaller then the average size of obstacles in the cell, the chamber is know as Hele-Shaw cell (e.g. *Tabeling* [2005]). The basic principle beyond the Hele-Shaw cell lies in the fact that the size a of the gap between the plates is small compared to the size L of

the obstacles between the plate. Consequently, the gap a controls the velocity profile in the direction perpendicular to the mean cell plane, and the local Stokes equations that govern the fluid dynamics results in the mean flow velocity across the cell thickness to be controlled by a Darcy equation.

For our purpose, we want to prevent the flow from being controlled by the thickness of the considered chamber (like in the case of the Hele-Shaw cell) and by a Darcy equation. Thus, we consider a Hele-Shaw cell whose thickness a is small compared to the overall horizontal dimensions of the cell, but not small with respect to the typical size of the obstacles in the chamber, L. The flow in a parallelepipedic channel where one of the transverse length is much smaller than the other one exhibits a velocity profile along the former smaller dimension that is parabolic, while the velocity profile along the latter larger dimension is that of a plug flow: almost uniform, with two narrow boundary layers at the walls (see Figure 5.3). In the standard Hele-Shaw setup the smallest section is the cell thickness, but in the case of our setup it is the horizontal distance between neighboring grains of the porous medium. Consequently the horizontal velocity field v (under stationary conditions) is governed by

$$\begin{aligned} \rho\left(\frac{\partial \mathbf{v}}{\partial t} + \mathbf{v}\cdot\nabla\mathbf{v}\right) &= -\nabla p + \mu\nabla^2\mathbf{v}, \\ \mathbf{v} &\sim \mathbf{v}(x,y), \\ \mathbf{v}\cdot\hat{z} &\sim 0 \end{aligned} \tag{5.4}$$

where ρ is the fluid density, p the pressure, μ is the (constant) dynamic viscosity.
With this quasi Hele-Shaw cell, due to the vertical flat velocity profile (except in the boundary layers), there is no vertical shearing inside the cell. So all shear occurs in the horizontal plane, which leads to a two-dimensional Navier-Stokes flow.

The porous medium

In the quasi Hele-Shaw cell we use the same pore geometry as the one used for the numerical simulations analyzed in the previous chapter. To resolve the flow and the reactions at the pore scale in the adopted porous medium with a digital camera and a standard optic (macro-lens), we build a quasi-Hele-Shaw cell of size $(100 \times 100 \times 1)$ mm. The grains of the porous medium have a size L between 1 mm and 7 mm, thus the thickness $a = 1$ mm of the chamber is not much smaller than L and the setup satisfies the conditions presented in the paragraph titled *A*

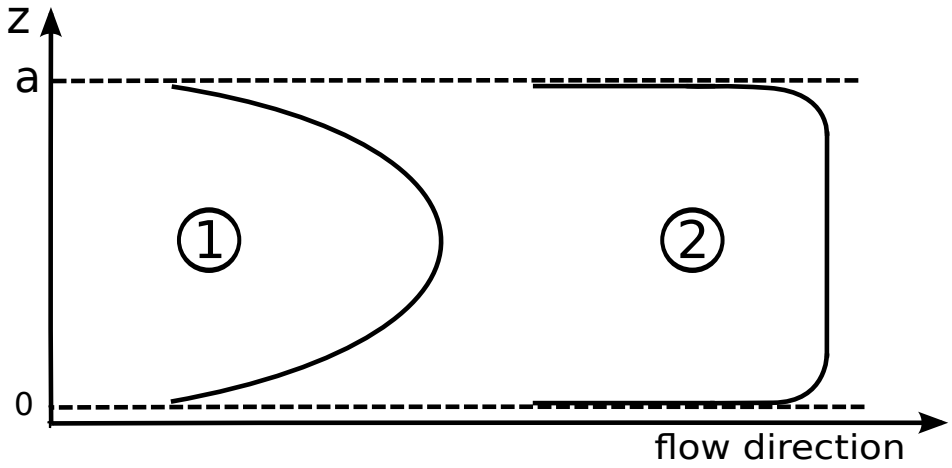

Figure 5.3: *A schematic picture of the velocity profile inside the Hele-Shaw cell in the vertical direction z for two extreme cases. Case* 1, $a/L \ll 1$, *the profile is parabolic in z; case* 2, *the ratio* a/L *is not a small quantity and over the vertical the velocity field has the same value almost everywhere.*

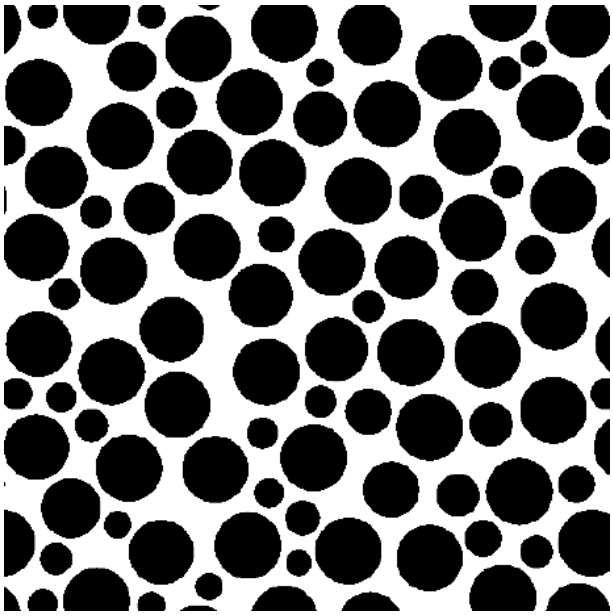

Figure 5.4: *The geometry of the adopted porous medium.*

quasi-Hele-Shaw cell, at least partly. We define the Reynolds number that characterize the ratio between inertial and viscous forces as

$$Re = \frac{\overline{v}L}{\nu} = \frac{qL}{\Sigma\nu} \tag{5.5}$$

where $\overline{v}$ is the average velocity over the length scale L, $\nu = \frac{\mu}{\rho}$ is the kinematic viscosity and $q = \overline{v}\Sigma$ is the flow across the surface Σ. To produce results that could be comparable with the numerical simulations analyzed in previous chapters, we will work in the same Reynolds

number regime. The Reynolds number of the numerical simulations was chosen to be $Re = 4$.

Lithography process

To build our cell, we use a lithographic technique. We adopt the technique described in *Harrison et al.* [2004], where between two glass plates a layer of UV-sensible glue is disposed. A mask with the negative image of the porous medium, shown in Figure 5.4, is printed at the high resolution of 128000 dots per inch (DPI) on a transparent film. The grains are represented by void circles and pores by black zones. This film is disposed on the top of the two glass plates, the space between which is filled with a UV sensible glue (Norland 81). Irradiating the glue in between the glass plates for a given time with a collimated UV light source we produce photopolymerization in the zones where the UV light can pass, as shown in Figure 5.5. As a

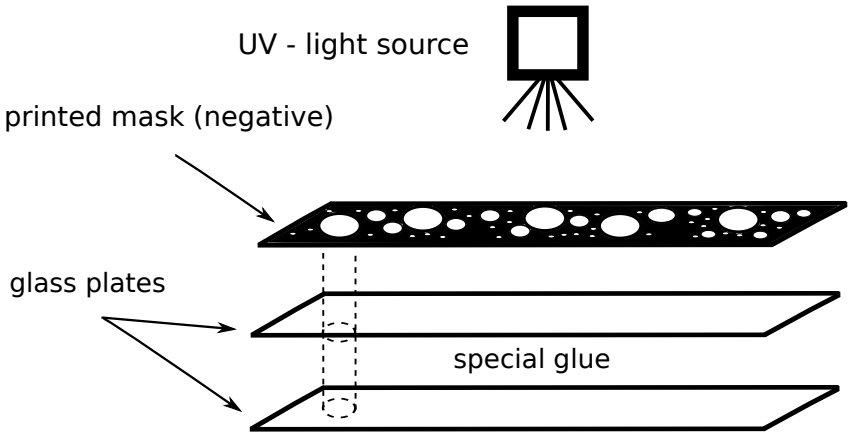

Figure 5.5: *A schematic view of the polymerization process.*

result we will obtain a series of cylinders between the glass plates made by a hard polymer. The used glue, *Norland Optical adhesive* 81, is sensitive to the entire range of long wave length from 320 to 400 nm, with a peak sensitivity around 365 nm. The cure time is dependent on light intensity and the thickness of the glue (in our case the distance between the glass plate). After this UV exposure phase, we clean the medium from the non polymerized glue that lies in the pores volume. This procedure is done using a combination of air pressure and a mixture of Ethanol and Acetone. The UV light source is a LED (*ThorLabs M365L2*) that emits UV at 365 nm. The used LED driver allows a variable power emission between 0 and 1 mW. Placing the UV source at a distance of 20 cm from the target we measured an homogeneous power per unit surface of 0.5 mW/cm^2 over an area of 10 cm^2. In order to obtain cylinder with sharp boundaries, we have to optimize the UV-light exposure time. In

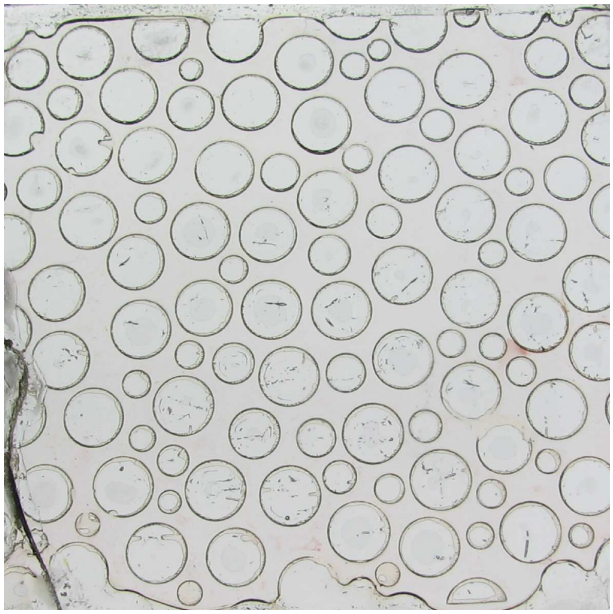

Figure 5.6: *A photo of the porous medium. The chamber's size is* $(100 \times 100 \times 1)mm$.

fact with underexposure the cleaning process will destroy totally or partially the solid grains. An overexposure will produce grains with a conic shape due to the diffusion of photons in the glue at the interface between the black and void zones in the mask. After several tests we optimized the exposure time τ_{exp} for a cell of thickness $a = 1$ mm exposed to a dose of 0.5 mW/cm^2, obtaining $\tau_{exp} = 135$ s (see Figure 5.6).

Once the grains are produced in between the glass plate, two opposite sides of the chamber are sealed using the same glue. The other two opposite sides will constitute the inlet and the outlet of the set up for the injection and the evacuation of the reactants.

The injection system

In order to produce the same flow as the one simulated through the SPH technique, we want to impose a homogeneous pressure at the opposite open sides of the chamber. To do this we build a suitable injection system using the following procedure. We superpose two glass plates with a isosceles triangle shape whose base $b = 10$ cm has the same size of the width of the chamber and a height u. The thickness of the glass plate is $d = 4$ mm. The gap between the glass plates is the same as the thickness of the chamber. We make a hole in one glass plate in the opposite corner of its basis. We seal this triangular structure against the open side of the chamber. We then close the other two border of this injection structure. We then produce another triangular structure similar to the previous one. This second structure is

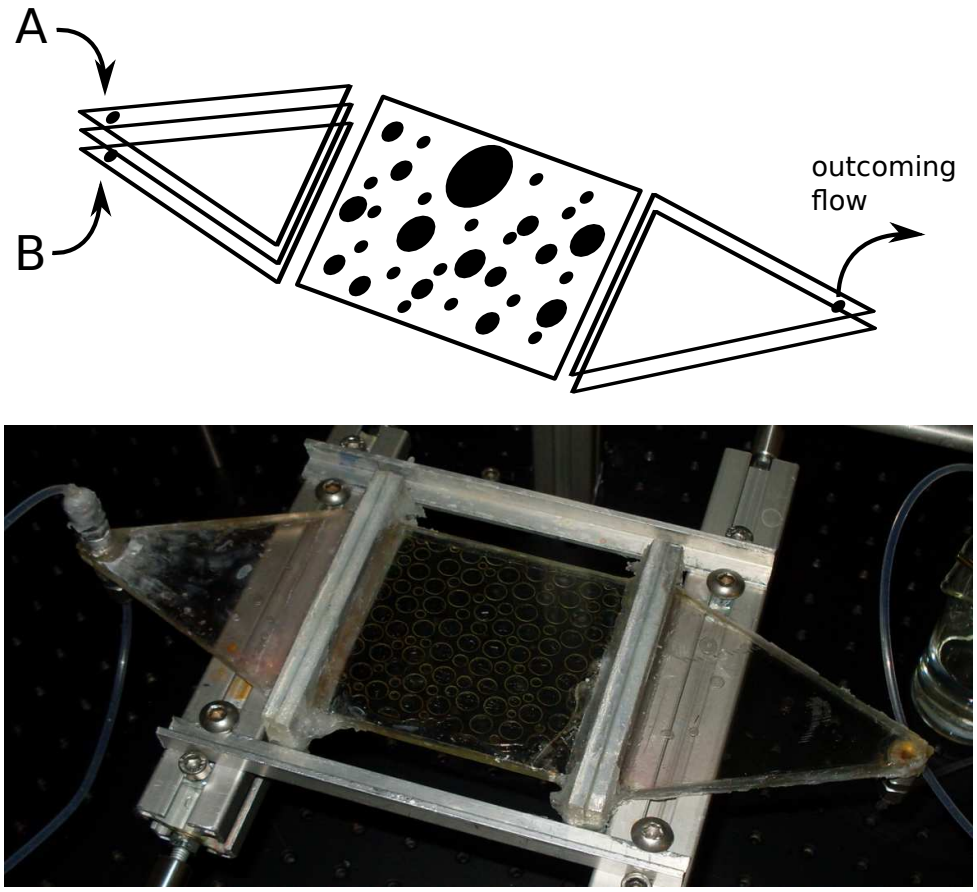

Figure 5.7: *On the top a schematic view of the injection system, on the bototm a photo of the real injection system and flow cell.*

made by the superposition of three isosceles triangular glass plate with the same base as the chamber width and an height u. The external triangle glass plate has a thickness $d = 4$ mm, the intermediate one has a thickness of 1 mm. The 2 gaps between the glass plates are both equal to 0.5 mm. We make a hole on the external glass plate in the opposite corner of its basis. A scheme of the injection system is shown in Figure 5.7. The height u of the triangles is chosen in order to have a flow at the entrance of the porous medium as homogeneous as possible. Figures 5.8 and 5.9 show the results of numerical simulations of the Navier-Stokes equations, with finite elements method, in the triangular injection structures with the same geometric properties already described and for two values of the height of the triangles: $u = 5$ cm and $u = 10$ cm. The velocity field profile obtained from numerical simulations suggest that 10 cm is a reasonable choice because the fluctuation of the flow about the average value are less then 10%.

We connect the two holes on the same injection structure to the reservoir of the reactant A and

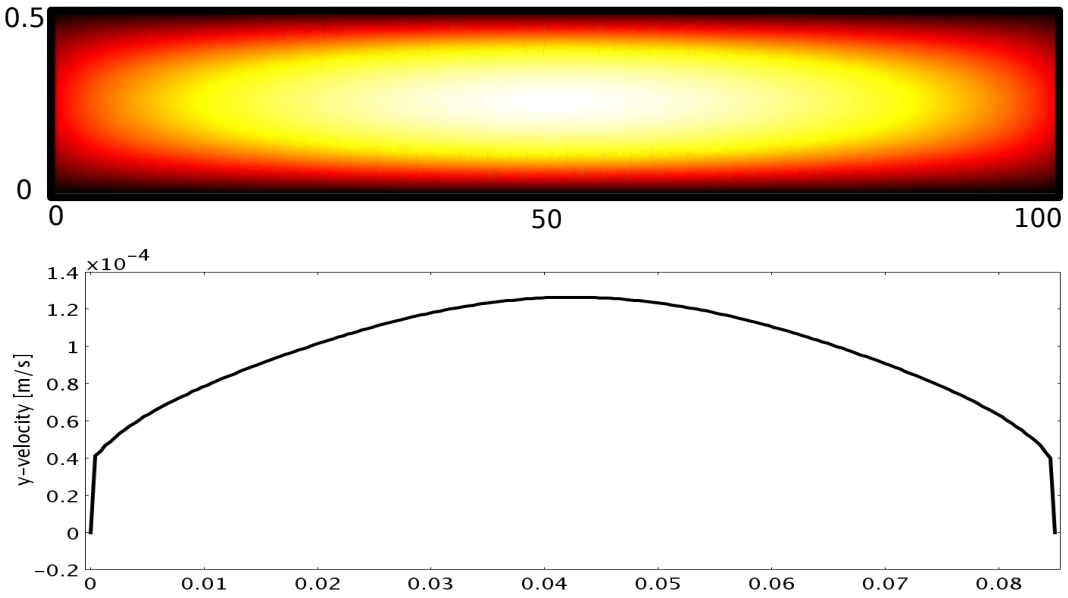

Figure 5.8: *Numerical simulation with finite element method for the flow in the injection system. On the top is shown the profile of the velocity field in the vertical cross section, where the triangular structure meet the porous medium. On the bottom the velocity profile in the line that cuts the cross section surface at mid-height. The gap between the glass plate is set to be* 0.5 *mm and the height is set to* $u = 5$ *cm*

B, respectively. The other structure is connected to a pump. By suction, we pump from one side of the chamber, injecting the reactants from the other side. A couple of faucet placed at the connection between the injection structure and the chemical reservoirs allows us to choose which chemical to inject. The pump is a cylindrical syringe whose piston is displaced by an electrical motor with constant rate. Knowing the diameter of the syringe, we can set the rate of the motor according to the flow that we want to impose. We can produce flow at volumetric flow rates ranging from $3 \cdot 10^{-2}$ mm^3/s up to 50 mm^3/s.

The chemical reaction

We chose a chemical reaction that follows the bimolecular irreversible kinetics $A + B \rightarrow C + \nu$ where C is some reaction product and ν is a photon. In this way the amount of light produced, and observed, will be proportional to the number of chemical reactions that have occurred.
We use the very fast peroxyoxalate chemiluminescence described in *Jonsson and Irgum* [1999], where the best combination of reaction speed and intensity of the emitted light is discussed. We use *bis(2.4.6-trichlorophenyl)oxalate* $(TCPO)$ under the catalytic influence of *1.8-diazabicyclo-*

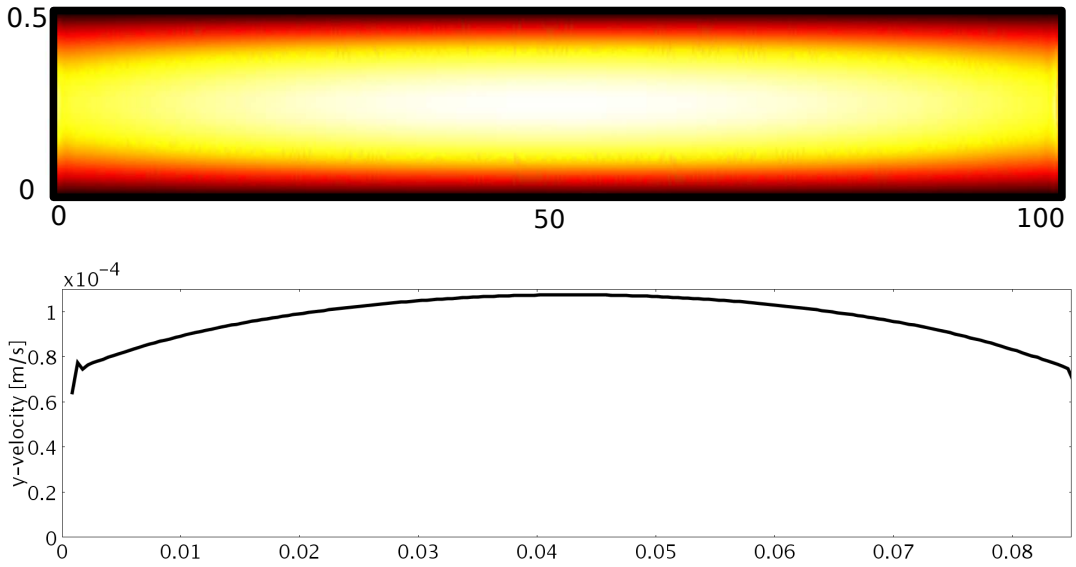

Figure 5.9: *Numerical simulation with finite element method for the flow in the injection system. On the top is shown the profile of the velocity field in the vertical cross section, where the triangular structure meet the porous medium. On the bottom the velocity profile in the line that cuts the cross section surface at mid-height. The gap between the glass plate is set to be* 0.5 *mm and the height is set to* $u = 10$ *cm*

[5.4.0]-undec-7-ene (DBU) and *1.2.4-Triazole* in a solution of Acetonitrile that when combined with the fluorescent dye *3-aminofluoranthene* ($3 - AFA$) and hydrogen peroxide (H_2O_2), will start a chemiluminescent reaction to glow a fluorescent color. From a kinetics point of view the limiting chemical species are the $TCPO$ and the H_2O_2, therefore, in order to reproduce the kinetics $A + B \rightarrow C$ we will use the same molar concentration of $TCPO$ and H_2O_2. Following *Jonsson and Irgum* [1999], we prepare two solutions. We will refer to A as a mixture of a molar concentration of 0.5mM of DBU, 5mM of *Triazole*, 50nM of $3 - AFA$ and 1mM of H_2O_2. We will refer to B as a solution of 1mM of $TCPO$. The solvent the same for both solutions, is the Acetonitrile. We define the t_k as the characteristic time for the reaction to reduce the emitted light by a factor 10 in a well mixed volume. As discussed in *Jonsson and Irgum* [1999] for the chemicals chosen and the adopted molar concentrations, t_k is around 2s. This implies that if the transport and mixing processes over the length scale of an observable pixel are larger than t_k we can use this chemical to reproduce a mixing limited reaction.

The diffusion coefficient of the limiting chemical species $TCPO$ and H_2O_2 are supposed to be the same.

The chosen solvent is Acetonitrile that is a very strong solvent. This constrains us to using, for

the injection system, materials that are not attacked by this solvent (glass and aluminum). We also tested the polymerized glue that constitutes the solid grains to be resistant to Acetonitrile. The test is positive for exposure time of the glue to Acetonitrile smaller then 24 hr; after this time the glue start to dissolve significantly in the solvent. The Acetonitrile at 25 Celsius degree has dynamic viscosity $\mu = 3.4 \cdot 10^{-4}$ Kg/(m·s), a density $\rho = 0.787$ Kg/m^3 and thus a kinematic viscosity $\nu = 0.45 \cdot 10^{-8}$ m^2/s.

The data acquisition chain

To measure the local reaction rate, the objective is to detect the intensity of the light produced by reactions in a dark room. This has been done with a digital camera that is remote controlled by a computer. We used a complementary metal-oxide-semiconductor ($S-CMOS$) based digital camera (Hamamatsu *Orca-Flash* 2.8). The $S-CMOS$ technology is highly performing to detect very low light emissions, this implies that to obtain a clear figure of the emitted light we do not need a large exposure time τ. A constraint of this measurement is that the exposure time τ have to be smaller than the characteristic mixing time scale. The camera has a spatial resolution of 1400×1900 pixels, with a pixel depth of $12-bit$. The used optics allows us to image the visible porous medium. Thus, each pixel corresponds to a length $h_p = \frac{L}{pixels} = \frac{100mm}{1400pixels} = 0.07$ mm/pixel. This pixel size represents the spatial resolution. The characteristic diffusion time over h_p is defined to be $t_D = \frac{h_p^2}{2D} \sim 3$s, where we assumed that the diffusion coefficient of the chemicals is of the order $D \sim 10^{-9}$m^2/s. Since our observation time scale is larger than the characteristic time of the chemistry t_k, with this experimental set-up we can resolve spatially the porous medium at a scale at which we can assume the reactants to be well mixed by diffusion.

The main control parameters of the $S-CMOS$ camera are the exposure time, and the frame rate, or the number of picture taken per unit time. The γ value associated with the taking of images is set to 0, in order to have a linear relationship between produced and detected light. Each image is a matrix A whose elements a_{ij} represent the intensity of the light detected at the pixel location ij. Each pixel has a value $0 < a_{ij} < 2^{bit} - 1 = 4095$ for the $12-bit$ camera that we use.

Experimental procedure

We place on an optical table the described injection system and the chamber. The quasi-Hele-Shaw cell lies in the horizontal plane to avoid gravitational effects on the flow. The camera is

placed on top of the porous medium at a distance of about 30 cm. We focus the optics onto the cell median horizontal plane, which is located at half the thickness of the porous medium. With a syringe pump, by suction, we saturate the injection system and the porous medium

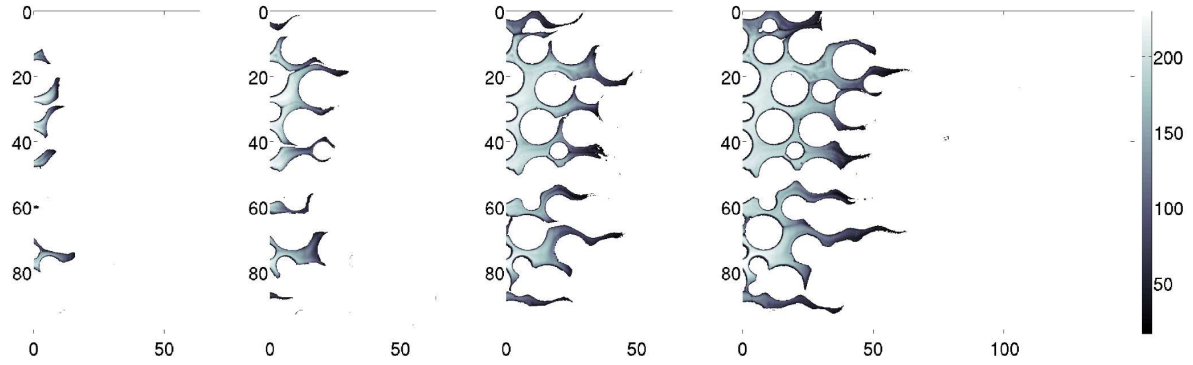

Figure 5.10: *Four images, at four consecutive times, of the porous medium while a conservative tracer is invading the pores volume. The color scale is normalized with respect to maximum value measured, on the pixel depth:* 255 *(over* 255 *corresponding to the* 8*bit of the camera). The imposed flow is* $q = 70mL/hr$. *The axis scales are in mm.*

with the chemical B. Then we start to inject the solution of A. As discussed in the previous chapter, the observed incoming reactant is organized in fingers inside the pores volume, see Figure 5.10. These fingers have an average transverse size $h_T = 1$ mm (that represent the smallest pore size that limits the thickness of invading fingers). For time smaller than the characteristic diffusion time over h_T, the reactants mix only at the finger interfaces. This corresponds to the invading regime discussed in the previous chapter. Thus the reactions will take place, and so the light will be emitted, at these fingers boundaries.

In practice the two solutions can mix before they are injected in the porous medium within the junction between the injection system and the chamber. This effect disturbs the observation and measurement. If we inject a mixture of the two chemicals the reactions will take place mainly inside the finger structures instead of on the finger's boundaries. To reduce this effect we reduce as much as we can the volume of the junction where A and B can mix while being injected. Furthermore, as soon as we can detect some light produced at the injection line of the porous medium, we stop the pumping for one minute. During this time the reactions will deplete completely the concentration of A and B in this junction zone. Thus we can start the injection and observe the reaction taking place mainly at the finger's boundaries (see Figures 5.12, 5.13 and 5.14). We tested 5 imposed flow rates with the syringe pump:

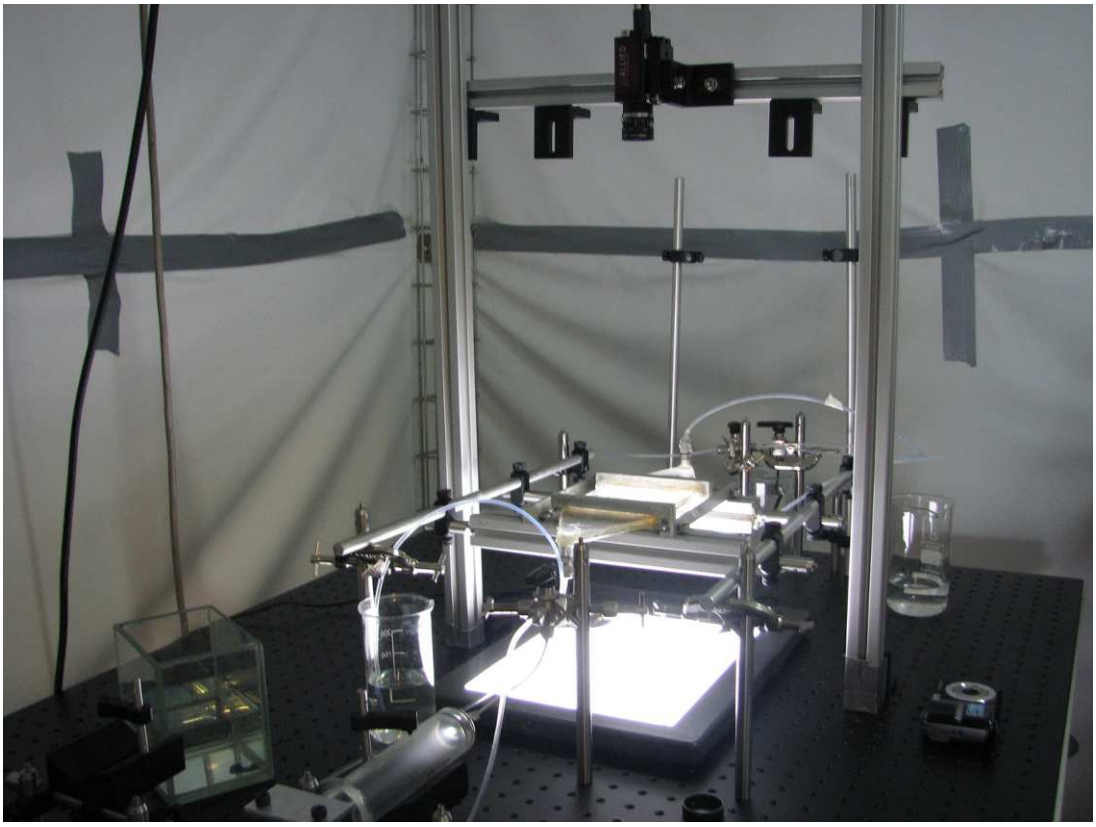

Figure 5.11: *A photo of the experimental set up. The camera takes pictures of the porous medium displaced between the injection system from the top. The latter is connected on one side to two reservoir where the chemicals are stored, on the other to the syringe pump. The optical table on which the experiment is displaced is within a dark room. An homogeneous source of light is here displaced under the porous medium in order to observe the injection of a conservative tracer. For the reactive experiment the light is removed and the experiment is run in the dark.*

$q = 70, 50, 40, 30, 20$ mL/hr. We define the Reynolds number over a length 1 mm (smallest pore size) as $Re = q\frac{L}{\Sigma\nu}$, where the surface of injection $\Sigma = 100 \times 1$ mm^2. For the imposed flow rates, we obtain a range of Reynolds number between 5.5 (corresponding to the lower flow rate) and 19.5 (corresponding to the fastest flow rate).

The exposure time τ of the camera should be the shortest possible in order to observe the dynamics of the fluid motion. However, it is necessary to consider that the exposure time of the camera fixes the number of photon, or the number of reactions, that we measure within one picture. Thus, if τ is too short the resulting picture will be very dark because not enough photons, produced during τ, will have reached the camera's sensor. In other words the camera's pixel depth (the amount of information that each pixel can provide) will be filled partially

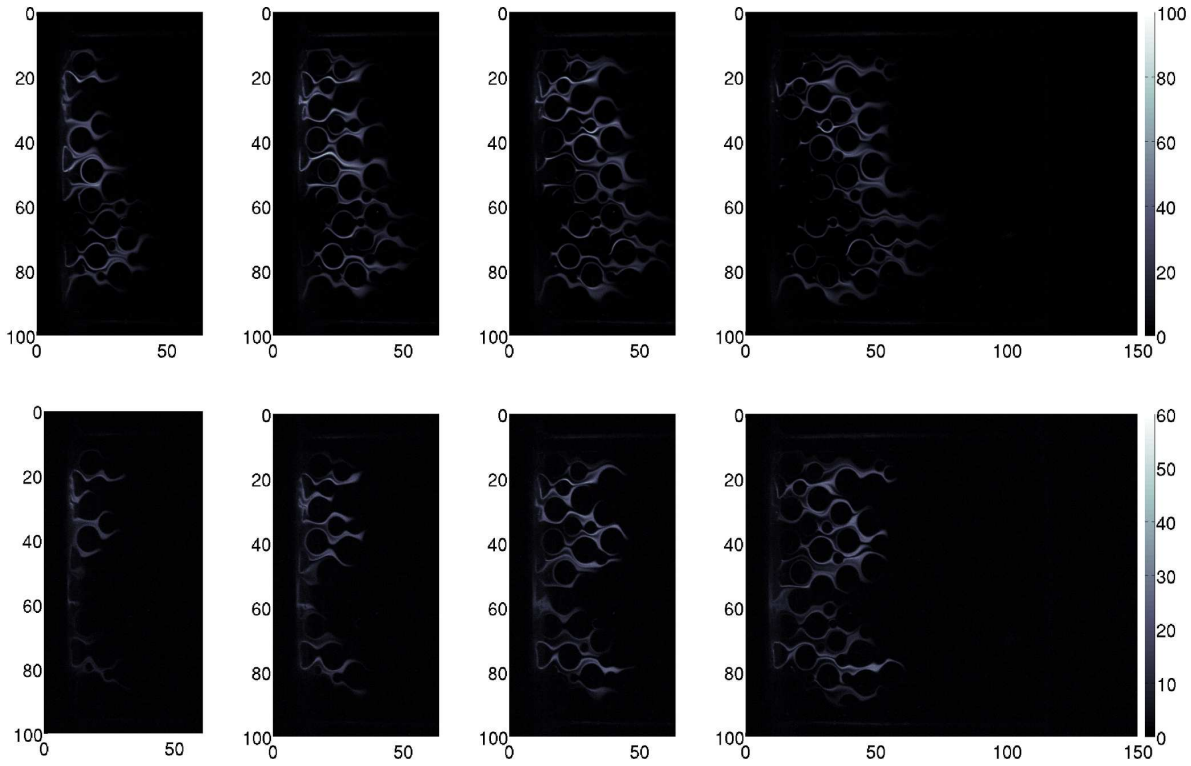

Figure 5.12: *Two sets of four images, at four consecutive times, of the porous medium while the reactions are taking place. The axis scales are in mm. The color scale is normalized with respect to maximum value measured, on the pixel depth (over* 4095 *corresponding to the* 12 *bits of the camera):* 100 *for the case* $q = 70$ *mL/hr (on the top) and* 60 *for the case* $q = 50$ *mL/hr (on the bottom).*

by the more intense detected light. On the other side, for a large τ the camera's pixel depth will be filled by the more intense detected light, but will not provide information about the dynamics of the fluid motion in the cell. In fact during τ the camera will integrate all the dynamical information while the fluid is moving. Thus, in practice we set up τ as the time that the dynamics takes to move the fluid over the size of one pixel. This quantity depends on the imposed flow rate: the larger the flow rate is, the smaller τ has to be. For a flow rate $q = 70$ mL/hr the optimized exposure time results to be $\tau = 1$ s, for a flow rate $q = 20$ mL/hr the optimized exposure time results to be $\tau = 3$ s, providing pixel values between 0 and 100 in the first case, between 0 and 60 for the other cases (see Figures 5.12 and 5.13). Figure 5.16 shows the detail of the spatial fingers structure of the reactions: chemical reactions take place only at the invading reactant finger's boundaries. This correspond to the zone of the system where the reactants are mixed.

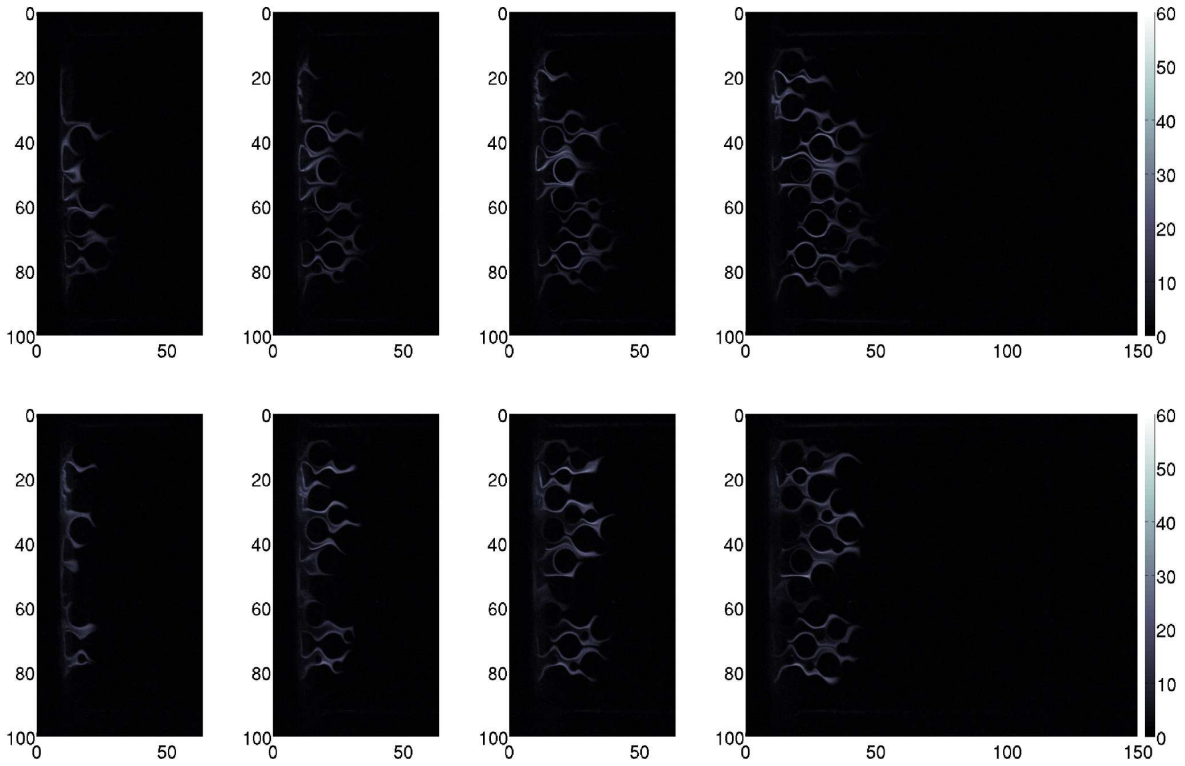

Figure 5.13: *Two sets of four images, at four consecutive times, of the porous medium while the reactions are taking place. The axis scales are in mm. The color scale is normalized with respect to maximum value measured, on the pixel depth* 60 *(over* 4095 *corresponding to the* 12 *bits of the camera). The top images are associated to* $q = 40$ *mL/hr, the lower to* $q = 30$ *mL/hr.*

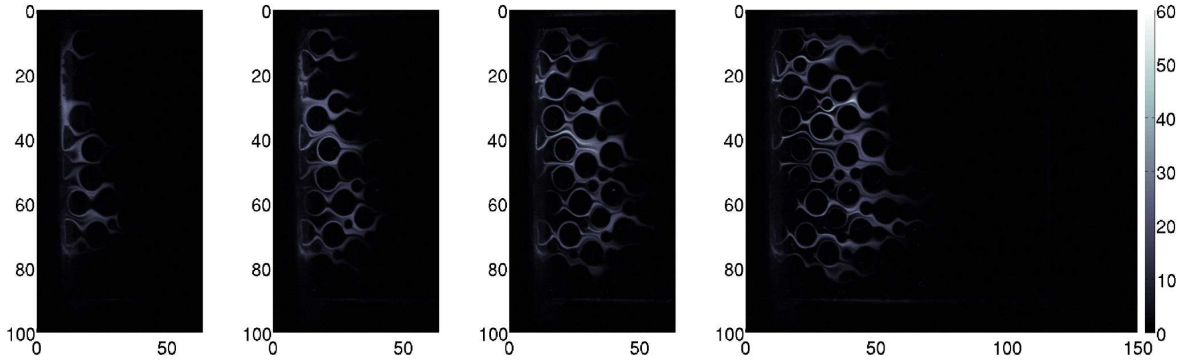

Figure 5.14: *Four images, at four consecutive times, of the porous medium while reactions are taking place. The axis scales are in mm. The color scale is normalized with respect to maximum value measured, on the pixel depth:* 60 *for the case* $q = 20$ *mL/hr (over* 4095 *corresponding to the* 12*bit of the camera).*

5.3 Results

We have taken images at regular time interval Δt; for a set of N pictures, we define the time as a vector of N component $t_i = i \cdot \Delta t$. The total amount of light detected by the $p-$th picture at time t_p represents the total amount of reactions, or C produced, in the time interval $[t_p, t_p + \tau_{exp}]$. This quantity is given by the sum over all the pixels $I_p = \sum_{ij} a_{ij}$ of the image p. We integrate I_p in time, obtaining a measure for the cumulative mass of produced C from the

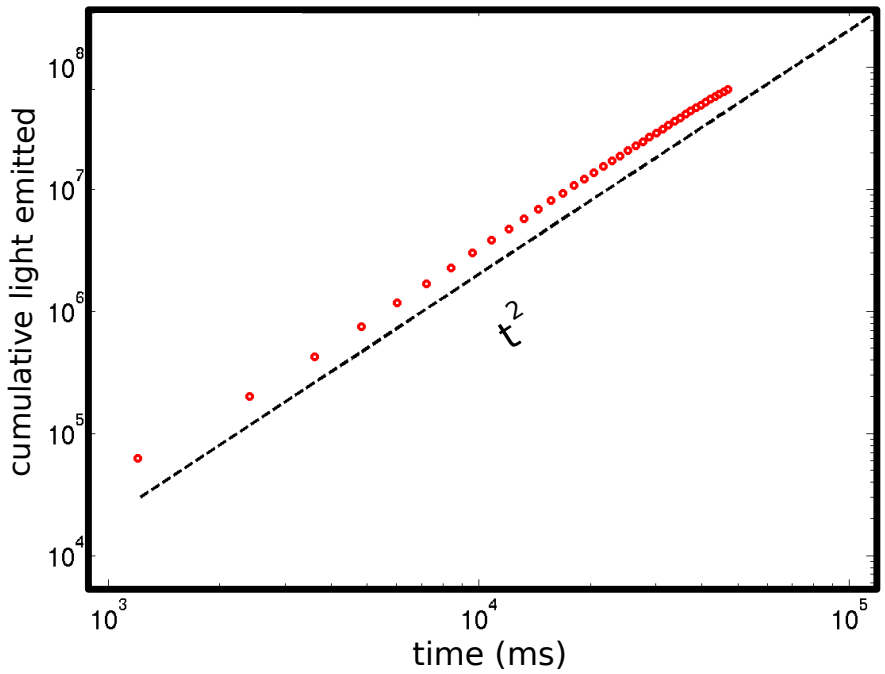

Figure 5.15: *Scaling of the cumulative mass of produced C measured as a function of time.*

injection to time t as

$$M_C(t_p) \propto \sum_{k=1}^{p} I_k = \sum_{k=1}^{p} \sum_{ij} (a_{ij})_k \tag{5.6}$$

Figure 5.15 shows the scaling of the the cumulative mass of produced C for flow rate $q = 70$ ml/hr. Its temporal scaling is $M_C(t) \propto t^2$. This scaling is in good agreement with the pore scale numerical simulations and the upscaled model proposed in the previous chapter for the first regime.

This quadratic scaling in time is related to the finger organization of the incoming reactant in the porous medium (see Figure 5.16). As discussed in the previous chapter, when diffusion homogenizes the reactants concentrations over the average transverse finger cross section $h_T \sim$

1 mm, these structures are destroyed. This happens after a characteristic diffusion time $t_D = \frac{h_T^2}{2D} \sim 500$ s, where we estimate the diffusion coefficient to about $D \sim 10^{-9}$ m^2/s. The kinetics is thus expected to change its scaling and slow down. To observe this second regime and the associated transition the experiment must have a duration larger (at least one order of magnitude) than t_D. The longer experiment we performed, for a flow of $q = 20$ ml/min, had a duration of 110 s preventing us from observing the second regime. For all the performed experiments the invading reactant is organized in fingers, on the surface of which reactions take place (see Figure 5.16) and the mass production is characterized by a quadratic scaling. To observe the destruction of the fingers structures and the consequent second regime, we should use very low flow rates q. This is not possible with the actual experimental set up because the local amount of chemical reactions depends on the flow rate: the lower it is, the slower the fingers growth will be, the less reactions take place and the less light is detected by the camera. To do this a possible development of this experiment is the use of a photomultiplier to measure amount of photons that are not detectable by the camera. Another option is the decrease of t_D using a porous medium with smaller pore volume and smaller average fingers cross section of size h_T.

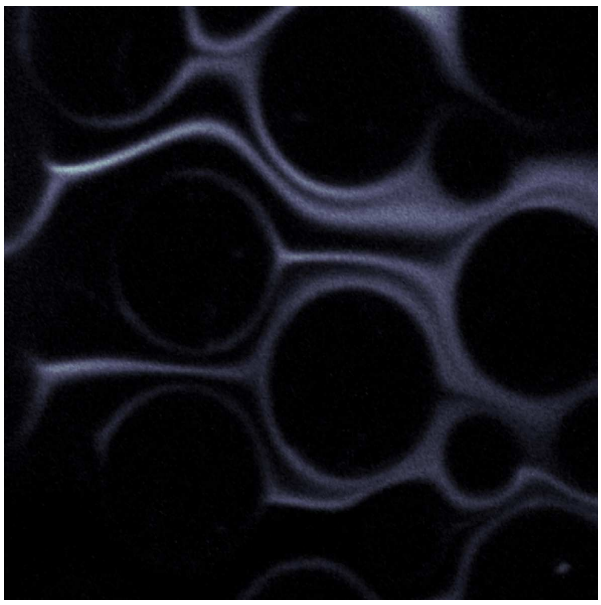

Figure 5.16: *Detail of the spatial organization of the chemical reactions at the pore scale. They take place where the reactants mix, at the fingers boundaries.*

Chapter 6

Conclusions and perspectives

The prediction of dispersion, mixing and reactive transport in heterogeneous flows is a challenging issue in the context of flow through porous media as the probability of reactive species to meet and react depends on the complex flow organization. Such a physical systems are described at small scale in terms of conservation laws that lead to well known governing equations (e.g. Navier-Stokes for flow, advection-diffusion-reaction equation for mass). On one hand the solution of such equations over the full domain is, in general, not known due to the mathematical difficulties (e.g. non linearity) and our ignorance on initial and boundary conditions for real systems. Typical observation scales are much larger than the small scale at which the governing equation are defined. Taking into account both of these critical aspects, simple, effective description consistent with respect to small scale are needed in order to provide solvable models at the desired observation scale. Several upscaling techniques have been discussed in the introduction. In this thesis we propose to investigate the multiscale nature of mixing limited reaction in porous media studying how the system behavior changes as the observation scale changes. We investigate the system behavior over a large range (temporal, spatial,...) of domains, in order to provide informations about how smaller scales can impact on larger ones.

Among the wide range of possible reactive systems that exist in porous media, we decided to study the mixing limited reactions where reactions are fast enough in depleting chemicals to be limited by mass transfer and mixing processes. In general mixing processes are complex and given by the coupling of different mass transport phenomena: the ones considered in this thesis are advection and diffusion. The concept of mixing is in general different from the one of spreading and thus, for transport in heterogeneous media, the two processes need to be

separated.

Diffusion limited reactions

To understand and characterize the basic mechanisms behind the coupling of mixing and reactions, we consider first a simple case. We reduce mixing to Fickian diffusion (no advection is considered). The chemistry considered is the irreversible bimolecular reaction between two chemicals A and B: $A + B \rightarrow C$. We consider that the governing processes (diffusion and chemical reactions) are stochastic and thus also the reactants concentrations are stochastic and defined by probability distributions. If the initial spatial distribution of reactants is perfectly homogeneous $c_A(x,0) = c_B(x,0) = c_0$ the diffusion plays no role and average concentrations of reactants scales following $c_A = c_B \propto t^{-1}$, as predicted by mass action law, here called the mean field description. In presence of heterogeneous fluctuations in initial conditions a deviation from the mass action law prediction is observed. When the average concentrations are almost depleted by reactions, reactants become spatially distributed in islands of A and islands of B that need to be diffusively displaced to meet and react, their scaling changes from t^{-1} to $t^{-1/4}$. This effect is the so-called Ovchinnikov-Zeldovich (OZ) segregation. We relate and quantify this anomalous kinetics to transition from a Gaussian to non-Gaussian shape of the concentrations pdf. The analytical results are complemented by numerical simulations based on the Gillespie algorithm. This results have been published on the *Journal of Chemical Physics* on 2011.

For the OZ segregation problem a full analytical solution has not been proposed in the past. The asymptotic behavior of concentration of reactants is predicted without knowing in detail the transition time between the mean field t^{-1} and the anomalous kinetics $t^{-1/4}$. We address this open question using the method of moment equations. We solved analytically the anomalous kinetics associated to the OZ segregation, providing a solution for all times, characterizing, hence, the transition time between the expected kinetics and its breakdown as a function of the Damkohler number. This results have been published on *Water Resources Research* on 2011. Within the same mathematical framework we then found an analytical solution for the OZ segregation when the diffusive mixing is not Fickian, but enhanced and described by Levy flights. This results have been published on *Advances in Water Resources* on 2012.

Diffusion limited reaction is the simplest system for studying anomalous kinetics. However, as has been shown in chapter 4, anomalous kinetics in more complex heterogeneous porous media can be understood in terms of diffusion limited systems.

Advective spreading in heterogeneous porous media

In order to relate the pore scale flow heterogeneity to advective spreading and subsequently to anomalous kinetics, we analyzed the Lagrangian velocity increments distribution and the associated accelerations correlation. We have shown the existence of long range temporal correlation of Lagrangian accelerations, which are at the root of the breakdown of classical Fickian dispersion models. Thus, similarly to turbulent media, flow through porous media displays strong intermittent properties. The advective dispersion in such a velocity field turns out to be non Fickian. Classical Random Walk models are associated to a dynamical description of Lagrangian particles in terms of a Langevin type equation characterized by a white noise. These models assume uncorrelation between Lagrangian accelerations and, hence, cannot represent our observations. We propose an extension of CTRW that takes into account correlations. We relate the parameters of the CTRW model to the observed Lagrangian acceleration correlation. In practice we evaluate from pore scale simulations the conditional probability $r(v|v')_{\Delta x}$ of the Lagrangian velocities to change from v to v' across a fixed spatial increment Δx. With this transition probabilities we define a correlated CTRW model to upscale the anomalous behavior observed. We show the good agreement between the scaling of longitudinal dispersion σ_x predicted by the proposed correlated CTRW model and the pore scale observation. This results has been published on *Water Resource Research* on 2011. The defined correlated CTRW, is also able to reproduce and predict the observed intermittent-like behavior of Lagrangian velocities (manuscript in preparation).

Anomalous kinetics of reactive front

In order to investigate the impact of heterogeneous advection on effective reactions, we consider the reactive front between two chemicals continuously injected, one displacing the other, in a $2d$ porous medium. The two solute react when in contact in the portion of the pores volume where they are mixed by the combination of heterogeneous advection and diffusion. While the two reactant are mixed a bimolecular reaction $A + B \rightarrow C$ take place. Upscaled Fickian dispersion models assume complete mixing at the pore scale and predict a scaling $M_C(t) \propto (D_{disp}t)^{\frac{1}{2}}$, where D_{disp} represent the effective dispersion coefficient. The upscaled picture resulting from our pore scale simulations is quite far from the Fickian case. We observe two time regimes in which the total product mass evolves faster then $t^{1/2}$. At early times the invading solute is organized in fingers of high velocity. Reactions take place only at

the fingers boundaries whose surface grows linearly in time. We show that this configuration leads to a mass scaling $M_C \propto t^2$. When diffusion mixes reactants and destroy these finger structures, the effective reaction rate slows down and we relate it to the longitudinal advective spreading providing $M_C \propto \sigma_x$. The transition time between these two regimes is characterized by the diffusion time over the transverse fingers cross section. This result is confirmed by $3d$ simulations. The proposed simple physical model explains both regimes and the transition time between them, providing a global upscaled framework for this mixing limited reaction. The behavior of the second regime, together with the upscaling analysis for σ_x presented in the third chapter, provides a consistent relationship between the local flow heterogeneity, anomalous dispersion and anomalous kinetics. Furthermore, we show that the kinetics of the peak of the longitudinal distribution of reaction product evolves in agreement with the OZ anomalous kinetics discussed in the second chapter, providing a link between reactive transport in complex advection and in diffusion limited systems.

A new experimental method for high precision quantification of reactive transport

In the framework of reactive transport in porous media laboratory experiments to measure the impact of incomplete mixing on global reaction kinetics represent a challenging goal. Thus, there exist relatively few experiments. We propose a new experimental set up based on chemiluminescence reactions that allows for high resolution quantification of the pore scale concentration pdf and reaction rate. Through a lithography technique we build a transparent quasi $2d$ (very thin) chamber filled with cylinders, representing soil grains, with the same geometry of the medium simulated in chapter 4. With a SCMOS camera we image the medium and measure the local reaction kinetics through a chemiluminescence reaction: each reaction produce a photon. Anomalous kinetics of the reactive front is observed and is very consistent with our theoretical predictions. While previous experiments provide indirect quantification of the produced mass by reactions (e.g. through the Beer-Lambert law), this method provides high precision measurements of the reaction rate and the pore scale concentration field.

Some perspectives

Mixing-driven reactions are determined by the geometry of the mixing interfaces whose dynamics derive from the interaction of microscopic mass transfer and reaction processes. The theoretical framework here presented for upscaling mixing limited reactions taking place at pore scale can be extended to different applications. As discussed, mixing limited reactions

in porous media are crucial in several scientific and industrial applications such as CO_2 sequestration, remediation, that are governed by complex chemical reactions. Reactive transport phenomena when coupled with growth of biofilms has important implications in aquifer storage and recovery, biobarriers, microbial enhanced oil recovery, CO_2 sequestration, seismic wave propagation, and in-situ bioremediation. Possible developments of this work include accounting for different mixing processes, such as viscous mixing, and more complex reactions that involve biological processes.

The proposed laboratory experiment is promising because it allows for imaging and, hence, measuring, the pore scale organization of flow, transported concentrations pdf and reactions. The characterization of the local velocity field in a chamber via particle tracking is currently developed (Master Thesis of Regis Turuban). Another interesting application of the proposed technique is the study of dispersion associated to unsaturated conditions, where numerical simulations are very limited in predicting the system behavior (current postdoctoral project of Joaquin Jimenez-Martinez).

The proposed chemiluminescence reaction technique could also be applied to $3d$ experiments. The same kind of set up could be used to inject the reactant A in a parallelepipedic chamber filled with transparent beads. Using index matching the whole system will be translucent and the light produced by reactions inside the medium can can be transmitted and detected with similar imaging techniques.

An interesting application of the chemiluminescence reaction is in non reactive experiments where the emitted light can be used as a tracer. If one of the two reactants, e.g. B, has a very large concentration with respect to the other, $c_A \ll c_B$ the kinetics of the reaction, following the mass action law, will be proportional to the concentration of the chemical with the lower concentration

$$\frac{dc_A}{dt} = -kc_Ac_B \sim -k'c_A \quad c_B \text{ is almost contant} \quad k' = kc_B$$

For a suitable choice of the chemical mixture for A and B, the resulting reaction constant k can be small and the kinetics very slow. This implies that the reaction cannot significantly modify the reactants concentrations for times smaller than the duration T of the experiment ($t_k = \frac{c_A(0)}{k} \gg T$). We could thus prepare a well mixed solution of A and B whose emitted light will be proportional to the concentration c_A. If the experiment have a duration T smaller than the characteristic chemical time $t_k = 1/k$, the variations in A concentrations can be associated only to transport mechanisms.

Appendix A

Appendix A

Advances in Water Resources 37 (2012) 86–93

Contents lists available at SciVerse ScienceDirect

Advances in Water Resources

journal homepage: www.elsevier.com/locate/advwatres

Incomplete mixing and reactions with fractional dispersion

Diogo Bolster [a,*], Pietro de Anna [b], David A. Benson [c], Alexandre M. Tartakovsky [d]

[a] Environmental Fluid Mechanics Laboratories, Dept. of Civil Engineering and Geological Sciences, University of Notre Dame, Notre Dame, IN, USA
[b] Géosciences Rennes, UMR 6118, CNRS, Université de Rennes 1, Rennes, France
[c] Hydrologic Science and Engineering, Colorado School of Mines, Golden, CO, USA
[d] Computational Mathematics Group, Pacific Northwestern National Laboratory, Richland, WA, USA

ARTICLE INFO

Article history:
Received 12 July 2011
Received in revised form 4 November 2011
Accepted 10 November 2011
Available online 23 November 2011

Keywords:
Fractional dispersion
Reactions
Incomplete mixing

ABSTRACT

A common barrier to accurately predicting the fate of reactive contaminants is accurately describing the role of incomplete mixing. In this paper we develop a stochastic analytical framework for an irreversible kinetic bimolecular reaction in a system with anomalous transport, governed by the fractional advection–dispersion equation (fADE). The classical well-mixed (thermodynamic) solution dictates that the concentration of reactants after an initial transient decreases proportional to t^{-1}. As the system becomes less and less well-mixed, the rate of reaction decreases relative to the thermodynamic solution, at late times scaling with $t^{-1/(2\alpha)}$ instead of t^{-1}, where $1 < \alpha \leqslant 2$ is the fractional order of the dispersion term in the fADE. The time at which this transition takes place is derived, giving an indication of the range of validity of the classical (well-mixed) equation. We verify these analytic results using particle-based simulations of random walks and reactions.

1. Introduction

Anomalous transport, or transport that does not follow Fick's Law of dispersive behavior, is common in a variety of hydrological and geophysical systems with heterogeneous velocity fields and typically arises due to nonlocal effects. Fields of interest where such anomalous behavior occurs include solute transport in surface [22] and subsurface water systems [33], turbulent environmental flows [12], sediment transport in rivers [8] and mechanical transport of soil constituents [19].

The classical 2nd-order advection–dispersion equation often cannot adequately model anomalous transport and a variety of mathematical models capable of doing so have emerged. Nonlocal effects can arise for a variety of reasons [11,32,13], but in short the concentration at some point should account for contributions from a variety of distances and/or the prior concentration history. Examples of the derivation of nonlocal methods in a variety of hydrological transport applications include delayed diffusion [15], projector formalisms [11], moment equations [32], multi-rate mass transfer [24], continuous time random walks [3] and fractional ADEs [40]. In this work we focus on the space-fractional ADE that is the continuum equation governing Lévy motion, which has been called ubiquitous [45]. The appeal lies in the fact that the model is sufficiently complex to display relevant dynamics while sufficiently simple to allow analytically tractable results that provide great insight into the influence of spatial nonlocality.

To date, the bulk of transport studies have focused on conservative transport. Many constituents of interest in hydrological systems do not behave conservatively, and their reactive character should be included, although predicting reactive transport in porous media can be quite challenging (see the recent review article by Dentz et al. [14]). Classical transport and reaction equations based on the assumption of perfect mixing fail to properly predict reactions within systems ranging from laboratory-scale in homogeneous material [36,23] to large-scale heterogeneous systems [29,47]. The deviations from classical reaction predictions can arise due to incomplete mixing [43,42], which must be accounted for in the correct upscaled model. For example, one might assume in an *ad hoc* manner that a kinetic reaction term is the result of upscaling the incomplete mixing process and arrive at accurate predictions of laboratory experiments (e.g. as done by [38] with the experiments of [23]).

Systems that can display anomalous transport for conservative constituents often display anomalous mixing characteristics (e.g., [37,9,46,5,28,27,4,10]). In some instances anomalous mixing can persist even when spreading of a conservative plume appears to be Fickian [28]. Such anomalous mixing in turn is expected to significantly impact chemical reactions where mixing is the mechanism that brings reactants together. The impact of anomalous transport on reactive systems of hydrological interest has to date received some attention (e.g., [6,16,17,47,29]). However, given the diverse nature of chemical reactions (e.g., instantaneous vs. kinetic, equilibrium, reversible vs. irreversible) a one-size-fits-all

* Corresponding author.
E-mail address: bolster@nd.edu (D. Bolster).

0309-1708/$ - see front matter © 2011 Elsevier Ltd. All rights reserved.
doi:10.1016/j.advwatres.2011.11.005

approach does not apply and interesting and important features arise depending on the specific type of reaction.

In this work we focus on irreversible kinetic reactions of the type $A + B \rightarrow C$. This is the simplest reactive system in which segregation or poor mixing of the species can lead to suppressed reactions. Therefore, the mechanics of transport and mixing bear directly on the ultimate reaction speed. For this system there is a competition between the rate of reaction between particles and the ability for A and B to mix by dispersive mechanisms. In a system that is continually well-mixed (say, as in a stirred beaker), the thermodynamic law follows

$$\frac{dC_A}{dt} = \frac{dC_B}{dt} = -kC_AC_B, \tag{1}$$

where C_i is the concentration of constituent i, and k [$L^d M^{-1} T^{-1}$] is the reaction rate coefficient. An especially interesting case is when the initial concentrations C_{A0} and C_{B0} are equal, then the solution to (1) is $C_A = C_B = C_{A0}(1 + C_{A0}kt)^{-1}$. It is important to note that these concentrations denote the ensemble average of a well-mixed process [20]. In a natural system that begins in an initially well-mixed state, the initial rate of reaction follows the thermodynamic law (1). The role of dispersive mechanisms in such a system is negligible (see [2,14]). However, as fluctuations of A or B become large with respect to the mean, isolated *islands* of A and B can form within which little or no reaction can occur, thus decreasing the rate at which the mean amount of A and B are consumed. This behavior was hypothesized and observed numerically for Fickian dispersion [35,26,44]. Using asymptotic arguments these authors showed that the rate of consumption of A and B changes from the initial thermodynamic value (which goes like t^{-1} after a brief initial time) to a rate that goes like $t^{-d/4}$, where d is the number of dimensions under consideration. It has subsequently been observed by other authors (e.g. [30,2,1]). This functional form of deviation from the thermodynamic law is valid for Fickian dispersion, but the deviation may be expected to be different in systems that do not display Fickian behavior.

Rather than rely on purely asymptotic arguments, we analytically derive solutions for the full time scaling of reaction rates associated with Lévy motion (including, as a subset, Brownian motion governed by Fick's Law). We do so using a stochastic model and the method of moments (e.g., [41,18]) and verify our results numerically with a particle-based reaction-dispersion model.

2. Model

Consider a system where two components A and B are distributed in space and can react chemically and irreversibly with one another. For simplicity we consider one-dimensional transport and reaction. The components are transported superdiffusively and are governed by the spatial fractional dispersion equation, so that

$$\frac{\partial C_i}{\partial t} = Dp\frac{\partial^\alpha C_i}{\partial x^\alpha} + Dq\frac{\partial^\alpha C_i}{\partial(-x)^\alpha} - kC_AC_B, \quad i = A, B, \tag{2}$$

where D [$L^\alpha T^{-1}$] is the dispersion coefficient, $1 \leqslant \alpha \leqslant 2$ is the fractional derivative exponent, and p and q are the weights of forward or backward dispersion, where $p + q = 1$ and $0 < p < 1$ (for symmetric dispersion $p = q = 0.5$). Mixing processes are given by both advective and dispersive mechanism. As a first step in understanding the impact of mixing on the global reaction rate, here we consider the case where the mixing processes are given only by fractional dispersion, neglecting the advective contribution. Note that the case of a constant advection term would cause a constant shift in time, but not affect mixing or reactions due to the principle of Gallillean invariance (i.e. the shift in the location of the center of mass is only affected by advection, while the rate of spreading of the plume around its center of mass, which influences mixing, is affected only by dispersion). In order to characterize the role incomplete mixing on the global chemical reaction rate, we focus on the dispersion-limited reaction case.

We begin by assuming that A and B are initially distributed in a uniformly random manner in a one-dimensional domain. This randomness persists, and we may decompose the random concentrations as $C_i(x,t) = \overline{C_i}(x,t) + C_i'(x,t), i = A, B$. The overbar refers to the ensemble average and the prime to fluctuations about this. We consider the initial average conditions:

$$\overline{C}_A(x,0) = \overline{C}_B(x,0) \equiv \overline{C}_{A0} \tag{3}$$

in an infinite domain with natural boundary conditions. Using (2) and the previous decomposition of concentration, the governing equations for the thermodynamic limit and the fluctuations from it can be written as

$$\frac{\partial \overline{C_i}}{\partial t} = -k\overline{C}_A\overline{C}_B - k\overline{C_A'C_B'} \tag{4}$$

and

$$\frac{\partial C_i'}{\partial t} = Dp\frac{\partial^\alpha C_i'}{\partial x^\alpha} + Dq\frac{\partial^\alpha C_i'}{\partial(-x)^\alpha} - k\overline{C}_AC_B' - kC_A'\overline{C}_B - kC_A'C_B' + k\overline{C_A'C_B'}, \tag{5}$$

where we used the fact that $\overline{C_i'} = 0$. We are interested in the evolution of $\overline{C}_i$, that depends on the evolution of the correlation structure of the local fluctuations. If both chemicals are initially distributed in the system through the same physical mechanism, it is reasonable to assume that the fluctuating components have initial identical correlation structure:

$$\overline{C_A'(x,0)C_A'(y,0)} = \overline{C_B'(x,0)C_B'(y,0)} = R(x,y). \tag{6}$$

Both A and B have similar initial correlation structures because the initial perturbations will arise due to small scale stochastic fluctuations (due to subscale noise/diffusion), which are expected to be similar for A and B as defined here.

A deviation from the thermodynamic law occurs when isolated patches of A and B emerge [44]. We select an initial condition for the fluctuation concentrations that reflects the emergence of such islands by taking A' and B' as initially anticorrelated such that

$$\overline{C_A'(x,0)C_B'(y,0)} = -R(x,y). \tag{7}$$

This is physically justifiable because in regions where there is an abundance of A relative to B, reactions will take place and result in a further depletion of B relative to the mean and excess of A relative to the mean. Similarly areas of excess B correspond to depleted A, thus giving rise to anti-correlation.

We can now write the equation for the covariance $f(x,y,t) = \overline{C_A'(x,t)C_B'(y,t)}$ as (see Appendix A)

$$\frac{\partial f(x,y,t)}{\partial t} = 2D\left(p\frac{\partial^\alpha f(x,y,t)}{\partial x^\alpha} + q\frac{\partial^\alpha f(x,y,t)}{\partial(-x)^\alpha}\right) \tag{8}$$

subject to initial condition $f(x, y, t = 0) = -R(x, y)$. The solution to (8) with natural boundary conditions on an infinite domain can be found with the Green's function, i.e.

$$f(x,y,t) = \int_{-\infty}^{\infty} -R(\xi,y)G(x,\xi,t)d\xi, \tag{9}$$

where

$$G(x,\xi,t) = \frac{1}{2\pi}\int_{-\infty}^{\infty} e^{2D[p(ik)^\alpha + q(-ik)^\alpha]t}e^{ik(x-\xi)}dk. \tag{10}$$

Because the initial correlation structure acts over a short range, we do not expect the specific initial correlation structure to play a major role. For simplicity we consider the limiting case of a delta correlated initial condition for f, i.e.

$$f(x,y,t=0) = -R(x,y) = -\sigma^2 l\delta(x-y), \tag{11}$$

where σ^2 is the variance and l the correlation length. This can be thought of as an approximation of an exponential or Gaussian correlation and it is straightforward to show that after some initial transient the solution for the delta correlation displays the same behavior (see Appendix B). In other studies it has been shown to give asymptotically similar results as short range correlation functions [34,7]. We are ultimately interested in the limit $y \to x$ and with the delta initial condition the solution for $f(x, y, t)$ is

$$\begin{aligned} f(x,y\to x,t) &= -\frac{\sigma^2 l}{2\pi}\int_{-\infty}^{\infty} e^{2D|p(ik)^\alpha + q(-ik)^\alpha|t}dk \\ &= -\frac{\sigma^2 l}{2\pi}t^{-1/\alpha}\int_{-\infty}^{\infty} e^{2D|p(im)^\alpha + q(-im)^\alpha|}dm = -\chi t^{-1/\alpha}, \end{aligned} \tag{12}$$

where $\chi = \frac{\sigma^2 l}{2\pi}\int_{-\infty}^{\infty} e^{2D|p(im)^\alpha+q(-im)^\alpha|}dm$ is a constant. Interestingly, the time scaling for f only depends on α, the fractional dispersion coefficient. Substituting (12) into (4) our equation for the mean concentration of A or B becomes

$$\frac{\partial \overline{C_i}}{\partial t} = -k\overline{C_i}^2 + k\chi t^{-1/\alpha}. \tag{13}$$

Strictly speaking, as written, Eq. (13) is not valid from time $t = 0$ as one has singular and nonphysical behavior associated with the term $k\chi t^{-1/\alpha}$. This problem is circumvented by accepting that this equation is only strictly valid after some initial "setting" time t_0 and defining the initial condition at this time such that $\overline{C}_A(t = t_0) = \overline{C}_{A0}$. It is equivalent to having an initial transient period during which the initial correlation and anticorrelation structure forms. We find that the solutions are insensitive to this small time [41].

3. Solution – discussion and implications

We will now work in nondimensional space. We nondimensionalize concentrations by the initial $\overline{C_{A0}}$ and time by $k\overline{C_{A0}}$ so that (13) can be written as

$$\frac{\partial \overline{C_i}}{\partial t} = -\overline{C_i}^2 + \chi^* t^{-1/\alpha} \quad \overline{C_A}(t = t_0) = 1, \tag{14}$$

where

$$\chi^* = \chi k^{\frac{1}{\alpha}}(C_{A0})^{\frac{1}{\alpha}-2} \tag{15}$$

$\chi^*$and α are now the only dimensionless numbers that play a role in this system. Note that the right side of (14) has a sink and a source term. At early time the well-mixed (first) term dominates, but at late time the well-mixed sink is balanced by the "source" that accounts for imperfect mixing.

3.1. Well mixed system (thermodynamic limit)

A well mixed system can be represented by $\chi^* = 0$. This is equivalent to the classical thermodynamic limit equations where the fluctuations in concentrations are zero, i.e.

$$\frac{\partial \overline{C_i}}{\partial t} = -\overline{C_i}^2 \quad \overline{C_A}(t = t_0) = 1. \tag{16}$$

The solution to this equation is well known and given by

$$\overline{C_A}(t) = \frac{1}{1 + (t - t_0)}. \tag{17}$$

In particular it is worth noting that at large times the concentration of A scales inversely with time, i.e. $\overline{C_A}(t) \sim t^{-1}$.

3.2. Incomplete mixing

We now look at the full solution of Eq. (14) accounting for the source terms that quantifies incomplete mixing. Eq. (14) is a Riccati equation and has solution

$$\overline{C_i}(t) = \frac{\sqrt{\chi^*}}{t^{\frac{1}{2\alpha}}}\frac{\left(I_{-\frac{\alpha-1}{2\alpha-1}}(z) - \kappa K_{\frac{\alpha-1}{2\alpha-1}}(z)\right)}{\left(I_{\frac{\alpha}{2\alpha-1}}(z) + \kappa K_{\frac{\alpha}{2\alpha-1}}(z)\right)}, \quad z = \frac{2\alpha\sqrt{\chi^*}}{2\alpha-1}t^{\frac{2\alpha-1}{2\alpha}}, \quad t \geqslant t_0, \tag{18}$$

where the I and K are modified Bessel functions of the first and second kind and κ is a constant that depends on the initial condition and is given by

$$\kappa = \frac{\left(I_{-\frac{\alpha-1}{2\alpha-1}}(z_0) - \chi^{*\frac{-1}{2}}t_0^{\frac{1}{2\alpha}}I_{\frac{\alpha}{2\alpha-1}}(z_0)\right)}{\left(K_{\frac{\alpha-1}{2\alpha-1}}(z_0) + \chi^{*\frac{-1}{2}}t_0^{\frac{1}{2\alpha}}K_{\frac{\alpha}{2\alpha-1}}(z_0)\right)}, \quad z_0 = \frac{2\alpha\sqrt{\chi^*}}{2\alpha-1}t_0^{\frac{2\alpha-1}{2\alpha}}. \tag{19}$$

3.3. Early time

At first glance the analytical solution in (18) may not appear to give much insight. However, early and late time expansions of this solution clarify the situation significantly. To leading order, at early time the solution in (18) is given by

$$\overline{C_A}(t) = \frac{1}{1 + (t - t_0)}, \tag{20}$$

which is identical to the well-mixed thermodynamic solution (Fig. 1) and shows consistency of the solution with an assumption of early conditions that are sufficiently mixed for the thermodynamic rate to dominate. If this thermodynamic solution held at all times one would expect a late time scaling that goes like inverse time, i.e., t^{-1}.

3.4. Late time

At late time, the fraction in parentheses in Eq. (18) containing the Bessel functions converges to unity, and the leading order behavior becomes

$$\overline{C_A}(t) \sim \sqrt{\chi^*}t^{-1/(2\alpha)}. \tag{21}$$

Unlike the thermodynamic solution, which scales as t^{-1}, the solution of (18) decreases at a slower rate of $t^{-1/(2\alpha)}$ (Fig. 1). For the Fickian case of $\alpha = 2$ this results in a late time scaling of $t^{-1/4}$, in agreement with previous predictions and observations (e.g. [35,26,44,2,1]).

3.5. Cross-over time

In the above discussion we talk about early and late times without clearly defining these. On physical grounds we define early times as times when the thermodynamic law still holds and late times as times when the anomalous kinetics emerge. The cross-over time that delineates early and late times can be found by balancing both terms on the right hand side of (14); i.e., it is when the terms that reflect well-mixed conditions and imperfectly mixed conditions become comparable in size. Thus we can define a dimensionless cross-over time τ such that $\frac{1}{\tau^2} = \chi^*\tau^{-1/\alpha}$. Solving for τ we obtain

$$\tau = \chi^{*\frac{\alpha}{1-2\alpha}}. \tag{22}$$

When $t > \tau$, anomalous kinetics are expected and at early time, when $t < \tau$, behavior consistent with the thermodynamic law is observed. The larger the value of χ^*, the earlier the onset of

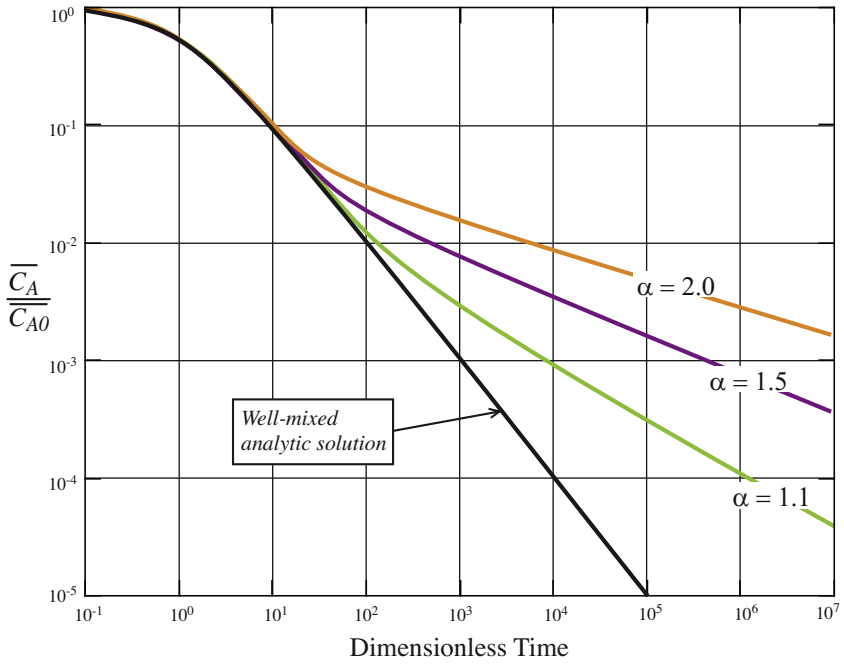

Fig. 1. Plots of the analytical solution (18) for a variety of values of α: 1.1, 1.5, and 2.0. Note that in all cases the solution pulls away from the well-mixed thermodynamic limit (black solid line) and at late times scales like $t^{-1/(2\alpha)}$. Each solution uses a value of $\chi^* = 0.005$.

anomalous kinetics. Recall that χ^* is a dimensionless number that reflects how noisy the initial concentration field is, as well as the competition between diffusion and reaction time scales. For illustration let us consider the Fickian case of $\alpha = 2$. Here

$$\chi^* = \sqrt{\frac{1}{8\pi}}\frac{\sigma^2}{C_{A0}^2}\sqrt{\frac{kl^2C_{A0}}{D}}, \tag{23}$$

which is closely related to the (dimensionless) dispersive Damkohler number $Da = \tau_D/\tau_R = kl^2C_{A0}/D$ (e.g. [39]). The Damkohler number is a ratio of the time scale of diffusion $\tau_D = l^2/D$ to the time scale of reaction $\tau_R = 1/kC_{A0}$, thereby quantifying how quickly reactions occur relative to dispersion. Our dimensionless χ^* is proportional to Da^2, with the constant of proportionality including a term $\frac{\sigma^2}{C_{A0}^2}$ that reflects the amplitude of initial "noise" in the distribution of A and B. An increase in Da means that reactions are faster relative to the rate of diffusion and the system has a quicker onset of incomplete mixing; i.e., A and B are consumed quickly relative to how quickly diffusion can bring them together. The additional term accounts for the smoothness in the initial condition, which directly affects that time of the onset of separate A and B islands and incomplete mixing.

4. Numerical simulations

To verify the theoretical results, we simulated random walks and particle/particle reactions using the method of [2] modified for Lévy motion. The details of the algorithm are given in [2] and the modified version is briefly outlined here. Time is discretized into steps of identical duration Δt. Each particle jumps a random distance in the domain of attraction (DOA) of an α-stable law (i.e. by the generalized central limit theorem they additively converge to an α-stable distribution [21]) so that the random walk approximates Lévy motion. We also must rapidly calculate the probability density of the sum of two random walks to estimate the probability that two particles will be co-located and potentially react. Therefore, we require jumps for which random values are easy to generate and the density function is also easy to calculate (effectively ruling out α-stable random variables themselves).

Due to the power-law tails, the shifted Pareto distribution $P(|X| > x) = s^\alpha(x+s)^{-\alpha}$ [25] is in the domain of attraction of the α-stable laws (by the generalized central limit theorem); therefore, a sum of random jumps drawn from this distribution will converge to Lévy motion. This is analogous to summing variables from a uniform distribution to simulate a Brownian motion by invoking the classical central limit theorem. However, relative to the corresponding α-stable density, the shifted Pareto density is too peaked at the origin and nearby particles are too likely to react. Instead we choose symmetric jumps X from a "chopped" Pareto (see for example Fig. 2) distribution following

$$P(|X| < x) = \begin{cases} mx & \text{if } x < ((1+\alpha)c)^{1/\alpha}, \\ 1 - cx^{-\alpha} & \text{otherwise.} \end{cases} \tag{24}$$

The constants c and m dictate the size of the jumps. Both c and m are functions of Δt and D. Each jump should be DOA α-stable with scale $(D\Delta t)^{1/\alpha}$, so that by (7.19)–(7.21) in [31], $c = D\Delta t/(\Gamma(1-\alpha)\cos(\pi\alpha/2))$. The slope m and cutoff $((1+\alpha)c)^{1/\alpha}$ are chosen to ensure a mono-modal density by making the small x uniform cumulative distribution tangent to the power law with prefactor c. The form we chose for this jump density is one that most closely approximates an α-stable variable, while still being computationally efficient. For $\alpha \geqslant 2$, the jumps are in the domain of attraction of a Gaussian and simpler traditional methods can be used. The separate probability density, denoted $v(s)$, that two particles will be co-located in any time interval given initial separation s is the convolution of two α-stable densities with each other. This is also α-stable. We use the chopped Pareto to calculate the density that approximates the α-stable law with scale $(2D\Delta t)^{1/\alpha}$.

An initial number N_0 of both A and B particles are (uniformly) randomly placed in a $1-D$ domain of size Ω. Note that we do not impose the initial conditions in equations (6) and (7) as done in the theory. Rather, we allow the randomness to naturally evolve from the uniform initial condition at $t = 0$. This evolution reflects the initial 'setting time' discussed in Section 2. The reactions are

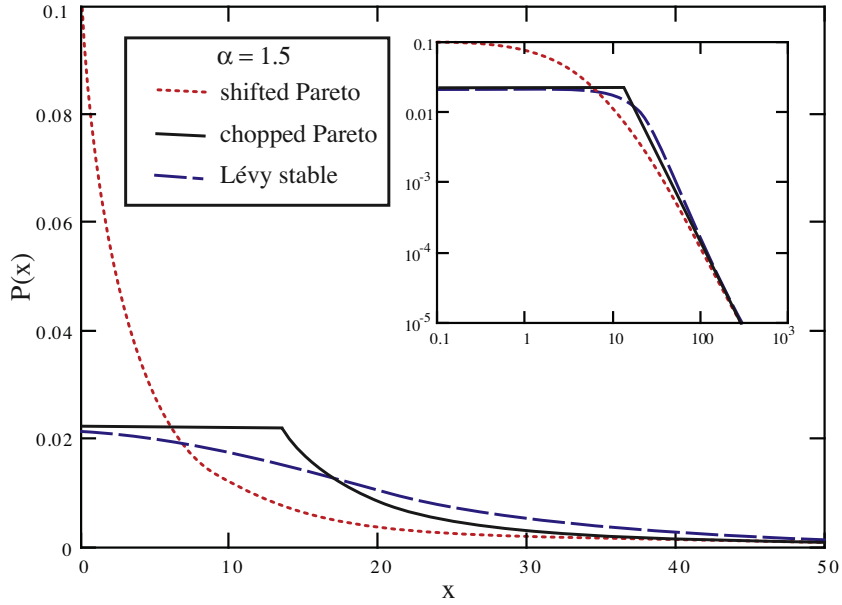

Fig. 2. Densities for random variables in the domain of attraction of a Lévy-stable with index $\alpha = 1.5$. Scale $(D\Delta t)^{1/\alpha} = 13.6$.

simulated by calculating the probability density of particle co-location ($v(s)$) by Lévy dispersion. This probability is multiplied by the thermodynamic probability of reaction given the co-location. Each particle represents a total mass $\Omega\overline{C_{A0}}/N_0$, so the probability of reaction [2] is $k\Delta t(\Omega\overline{C_{A0}}/N_0)v(s)$. This probability for each A and B particle pair is compared to a new Uniform(0,1) random variable until a reaction takes place or pairs are exhausted. The particles then diffuse by random walks and react again *ad nauseum*.

In all of the Lagrangian simulations, the reaction rate follows the well-mixed solution until the late time scaling sets in. In agreement with our theoretical development, the late time solution scales with $t^{-1/(2\alpha)}$ (Fig. 3). Each simulation used representative values for aqueous environments: domain size $\Omega = 200$ cm; $\overline{C_{A0}} = \overline{C_{B0}} = 0.001$ and $k = 1.0$, where the latter two constants use consistent concentration units. The dispersion coefficients were varied to get ample separation of data points for visual clarity: For $\alpha = 1.1$, 1.5, and 2.0, $D = 5 \times 10^{-6}$, 2.5×10^{-6}, and 1×10^{-6} cm$^\alpha$/s, respectively. The initial number of both A and B particles was 20,000; each simulation was run 40 times and the ensemble average concentrations were calculated. Even single realizations display the anomalous behavior clearly and 40 were chosen to smooth any existing noise. Doubling the number of realizations does not appear to change the solution and so 40 realizations are deemed sufficient.

At the latest time in the numerical simulations, another (approximately exponential) scaling arises that is not predicted by our analytical development. This deviation from the theoretical

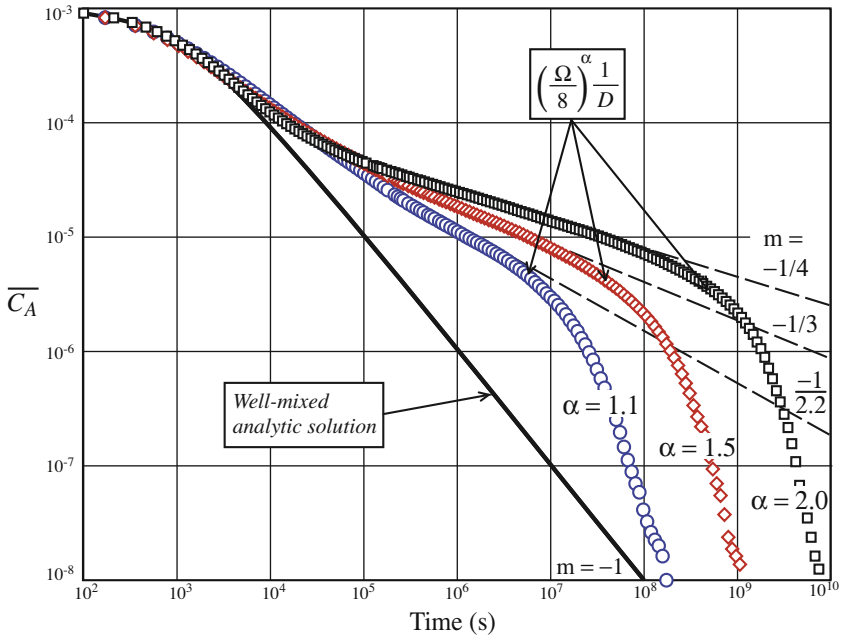

Fig. 3. Concentration change simulated by particle models (symbols) and analytic solutions to well-mixed equation (solid curve). All solutions transition from the perfectly mixed solution of to the $t^{-1/(2\alpha)}$ asymptotic solution. The approximate time $(\Omega/8)^\alpha/D$ at which the boundaries are felt, on average, is denoted on the plots.

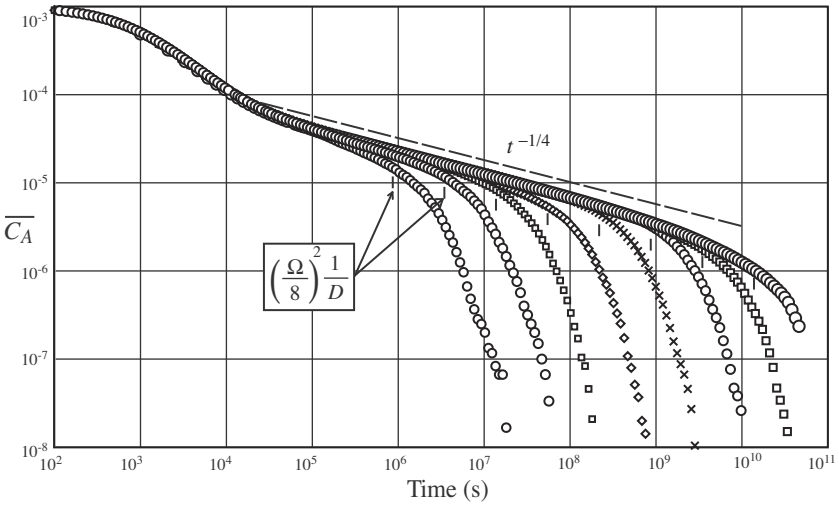

Fig. 4. Effect of finite-sized domains on Brownian motion dispersion ($\alpha = 2$) and reactions. Each simulation is identical except for a doubling of domain size, which theoretically quadruples the time at which boundaries impede segregation of A and B into separate islands. The theoretical transition time $(\Omega/8)^\alpha/D$ at which the boundaries are felt, on average, is denoted by vertical ticks.

prediction can be attributed to the finite size of the computational domain and the fact that the theoretical development is for an infinite medium. While one might expect that the boundaries would increase reaction rates at all times because of the very large (inter-island) distances that the particles may take at any time, it is the average size of the islands that dictates the late-time transition back to well-mixed rates (Fig. 3). A simple argument shows that the islands grow at a Lévy diffusive rate of $(Dt)^{1/\alpha}$, so that the fringes of the largest island may feel the boundary at time $t = (\Omega/K)^\alpha/D$, where K is some empirical constant that describes the distance out along an island where the reactions are taking place. We find that a value of $K = 8$ is a reasonable guide to the onset of boundary effects (Fig. 3). To demonstrate that this is truly a boundary effect and test this approximation, we ran the simulations for Fickian dispersion and reaction as shown in Fig. 4. In this case the ratio of the initial number of particles to the domain size is fixed at $N_0/\Omega = 40$ so that the average particle spacing is the same for any domain size. The domain size is doubled successively, which increases by a factor of four the time at which the boundaries are felt by the reaction (Fig. 4).

5. Conclusions

The role of incomplete mixing greatly complicates the accurate predictions of effective chemical reaction rates. Not only is the overall rate different from the well-mixed case, but the functional form is different, pointing to the insufficiency of the classical (thermodynamic) rate equation. We showed, for a simple set of cases, how the correct ensemble concentration evolution equation can be derived using stochastic analytic methods. In particular, as incomplete mixing effects dominate, the rate of decay of chemical species changes from t^{-1} to $t^{-1/(2\alpha)}$, which for the Fickian case of $\alpha = 2$ is consistent with previous observations [2,1]. Enhanced dispersion leads to faster decay than the Fickian counterpart, but the system is still slowed and dispersion-limited relative to the well-mixed system.

The mechanics of the underlying dispersion and mixing process is directly incorporated into the ensemble governing equation through the action of the fractional dispersion Green function on the initial degree of imperfect mixing in the system. This analysis leads to a dimensionless number that marks the transition from good mixing and the classical governing equation to poor mixing and the equation with a new term. Analytic arguments also show the time at which the domain boundaries destroy the poor mixing by limiting the size of the islands that are enriched in one or the other reactant.

The work here focuses purely on the role of fractional dispersion on incomplete mixing and reactions. However, the methodologies (both analytic and numerical) developed here are quite general and should allow for the analyses of more complicated and realistic geometries and mixing mechanisms. Incorporating the small scale mixing limitations imposed by heterogeneous velocity fields and local dispersion within larger scale reaction predictions is of significant practical interest to the water resources community as a whole.

Acknowledgements

Diogo Bolster would like to express thanks for financial support from NSF via Grant EAR-1113704. David Benson would like to express thanks for financial support from NSF via Grants EAR-0749035 and DMS-0539176 and the Department of Energy through Grant DOE DE-FG02-07ER15841. Any opinions, findings, conclusions, or recommendations do not necessarily reflect the views of the funding agencies. Pietro de Anna would like to express thanks for the financial support of the European Commission through FP7 project, IMVUL (Grant Agreement 212298). Alexander Tartakovsky was partially supported by the Office of Advanced Scientific Computational Research of the Department of Energy.

Appendix A. Covariance equation

Multiplying (5) for $i = A$ by $C'_B(y)$ and discarding terms of higher than second order in fluctuations we obtain

$$C'_B(y)\frac{\partial C'_A(x)}{\partial t} = D\left(p\frac{\partial^\alpha C'_A(x)C'_B(y)}{\partial x^\alpha} + q\frac{\partial^\alpha C'_A(x)C'_B(y)}{\partial(-x)^\alpha}\right) - k\overline{C_A(x)}C'_B(x)C'_B(y) - k\overline{C_A(x)}C'_A(x)C'_B(y). \quad (A.1)$$

Similarly multiplying (5) for $i = B$ by $C'_A(y)$ and discarding terms of higher than second order in fluctuations we obtain

$$C'_A(y)\frac{\partial C'_B(x)}{\partial t} = D\left(p\frac{\partial^\alpha C_B(x)C'_A(y)}{\partial x^\alpha} + q\frac{\partial^\alpha C'_B(x)C'_A(y)}{\partial(-x)^\alpha}\right) - k\overline{C_B(x)}C'_A(x)C'_A(y) - k\overline{C_B(x)}C'_B(x)C'_A(y). \quad (A.2)$$

Taking the ensemble average of (A.1) and (A.2) and recognizing that by stationarity $\overline{C'_B(y)C'_A(x)} = \overline{C'_A(y)C'_B(x)}$, we sum the equations and obtain the following equation for the covariance

$$\overline{C'_B(y)\frac{\partial C'_A(x)}{\partial t} + C'_A(y)\frac{\partial C'_B(x)}{\partial t}} = 2D\left(p\frac{\partial^\alpha \overline{C'_A(x)C'_B(y)}}{\partial x^\alpha} + q\frac{\partial^\alpha \overline{C'_A(x)C'_B(y)}}{\partial(-x)^\alpha}\right) - 2k\overline{C_A(x)C'_A(x)C'_A(y)} - 2k\overline{C_A(x)C'_A(x)C'_B(y)}, \quad (A.3)$$

which can be rewritten as

$$\frac{\partial \overline{C'_A(x)C'_B(y)}}{\partial t} = 2D\left(p\frac{\partial^\alpha \overline{C'_A(x)C'_B(y)}}{\partial x^\alpha} + q\frac{\partial^\alpha \overline{C'_A(x)C'_B(y)}}{\partial(-x)^\alpha}\right) - 2k\overline{C_A(x)C'_A(x)C'_A(y)} - 2k\overline{C_A(x)C'_A(x)C'_B(y)}. \quad (A.4)$$

Similarly, an equation for $\overline{C'_A(x)C'_A(y)}$ is given by

$$\frac{\partial \overline{C'_A(x)C'_A(y)}}{\partial t} = 2D\left(p\frac{\partial^\alpha \overline{C'_A(x)C'_A(y)}}{\partial x^\alpha} + q\frac{\partial^\alpha \overline{C'_A(x)C'_A(y)}}{\partial(-x)^\alpha}\right) - 2k\overline{C_A(x)C'_B(x)C'_A(y)} - 2k\overline{C_B(x)C'_A(x)C'_A(y)}. \quad (A.5)$$

Subtracting Eq. (A.5) from Eq. (A.4) gives:

$$\frac{\partial[\overline{C'_A(x,t)C'_B(y,t)} - \overline{C'_A(x,t)C'_A(y,t)}]}{\partial t} = 2D\left(p\frac{\partial^\alpha\left(\overline{C'_A(x)C'_B(y)} - \overline{C'_A(x)C'_A(y)}\right)}{\partial x^\alpha} + q\frac{\partial^\alpha\left(\overline{C'_A(x)C'_B(y)} - \overline{C'_A(x)C'_A(y)}\right)}{\partial(-x)^\alpha}\right). \quad (A.6)$$

As laid out in the main body of the text the initial conditions for these are

$$\overline{C'_A(x,0)C'_A(y,0)} = -\overline{C'_A(x,0)C'_B(y,0)} = R(x,y). \quad (A.7)$$

Therefore, from moment Eqs. (A.4) and (A.5) it follows that

$$\overline{C'_A(x,y,t)C'_B(x,y,t)} = -\overline{C'_A(x,y,t)C'_A(x,y,t)} \quad (A.8)$$

and with this is mind, we can rewrite the 1-D Eq. (A.6)

$$\frac{\partial[\overline{C'_A(x,t)C'_B(y,t)}]}{\partial t} = 2D\left(p\frac{\partial^\alpha\left(\overline{C'_A(x)C'_B(y)}\right)}{\partial x^\alpha} + q\frac{\partial^\alpha\left(\overline{C'_A(x)C'_B(y)}\right)}{\partial(-x)^\alpha}\right). \quad (A.9)$$

Appendix B. Alternative initial correlation structures

In this appendix we demonstrate that another short range correlation structure, namely the exponential, give the same long time behavior as the delta correlation, thus justifying its selection. Specify now:

$$f(x,y,t=0) = R(x,y) = -\sigma^2 e^{-\frac{|x-y|}{l}}. \quad (B.1)$$

Substituting into (9) for the limit of $y \to x$

$$f(x,y\to x,t) = -\frac{\sigma^2}{\pi}\int_{-\infty}^{\infty}\frac{l}{k^2l^2+1}e^{2D[p(ik)^\alpha]+q(-ik)^\alpha]t}dk = -\frac{\sigma^2}{\pi}\int_{-\infty}^{\infty}\frac{lt^{\frac{1}{\alpha}}}{m^2l^2+t^{\frac{2}{\alpha}}}e^{2D[p(im)^\alpha]+q(-im)^\alpha]}dm. \quad (B.2)$$

If we take the limit of long time ($t \to \infty$)

$$f(x,y\to x,t) \sim -t^{-1/\alpha}\frac{\sigma^2 l}{2}\int_{-\infty}^{\infty}e^{2D[p(im)^\alpha]+q(-im)^\alpha]}dm \quad (B.3)$$

which is the same scaling that arises for the delta initial correlation for all times. Similar results can be shown for other short range correlation structures such a Gaussian one.

References

[1] de Anna P, Le Borgne T, Dentz M, Bolster D, Davy P. Anomalous kinetics in diffusion limited reactions linked to non-Gaussian concentration PDF. J Chem Phys 2011;135:174104.

[2] Benson DA, Meerschaert MM. Simulation of chemical reaction via particle tracking: diffusion-limited versus thermodynamic rate-limited regimes. Water Resour Res 2008;44:W12201. doi:10.1029/2008WR007111.

[3] Berkowitz B, Cortis A, Dentz M, Scher H. Modeling non-Fickian transport in geological formations as a continuous time random walk. Rev Geophys 2006;44:RG2003.

[4] Bolster D, Dentz M, Le Borgne T. Hyper mixing in shear flow. Water Resour Res 2011;47:W09602. doi:10.1029/2011WR010737.

[5] Bolster D, Valdes-Parada FJ, Le Borgne T, Dentz M, Carrera J. Mixing in confined stratified aquifers. J Contam Hydrol 2011;120–121:P198–21. doi:10.1016/j.jconhyd.2010.02.003.

[6] Bolster D, Benson DA, LeBorgne T, Dentz M. Anomalous mixing and reaction induced by superdiffusive nonlocal transport. Phys Rev E 2010;82:021119. doi:10.1103/PhysRevE.82.021119.

[7] Bolster D, Dentz M, Carrera J. Effective two-phase flow in heterogeneous media under temporal pressure fluctuations. Water Resour Res 2009;45:W05408.

[8] Bradley D, Tucker G, Benson D. Fractional dispersion in a sand bed river. J Geophys Res F Earth Surf 2010;115:F00A09. doi:10.1029/2009JF001268.

[9] Chiogna G, Cirpka OA, Gratwohl P, Rolle M. Transverse mixing of conservative and reactive tracers in porous media: quantification through the concepts of flux-related and critical dilution indices. Water Resour Res 2011;47:W02505.

[10] Cirpka OA, de Barros FPJ, Chiogna G, Rolle M, Nowak W. Stochastic flux-related analysis of transverse mixing in two-dimensional heterogeneous porous media. Water Resour Res 2011;47:W06515.

[11] Cushman JH, Ginn TR. Nonlocal dispersion in media with continuously evolving scales of heterogeneity. Transport Porous Med 1993;13:123–38.

[12] Cushman-Roisin B. Beyond eddy diffusivity: an alternative model for turbulent dispersion. Environ Fluid Mech 2008;8:543–9.

[13] Dentz M, Bolster D. Distribution versus correlation-induced anomalous transport in quenched random velocity fields. Phys Rev Lett 2010;105:244301.

[14] Dentz M, LeBorgne T, Englert A, Bijeljic B. Mixing, spreading and reaction in heterogeneous media: a brief review. J Contam Hydrol 2011;120–121:1–17.

[15] Dentz M, Tartakovsky DM. Delay mechanisms of non-Fickian transport in heterogeneous media. Geophys Res Lett 2006;33(16):L16406.

[16] Donado LD, Sánchez-Vila X, Dentz M, Carrera J, Bolster D. Multicomponent reactive transport in multicontinuum media. Water Resour Res 2009;45:W11402.

[17] Edery Y, Scher H, Berkowitz B. Modeling bimolecular reactions and transport in porous media. Geophys Res Lett 2009;35:L02407.

[18] Fiori A, Jankovic I. Can we determine the transverse macrodispersivity by using the method of moments. Adv Water Resour 2005;28(6):589–99.

[19] Furbish D, Childs E, Haff P, Schmeeckle M. Rain splash of soil grains as a stochastic advection–dispersion process, with implications for desert plant–soil interactions and land-surface evolution. J Geophys Res 2009;114:F00A03.

[20] Gillespie DT. The chemical Langevin equation. J Chem Phys 2000;113(1):297–306.

[21] Gnedenko BV, Kolmogorov AN. Limit distributions for sums of independent random variables. Addison-Wesley; 1954 [Translated from Russian].

[22] Gooseff MN, Wondzell SM, Haggerty R, Anderson J. Comparing transient storage modeling and residence time distribution (RTD) analysis in geomorphically varied reaches in the Lookout Creek basin, Oregon, USA. Adv Water Resour 2003;26:925–37.

[23] Gramling C, Harvey CF, Meigs LC. Reactive transport in porous media: a comparison of model prediction with laboratory visualization. Environ Sci Technol 2002;36:2508–14.

[24] Haggerty R, Gorelick SM. Multiple-rate mass transfer for modeling diffusion and surface reactions in media with pore-scale heterogeneity. Water Resour Res 1995;31(10):2383–400.

[25] Van Hauwermeiren M, Vose D. A compendium of distributions. [ebook]. Ghent, Belgium: Vose Software; 2009.

[26] Kang K, Redner S. Fluctuation dominated kinetics in diffusion-controlled reactions. Phys Rev A 1985;32:435–47.

[27] Le Borgne T, Dentz M, Bolster D, Carrera J, de Dreuzy J-R, Bour O. Persistence of incomplete mixing: a key to anomalous transport. Phys Rev E 2011;84:015301(R).

[28] Le Borgne T, Dentz M, Bolster D, Carrera J, de Dreuzy J-R, Davy P. Non-Fickian mixing: temporal evolution of the scalar dissipation rate in porous media. Adv Water Resour 2010;33:1468–75.

[29] Luo J, Cirpka OA. How well do mean breakthrough curves predict mixing-controlled reactive transport? Water Resour Res 2011;47:W02520.

[30] Monson E, Kopelman R. Nonclassical kinetics of an elementary $A+B\to C$ reaction–diffusion system showing effects of a speckled initial reactant distribution and eventual self-segregation. Exp Phys Rev E 2004;69:021103.

[31] Meerschaert MM, Scheffler H-P. Limit distributions for sums of independent random vectors: heavy tails in theory and practice. Wiley Interscience; 2001.

[32] Neuman SP. Lagrangian theory of transport in space-time nonstationary velocity fields: exact nonlocal formalisms by conditional moments and weak approximation. Water Resour Res 1993;29:633–45.

[33] Neuman SP, Tartakovsky DM. Perspective on theories of anomalous transport in heterogeneous media. Adv Water Resour 2009;32:670–80.
[34] Neuweiler I, Attinger S, Kinzelbach W, King P. Large scale mixing for immiscible displacement in heterogeneous porous media. Transport Porous Med 2003;51:287–314.
[35] Ovchinnikov AA, Zeldovich YB. Role of density fluctuations in bimolecular reactions. Chem Phys 1978;28:215–8.
[36] Raje D, Kapoor V. Experimental study of bimolecular reaction kinetics in porous media. Environ Sci Technol 2000;34:1234–9.
[37] Rolle M, Eberhardt C, Chiogna G, Cirpka OA, Gratwohl P. Enhancement of dilution and transverse reactive mixing in porous media: experiments and model-based interpretation. J Contam Hydrol 2009;110:130–42.
[38] Sánchez-Vila X, Fernández-Garcia D, Guadagnini A. Interpretation of column experiments of transport of solutes undergoing an irreversible bimolecular reaction using a continuum approximation. Water Resour Res 2010;46: W12510.
[39] Sanchez-Vila X, Dentz M, Donado LD. Transport-controlled reaction rates under local non-equilibrium conditions. Geophys Res Lett 2007;34:L10404. doi:10.1029/2007GL029410.
[40] Schumer R, Meerschaert MM, Baeumer B. Fractional advection–dispersion equations for modeling transport at the earth surface. J Geophys Res 2009;114:F00A07.
[41] Tartakovsky AM, de Anna P, Borgne TL, Balter A, Bolster D. Effects of spatial concentration fluctuations on non-linear reactions. Water Resour Res [submitted for publication].
[42] Tartakovsky AM, Tartakovsky DM, Meakin P. Stochastic Langevin model for flow and transport in porous media. Phys Rev Lett 2008;101:044502.
[43] Tartakovsky AM, Tartakovsky GD, Scheibe TD. Effects of incomplete mixing on multicomponent reactive transport. Adv Water Resour 2009; 32:1674–9.
[44] Toussaint D, Wilczek F. Particle–antiparticle annihilation in diffusive motion. J Chem Phys 1983;78:2642–7.
[45] Tsallis C, Levy SVF, Souza AMC, Maynard R. Statistical–mechanical foundation of the ubiquity of the Lévy distributions in Nature. Phys Rev Lett 1996;77:5442.
[46] Werth CJ, Cirpka OA, Grathwohl P. Enhanced mixing and reaction through flow focusing in heterogeneous porous media. Water Resour Res 2006;42:W12414. doi:10.1029/2005WR004511.
[47] Willmann M, Carrera J, Sánchez-Vila X, Silva O, Dentz M. Coupling of mass transfer and reactive transport for nonlinear reactions in heterogeneous media. Water Resour Res 2010;44:W12437.

Appendix B

Appendix B

Effective pore-scale dispersion upscaling with a correlated continuous time random walk approach

T. Le Borgne,[1] D. Bolster,[2] M. Dentz,[3] P. de Anna,[1] and A. Tartakovsky[4]

Received 23 January 2011; revised 29 September 2011; accepted 22 October 2011; published 29 December 2011.

[1] We investigate the upscaling of dispersion from a pore-scale analysis of Lagrangian velocities. A key challenge in the upscaling procedure is to relate the temporal evolution of spreading to the pore-scale velocity field properties. We test the hypothesis that one can represent Lagrangian velocities at the pore scale as a Markov process in space. The resulting effective transport model is a continuous time random walk (CTRW) characterized by a correlated random time increment, here denoted as correlated CTRW. We consider a simplified sinusoidal wavy channel model as well as a more complex heterogeneous pore space. For both systems, the predictions of the correlated CTRW model, with parameters defined from the velocity field properties (both distribution and correlation), are found to be in good agreement with results from direct pore-scale simulations over preasymptotic and asymptotic times. In this framework, the nontrivial dependence of dispersion on the pore boundary fluctuations is shown to be related to the competition between distribution and correlation effects. In particular, explicit inclusion of spatial velocity correlation in the effective CTRW model is found to be important to represent incomplete mixing in the pore throats.

Citation: Le Borgne, T., D. Bolster, M. Dentz, P. de Anna, and A. Tartakovsky (2011), Effective pore-scale dispersion upscaling with a correlated continuous time random walk approach, *Water Resour. Res.*, *47*, W12538, doi:10.1029/2011WR010457.

1. Introduction

[2] The ability to upscale dispersion is an important step in predicting solute transport through porous media. This topic has received continuous attention since the pioneering work of Taylor, who studied dispersion in a tube [*Taylor*, 1953]. Taylor showed that this system, at late times, once transverse diffusion has allowed the plume to sample all the velocities in the tube cross section, can be characterized by an effective one-dimensional advection-dispersion equation with an enhanced dispersion coefficient. This enhanced dispersion coefficient can be quantified by the second centered moment of the concentration distribution [*Aris*, 1956]. The Taylor dispersion coefficient reflects the interaction between spreading driven by the heterogeneous velocity field and diffusion that attenuates the resulting concentration contrasts.

[3] Since this seminal study there has been a large amount of work dedicated to quantifying dispersion in more complex flow fields. A variety of methodologies, including the method of local moments [*Brenner*, 1980; *Brenner and Adler*, 1982; *Frankel and Brenner*, 1989; *Edwards and Brenner*, 1993], volume averaging [*Bear*, 1972; *Plumb and Whitaker*, 1988; *Valdes-Parada et al.*, 2009; *Wood*, 2009], and the method of multiple scales [*Auriault and Adler*, 1995; *Lunati et al.*, 2002; *Attinger et al.*, 2001], have emerged. The main goal of these methods is to develop an effective asymptotic dispersion coefficient that quantifies spreading and mixing in an upscaled effective equation and in many cases they have been successful [*Edwards et al.*, 1991; *Porter et al.*, 2010].

[4] Macrodispersion approaches describe asymptotic heterogeneity-induced transport, which can be cast in an advection-dispersion equation for the macroscale solute concentration. Such Fickian models are characterized typically by a diffusive growth of the plume size. In many applications, however, such an asymptotic regime is often not reached on realistic space and time scales. In fact, there is a large amount of data from field [*Rehfeldt et al.*, 1992; *Gelhar et al.*, 1992; *Sidle et al.*, 1998; *Le Borgne and Gouze*, 2008] and laboratory experiments [*Silliman and Simpson*, 1987; *Silliman et al.*, 1987; *Moroni et al.*, 2007; *Levy and Berkowitz*, 2003] that suggests that the Fickian behavior is often not observed. Theoretical predictions in heterogeneous velocity fields anticipated this [*Matheron and de Marsily*, 1980; *Deng et al.*, 1993; *Deng and Cushman*, 1995; *Dentz et al.*, 2000; *Berkowitz et al.*, 2006; *Bijeljic and Blunt*, 2006; *Nicolaides et al.*, 2010; *Wood*, 2009]. This behavior can be traced back to incomplete mixing on the macroscopic support scale [*Le Borgne et al.*, 2011; *Dentz et al.*, 2011].

[5] Thus, for the realistic modeling of transport in heterogeneous porous media, it is necessary to predict transport

[1]Geosciences Rennes, UMR 6118, CNRS, Université de Rennes 1, Rennes, France.
[2]Environmental Fluid Dynamics Laboratories, Department of Civil Engineering and Geological Sciences, University of Notre Dame, Notre Dame, Indiana, USA.
[3]Institute of Environmental Assessment and Water Research, Barcelona, Spain.
[4]Computational Mathematics Group, Pacific Northwest National Laboratory, Richland, Washington, USA.

0043-1397/11/2011WR010457

during this preasymptotic regime [e.g., *Gill and Sankarasubramanian*, 1970; *Latini and Bernoff*, 2001; *Bijeljic and Blunt*, 2006] and in particular capture the anomalous non-Fickian behavior. Several nonlocal models have emerged to model this behavior in porous media, including moment equation approaches [*Neuman*, 1993; *Morales-Casique et al.*, 2006], projector formalisms [*Cushman and Ginn*, 1993, 1994], multirate mass transfer [*Haggerty and Gorelick*, 1995; *Carrera et al.*, 1998; *Cherblanc et al.*, 2007; *Chastanet and Wood*, 2008], fractional advection-dispersion equations [*Benson et al.*, 2000, 2001; *Cushman and Ginn*, 2000], continuous time random walks [*Berkowitz and Scher*, 1995; *Berkowitz et al.*, 2006; *Bijeljic and Blunt*, 2006] and continuous Markovian stochastic processes in time [*Meyer and Tchelepi*, 2010]. A review of these models is provided by *Neuman and Tartakovsky* [2009]. One of the main challenges within nonlocal modeling approaches is how to relate microscale properties (e.g., velocity statistics) to the effective macroscale models.

[6] In this paper we will focus on the continuous time random walk (CTRW) approach. A popular approach for defining CTRW model parameters is breakthrough curves fitting [e.g., *Berkowitz and Scher*, 2010]. While useful in practice, the limitation of this approach is that it is difficult in general to relate the derived effective parameters to the velocity field properties. Some analytical approaches considering simplified forms of heterogeneity have been developed that upscale exactly to a CTRW [*Dentz and Castro*, 2009; *Dentz et al.*, 2009; *Dentz and Bolster*, 2011]. In particular, the importance of spatial velocity correlation and its impact on anomalous transport is explicitly illustrated in the simplified model of *Dentz and Bolster* [2011]. A different approach that is not restricted to simplified types of heterogeneity was developed by *Le Borgne et al.* [2008a, 2008b]. By using the spatial Markov property of Lagrangian velocities, one can define a correlated CTRW model, whose parameters are defined from the velocity field distribution and spatial correlation properties. Thus, the upscaled CTRW model is obtained without fitting its parameters to the dispersion data; instead they are estimated from the Lagrangian velocity field analysis. Velocity distribution and spatial correlation are known two govern dispersion heterogeneous media [*Bouchaud and Georges*, 1990]. Solute dispersion is enhanced when the width of the velocity distribution is increased. It is also enhanced when the spatial correlation of the velocity field is stronger. In other words, when each solute particle tends to keep similar velocities for a long time, the ensemble of particles is more dispersed. The correlated CTRW approach quantifies separately distribution and correlation effects. We will show in the following that this is critical to understand and quantify pore-scale dispersion as velocity distribution and spatial correlation can have antagonist effects, hence competing for governing the global dispersion.

[7] Here we invoke a CTRW approach characterized by correlated successive particle velocities (termed correlated CTRW in the following) to study dispersion in a pore-scale context. To this end, we first consider a simplified periodic representation of a pore introduced by *Dykaar and Kitanidis* [1996] (Figure 1) and then a more complex two-dimensional heterogeneous porous medium [*Tartakovsky and Neuman*, 2008]. Because of its simplicity, the sinusoidal channel model can provide much insight to the understanding of basic mechanisms that occur at the pore scale. The conclusions derived from the analysis of this system can also be used to understand and quantify the role of boundary fluctuations, which is relevant for example for transport at the fracture scale [*Drazer et al.*, 2004; *Drazer and Koplick*, 2002]. Additionally this model is appealing, because, while quite simple, it displays some interesting and perhaps unexpected features. For example, *Bolster et al.* [2009] showed that increasing the fluctuation of the pore wall does not necessarily result in an increase in asymptotic dispersion, a result that may be counterintuitive on the basis of other predictions [e.g., *Gelhar*, 1993; *Prude'Homme and Hoagland*, 1999; *Tartakovsky and Xiu*, 2006] that suggest that as the fluctuations increase, so too should dispersion. Some experimental evidence [*Drazer et al.*, 2004; *Drazer and Koplick*, 2002] and heuristic mathematical arguments [*Rosencrans*, 1997] support this prediction of a reduction in asymptotic dispersion. The reduction cannot be explained by a classical Taylor-Aris type approach (see *Bolster et al.* [2009] for details).

[8] In this work, we argue and illustrate that the correlated CTRW model provides a solid framework that can be used to physically interpret and understand such observations. Additionally we illustrate that it is capable of accurately predicting the evolution of observed preasymptotic non-Fickian dispersion. In section 2, we describe the periodic pore representation for which we seek to upscale dispersion. In section 3, we introduce the correlated CTRW model and compute the transition time distribution and the probability transition matrix that parametrize it. In section 4, we compare the prediction of this upscaled model to the results obtained from the fully resolved pore-scale simulations. In section 5, we demonstrate the applicability of this upscaling approach to a more complex heterogeneous porous medium.

2. Sinusoidal Channel Model

[9] We consider flow in a two-dimensional channel that is symmetric about the central axis at $y = 0$. The boundaries of the channel fluctuate periodically in the horizontal direction as

$$h(x) = \overline{h} + h' \sin\left(2\pi \frac{x}{L}\right), \tag{1}$$

where $\overline{h}$ is the average channel height. The aspect ratio is defined by

$$\epsilon = \frac{2\overline{h}}{L}. \tag{2}$$

The ratio between the amplitude of the aperture fluctuations h' and the mean aperture, called the fluctuation ratio, is denoted by

$$a = \frac{h'}{2\overline{h}}. \tag{3}$$

The flow at low Reynolds numbers within such a sinusoidal channel, whose boundary changes slowly (i.e., $\epsilon = \frac{\overline{h}}{L} < 1$) was studied and derived analytically using a perturbation method in ϵ by *Kitanidis and Dykaar* [1997]. In order to

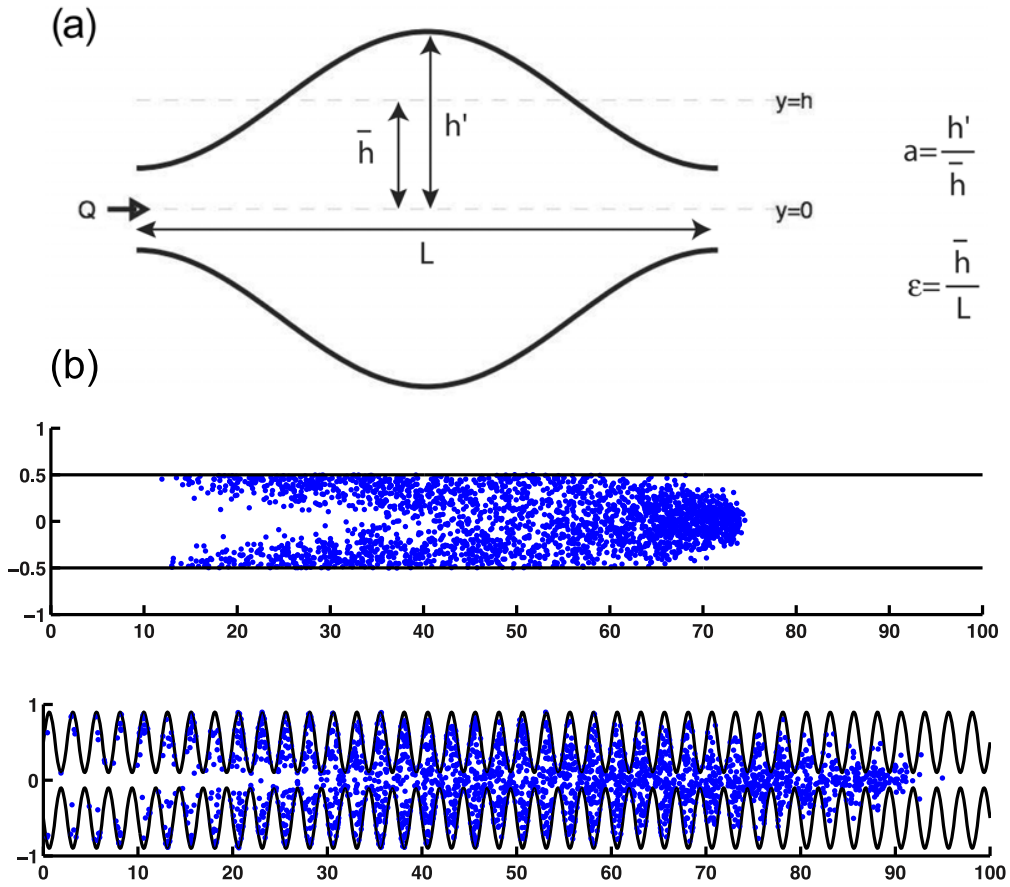

Figure 1. (a) A schematic of the pore we are considering and (b) random walk simulations for $Pe = 10^3$ after a time of 50τ (where τ is the mean travel time of one pore). In Figure 1b, the top plot corresponds to $a = 0$, and the bottom plot corresponds to $a = 0.4$ and $\epsilon = 0.4$.

illustrate the different types of flow that can arise within such a geometry, two sets of streamlines calculated using this method are shown in Figure 1. A feature of this model is that recirculation zones appear for aspect and fluctuation ratios close to 0.4 [*Bolster et al.*, 2009].

[10] We simulate transport in this flow field using a particle tracking approach. The Peclet number Pe, which characterizes the ratio between the advective and diffusive time scales, is defined by

$$Pe = \frac{2\bar{h}\overline{u}}{D}, \tag{4}$$

where D is the diffusion coefficient and $\overline{u}$ is the mean velocity. In the following simulations, we set the parameter values as $Pe = 10^3$, $\overline{u} = 1$, and $\overline{h} = 1/2$. Figure 2 shows an example of particle trajectories in a flow field characterized by $a = 0.4$ and $\epsilon = 0.4$. Particles travel fast at the center of the pore and move slowly close to the pore wall where they can be trapped in recirculation zones. They jump from one streamline to another by diffusion. The resulting longitudinal dispersion can be characterized in terms of the longitudinal width σ of the solute distribution $c(\mathbf{x}, t)$

$$\sigma^2(t) = \int \mathrm{d}\mathbf{x} x^2 c(\mathbf{x}, t) - \left[\int \mathrm{d}\mathbf{x} x c(\mathbf{x}, t)\right]^2. \tag{5}$$

Specifically, asymptotic longitudinal dispersion is quantified in terms of the effective dispersion coefficient

$$D^e = \frac{1}{2}\lim_{t\to\infty} \frac{\mathrm{d}\sigma^2(t)}{\mathrm{d}t}. \tag{6}$$

[11] The dependence of the asymptotic coefficient on the aspect and fluctuation ratios, obtained by *Bolster et al.* [2009], is displayed in Figure 3. When the aspect ratio ϵ is small, the increase of the fluctuation ratio a leads to a decrease of the asymptotic dispersion coefficient. On the other hand, when the aspect ratio ϵ is large, the increase of the fluctuation ratio a leads to an increase of the asymptotic dispersion coefficient. We demonstrate in the following that this nontrivial behavior can be understood qualitatively by the competition between distribution effects and correlation effects and can be quantified formally through a correlated CTRW model.

3. Correlated CTRW Model

[12] We seek to represent the longitudinal dispersion process in the wavy channel model as a one-dimensional random walk with distributed spatial and temporal increments (CTRW). The series of successive longitudinal particle positions $\{x^{(n)}\}_{n=0}^{\infty}$ and travel times $\{t^{(n)}\}_{n=0}^{\infty}$ are

$$x^{(n+1)} = x^{(n)} + \Delta x^{(n)} \tag{7}$$

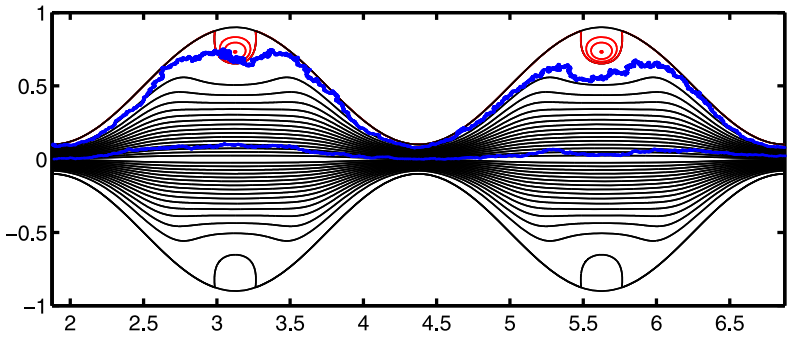

Figure 2. Examples of particle trajectories over two pores for two particles starting initially close to the pore wall and at the center of the pore throat, respectively. The pore shape parameters are $\epsilon = 0.4$ and $a = 0.4$. The detailed streamlines in the upper recirculation zones are shown in red.

$$t^{(n+1)} = t^{(n)} + \Delta t^{(n)}, \tag{8}$$

where $\{\Delta x^{(n)}\}_{n=0}^{\infty}$ and $\{\Delta t^{(n)}\}_{n=0}^{\infty}$ are the successive spatial and temporal increments. In many CTRW models, the successive temporal increments $\Delta t^{(n)}$ are taken as independent random variables. Thus, the dispersion dynamics depend entirely on the increment distributions [*Berkowitz and Scher*, 2010; *Dentz and Bolster*, 2011]. Figure 2 suggests that, in the absence of complete mixing at pore throats, there can be a significant correlation between successive particle travel times. Particles moving quickly at the pore center have a high probability to remain in a high-velocity zone in the next pore. Similarly, particles have a significant probability to be successively trapped in successive pores when they travel close to the pore walls.

[13] Transit times are related to Lagrangian velocities by $\{\Delta t^{(n)} = \Delta x / v^{(n)}\}_{n=0}^{\infty}$, where $v^{(n)}$ is the mean particle velocity across the length Δx. Diffusive jumps of particles across streamlines induce a certain velocity decorrelation such that ultimately the velocity memory is lost when the particle has traveled over many pores. The process of velocity decorrelation by diffusion is most efficient at the pore throat where streamlines converge close to each other. Figure 4 displays the pore-scale Lagrangian velocity correlation functions as a function of travel time and as a function of travel distance for the case $a = 0.4$ and $\epsilon = 0.4$. The Lagrangian velocities are found to have a short-range correlation in space and a long-range correlation in time. The latter is related to the low-velocity areas close to the pore wall and to the recirculation areas, where particles can remain trapped for a long time.

[14] In order to quantify the correlation between successive temporal increments, due to incomplete mixing at pore throats, we represent the series of successive transit times over one pore length $\{\Delta t^{(n)}\}_{n=0}^{\infty}$ as a Markov chain, which is motivated by the short range spatial correlation of Lagrangian velocities (Figure 4). Note that this the Markov property does not mean that the correlation length is assumed to be equal to one pore size. The corresponding correlation length depends on the transition probabilities for successive transit times. Thus, setting the spatial increment equal to the pore length $\Delta x^{(n)} = L$ in (7), the corresponding effective transport model is a correlated CTRW defined by the probability distribution density $p(\Delta t)$ and the conditional probability density $r(\Delta t|\Delta t')$, where Δt

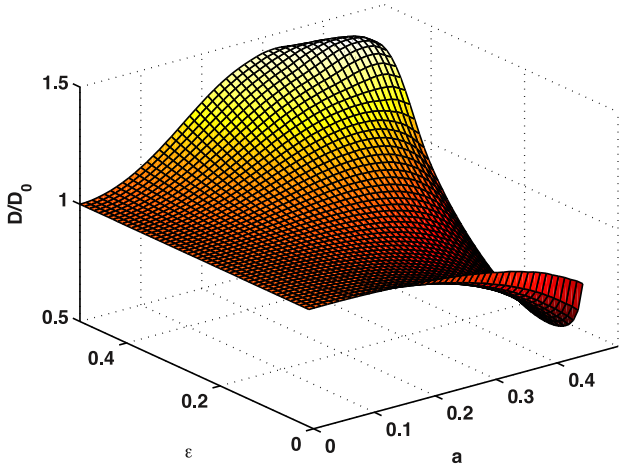

Figure 3. Dependence of the asymptotic dispersion coefficient on ϵ and a for $Pe = 10^3$, from *Bolster et al.* [2009]. The dispersion coefficient is normalized by D_0, the value corresponding to a parallel wall channel ($\epsilon = 0, a = 0$).

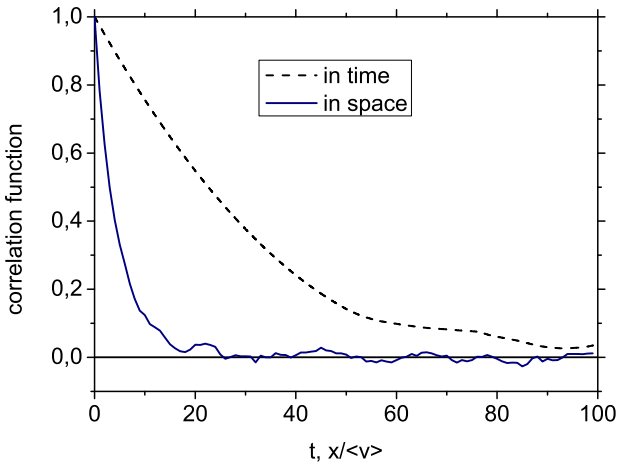

Figure 4. Comparison of pore-scale Lagrangian velocity correlation function in time and in space for parameters $a = 0.4$ and $\epsilon = 0.4$.

and $\Delta t'$ are successive transit times across one pore. To test the applicability of this model to upscale longitudinal dispersion, we numerically compute the transit time distributions across one pore $p(\Delta t)$ and the conditional probability density $r(\Delta t|\Delta t')$ from transport simulations over two pores (Figure 2).

[15] The Lagrangian transit time distributions across one pore $p(\Delta t)$, computed from particle tracking simulations, are displayed in Figure 5 for different values of the aspect and fluctuation ratios. They are characterized by a peak at small times and a tail at large times, with a significant probability for particles to experience large transit times. The maximum transit time is defined by an upper cut off. Both the minimum and maximum times depend on the pore shape. A special case is $a = 0.4$ and $\epsilon = 0.4$ for which recirculation zones exist (Figure 1c). The impact of these recirculation zones is that the width of the transit time distribution increases by about 1 order of magnitude compared to cases without recirculation zones. The probability of large transit times increases because of trapping of particles in these recirculation zones. At the same time, the smallest transit time decreases, i.e., the maximum velocity increases. This is due to an enhanced focusing of flow lines in the center of the pore (Figure 1c). For the other cases, the increase of the aspect ratio ϵ tends to slightly decrease the minimum transit time while increasing slightly the maximum transit time. The increase of the fluctuation ratio a does not appear to affect the minimum transit time, but does increase slightly the maximum transit time.

[16] We now quantify the conditional probability density $r(\Delta t|\Delta t')$ from particle tracking simulations over two successive pores, where $\Delta t'$ is the transit time across the first pore and Δt is the transit time across the second pore. This quantifies the correlation between successive transit time, illustrated in Figure 2. For this purpose, we discretize the transit time distribution $p(\Delta t)$ into n classes $\{C_i\}_{1\le i\le n-1}$ of equal probability of occurrence [*Le Borgne et al.*, 2008b]. We define $\eta = P(\Delta t)$ as the score corresponding to the transit time Δt, where $P(\Delta t)$ is the cumulative transit time

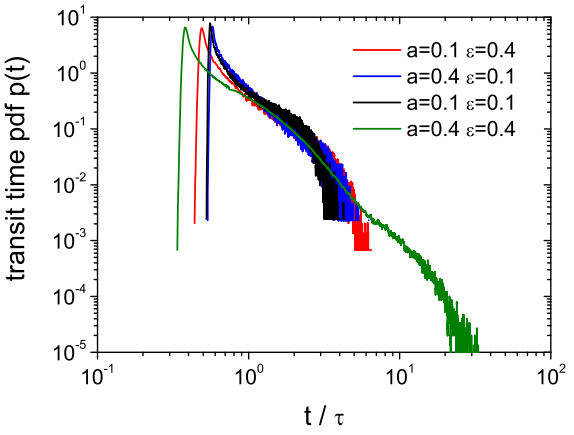

Figure 5. Transit time probability density function $p(t)$ across one pore corresponding to different values of the pore shape parameters ϵ and a. The transit time is normalized by the mean transit time over one pore τ.

distribution. We discretize the η domain, which is bounded between 0 and 1, into n classes of equal width $1/n$, defined by their boundaries η_i. The smallest transit time (largest velocity) corresponds to $\eta_1 = 0$ and the largest transit time (smallest velocity) to $\eta_{n+1} = 1$. In this study, we use $n = 49$ classes. The influence of the number of classes on the prediction of spreading is discussed in section 4. For a given transit time Δt, the corresponding class C_i is determined as follows: $\Delta t \in C_i$ if $\eta_i \le P(\Delta t) < \eta_{i+1}$. The corresponding class boundaries in the temporal increment space are $\Delta t_i = P^{-1}(\eta_i)$.

[17] The probability for a particle to travel through a pore in a time $\Delta t \in C_i$ given that it traveled through the previous pore in a time $\Delta t' \in C_j$ is given by,

$$T_{ij} = \int_{\Delta t_i}^{\Delta t_{i+1}} \mathrm{d}t \int_{\Delta t_j}^{\Delta t_{j+1}} \mathrm{d}t' r(t|t'), \tag{9}$$

The transition matrix $\mathbf{T}$ is the discrete form of the conditional probability density $r(\Delta t|\Delta t')$ and describes the transition probability from class i to class j. The transition matrix is shown for different pore shapes in Figure 6. The transition probabilities are largest in the diagonal region and tend to zero away from the diagonal. The probabilities on the diagonal, i.e., T_{ii}, are the probabilities for a particle to remain in the same class C_i, i.e., to keep a similar transit time over successive pores. The probabilities away from the diagonal correspond to probabilities for a particle to change its transit time from one pore to another, which depends on its diffusion across streamlines.

[18] The correlation of successive times can be measured by the probability to remain in the original class and by the width of the banded matrix area around the diagonal, which reflects the probability for particles to remain in neighboring transit time classes over successive pores. Notice that the transition matrix quantifies some complex correlation properties of the flow field. For instance, the correlation is systematically stronger for small transit times (i.e., large velocities) than for large transit times (Figure 6). As shown in Figure 6, conditional probabilities in the upper left corner, corresponding to the probabilities for particles to keep small transit times, are higher than the other conditional probabilities, e.g., the probability for particles to keep intermediate or large transit times across successive pores.

[19] The comparison of transition matrices in Figure 6 can be used to understand the effect of the pore shape parameters (equation (2) and Figure 1a) on the transit time correlation. The effect of increasing the aspect ratio ϵ from 0.1 to 0.4 is to decrease the width of the banded area in the transition matrix around the diagonal, i.e., to increase the correlation of the successive transit times, as successive particle transit times have a high probability to be close to each other. This can be explained as follows. For a given mean channel height $\overline{h}$, increasing ϵ is equivalent to decreasing the pore length L. Decreasing L implies decreasing the distance available for particles to diffuse across streamlines. Thus, for large ϵ the correlation of successive transit times is strong.

[20] For a given aspect ratio ϵ, the effect of increasing the fluctuation ratio a from 0.1 to 0.4 is to decrease the

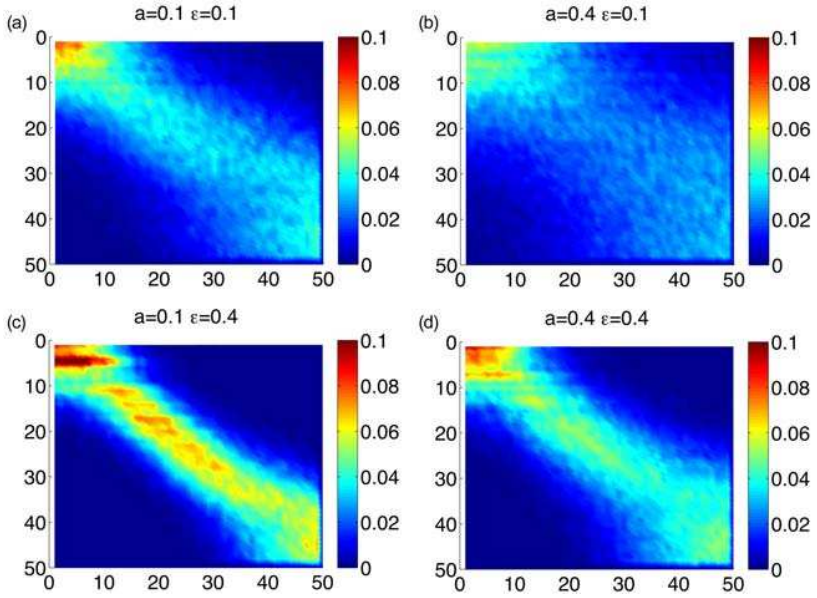

Figure 6. Spatial transition matrices T corresponding to different values of the pore shape parameters ϵ and a (equation (9)). The horizontal axis represents the initial transit time class and the vertical axis represents the next transit time class. Small matrix indices correspond to small transit times (large Lagrangian velocities), and large matrix indices correspond to large transit times (small Lagrangian velocities). The color scale represents the transit time transition probabilities along particle paths.

correlation of successive transit times, as shown by the increase of the width of the banded area in the transition matrix which implies that particle have a significant probability to change transit times over successive pores. This in turn can be explained by the small width of the pore necks for large a (Figure 1a) that induces a focusing of flow lines, thus enhancing mixing between stream lines at the pore necks. Thus, for large a, the correlation between successive transit times is weak.

[21] The transit time distributions and correlation matrices can be used to understand the nontrivial dependence of the asymptotic dispersion coefficient on the pore shape parameters shown in Figure 3. In general, an increase in the width of transit time distribution and an increase of the correlation of successive transit times are both expected to contribute to an increase of the asymptotic dispersion coefficient. These effects are known as distribution- and correlation-induced dispersion [*Bouchaud and Georges*, 1990; *Dentz and Bolster*, 2011]. When changing the fluctuation ratio a, these two effects evolve in opposite directions, thus competing for controlling dispersion. An increase of the fluctuation ratio a produces an increase the transit time variability but a decrease of there correlation over successive pores. In the absence of recirculation zones ($\epsilon < 0.4$), the transit time variability depends only slightly on the fluctuation ratio a. Since transit time decorrelation is the dominant effect in this case, the increase of the fluctuation ratio a leads to a decrease of the asymptotic dispersion coefficient. Conversely, for large aspect ratios ($\epsilon \geq 0.4$), the appearance of recirculation zones leads to a strong dependence of the transit time distribution on the fluctuation ratio a. This effect dominates over the effect of transit time decorrelation, which implies that the asymptotic dispersion coefficient increases with the fluctuation ratio a in this case. Thus, the dependence of dispersion coefficient on the pore shape parameters is controlled here by the competition between distribution and correlation effects.

4. Predictions of the Correlated CTRW Model

[22] The transit time distribution $p(\Delta t)$ and the transition matrix $\mathbf{T}$ together with the spatial Markov property define the correlated CTRW model in (8). Using this effective description, we can make predictions of the transport behavior over a large range of temporal and spatial scales. The equations of motion (8) of a particle are solved numerically using random walk particle tracking, which allows for efficient transport simulations. We compare the predictions of this effective random walk model with the numerical random walk simulations of transport through the fully resolved two-dimensional velocity fields (Figure 2) for $a = 0.4$ and $\epsilon = 0.4$. To probe the role of correlation we also compare the transport behavior resulting from the correlated CTRW with the predictions of a CTRW model without correlation, defined by (7) and (8) with the transition probability given as $r(\Delta t|\Delta t') = p(\Delta t)$. Notice that the predictions of both models are obtained without fitting the model parameters to the dispersion data. Instead the model's parameters, here $p(\Delta t)$ and $r(\Delta t|\Delta t')$ are estimated from the Lagrangian velocity field analysis.

[23] Figure 7 displays the temporal evolution of the second centered moment of the particle positions in the direction of the mean flow $\sigma^2(t)$ for the case $a = 0.4$ and $\epsilon = 0.4$. The initial preasymptotic regime, where $\sigma^2(t)$ evolves nonlinearly in time, lasts for about 30τ, where τ is the mean transit time across one pore. Hence, the Fickian behavior is reached when the average position of the plume has traveled over 30 pores. The spatial distribution of

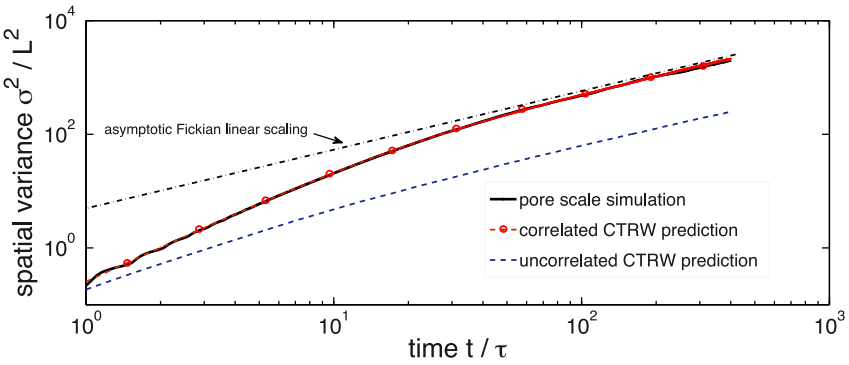

Figure 7. Comparison of the prediction of the correlated CTRW (red dashed line) and uncorrelated CTRW (blue dashed line) with the numerical simulations for the second centered spatial moment in the longitudinal direction σ^2, with $a = 0.4$ and $\epsilon = 0.4$ (black dots). The time is normalized by the mean transit time over one pore τ, and the spatial variance is normalized by L^2. Notice the overlap of the correlated CTRW model predictions and the full pore-scale simulations.

particle positions, shown in Figure 8, is strongly non-Gaussian during the preasymptotic regime.

[24] The correlated CTRW model is found to provide very good predictions of the temporal evolution of the second centered moment $\sigma^2(t)$ at all times and is able to predict accurately the evolution of the spatial particle position distributions from non-Gaussian to Gaussian. In particular, the persistent asymmetry of the spatial distributions, which is due to trapping in low-velocity and recirculation zones, is well captured. The uncorrelated CTRW model is found to underestimate dispersion significantly. The discrepancy for the second centered moment $\sigma^2(t)$ is about 1 order of magnitude at large times. The uncorrelated CTRW model used here has the same transit time distribution as the correlated CTRW model but no correlation of successive transit times. Thus, the comparison of these two models shows the role of spatial correlations of particle motions, which are due in this example to incomplete mixing at the pore throats. Thus, successive transit time correlation, related for instance the fact that particles traveling close to the pore walls have a high probability of being successively trapped in recirculation zones (Figure 2), is found to have an important impact on dispersion.

[25] The good agreement of the correlated CTRW model with pore-scale simulations validates the spatial Markov property of Lagrangian velocities. This property implies that large-scale dispersion can be predicted from solving transport in just two characteristic pore sizes. The model parameters are fully defined from the Lagrangian velocity properties. We have performed the same comparison for a variety of other pore shape parameters and found a similar agreement between effective and pore-scale random walk simulations. The transition matrices quantify high-order correlation effects that are not included in classical two-point correlation functions. The high probability region in the left upper part of the transition matrices (Figure 6) indicate that small transit times are more correlated than large transit times. This implies that large velocities at the center of the pore are more correlated over successive pores than small velocities. The dependency of correlation on the local velocity was previously demonstrated by *Le Borgne et al.* [2007].

[26] In order to probe the minimum number of parameters sufficient to capture this effect, we ran correlated CTRW simulations with different numbers of transit time classes (Figure 9). Decreasing the number of classes from 49 to 12 we found only a slight change in the prediction of spatial variance. However, for a smaller number of classes, the spatial variance is significantly underestimated. For instance, the underestimation is about 40 percent when using only 3 velocity classes. Thus, we estimate that the minimum number of classes required in this case for capturing the whole range of correlation effects may be around 10. This suggests that, although the transition matrix can be simplified, it should contain a minimum of information for representing complex correlation properties such as the dependency of correlation on velocity.

5. Application to a Heterogeneous Porous Medium

[27] In section 5, we apply the methodology to the more complex 2-D heterogeneous porous medium studied by *Tartakovsky and Neuman* [2008] and *Tartakovsky et al.* [2008]. The Navier-Stokes equations for flow in the pore network are solved using smoothed particle hydrodynamics

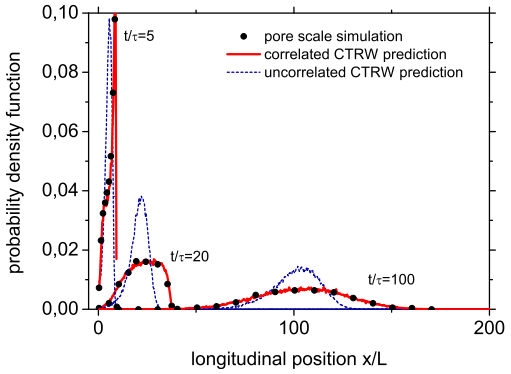

Figure 8. Comparison of the prediction of the correlated CTRW (red lines) and uncorrelated CTRW (blue lines) with the numerical simulations for the spatial distribution of longitudinal particle positions (black line with dots). Notice the overlap of the correlated CTRW model predictions and the full pore-scale simulations.

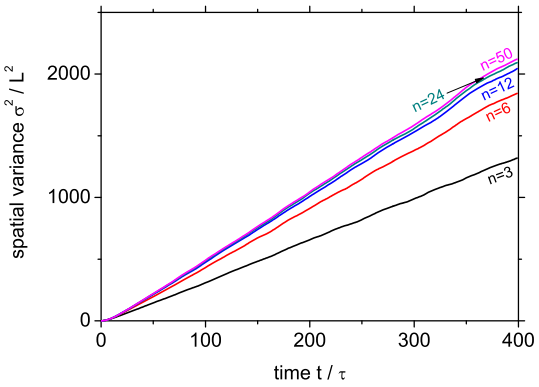

Figure 9. Prediction of the correlated CTRW model for the second centered moment with different numbers of velocity classes, $n = 3, 6, 12, 24, 49$.

(SPH) (Figure 10). The medium is composed of void and circular grains with mean porosity $\phi = 0.42$. The average velocity of $\overline{v} = 10^{-2}$ results from application of a hydraulic head gradient from top to bottom. The boundary conditions for flux are periodic on all sides. All details of computations are given by *Tartakovsky and Neuman* [2008]. The resulting velocity field shows the existence of a braided network of preferential flow paths as well as low-velocity or stagnation zones.

[28] In order to quantify the dispersion process in this medium, we apply the methodology to analyze the statistics of transit times along the SPH particle trajectories. SPH is a Lagrangian particle method where particles representing elementary fluid volumes are advected with the flow and exchange mass between them by diffusion. Advective Lagrangian trajectories are thus given by the trajectories of the SPH particles. The Lagrangian velocities analyzed along SPH particles trajectories can change because of advective heterogeneities but not because of diffusion across streamlines. Hence, velocity decorrelation occurs solely because of randomness in the velocity resulting from the heterogeneous nature of the porous medium.

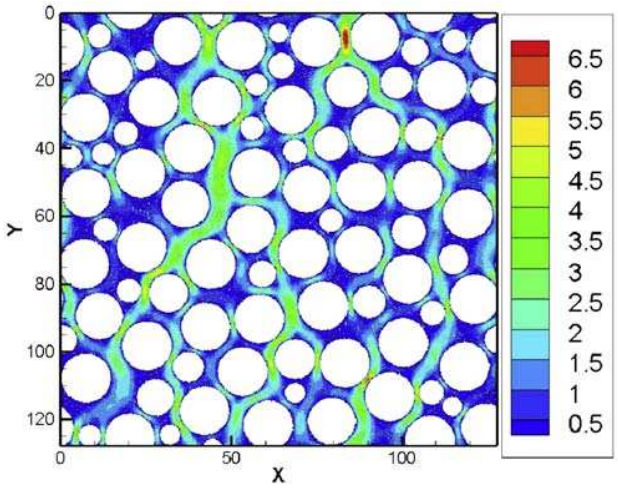

Figure 10. Heterogeneous pore-scale flow field showing the distribution of $v/\overline{v}$ (the magnitude of velocity relative to its spatial average), from *Tartakovsky and Neuman* [2008].

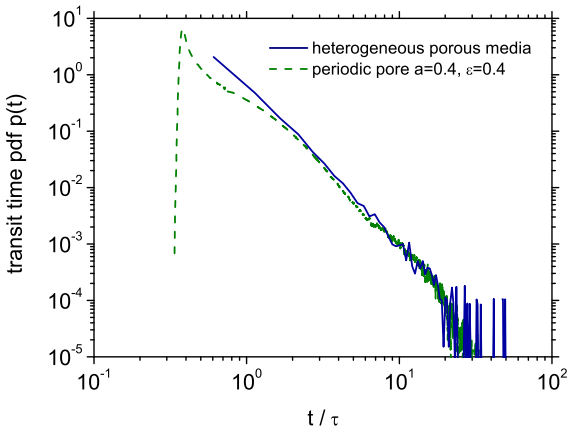

Figure 11. Transit time distribution across the mean pore size $\Delta x = 2.6$ for the heterogeneous porous media. It is compared here to the sinusoidal channel distribution for $a = 0.4$ and $\epsilon = 0.4$.

[29] The transit time distribution and transition matrix over the mean pore length $\Delta x = 2.6$ are computed by using $N = 27{,}620$ SPH particles (Figure 11). The comparison with the sinusoidal pore results shows that the large time distributions are strikingly similar for the two systems. The transition matrix (Figure 12) also shares some common features with those of the sinusoidal channel. The small transit times, corresponding to larger velocity channels, are found to be more correlated than other transit time classes. The large transit times are also more correlated than intermediate transit times, showing the existence of repetitive trapping phenomena. Thus, although the wavy channel model may appear simplified, it contains several features relevant to

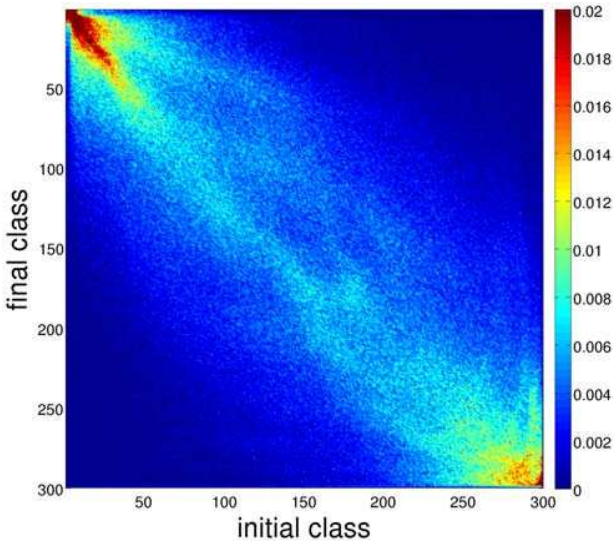

Figure 12. Spatial transition matrix T across the mean pore size $\Delta x = 2.6$ for the heterogeneous porous medium. Small matrix indices correspond to small transit times (large Lagrangian velocities), and large matrix indices correspond to large transit times (small Lagrangian velocities). Here the matrix is discretized into 300 classes.

Bibliography

Ackerer, P. (2010), Preface, *Computational Geosciences*, *14*(3), 383–383, doi:10.1007/s10596-010-9189-z.

Aris, R. (1956), On the dispersion of a solute in a fluid flowing through a tube, *Proc. Roy. Soc. A*, *253*, 67–77.

Baras, F., and M. Mansour (1996), Reaction-diffusion master equation: A comparison with microscopic simulations., *Physical review. E, Statistical physics, plasmas, fluids, and related interdisciplinary topics*, *54*(6), 6139–6148.

Battiato, I., D. M. Tartakovsky, a.M. Tartakovsky, and T. Scheibe (2009), On breakdown of macroscopic models of mixing-controlled heterogeneous reactions in porous media, *Advances in Water Resources*, *32*(11), 1664–1673, doi:10.1016/j.advwatres.2009.08.008.

Bear, J. (1988), *Dynamics of Fluyds in Porous Media*, Dove Publications, Inc., New York.

Bellin, a., G. Severino, and A. Fiori (2011), On the local concentration probability density function of solutes reacting upon mixing, *Water Resources Research*, *47*(1), 1–15, doi:10.1029/2010WR009696.

Benson, D. a., and M. M. Meerschaert (2008), Simulation of chemical reaction via particle tracking: Diffusion-limited versus thermodynamic rate-limited regimes, *Water Resources Research*, *44*(12), 1–7, doi:10.1029/2008WR007111.

Benson, D. A., S. W. Wheatcraft, and M. M. Meerschaert (2000), The fractional-order governing equation of Lévy Motion, *Water Resources Research*, *36*(6), 1413, doi:10.1029/2000WR900032.

Berkowitz, B., and H. Scher (1998), Theory of anomalous chemical transport in random fracture networks, *57*(5), 5858–5869.

Berkowitz, B., A. Cortis, M. Dentz, and H. Scher (2006), Modeling non-Fickian transport in geological formations as a continuous time random walk, *Reviews of Geophysics*, *44*(2), 1–49, doi:10.1029/2005RG000178.

Bernstein, D. (2005), Simulating mesoscopic reaction-diffusion systems using the Gillespie algorithm, *Physical Review E*, *71*(4), 1–13, doi:10.1103/PhysRevE.71.041103.

Bijeljic, B., P. Mostaghimi, and M. Blunt (2011), Signature of Non-Fickian Solute Transport in Complex Heterogeneous Porous Media, *Physical Review Letters*, *107*(20), 20–23, doi:10.1103/PhysRevLett.107.204502.

Bolster, D., D. Benson, T. Le Borgne, and M. Dentz (2010), Anomalous mixing and reaction induced by superdiffusive nonlocal transport, *Physical Review E*, *82*(2), doi:10.1103/PhysRevE.82.021119.

Bolster, D., P. de Anna, D. a. Benson, and A. M. Tartakovsky (2012), Incomplete mixing and reactions with fractional dispersion, *Advances in Water Resources*, *37*, 86–93, doi:10.1016/j.advwatres.2011.11.005.

Boon, J. P., D. Dab, R. Kapral, and A. Lawniczak (1996), Lattice gas automata for reactive systems, *Physics Reports*, *273*(2), 55–147, doi:10.1016/0370-1573(95)00080-1.

Bouchaud, J. (1990), Anomalous diffusion in disordered media: Statistical mechanisms, models and physical applications, *Physics Reports*, *195*(4-5), 127–293, doi:10.1016/0370-1573(90)90099-N.

Carrera, J., X. Sanchez-Vila, I. Bennet, A. Medina, G. Galaraza, and J. Guimera (1998), On matrix diffusion: formulations, solution methods and qualitative effects, *Hydrogeol. J.*, *6*, 178–190.

Chiogna, G., O. A. Cirpka, P. Grathwohl, and M. Rolle (2011), Transverse mixing of conservative and reactive tracers in porous media: Quantification through the concepts of flux-related and critical dilution indices, *Water Resources Research*, *47*(2), doi:10.1029/2010WR009608.

Connors, K. A. (1990), *Chemical Kinetics*, VCH publishers, New York.

Cushman, J. H., and T. R. Ginn (1993), Non local dispersion in media with continuously evolving scales of heterogeneity, *Transp. in Porous Media*, *13*(1), 123–138.

Cushman, J. H., L. S. Bennethum, and B. X. Hu (2002), A primer on upscaling tools for porous media, *Advances in Water Resources*, *25*(8-12), 1043–1067, doi:10.1016/S0309-1708(02)00047-7.

Dagan, G., a. Fiori, and I. Jankovic (2012), Upscaling of flow in heterogeneous porous formations: Critical examination and issues of principle, *Advances in Water Resources*, doi:10.1016/j.advwatres.2011.12.017.

Dauxois, T., F. Di Patti, D. Fanelli, and A. McKane (2009), Enhanced stochastic oscillations in autocatalytic reactions, *Physical Review E*, *79*(3), doi:10.1103/PhysRevE.79.036112.

de Anna, P., F. Di Patti, D. Fanelli, A. J. McKane, and T. Dauxois (2010), Spatial model of autocatalytic reactions, *Physical Review E*, *81*(5), doi:10.1103/PhysRevE.81.056110.

de Anna, P., T. Le Borgne, M. Dentz, D. Bolster, and P. Davy (2011), Anomalous kinetics in diffusion limited reactions linked to non-Gaussian concentration probability distribution function., *The Journal of chemical physics*, *135*(17), 174,104, doi:10.1063/1.3655895.

De Simoni, M., J. Carrera, X. Sánchez-Vila, and A. Guadagnini (2005), A procedure for the solution of multicomponent reactive transport problems, *Water Resources Research*, *41*(11), 1–16, doi:10.1029/2005WR004056.

De Simoni, M., X. Sanchez-Vila, J. Carrera, and M. W. Saaltink (2007), A mixing ratios-based formulation for multicomponent reactive transport, *Water Resources Research*, *43*(7), 1–10, doi:10.1029/2006WR005256.

Delay, F., P. Ackerer, and C. Danquigny (2005), Simulating Solute Transport in Porous or Fractured Formations Using Random Walk Particle Tracking, *Vadose Zone Journal*, *4*(2), 360, doi:10.2136/vzj2004.0125.

Dentz, M., T. Le Borgne, A. Englert, and B. Bijeljic (2010), Mixing, spreading and reaction in heterogeneous media: A brief review., *Journal of contaminant hydrology*, doi:10.1016/j.jconhyd.2010.05.002.

Dentz, M., T. Le Borgne, A. Englert, and B. Bijeljic (2011), Mixing, spreading and reaction in heterogeneous media: a brief review., *Journal of contaminant hydrology*, *120-121*, 1–17, doi:10.1016/j.jconhyd.2010.05.002.

Di Patti, F., S. Azaele, J. R. Banavar, and A. Maritan (2010), System size expansion for systems with an absorbing state, *Population (English Edition)*, p. 5.

Duplat, J., and E. Villermaux (2008), Mixing by random stirring in confined mixtures, *Journal of Fluid Mechanics*, *617*, 51, doi:10.1017/S0022112008003789.

Duplat, J., a. Jouary, and E. Villermaux (2010a), Entanglement Rules for Random Mixtures, *Physical Review Letters*, *105*(3), 8–11, doi:10.1103/PhysRevLett.105.034504.

Duplat, J., C. Innocenti, and E. Villermaux (2010b), A nonsequential turbulent mixing process, *Physics of Fluids*, *22*(3), 35,104, doi:10.1063/1.3319821.

Edery, Y., H. Scher, and B. Berkowitz (2010), Particle tracking model of bimolecular reactive transport in porous media, *Water Resources Research*, *46*(7), 1–12, doi:10.1029/2009WR009017.

Fahs, M., A. Younes, and P. Ackerer (2010), An Efficient Implementation of the Method of Lines for Multicomponent Reactive Transport Equations, *Water, Air, & Soil Pollution*, *215*(1-4), 273–283, doi:10.1007/s11270-010-0477-y.

Feller, W. (1966), *An Introduction to Probability Theory and Its Applications*, second edi ed., Wiley Series in Probability and Mathematical Statistics.

Gálfi, L., and Z. Rácz (1988), Properties of the reaction front in an A+BâĘŠC type reaction-diffusion process, *Physical Review A*, *38*(6), 3151–3154, doi:10.1103/PhysRevA.38.3151.

Gardiner, C. W. (2004), *Handbook of stochastic Methods*, third ed., Springer-Verlag, Berlin.

Gelhar, L. W., and C. L. Axness (1983), Three-Dimensional Stochastic Analysis of Macrodispersion in Aquifers, *19*(1), 161–180.

Gillespie, D. T. (1976), A general method for numerically simulating the stochastic time evolution of coupled chemical reactions, *Journal of Computational Physics*, *22*(4), 403–434, doi:10.1016/0021-9991(76)90041-3.

Gillespie, D. T. (1977), Exact stochastic simulation of coupled chemical reactions, *The Journal of Physical Chemistry*, *81*(25), 2340–2361, doi:10.1021/j100540a008.

Gramling, C. M., C. F. Harvey, and L. C. Meigs (2002), Reactive Transport in Porous Media: A Comparison of Model Prediction with Laboratory Visualization, *Environmental Science & Technology*, *36*(11), 2508–2514, doi:10.1021/es0157144.

Haggerty, R., and S. M. Gorelick (1995), Multiple-Rate Mass Transfer for Modeling Diffusion and Surface Reactions in Media with Pore-Scale Heterogeneity, *Water Resources Research*, *31*(10), 2383, doi:10.1029/95WR10583.

Haggerty, R., S. A. McKenna, and L. C. Meigs (2000), On the late-time behavior of tracer test breakthrough curves, *Water Resources Research*, *36*(12), 3467, doi:10.1029/2000WR900214.

Harrison, C., J. a. T. Cabral, C. M. Stafford, A. Karim, and E. J. Amis (2004), A rapid prototyping technique for the fabrication of solvent-resistant structures, *Journal of Micromechanics and Microengineering*, *14*(1), 153–158, doi:10.1088/0960-1317/14/1/021.

Harvey, C. F., and S. M. Gorelick (1995), Temporal Moment-Generating Equations: Modeling Transport and Mass Transfer in Heterogeneous Aquifers, *Water Resources Research*, *31*(8), 1895, doi:10.1029/95WR01231.

Havlin, S., M. Araujo, H. Larralde, A. Shehter, and H. E. Stanley (1995), Anomalous kinetics in A + B âĘŠ C with initially-separated reactants, *Chaos, Solitons & Fractals*, *6*, 157–169, doi:10.1016/0960-0779(95)80024-B.

Hornung, U. (1997), *Homogeneization and porous media*, Springer-Verlag, New York.

Horsthemke, W., S. Fedotov, and V. Mendez (2010), *Reaction-Transport Systems*, Springer Series in Synergetics, 1st ed., Springer Berlin Heidelberg, Berlin, Heidelberg, doi:10.1007/978-3-642-11443-4.

Janković, I., A. Fiori, and G. Dagan (2009), The impact of local diffusion on longitudinal macrodispersivity and its major effect upon anomalous transport in highly heterogeneous aquifers, *Advances in Water Resources*, *32*(5), 659–669, doi:10.1016/j.advwatres.2008.08.012.

Jonsson, T., and K. Irgum (1999), Very fast peroxyoxalate chemiluminescence, *Analytica Chimica Acta*, *400*, 257–264.

Kang, K., and S. Redner (1985), Fluctuation-dominated kinetics in diffusion-controlled reactions, *Physical Review A*, *32*(1), 435.

Kang, P., M. Dentz, T. Le Borgne, and R. Juanes (2011), Spatial Markov Model of Anomalous Transport Through Random Lattice Networks, *Physical Review Letters*, *107*(18), 1–5, doi: 10.1103/PhysRevLett.107.180602.

Kapoor, V., L. W. Gelhar, and F. Miralles-Wilhelm (1997), Bimolecular second-order reactions in spatially varying flows: Segregation induced scale-dependent transformation rates, *Water Resources Research*, *33*(4), 527, doi:10.1029/96WR03687.

Kitanidis, P. K. (1994), The concept of the Dilution Index, *Water Resources Research*, *30*(7), 2011, doi: 10.1029/94WR00762.

Konz, M., P. Ackerer, P. Huggenberger, and C. Veit (2009), Comparison of light transmission and reflection techniques to determine concentrations in flow tank experiments, *Experiments in Fluids*, *47*(1), 85–93, doi:10.1007/s00348-009-0639-0.

Le Borgne, T., M. Dentz, and J. Carrera (2008a), Lagrangian Statistical Model for Transport in Highly Heterogeneous Velocity Fields, *Physical Review Letters*, *101*(9), 1–4, doi: 10.1103/PhysRevLett.101.090601.

Le Borgne, T., M. Dentz, and J. Carrera (2008b), Lagrangian Statistical Model for Transport in Highly Heterogeneous Velocity Fields, *Physical Review Letters*, *101*(9), 1–4, doi: 10.1103/PhysRevLett.101.090601.

Le Borgne, T., M. Dentz, and J. Carrera (2008c), Spatial Markov processes for modeling Lagrangian particle dynamics in heterogeneous porous media, *Physical Review E*, *78*(2), 1–9, doi: 10.1103/PhysRevE.78.026308.

Le Borgne, T., M. Dentz, P. Davy, D. Bolster, J. Carrera, J.-R. de Dreuzy, and O. Bour (2011a), Persistence of incomplete mixing: A key to anomalous transport, *Physical Review E*, *84*(1), 1–4, doi: 10.1103/PhysRevE.84.015301.

Le Borgne, T., D. Bolster, M. Dentz, P. de Anna, and A. Tartakovsky (2011b), Effective pore-scale dispersion upscaling with a correlated continuous time random walk approach, *Water Resources Research*, *47*(12), 1–10, doi:10.1029/2011WR010457.

Levy, M., and B. Berkowitz (2003), Measurement and analysis of non-Fickian dispersion in heterogeneous porous media., *Journal of contaminant hydrology*, *64*(3-4), 203–26, doi:10.1016/S0169-7722(02)00204-8.

Leyvraz, F., and S. Redner (1992), Spatial structure in diffusion-limited two-species annihilation, *Physical Review A*, *46*(6), 3132–3147, doi:10.1103/PhysRevA.46.3132.

Lugo, C., and A. McKane (2008), Quasicycles in a spatial predator-prey model, *Physical Review E*, *78*(5), 1–15, doi:10.1103/PhysRevE.78.051911.

Luo, J., M. Dentz, J. Carrera, and P. Kitanidis (2008), Effective reaction parameters for mixing controlled reactions in heterogeneous media, *Water Resources Research*, *44*(2), 1–12, doi:10.1029/2006WR005658.

Majdalani, S., and P. Ackerer (2011), Identification of Groundwater Parameters Using an Adaptative Multiscale Method, *Ground Water*, *49*(4), 548–559, doi:10.1111/j.1745-6584.2010.00750.x.

McKane, A. J., and T. J. Newman (2005), Predator-Prey Cycles from Resonant Amplification of Demographic Stochasticity, *Physical Review Letters*, *94*(21), doi:10.1103/PhysRevLett.94.218102.

Meerschaert, M., D. Benson, and B. Bäumer (1999), Multidimensional advection and fractional dispersion, *Physical Review E*, *59*(5), 5026–5028, doi:10.1103/PhysRevE.59.5026.

Metzler, R., and J. Klafter (2000), The random walk's guide to anomalous diffusion: a fractional dynamics approach, *Physics Reports*, *339*.

Meunier, P., and E. Villermaux (2010), The diffusive strip method for scalar mixing in two dimensions, *Journal of Fluid Mechanics*, *662*, 134–172, doi:10.1017/S0022112010003162.

Monson, E., and R. Kopelman (2004), Nonclassical kinetics of an elementary A+B[over âĘŠ]C reaction-diffusion system showing effects of a speckled initial reactant distribution and eventual self-segregation: Experiments, *Physical Review E*, *69*(2), 1–12, doi:10.1103/PhysRevE.69.021103.

Montroll, E. W., and G. H. Weiss (1965), Random walks on lattices, *J. Math. Phys.*, *6*(2), 167.

Mordant, N., J. Delour, E. Léveque, a. Arnéodo, and J.-F. Pinton (2002), Long Time Correlations in Lagrangian Dynamics: A Key to Intermittency in Turbulence, *Physical Review Letters*, *89*(25), 2–5, doi:10.1103/PhysRevLett.89.254502.

Neufeld, Z., and E. Hernandez-Garcia (2010), *Chemical and Biological Processes in Fluid Flows: A dynamical System Approach*, Imperial College Press.

Neuman, S. P. (1993), Eulerian-Lagrangian Theory of transport in space-time nonstationary velocity fields: Exact nonlocal formalism by conditional moments and weak approximation, *Water Resources Research*, *29*(3), 633, doi:10.1029/92WR02306.

Neuman, S. P., and D. M. Tartakovsky (2009), Perspective on theories of non-Fickian transport in heterogeneous media, *Advances in Water Resources*, *32*(5), 670–680, doi:10.1016/j.advwatres.2008.08.005.

Oates, P. M. (2007), Upscaling reactive transport in porous media: laboratory visualization and stochastic models, Ph.D. thesis, MIT.

Oates, P. M., and C. F. Harvey (2006), A colorimetric reaction to quantify fluid mixing, *Experiments in Fluids*, *41*(5), 673–683, doi:10.1007/s00348-006-0184-z.

Ottino, J. (1989), *The kinematics of mixing: stretching, chaos, and transport*, Cambridge University Press.

Ovchinnikov, A. I. A., and Y. B. Zeldovich (1978), ROLE OF DENSITY FLUCTUATIONS IN BIMOLECULAR REACTION KINETICS, *Chemical Physics*, *28*, 215–218.

Pinder, G. F., and M. A. Celia (2006), *Subsurface Hydrology*, Wiley, Hoboken, New Jersey.

Pope, S. B. (2000), *Turbulent Flows*, Cambridge University Press, New York.

Quintard, M., and S. Whitaker (1994), Convection, dispersion, and interfacial transport of contaminants: Homogeneous porous media, *Advances in Water Resources*, *17*(221-239).

Saaltink, M. W. (2004), RETRASO, a code for modeling reactive transport in saturated and, *Geol. Acta*, *2*, 235–251.

Schweitzer, F. (2003), *Brownian Agents and Active Particles Brownian Agents and Active Particles*, 420 pp., Springer Series in Synergetics, New York.

Strogatz, S. H. (2000), *Non linear dynamics and chaos*, Westview Press.

Tabeling, P. (2005), *Introduction to microfluidics*, Oxford University Press, New York, NY, US.

Tartakovsky, A. (2010), Langevin model for reactive transport in porous media, *Physical Review E*, *82*(2), 1–11, doi:10.1103/PhysRevE.82.026302.

Tartakovsky, A., D. Tartakovsky, and P. Meakin (2008a), Stochastic Langevin Model for Flow and Transport in Porous Media, *Physical Review Letters*, *101*(4), 1–4, doi:10.1103/PhysRevLett.101.044502.

Tartakovsky, A. M., and P. Meakin (2005), A smoothed particle hydrodynamics model for miscible flow in three-dimensional fractures and the two-dimensional RayleighâĂŞTaylor instability, *Journal of Computational Physics*, *207*(2), 610–624, doi:10.1016/j.jcp.2005.02.001.

Tartakovsky, A. M., and S. P. Neuman (2008), Effects of Peclet number on pore-scale mixing and channeling of a tracer and on directional advective porosity, *Geophysical Research Letters*, *35*(21), doi:10.1029/2008GL035895.

Tartakovsky, a. M., G. Redden, P. C. Lichtner, T. D. Scheibe, and P. Meakin (2008b), Mixing-induced precipitation: Experimental study and multiscale numerical analysis, *Water Resources Research*, *44*(6), 1–19, doi:10.1029/2006WR005725.

Tartakovsky, A. M., G. D. Tartakovsky, and T. D. Scheibe (2009), Effects of incomplete mixing on multicomponent reactive transport, *Advances in Water Resources*, *32*(11), 1674–1679, doi:10.1016/j.advwatres.2009.08.012.

Taylor, G. (1953), Dispersion of Soluble Matter in Solvent Flowing Slowly through a Tube, *Proceedings of the Royal Society A: Mathematical, Physical and Engineering Sciences*, *219*(1137), 186–203, doi:10.1098/rspa.1953.0139.

Tel, T., A. Demoura, C. Grebogi, and G. Karolyi (2005), Chemical and biological activity in open flows: A dynamical system approach, *Physics Reports*, *413*(2-3), 91–196, doi:10.1016/j.physrep.2005.01.005.

Toussaint, D., and F. Wilczek (1983), Particle-antiparticle annihilation in diffusive motion, *The Journal of Chemical Physics*, *78*(5), 2642, doi:10.1063/1.445022.

van Kampen, N. (2007), *Stochastic Processes in Physics and Chemistry*, third ed., Elsevier, Amsterdam.

Villermaux, E., and J. Duplat (2003), Mixing as an Aggregation Process, *Physical Review Letters*, *91*(18), 3–6, doi:10.1103/PhysRevLett.91.184501.

Whitaker, S. (1999), *The Method of Volume Averaging*, Kluwer Academic Publisher, Dordrecht.

Zinn, B., L. C. Meigs, C. F. Harvey, R. Haggerty, W. J. Peplinski, and C. F. Von Schwerin (2004), Experimental visualization of solute transport and mass transfer processes in two-dimensional conductivity fields with connected regions of high conductivity., *Environmental science & technology*, *38*(14), 3916–26.

Zumofen, G., J. Klafter, and M. Shlesinger (1996), Breakdown of Ovchinnikov-Zeldovich Segregation in the A+B–>0 Reaction under Lévy Mixing., *Physical review letters*, *77*(13), 2830–2833.

ANNEXE 2 (Modèle dernière page de thèse)

VU :

Le Directeur de Thèse
(DAVY, Philippe)

VU :

Le Responsable de l'École Doctorale

DAVY Philippe

VU pour autorisation de soutenance

Rennes, le

Le Président de l'Université de Rennes 1

Guy CATHELINEAU

VU après soutenance pour autorisation de publication :

Le Président de Jury,